Investigating the Role of *Runx2* in Haematopoiesis

Grace Ann Meaker

St Cross College

University of Oxford

A thesis submitted for the degree of

Doctor of Philosophy

September 2025

Abstract

Self-renewing multipotent haematopoietic stem cells (HSCs) are a rare but vital cell population supporting life-long homeostasis of the entire blood and immune system. Due to the paucity of HSCs and limitations in *ex vivo* HSC expansion, it has been difficult to comprehensively study the genetic regulators of the balancing of HSC self-renewal and differentiation.

Investigation of a genome-wide *ex vivo* CRISPR screen in mouse haematopoietic stem and progenitor cells (HSPCs) uncovered many putative negative regulators and essential genes which have previously been uncharacterised in HSCs. The RUNX transcription factor family were identified as putative negative regulators of HSC expansion. *Runx1* and *Runx2* loss promoted HSC expansion *ex vivo* and increased engraftment *in vivo* but had contrasting effects on the reconstitution of the broader haematopoietic system, therefore revealing non-redundant roles for *Runx* family members in haematopoiesis.

Runx2 was further validated as a potent regulator of haematopoiesis, using a haematopoietic-specific *Runx2*^{flox} mouse. Heterozygosity of *Runx2* was sufficient for increased HSC expansion *ex vivo* and increased engraftment *in vivo*. *Runx2* was found to have a role in regulation of HSC self-renewal potential. Its loss, however, had no effect on steady-state haematopoiesis.

Runx2 loss also decreased T-cell output and partially blocked progression of early T-cell differentiation in the thymus. This supports a model where *Runx2* regulates migration of lymphoid progenitor cells through T-cell differentiation, as *Runx2*-deficient lymphoid progenitor cells accumulated in the bone marrow and thymus.

In summary, the findings presented in this thesis demonstrated new roles for *Runx2* in regulating T-cell output and self-renewal potential of HSCs.

Declaration

I declare that this work is my own research, except where explicitly stated. This thesis has not been submitted, either partially or in full, for another qualification at this University, or for a qualification at any other institution. The total length of the main body of this thesis is 38,328 words and therefore does not exceed the limit of 50,000 words for such a thesis.

Acknowledgements

I would first like to thank my supervisor Adam Wilkinson for his patience, support and undying enthusiasm for this project. I would also like to thank my co-supervisor Tom Milne, for helping me develop so many of the key skills needed during a PhD – not least the ability to answer hard questions on the spot!

I extend my thanks to the Medical Research Council for my scholarship and funding and to my thesis, transfer and confirmation committees for their input on the direction of my project.

To the WIMM Flow Cytometry Facility for helping me out countless times – especially Kevin who always had a friendly smile despite cytometer-related dramas. I thank the BMS and FGF Facilities for technical support with *in vivo* work and the WIMM Virus Core for generating lentivirus for gene-editing.

I thank members of the Wilkinson lab past and present for their support and guidance. In particular Hwei Minn, who trained me alongside Adam in those early days of the lab. Thanks also go to Matt Nicholls for performing *ex vivo* T-cell assays, and to Ian Hsu for CRISPR screen analysis. I also am very grateful to Catherine Chahrour for her assistance with bioinformatic analyses, and to Dr Alastair Smith for performing CUT&Tag experiments.

Dedications

I could not have got through the last four years without the incredible friends I have made along the way. I thank Liz and Shanissa for silly coffee breaks and being my conference buddies.

I am so grateful to Maya, Olly and Joe for being there with me from day one of my PhD and providing much needed laughter and light. Also, to Nicole for providing someone to look up to (despite being 5'2) and always having time for a coffee and a chat. To Matt Baxter, who's been there for me professionally and personally throughout my PhD journey in so many ways.

I must also thank my undergraduate placement year supervisor Tom Gorochowski, who helped me to believe in myself and my ability as a scientist – without whom I would never have done a PhD.

I thank my little buddy Darwin for keeping me sane during those long days of writing by being his chaotic chirpy self.

My final thanks go to my Mum and Dad, for nurturing my interest in science from such a young age and giving me the foundation to get to where I always dreamed of.

"Science, for me, gives a partial explanation for life. In so far as it goes, it is based on fact, experience, and experiment." – Rosalind Franklin

Glossary

ACK - ammonium-chloride-potassium

AGM - aorta-gonad mesonephros

ALL - acute lymphoblastic leukemia

AML - acute myeloid leukaemia

APC - antigen-presenting cell

BM - bone marrow

CCD - cleidocranial dysplasia

cKO - conditional knockout

CLP - common lymphoid progenitor

CM junction - cortico-medullary junction

CMP - common myeloid progenitor

CRISPR - clustered regularly interspaced short palindromic repeats

cTEC - cortical thymic epithelial cell

CUT&Tag - cleavage under targets and tagmentation

DC - dendritic cell

ddPCR - droplet digital PCR

DEG - differentially expressed gene

DMEM - Dulbecco's modified eagle medium

DN - double negative

DNA - deoxyribonucleic acid

DP - double positive

EHT - endothelial-to-haematopoietic transition

ETP - early T-lineage precursor

FACS - fluorescence activated cell sorting

FBS - foetal bovine serum

FDR - false discovery rate

FL - fetal liver

FPD - familial platelet disorder

gDNA - genomic DNA

GMP - granulocyte-monocyte progenitor cell

GO:BP - gene ontology: biological process

gRNA - guide RNA

GSEA - gene set enrichment analysis

GvHD - graft versus host disease

HLA - human leukocyte antigen

HPC - haematopoietic progenitor cell

HSC - haematopoietic stem cell

HSCT - haematopoietic stem cell transplantation

HSPC - haematopoietic stem and progenitor cell

IFN - interferon

IT-HSC - intermediate-term haematopoietic stem cell

ITS-X - insulin-transferrin-selenium

KO - knockout

KSL - c-Kit^{+}Sca-1^{+}Lin-

LMPP - lymphoid-myeloid-primed progenitor cell

LT-HSC - long-term haematopoietic stem cell, CD150^{+}CD48^{-}CD34^{-}c-Kit^{+}Sca-1^{+}Lin^{-}

LyMPP - lymphoid-primed multipotent progenitor cell

MACS - magnetic-activated cell sorting

MAGeCK - model-based analysis of genome-wide CRISPR/Cas9 knockout

MEP - megakaryocyte-erythroid progenitor cell

MF - mesenchymal fibroblast

MHC - major histocompatibility complex

MPP - multipotent progenitor cell

MPP$^{G/M}$ - granulocytic-monocyte-biased multipotent progenitor cell

MPP$^{Mk/E}$ - megakaryocytic-erythroid-biased multipotent progenitor cell

mRNA - messenger RNA

MSC - mesenchymal stromal cell

mTEC - medullary thymic epithelial cell

NEAA - non-essential amino acids

NK cell – natural killer cell

NLS - nuclear localisation signal

NMTS - nuclear matrix targeting signal

PB - peripheral blood

PBS - phosphate-buffered saline

PCR - polymerase chain reaction

pDC - plasmacytoid dendritic cell

pHPC - CD201$^-$CD150$^-$KSL

pHSC - CD201$^+$CD150$^+$KSL

PI - propidium iodide

PSG - penicillin-streptomycin-glutamine

PST - proline-serine-threonine

PVA - polyvinyl alcohol

RHD - Runt homology domain

RNA - ribonucleic acid

RNA-pol II - RNA-polymerase II

RRA - robust rank aggregation

SCF - stem cell factor

sgRNA - single guide RNA

shRNA - short hairpin RNA

siRNA - short interfering RNA

SP - single positive

ST-HSC - short-term haematopoietic stem cell

TCR - T-cell receptor

TF - transcription factor

TNF - tumour necrosis factor

TPO - thrombopoietin

UCB - umbilical cord blood

VWRPY - C-terminal repressive domain

WT - wild-type

Papers arising from this DPhil

Meaker G.A., et al. A genome-wide screen identifies Runx2 as a novel regulator of hematopoietic stem cell expansion and T-cell commitment. *In press*, *Blood*, 2025.

Haney M., ... **Meaker G.A** et al. *In vivo* CRISPR screening identifies SAGA complex members as key regulators of hematopoiesis. *Under review at Nature Comms,* 2025

Meaker G.A., Wilkinson A.C. Ex vivo Hematopoietic Stem Cell Expansion Technologies: Recent Progress, Applications, and Open Questions. *Experimental Hematology*, 2024.

Meaker G.A.*, Khoo H.M.*, Wilkinson A.C. Ex vivo Expansion and Genetic Manipulation of Mouse Hematopoietic Stem Cells in Polyvinyl Alcohol-Based Cultures. *J. Vis. Exp.* 2023

(* denotes co-first authorship)

Table of Contents

Figures in this thesis

Tables in this thesis

Chapter 1: Introduction and Background

1.1 Overview of haematopoiesis

1.1.1 Haematopoiesis and the blood system

Haematopoiesis is defined by the production of blood components, maintained over an organism's lifetime by a complex balance of cellular migration, differentiation and proliferation. Haematopoietic stem cells (HSCs) support long-term haematopoietic homeostasis by producing erythrocytes, megakaryocytes (and platelets), monocytes, eosinophils, neutrophils, dendritic cells, mast cells, B-cells, T-cells, natural killer cells and innate lymphoid cells[1,2]. These cell types have a variety of roles in innate and adaptive immunity, allowing the organism to respond to pathogenic threat and protect from infection. Additionally, erythrocytes transport oxygen to tissues using haemoglobin, while platelets help prevent blood loss by forming clots at sites of injury. After entering circulation, these cells have a finite lifespan, hence HSCs need to maintain a constant delivery of fresh mature cells to sustain lifetime immune function. For example in the mouse, neutrophils have a half-life of only 12.5 hours[3,4], monocytes ~20-50 hours[3,5], and macrophages up to 24-35 weeks depending on tissue-specificity[3,6–9].

The traditional model of adult haematopoiesis proposed a tree-like hierarchy, with a small pool of multipotent self-renewing HSCs at the apex that progressively lose self-renewal ability (to produce another HSC[10]) and lineage potential (to differentiate into multiple cell types) as they specify into mature blood lineages (**Figure 1.1A**). This classical model describes a key bifurcation into common myeloid progenitor cells (CMPs) and common lymphoid progenitor cells (CLPs)[1]. CMPs have megakaryocytic, erythroid and myeloid potential, whereas CLPs produce T-cells, B-cells and natural killer (NK) cells. The existence of CLPs has been hotly debated in the field, with the identification of lymphoid-restricted progenitor cells in the 1990s[11–13], to the finding that the most immature T-progenitor cells are earlier than the CLPs

in haematopoiesis and still retain some myeloid potential, termed early T-lineage precursor cells or ETPs[14].

As the field has developed, deeper understanding of the stages of differentiation has highlighted the existence of various different types of progenitors, with some displaying lineage restriction (**Figure 1.1B**)[1,15,16]. A number of different HSC and progenitor cell populations have been resolved[17]. Long-term HSCs (LT-HSCs) are rare and quiescent - residing in G0 of the cell cycle - and can reconstitute haematopoiesis over the long-term whereas short-term HSCs (ST-HSCs) have a short-term reconstitution capacity[18,19]. LT-HSCs differentiate into ST-HSCs and ST-HSCs differentiate into multipotent progenitor cells (MPPs) which cannot self-renew[19]. Intermediate-term HSCs (IT-HSCs) sit between the LT- and ST-HSCs, with medium-term reconstitution ability[20,21].

Heterogeneity in MPPs was characterised by the Trumpp and Passegue groups who defined MPP1 as having similar lineage potential and reconstitution ability to ST-HSCs, and MPP2, MPP3 and MPP4 as having no self-renewal potential and a short-term myeloid reconstitution potential[16,22]. Myeloid potential was found to persist alongside lymphoid potential further down the 'tree'[20,23,24]. Challen and colleagues provided an updated definition of MPP subsets in 2021, defining MPP as having medium term (~2 month) multilineage reconstitution, but no self-renewal ability[25]. They defined lineage-restricted MPPs as having short to medium term (~1-2 month) lineage reconstitution ability, with $MPP^{G/M}$ displaying a granulocyte/monocyte bias, LyMPP displaying a B/T-lymphoid bias, and $MPP^{Mk/E}$ displaying a megakaryocyte/erythroid bias[25].

Advances in single-cell techniques such as single-cell RNA-sequencing and lineage tracing have suggested further updates to these models for haematopoiesis, such as the hypothesis that lineage-specificity occurs without progression through multipotent stages[24,26,27]. The current understanding is that haematopoiesis is a continuous process, with heterogeneous populations at all stages of differentiation and flexibility to meet homeostatic demands in

response to infection, inflammation and haematopoietic stress (**Figure 1.1C**).

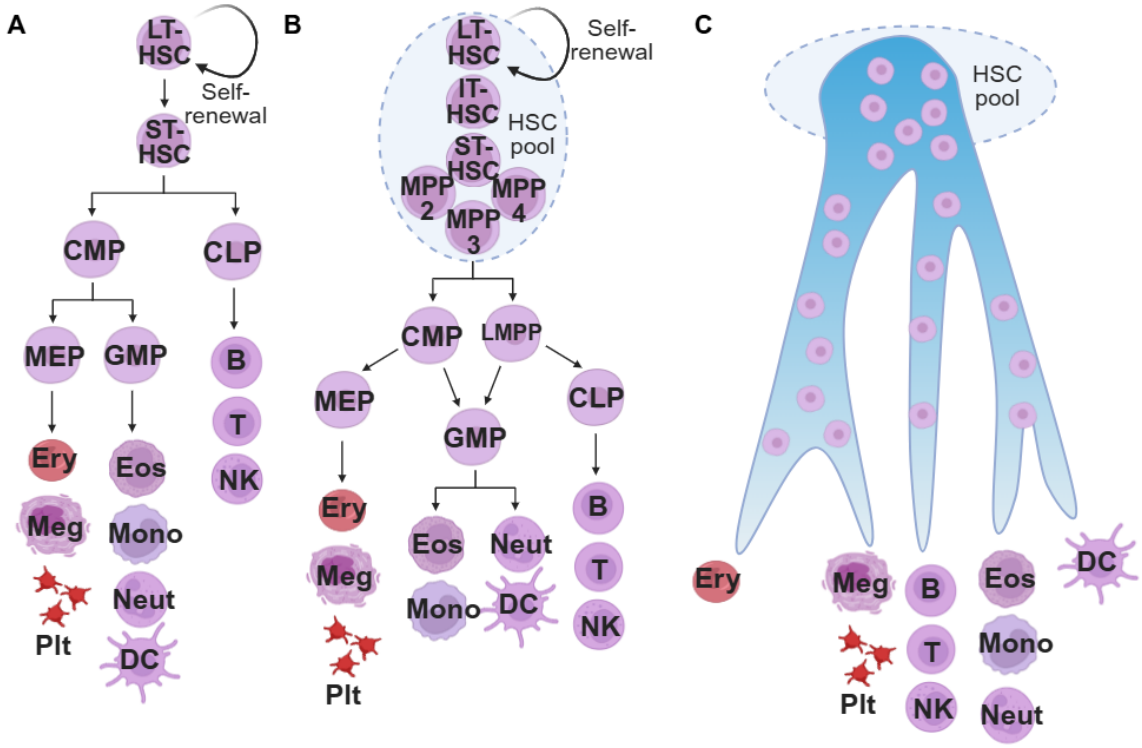

Figure 1.1: Proposed models of haematopoiesis.

(A) Model of haematopoiesis circa the year 2000. HSCs are either self-renewing or differentiating (LT-HSC and ST-HSC respectively). ST-HSCs differentiate into two clear lineages to produce myeloid or lymphoid cells.

(B) Model between 2005-2015. HSCs are considered more heterogenous, and the myeloid and lymphoid lineages maintain multipotent lineage potential further into differentiation, contrasting the clear bifurcation in A.

(C) Model from 2016 to now. Single-cell transcriptomics has revealed a complex landscape of differentiation, responding to haematopoietic requirements.

LT-HSC = long-term HSC. ST-HSC = short-term HSC. CMP = common myeloid progenitor cell. CLP = common lymphoid progenitor cell. MEP = megakaryocyte-erythroid progenitor cell. GMP = granulocyte-monocyte progenitor cell. Ery = erythroid cell. Meg = megakaryocyte. Plt = platelet. Eos = eosinophil. Mono = monocyte. Neut = neutrophil. DC = dendritic cell. B = B-cell. T= T-cell. NK = natural killer cell. IT-HSC = intermediate-term HSC. MPP = multipotent progenitor cell. LMPP = lymphoid-myeloid primed-progenitor cell. Adapted from Laurenti and Gottgens, 2018[24]. Reproduced with permission from Springer Nature. Created in BioRender.

1.1.2 Haematopoietic stem cells

HSCs are a rare and essential cell type, responsible for lifetime haematopoietic homeostasis[28,29]. They are primarily found in the bone marrow with ~100,000 present in

humans[28]. HSCs can either asymmetrically divide to produce another HSC and a progenitor cell (HSC maintenance and self-renewal), symmetrically divide to produce two progenitor cells (differentiation) or symmetrically divide to produce two HSCs (symmetrical self-renewal)[1,30]. The first identification of the HSC concept came from an *in vivo* assay by Till and McCulloch[31] wherein lethal irradiation of mice was rescued by bone marrow transplantation. They used a spleen colony forming unit assay to estimate stem cell numbers and provided the first evidence of multipotent progenitor cells *in vivo* which were able to generate multiple blood lineages[1,31]. Weissman and colleagues in 1988 refined this by identifying distinct populations of multipotent progenitor cells (which could not self-renew or persist over time) and self-renewing HSCs[32]. Stable reconstitution of the haematopoietic system following transplantation into a bone marrow ablated recipient remains the gold-standard functional definition of an HSC[29]. This functional definition characterises HSC activity in terms of their 'engraftment' into the recipient. Engraftment is defined as the ability of HSCs to establish a proliferative HSC pool and produce multipotent progenitors to support haematopoiesis[33]. Interactions between haematopoietic stem cells and the bone marrow microenvironment play a critical role in regulating engraftment, particularly through chemokine and cytokine signalling[34]. For example, expression of the CXC chemokine ligand CXCL12 is upregulated in the bone marrow following ablation of the recipient haematopoietic system and prior to transplantation[35]. Other key players in the mechanisms of HSC engraftment include cell adhesion molecules such as endothelial secretins for HSC movement within the niche[34]. α4β1/VLA-4 integrin and lectins are important for HSC interaction and attachment to niche cells[36,37].

1.1.3 Haematopoietic stem cell transplantation and clinical relevance of HSCs

Haematopoietic stem cell transplantation (HSCT) has been an established therapy for many blood disorders for nearly 60 years[38,39]. It is used in treatment for leukaemias, myeloproliferative disorders such as myelodysplastic syndrome and genetic haematological disorders such as anaemias and severe combined immunodeficiency[39]. It involves replacing

the defective haematopoietic system of a patient with a healthy one by transplantation of donor HSCs and immune cells. This usually requires the patient's bone marrow to be depleted by a regimen of chemotherapy or radiotherapy. The donor HSCs can be derived from a healthy, matched donor (allogenic HSCT) or their own stem cells (autologous HSCT)[40].

In most cases of allogeneic HSCT, HSCs are obtained from mobilised peripheral blood but can also be sourced from the bone marrow of a suitable donor[41]. This requires human leukocyte antigen (HLA) matching to reduce the chance of the patient developing graft versus host disease (GvHD), a potentially fatal condition in which transplanted cells attack the patient. The requirement for a matched donor means 70% of patients have no donor accessible, and even with a matched donor they still have the risk of serious complications such as graft rejection, graft failure and infections as a result of long regimens of immunosuppressive drugs[42]. To reduce the risk of GvHD, HSCs can be sourced from umbilical cord blood (UCB)[42]. The limitation of UCB is that single units have very low cell numbers, making them impractical or impossible to use for proper donor HSC engraftment in adults.

There is therefore much research interest in developing methods for expanding HSCs *ex vivo*, to improve the safety, efficacy and availability of HSCT[43]. To understand how to boost HSC expansion *ex vivo*, the field must understand the genetic effectors of HSC biology and function.

1.1.4 The bone marrow niche

Inconsistencies in the behaviour of the multipotent progenitor cells discovered by Till and McCullough led to the proposal by Schofield in 1978 that haematopoietic stem and progenitor cells (HSPCs) require interactions with a stem cell 'niche' to maintain stemness and reconstitution ability[44,45]. Discovery of the requirement of the genomic locus encoding c-Kit (CD117), a cellular receptor, and the locus encoding stem cell factor (SCF), the c-Kit receptor's ligand, for HSC function also supported the idea that HSCs require extrinsic signalling for their behavioural regulation[2]. Further investigation revealed that osteoblasts derived from bone marrow stromal cells interact with blood vessel cells such as sinusoids, to regulate HSPCs

and produce haematopoietic cytokines[46–50]. Since then the niche has been characterised as containing fourteen main clusters of cell types which cooperate to support the fitness of the overall 'ecosystem'[51–53]. The bone marrow niche has a predictable structure, with different regions containing patterns of cell types with different functions and lineage potentials. For example, HSCs are five times more likely than other cell types to be in proximity to a sinusoid and are mostly found in the trabecular region of the bone marrow, suggesting their regulation by various bone cells[49,54,55]. A key role of niche cells is to produce haematopoietic cytokines, including SCF and CXCL12, to promote HSC survival and function. CXCL12 (stromal-derived factor 1, SDF-1) is produced by early mesenchymal progenitor cells and is essential for HSC survival, long-term reconstitution ability, quiescence and production of CLPs[56]. SCF is produced by perivascular cells and promotes HSC self-renewal in collaboration with other cytokines, such as thrombopoietin (TPO) which is produced in the liver[57–59]. Myeloid progenitor cells localise in proximity to a subset of blood vessels expressing the myelopoietic regulator CSF1[60,61]. Changes in the structure of the niche and the secretion of cytokines are observed with aging[62], discussed further in Chapter 1.1.8. An overview of the distinct niches occupied by HSCs and progenitor cells is shown in **Figure 1.2**.

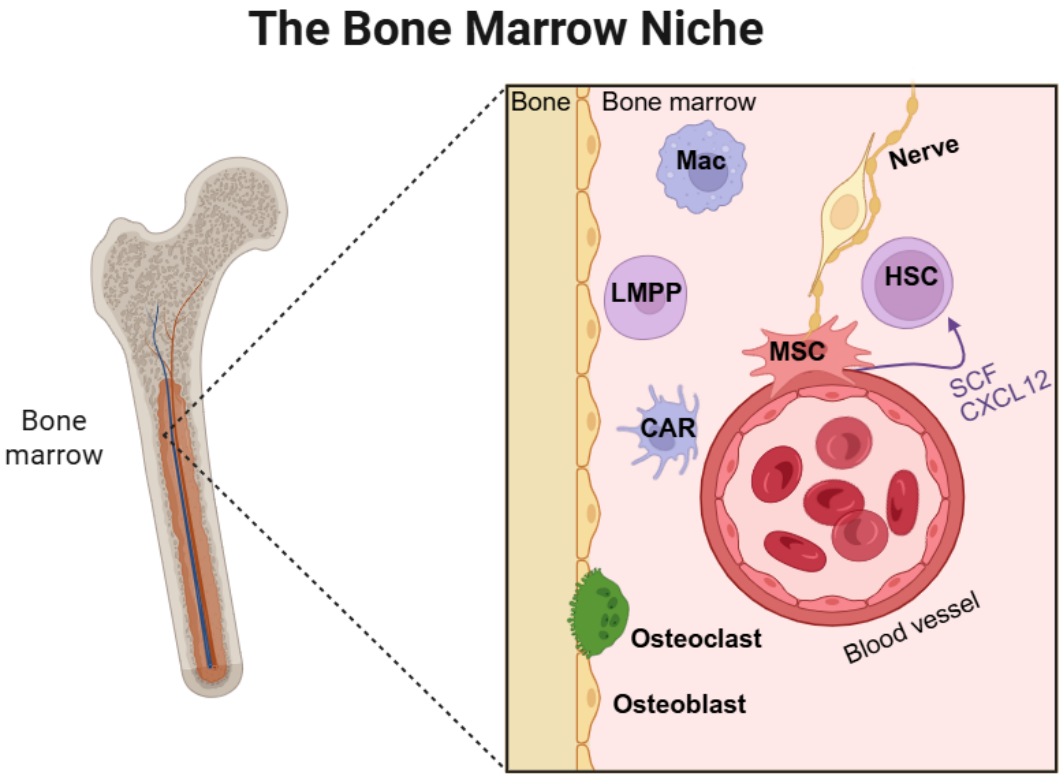

Figure 1.2: Simplified overview of the bone marrow niche. HSCs primarily reside in proximity to bone and adjacent to sinusoid blood vessels, with SCF and CXCL12 promoting their maintenance. Mac = macrophage, LMPP = lymphoid-myeloid-primed progenitor cell, MSC = mesenchymal stromal cell. CAR = CXCL12-abundant reticular cells. Figure adapted from Morrison and Scadden[49]. Reproduced with permission from Springer Nature. Created in BioRender.

1.1.5 Developmental haematopoiesis

There are three waves of haematopoiesis during embryonic development: the primitive wave, the pro-definitive (also known as transient-definitive) wave and the definitive wave (**Figure 1.3**). In the mouse, primitive haematopoiesis occurs between ~E7.0 and E8.5 and produces only erythrocytes, macrophages and megakaryocytes[63–66]. Pro-definitive haematopoiesis generates erythromyeloid progenitor cells and occurs between ~E8.5 and E10.5[67]. Definitive haematopoiesis, between E11.5 and birth, produces myeloid cells, lymphoid cells, erythroid cells, megakaryocytic cells and definitive HSCs[64,68,69]. HSCs originate from hemogenic endothelium in the aorta-gonad mesonephros (AGM) region of the dorsal aorta before

migrating to the fetal liver[70–72], where they undergo maturation, self-renewal, and differentiation to generate progenitor cells[73]. The definitive HSCs in the fetal liver (FL HSCs) are highly proliferative[74], contrasting to the quiescent (non-cycling) state in which 98% of adult bone marrow HSCs are maintained at the steady-state[75–77]. After maturation, the FL HSCs migrate to the bone marrow, where they will remain for lifetime haematopoiesis[78,79]. Recent work has identified a population of embryonically derived progenitor cells that persist into adulthood and contribute to blood cell production throughout life, with a particularly prominent but progressively declining contribution to the lymphoid lineage[80]. This discovery calls into question the contribution of HSCs to lifelong haematopoiesis.

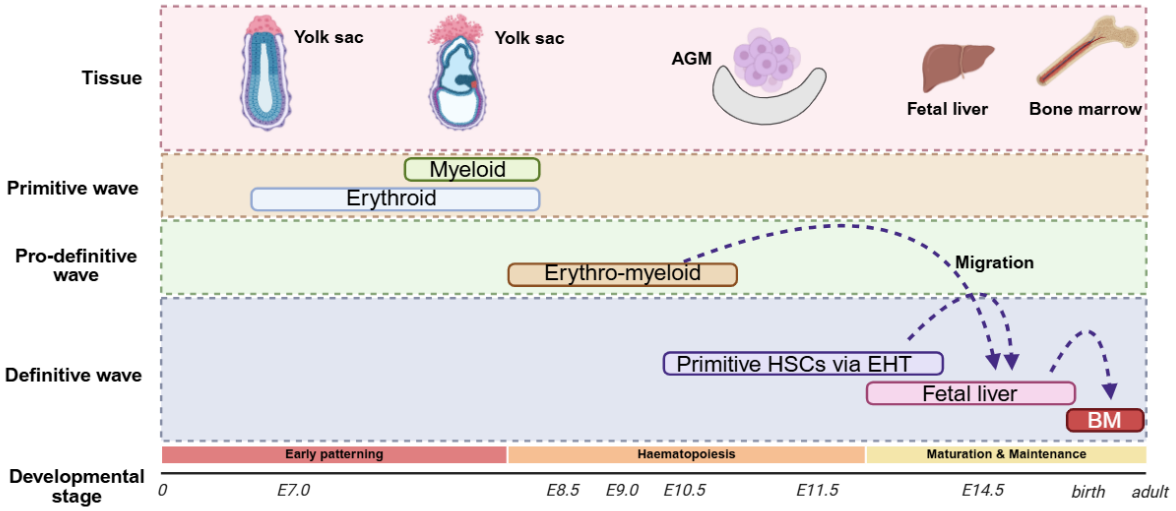

Figure 1.3. Waves of haematopoiesis during embryonic development in the mouse. Blood formation occurs in three successive waves. The primitive wave in the yolk sac (from ~E7.0) produces early erythroid and myeloid cells. The pro-definitive wave (from ~E8.5) generates erythro-myeloid progenitor cells. The definitive wave begins in the aorta-gonad mesonephros (AGM) (~E10.5), where HSCs emerge via endothelial-to-haematopoietic transition (EHT), then expand in the fetal liver before establishing lifelong haematopoiesis in the bone marrow. Figure adapted from Ciau-Uitz et al., 2014[67], with permission from Elsevier. Created in BioRender.

The behavioural differences between fetal and adult HSCs have been ascribed to differences in gene expression programmes[81], epigenetic changes and reorganisation of the genome[82]. Given the increased engraftment ability of FL HSCs, it is of interest to characterise the ontological differences with a view to promoting a more regenerative adult HSC[83]. LIN28B, an RNA-binding protein[84,85], is an important regulator of self-renewal in FL HSCs via the LIN28B-

Let-7-HMGA2 axis[86]. Overexpression of *Lin28b* in adult bone marrow HSCs increases their engraftment into recipient mice by 10-fold[86] via epigenetic silencing of adult HSC genes[87]. Investigation into genetic proponents of self-renewal throughout ontogeny therefore represents an interesting clinical avenue to promote HSC expansion and increased engraftment.

1.1.6 Steady-state vs emergency haematopoiesis

HSCs play a key role in maintaining haematopoietic system homeostasis throughout life. This means blood cell populations must be replenished in response to loss due to injury (causing tissue damage or blood loss), disease or infection. At such times, massive increases in the numbers of new mature cells are required, which are produced through a state called 'stress haematopoiesis'[30]. At the steady-state, the HSCs are largely quiescent which prevents replicative stress and helps to preserve DNA integrity, but during emergency haematopoiesis they become more proliferative and increase output of progenitor cells via differentiation[88–90]. In times of prolonged stress, either self-renewal or progenitor cell production can become unbalanced leading to HSC depletion or lack of effective blood system reconstitution. This can then lead to HSC exhaustion[30].

1.1.7 Interferons in haematopoiesis and beyond

Interferons (IFNs) are a family of cytokines with critical roles in immunity, antiviral responses, inflammation and cancer biology[91,92]. This topic is introduced here to provide necessary context for results discussed later in the thesis. IFNs are classified into three main groups: Type I, Type II and Type III. Type I includes IFNs α, β, δ, ε, κ, τ and ω, Type II IFN-γ[92] and Type III IFN-λ[93(p28),94]. They are produced in response to inflammation by immune cells such as macrophages[95] and dendritic cells (DCs)[96]. These are stimulated to produce pro-inflammatory cytokines such as Type I IFNs by the detection of viruses using their Toll-like receptors[96–98]. Type II IFN is produced by NK cells, $CD4^+$ T-helper cells and $CD8^+$ T-cells and promotes antigen recognition by macrophages and dendritic cells[99]. Type III IFN is produced

by dendritic cells and regulates CD4+ T-cell and B-cell differentiation, CD8+ T-cell and B-cell cytokine production and has several other roles in immune modulation[100]. The results in this thesis necessitate focus on Types I and II.

IFNs transduce their signal by the STAT (signal transducers and activators of transcription) transcription factor family members to activate interferon-stimulated genes (ISGs), utilising the JAK (Janus Kinase)/STAT signalling pathway[101]. Type I interferons (e.g. IFN-α) bind the heteromeric IFNAR receptor (composed of IFNAR1 and IFNAR2), triggering intracellular signalling cascades that activate downstream effector responses[102].

Type I and II IFNs exert diverse effects on haematopoiesis. IFN-γ plays several roles in HSC and progenitor cell biology. IFN-γ signalling is required for myelopoiesis in response to bacterial infection[103], and treatment with IFN-γ expanded HSPCs (KSL)[104] while depleting HSPCs (c-Kit$^+$CD150$^+$CD48$^-$) in the murine bone marrow[105]. These HSPCs had impaired reconstitution capacity, displaying poor engraftment in competitive transplantation assays[105]. IFN-γ has also been implicated in bone marrow failure, as mice lacking the IFN-γ receptor had decreased bone marrow depletion in a bone marrow failure model[105]. At the steady-state, IFN-γ is required for myeloid differentiation[106] and transgenic mice with elevated IFN-γ production exhibited skews in haematopoiesis; B-cell numbers were reduced in haematopoietic organs, thymic T-cells were increased, and myeloid progenitor cells were decreased in number and frequency in the bone marrow[107].

These findings represent IFN-γ as promoting differentiation at the cost of HSC depletion. In contrast to this, an early study by Shiohara and colleagues showed that SCF and IFN-γ synergise to produce more primitive haematopoietic cells – however this has not been revisited since the development of an immunophenotypic definition of an HSC[108]. More recently, Baldridge and colleagues found that IFN-γ treatment of mice mobilised HSCs and increased their proliferation, but that the long-term reconstitution potential of the HSCs was attenuated as a result[109]. They also demonstrated that IFN-γ regulates HSC activity even at

the steady-state and therefore has a role in normal haematopoietic homeostasis. Similar dynamics were observed for Type I IFNs: Essers and colleagues reported that acute IFN-α, treatment increases proliferation of HSCs and early progenitor cells, whereas chronic activation functionally attenuates their repopulation ability[110]. Consistent with this, β-glucan, a component of fungal cell walls, was found to induce IFN-α production by pDCs in mice, increasing the frequency of KSL cells, reducing the frequency of ST-HSCs and leaving LT-HSCs unchanged[111]. Thus, IFNs have a complex role in haematopoiesis – they are essential for immune function and mobilisation of immune cells during infection, but chronic activation compromises HSC self-renewal and therefore haematopoietic integrity.

These studies describe the role of canonical IFN signalling in haematopoiesis, mediated by extrinsic IFN stimulating expression of ISGs. ISG expression can also be driven intrinsically. Observations that an oncolytic poxvirus, Myxoma virus, was unable to infect human HSCs but was able to infect their progeny (monocytes, B-cells, NK cells)[112] together with the finding that pluripotent embryonic stem cells cannot produce Type I IFN or respond to it exogenously[113], suggested that stem cells intrinsically promote ISG expression rather than canonical IFN signalling for antiviral defence. Building on this, Wu and colleagues demonstrated that multiple stem cell types, including HSCs, are resistant to viral infections through intrinsic ISG expression, and that this intrinsic antiviral programme decreases with differentiation as cells become more dependent on IFN responsiveness[114].

Interferon signalling in haematopoiesis is therefore understood to be a delicate balance, ensuring enough differentiated cells reach tissues in times of injury or stress but without compromising the function of HSCs to self-renew over lifelong haematopoiesis.

1.1.8 The aged haematopoietic system

Cellular aging is defined as a gradual decline of cellular and physiological function and integrity over time[115,116]. In the HSC compartment, aging is associated with an increased myeloid biased output[117,118], loss of self-renewal ability[117,119,120] and an increase in immunophenotypic

HSC number in the bone marrow[121–123]. Indeed, the decline of haematopoietic function and homeostasis with age, including loss of HSC function, has been linked to many conditions such as an increased risk of myeloid leukaemias[124], anemia[125] and decreased immune system function and response to infection[126–128]. As the function and differentiation of the HSCs declines with age, the myeloid-biased output compensates for the myeloid lineages but this is not present in the lymphoid lineages[129].

A key hallmark of aging in haematopoiesis is the loss of lymphoid output. Lymphoid differentiation is impaired in the aged mouse[127,129], the number of T-progenitor cells in the bone marrow and thymus is reduced, as are the number of mature T-cells in the spleen[127]. A strong contributor to the loss of lymphoid output is the effect of ageing on the thymus, which experiences regression or involution during ageing, characterised by a decrease in thymic mass and cellularity[130,131] as well as decreased T-cell output and TCR repertoire diversity[132]. Changes also occur in the thymic stromal environment such as alterations in marker expression of thymic epithelial cells[132]. Physical changes occur within the thymic niche, with aged thymi displaying increased fibrosis and adipose tissue, as well as alterations in corticomedullary junction organisation[132].

The mechanisms driving hallmarks of haematopoietic aging are both cell-intrinsic and cell-extrinsic. Cell-intrinsic changes through ontogeny include alterations in gene expression programmes, impaired DNA damage responses[133], and increased clonality[62]. Expression of genes involved in lineage specification change with age, with downregulation of lymphoid genes and upregulation of myeloid genes driving the myeloid bias seen in aged haematopoiesis[133,134].

Chromatin/epigenetic regulation also changes during aging. Chromatin is the complex of DNA and protein packaging the eukaryotic genome and undergoes diverse chemical and structural modifications for regulation of gene expression[135]. In aged HSCs, dysregulation of chromatin

remodelling genes are linked to global changes in the epigenetic landscape postulated to drive functional decline and increased risk of malignant transformation[62,136–138].

Aged mouse HSCs have shortened telomeres - repetitive sequences acting as protective caps at the end of chromosomes[62,139,140]. Telomeres prevent chromosome ends from being mistaken for damaged or broken DNA and prevent them from fusing together, but with every cell division they shorten[141]. When they become too short, DNA damage pathways are activated which leads to senescence or apoptosis[142].

The clonality of the HSC pool also changes in ontogeny as a result of these cell-intrinsic features, with the aged bone marrow containing an accumulation of myeloid-biased and myeloid-restricted HSCs compared with the young adult bone marrow[62,143]. These aged HSCs have a two-fold decrease in engraftment ability and a decreased lymphoid potential[121,133,144,145].

Cell-extrinsic mechanisms contributing to HSC aging occur in the bone marrow niche. The bone marrow niche, as discussed in Chapter 1.1.4, interacts with HSCs to regulate their behaviour. Changes in the niche with age include changes in extracellular matrix components and decreased bone formation, as well as increased adipogenesis[62]. Another change is in the secretion of cytokines, for example CCL5 which promotes skewing of HSC output towards the myeloid lineage, at the expense of lymphoid output via downregulation of pro-lymphoid genes[146].

The cell-intrinsic and cell-extrinsic mechanisms driving HSC aging contribute to functional decline and predisposition to haematological malignancies. There is therefore great research interest in understanding how haematopoiesis is maintained throughout ontogeny to improve the quality of life as we age. Understanding the subtle differences in HSC activity with age may also improve clinical outcomes of patients receiving treatments for haematological malignancies, such as HSCT.

1.2 T-cell differentiation and function

1.2.1 T-cell development from lymphoid progenitor cells

T-cells are essential effectors of the adaptive immune response[147]. The definition of a T-cell is a lymphocyte expressing a T-cell receptor, or TCR. T-cells are produced from lymphoid progenitor cells which migrate from the bone marrow to the thymus[148,149]. T-cell development in the thymus is a complex multi-step process, summarised in **Figure 1.4**. The ability of multipotent progenitor cells to produce lymphoid progenitor cells becomes lessened over time, decreasing the efficacy of the T-cell response and subsequently the immune system's capacity to fight off infections.

1.2.2 Immunophenotypic definitions of thymocytes

Once lymphoid progenitor cells migrate to the thymus they initially commit to the T-lineage as $CD4^-CD8^-$, also known as double negative (DN)[149]. The mouse DN compartment can be further divided into stages DN1-DN4 by the cell surface expression of CD25 and CD44 markers[150]. They then become $CD4^+CD8^+$ (double positive) before becoming single positive and only expressing CD4 or CD8 in a process known as positive selection[151,152].

1.2.3 T-cell receptor and major histocompatibility complex biology

TCRs recognise the major histocompatibility complex (MHC), also known as the human leukocyte antigen or HLA in humans. The MHC is expressed on all nucleated cells and displays intracellular peptide fragments which can be 'self' (from the host) or 'non-self' (from a pathogen)[153]. MHC complexes on infected cells display peptide fragments from pathogens for recognition by immune cells. MHCs can either be class I or class II. Class I molecules interact with TCRs on CD8-expressing T-cells, class II interact with those expressing CD4[154].

1.2.4 Thymic selection stages

There are several selection stages through T-development in the thymus. During the developmental transition from DN-DP, V(D)J recombination (genetic rearrangement) at the TCRβ locus occurs[155] and cells enlarge and proliferate[156,157]. TCR is an antigen-binding molecule consisting of two key proteins, the TCR-α and TCR-β[147,158]. These are encoded by the two TCR genes, *TRA* and *TRB*, which undergo stochastic genetic rearrangement during thymocyte maturation in the thymus to produce a diversity of TCR receptors[149,158].

DN1 cells, also known as the ETP stage (early T-cell precursor) strongly express Notch-promoted genes and low to no expression of T-cell identity genes and as such, retain pDC and NK cell potential[159,160]. As they proliferate and transition to DN2, they begin to commit more strongly to the T-cell lineage, with expression of T-cell genes such as *CD3g*, *Cd3e*, *Zap70* and *Il7ra* (CD127)[161,162]. Progression into and through DN2 depends on transcription factors (TFs) TCF1 and GFI1[163,164], with TCF1 (activated downstream of Notch and WNT pathways) likely acting as a rate-limiting regulator by promoting transcription of T-lineage genes[165]. GFI1's role is less clear, but it may help prime ETPs for this transition[161]. Importantly, additional thymic microenvironmental signals act to restrain premature ETP progression, ensuring a controlled entry into the DN2 stage[166–168].

The first selection stage is β selection at DN3. Here, DN3 thymocytes must produce a functional TCRβ chain that pairs with the pre-Tα to form a pre-TCR[155]. If they are successful, they can pass to DN4 and to the DP stage by migration to the cortex. If they are unsuccessful, they undergo apoptosis. This selection is mediated by interactions with thymic stromal cells and changes in the transcriptome and epigenome in DN3 cells, ensuring only those with a properly rearranged TCRβ chain survive[169–171]. Cells expressing a pre-TCR are stimulated to proliferate by signals such as Notch and CXCL12-CXCR4 chemokine signalling to maximise TCR diversity[172,173].

Once cells reach the DP stage, positive selection occurs in the cortex where TCRs interact with self-MHC molecules presented by cortical thymic epithelial cells (cTECs)[152,174]. Only thymocytes with sufficient recognition of the self-MHC progress to the next stage.

DP cells that survive migrate to the thymus medulla, where negative selection removes cells with overly strong recognition of self-MHC presented by DCs and medullary thymus epithelial cells (mTECs)[175]. Weak self-MHC interaction can direct cells to differentiate into the regulatory T-cell lineage, discussed further in Chapter 1.2.5[152]. This stage is crucial for eliminating cells which express strongly self-reactive TCRs – it is important to maintain TCR diversity for immunity against a wide range of pathogens but cells expressing strongly self-reactive TCRs contribute to autoimmunity so must be destroyed[176].

Post negative selection, thymocytes express either CD4 or CD8 as single positive T-cells, which then emigrate into the peripheral blood[149,157]. Once in the blood, naïve $CD4^+$ and $CD8^+$ T-cells interact with signalling molecules and immune cells to mature into relevant subtypes.

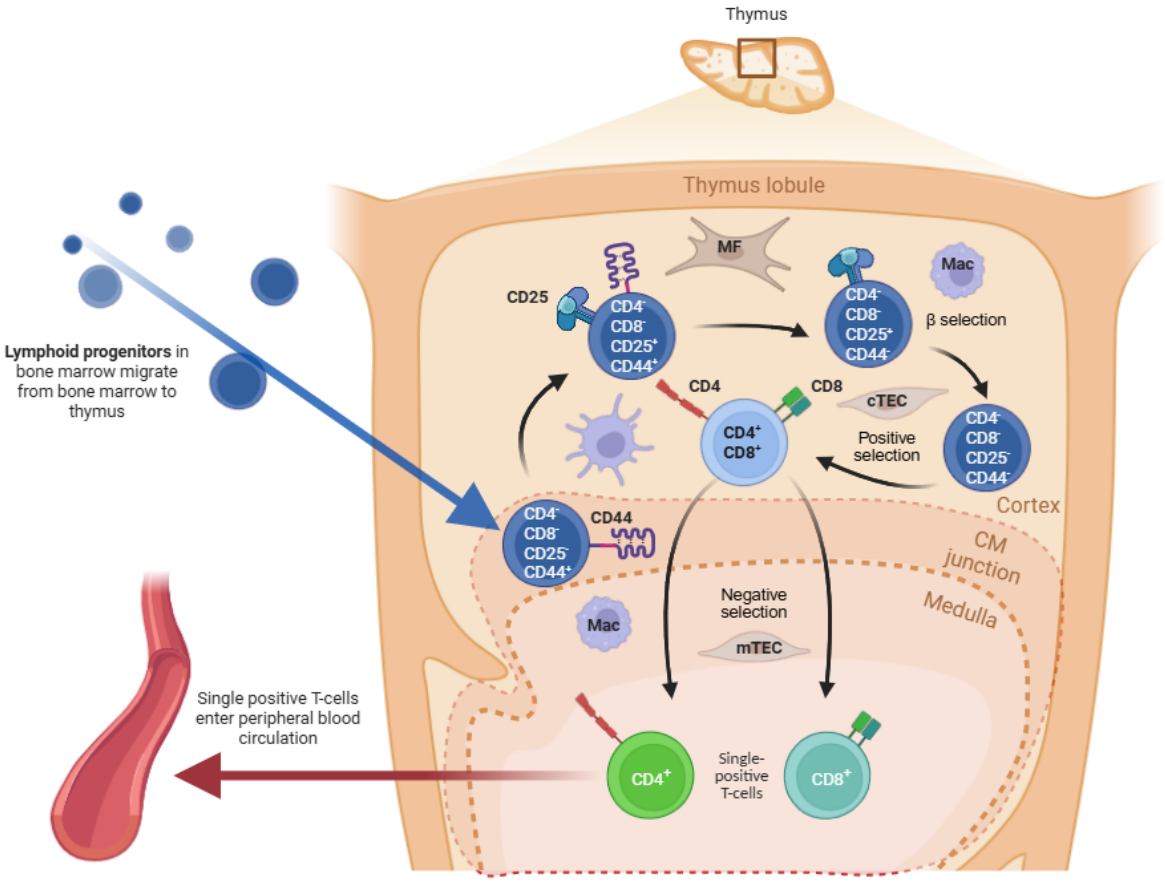

Figure 1.4: T-cell development in the thymus. The distinct areas of the thymus have different functions in T-differentiation, with specific stromal cell types in each contributing to this. Lymphoid progenitor cells migrate from the bone marrow to the thymus, where they progress through stages defined by CD4, CD8, CD25, and CD44 expression. Thymocytes undergo β-selection, positive selection (MHC recognition), and negative selection. Surviving cells mature into single-positive $CD4^+$ or $CD8^+$ T-cells, which then exit to the peripheral blood circulation. Mac = macrophage. MF = mesenchymal fibroblast. cTEC = cortical epithelial cell. mTEC = medullary epithelial cell. CM junction = cortico-medullary junction. Figure adapted from Zúñiga-Pflücker and Carlos, 2004[149]. Reproduced with permission from Springer Nature. Created in BioRender.

1.2.5 T-cell diversity

In lymphoid organs such as the spleen, thymus and lymph nodes, the naïve single-positive T-cells scan antigen presenting cells (APCs) displaying peptide-MHC complexes[177] and differentiate into relevant T-cell subtypes. These subtypes have a range of roles in coordination of the immune response - by scanning the MHC on infected cells, activating other immune cells such as B-cells, killing infected cells and providing an immune 'memory' to accelerate the immune response if the body encounters the same pathogen again[178]. Upon

activation by interaction with relevant MHC class II complexes, $CD4^+$ T-cells can differentiate into subsets of helper T-cells such as the best characterised Th1 and Th2 which produce diverse cytokines and antibody responses[179]. $CD8^+$ T-cells recognise MHC class I complexes, and can differentiate into cytotoxic T-cells which, post-pathogen clearance, can persist in the body as T-memory cells[180].

Helper T-cells are essential for coordination of adaptive immunity. They recognise peptides displayed by the MHC class II molecules on APCs such as dendritic cells and, once activated, are essential for cytokine-mediated activation of B-cells to secrete antibodies[179]. They also activate cytotoxic T-cells to kill infected cells, stimulating them to release cytokines and other signalling molecules such as IFNs[181]. Helper T-cells also enhance APC function, amplifying the immune response[178]. This then drives activation of the naïve helper T-cells to become effector cells. Their functional subsets have specific roles but overall act to activate and recruit cytotoxic T-cells, B-cells, eosinophils, macrophages to both elicit an effective immune response against the pathogen/s and repress the immune response to mitigate the risk of autoimmunity[181].

Regulatory T-cells or Tregs, act to restrain the immune response to mitigate autoimmunity[182]. Tregs arise during positive thymic selection or from naïve T-helper cells. T-helper cells are stimulated to become Tregs by the presence of TGF-β which promotes expression of the critical Foxp3 TF[183,184]. They enact their function by the release of cytokines TGF-β, IL-2 and IL-10. TGF-β and IL-2 can promote the differentiation and activation of Tregs in a positive feedback loop[181]. IL-10 acts by downregulation of MHC class II on APCs, thereby dampening the immune response.

Cytotoxic T-cells develop from naïve $CD8^+$ T-cells. They use their TCR to recognise MHC class I molecules displayed on infected nucleated cells, before killing those cells via apoptosis using one of two main mechanisms. The first mechanism is binding of the Fas ligand (a molecule present on the surface of cytotoxic T-cells) to the Fas receptor on the target cell[185–

[187]. This initiates apoptosis via activation of the caspase pathway. The second is the release of perforin and granzyme molecules onto the target cell, which punch holes in the membrane and trigger apoptosis respectively[188,189]. There is an additional cytokine-facilitated mechanism, wherein activated cytotoxic T-cells enlist IFN-γ and tumour necrosis factor-α (TNF-α). IFN-γ stimulates increased MHC class I and Fas receptor presentation of the target cells, initiating apoptosis via the caspase pathway[190]. TNF-α binds its receptor expressed on the target cell and initiates apoptosis via the caspase pathway[191].

Following the resolution of an immune response, ~90% of effector $CD8^+$ cytotoxic T-cells undergo apoptosis[192,193]. Memory T-cells differentiate from the remaining pool and serve as immunological memory to rapidly respond to secondary infections of the same pathogen. They are transcriptionally primed to elicit a rapid immune response, for example by maintaining expression of inflammatory cytokine receptors[194]. They are long-lived (some can self-renew[195]) and have some resistance to the suppressive action of Tregs, to provide long-term protection from previously-encountered infections[178,196].

T-cells therefore represent a diverse range of immunological effectors, essential for lifelong capability of the adaptive immune response.

1.3 Transcriptional regulation of HSC activity

Transcription is an RNA polymerase II (RNA Pol II)–dependent process in which the DNA template is copied into messenger RNA, representing the first step in gene expression[197]. At its simplest, RNA Pol II is recruited to gene promoters, where it initiates RNA synthesis[198]. However, transcriptional regulation is highly complex and requires the coordinated action of numerous TFs and co-factors[199]. TFs are DNA binding proteins that are key modulators of cellular behaviour and activity via control of gene transcription and often act together with other TFs and chromatin modifiers[200]. TFs are classically described as engaging with gene promoters, but can also interact with enhancer elements, regulatory elements that

communicate with promoters via chromatin looping to modulate transcription[201,202]. TF specificity is mediated by consensus recognition sequences (motifs) in the genome, but is also affected by chromatin accessibility, histone modifications and cooperative interactions with other co-factors such as other TFs[135,199].

The TFs which are critical for haematopoiesis range across all classes of DNA-binding proteins. Knowledge of their specific roles is essential for determining how haematological malignancies such as leukaemia emerge and, in turn, understanding the genetic abnormalities contributing to leukaemic development has informed which TFs are essential for normal haematopoiesis[203]. The field has built up an understanding of transcriptional regulation in haematopoiesis by gene knockout (KO) studies in mice, revealing the effects of their loss. The critical regulators of the long-term stem cell pool in the adult include the TFs *Runx1*, *Scl*, *Lmo-2*, *Tel*, *Gfi-1* and *Gata-2* and the chromatin modifiers *Mll* and *Bmi-1*[203]. These also have roles in regulating the lineage output of HSCs, and modulation of expression of TFs throughout differentiation is essential for the haematopoietic system to react to homeostatic demands[203]. Several of these factors play roles in the emergence of definitive HSCs during development, for example SCL and its binding partner LMO-2 are both required for both primitive and definitive waves of haematopoiesis, with their loss resulting in an absence of blood formation[204]. MLL and RUNX1 are required for formation of HSCs in the AGM, and RUNX1 loss results in a lack of haematopoietic development[205].

In vertebrates, ETS factors play an essential role in development and maintenance of haematopoietic cells via interaction with GATA factors[206,207]. The ETS family is a large, highly evolutionarily conserved TF family in metazoans[208–211]. ETS TFs co-regulate each other's expression, and RUNX1 physically binds ETS TFs[212–216]. Whilst many of the roles of the ETS TFs are enacted during developmental haematopoiesis, the ETS TF Erg is required for HSC self-renewal and therefore plays a role in adult haematopoietic reconstitution[217]. Loss of one allele of *Erg* has no effect on self-renewal at the steady-state as the HSC pool can still be

maintained, but causes defective HSC engraftment. This exemplifies the dosage dependencies for transcriptional regulators in haematopoiesis[217].

Within the adult mouse, there is gerontological specificity of TF expression. As mentioned in 1.1.8, aged HSCs have a decreased engraftment ability and a myeloid bias with a decreased lymphoid potential[121]. They also display a different transcriptional landscape, with genes involved in DNA damage repair, chromatin remodelling and maintenance of genomic integrity altered in expression between young and aged HSCs[128,203,218]. Given many of these gene expression changes have been postulated to predispose aged HSCs and therefore patients to leukaemia and other malignancies[128], there is clinical relevance in modulating gene expression as a way to rejuvenate aged HSCs[117]. For example, overexpression of the TF and chromatin remodeller SAT1B improved T-cell, B-cell and NK cell output from aged mouse HSPCs in vitro[117,219]. This rejuvenation approach via gene expression alterations is a contemporary focus of the field, with many groups publishing recent papers outlining transcriptional differences between young and aged HSCs[220–222]. Temporal and lineage-specific expression of TFs therefore represents a key paradigm for initiating and sustaining haematopoiesis across a lifetime. To fully understand how gene expression changes alter haematopoietic output and homeostasis, genome-wide approaches must be employed in a variety of haematopoietic contexts such as emergency/stress haematopoiesis, developmental haematopoiesis, aged haematopoiesis and steady-state haematopoiesis.

1.4 The *Runx* family genes

1.4.1 Overview of the *Runx* family

The RUNX TF family, also known as the AML, CBFα and PEBP2α family, consists of *Runx1*, *Runx2*, and *Runx3*[223,224]. Their consensus name, RUNX, references their homology to *runt* which was identified as a segmentation gene in *Drosophila melanogaster*[225]. Mutations in *runt* resulted in deletions in anteroposterior segments of the embryo, resulting in the eponymous

'runt' phenotype[226]. The RUNX factors bind their stabilising cofactor, CBFβ to increase their DNA-binding affinity by 5-10-fold[227,228]. They have a myriad of roles in development and cancer, summarised in **Figure 1.5**.

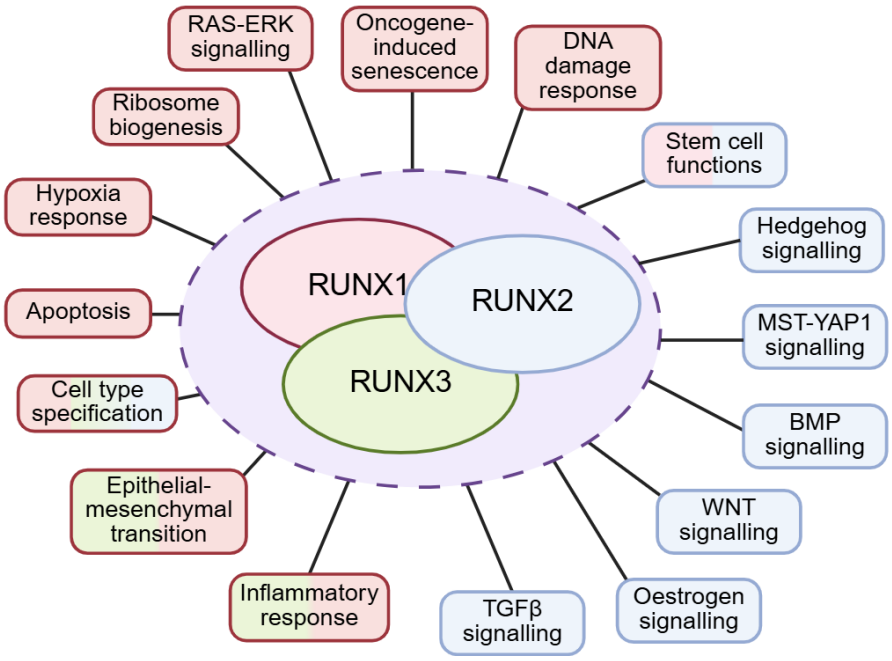

Figure 1.5: Roles and regulatory pathways of the Runx family – *Runx1*, *Runx2* and *Runx3*. Colour of text boxes indicates the RUNX protein primarily associated with that function. Where one or more RUNX proteins have a role, this is indicated by a colour gradient. Figure adapted from Ito et al., 2015[229]. Reproduced with permission from Springer Nature.

Each *Runx* gene can be transcribed from one of two distinct promoters, a distal P1 promoter and proximal P2 promoter[225]. The RUNX family proteins share a high degree of conservation, owing to their origins as a gene triplication event around 500 million years ago during early vertebrate evolution[230]. All three share a similar structure, with the DNA-binding Runt domain, a transactivation domain and an inhibitory domain, followed by a VWRPY motif (**Figure 1.6**). The primary difference is that RUNX2 contains a polyalanine polyglutamine (QA) tract which has a role in target gene transactivation and determination of skull shape[231–233].

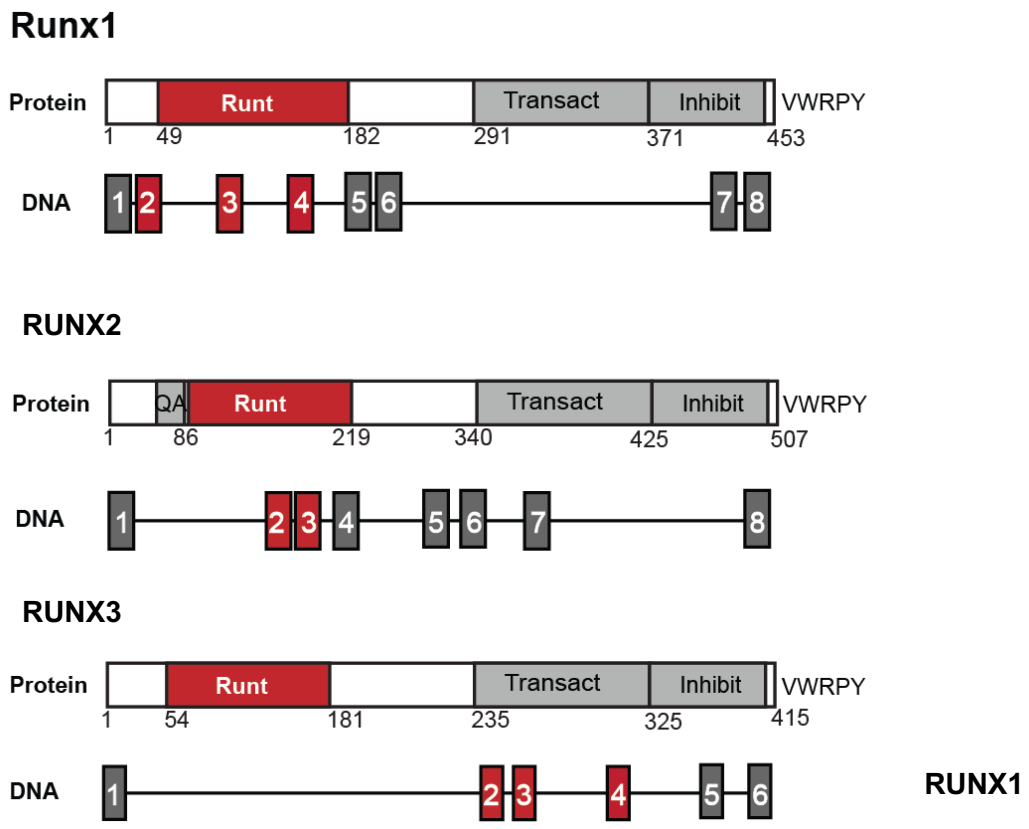

Figure 1.6: Structure of the mammalian Runx proteins and gene loci – Runx1, Runx2 and Runx3[229]. Transact = transactivation domain. Inhibi = inhibitory domain. QA = polyalanine polyglutamine tract.

1.4.2 RUNX proteins as transcriptional regulators

The RUNX proteins recognise a consensus (Py)G(Py)GGT motif on DNA with their Runt domain[234,235]. As they can function as both activators and repressors, they interact and bind with many different proteins. The conserved VWRPY motif serves as a binding site for corepressors such as the transducing-like enhancer of split family[236–238]. For example, RUNX proteins bind the transcriptional corepressor mSin3 just C-terminal of the Runt domain[238,239]. mSin3 can then recruit other corepressors such as HDACs to the chromatin and repress transcription of target genes[240]. RUNX proteins can also recruit HDACs themselves[241].

The RUNX proteins can drive transcriptional activation by interaction with coactivators such as histone acetyltransferases like p300/CBP[242,243], C/EBPa[244], ETS family members[245–247] and

SMADs[248,249]. In some cases, the RUNX proteins can function as activators and repressors of the same gene in different contexts, giving a context-dependent activity[250]. For example, RUNX1 promotes *Spi1* expression in myeloid and B lineages, but represses its expression in megakaryocytes and T-cells[251,252].

Overall, the RUNX proteins have a myriad of roles in gene expression regulation, orchestrated by a host of cofactors which vary depending on the cellular context. This thesis primarily focuses on *Runx2* in haematopoiesis, with Chapter 3 providing a brief exploration of *Runx1*. Accordingly, *Runx1* and *Runx2* will be reviewed below in greatest detail.

1.4.3 Overview of *Runx1*

Runx1 is a well-described haematopoietic TF, required for HSC formation during definitive haematopoiesis[213,253–256]. It is expressed in the mesoderm and the primitive haematopoietic progenitor cells and is required for normal development of the blood lineages[256,257]. As with the other *Runx* genes, it has two promoters, the distal P1 and proximal P2[258]. Transcription from these promoters and alternative splicing of the 9 exons permits 12 isoforms of *Runx1*, with those expressed from P1 being primarily restricted to the haematopoietic system[259]. Autoregulation also occurs at the *Runx1* locus, with a RUNX protein binding site present in the P1 promoter and first exon[260].

In adult haematopoiesis, *Runx1* is expressed in all lineages except erythrocytes[224,261,262]. Conditional deletion of *Runx1* in the bone marrow of mice causes an increase in cKit^{+}Sca-1^{+}Lin^{-} HSPCs but has no effect on long-term HSCs[263,264]. Cai and colleagues showed that loss of *Runx1* reduces ribosome biogenesis in HSPCs, generating a stress resistant phenotype[265] and allowing them to outcompete wild-type HSPCs in the bone marrow. *Runx1* is dispensable for adult haematopoiesis, but its loss causes defects in B and T-cell differentiation and a mild myeloproliferative phenotype[263,266,267]. Haploinsufficiency produces a different phenotype, with transplantation of *Runx1*$^{+/-}$ HSCs resulting in a decrease in long-term HSCs and an expansion of multipotent progenitor cells in the recipient mice[268]. This expansion resulted in increased

engraftment, but these progenitor cells had a defect in production of $CD4^+$ T-cells and platelets. This differentiation impairment was also seen in granulocyte production[269].

These mouse phenotypes reflect what is seen in familial platelet disorder (FPD), a *RUNX1* haploinsufficiency in humans[268,270]. FPD is characterized by thrombocytopenia, platelet dysfunction, predisposition to myeloid malignancies such as acute myeloid leukaemia (AML) and myelodysplastic syndrome and predisposition to lymphoid malignancies such as acute lymphoblastic leukaemia (ALL) and lymphomas[271,272].

RUNX1 is well established as a commonly mutated gene in AML[254,273,274]. The reoccurring AML chromosomal translocation t(8;21) results in a fusion of the N-terminal region of RUNX1 with ETO, encoded by *RUNX1T1*[254]. This fusion protein cannot cause AML alone but requires a further oncogenic driver. RUNX1 therefore represents a key TF involved in developmental, adult, and malignant haematopoiesis.

1.4.4 Overview of *Runx2*

Runx2 is considered the master osteoblast regulator. It was first identified in adult mouse thymi and was postulated to be a T-cell specific TF[275,276]. It has an essential role in regulation of skeletal development via Sp7 and WNT signalling and loss of *Runx2* prevents osteoblast formation[277–280]. As the other *Runx* factors, it has tissue-specific transcript utilisation[281]. The P2-derived isoforms are broadly expressed throughout the body in mesenchymal tissues[282] whereas P1-derived isoforms tend to be expressed more specifically in the bone cells such as osteoblasts and chondrocytes[283–285].

1.4.5 *Runx2* genomic locus and structure

There are 9 isoforms of *Runx2* present in mammals, with 2 being the best characterised, Type I and Type II[286]. P1 promoter activity is essential for osteogenesis, with activity in bone cell types such as osteoblasts and chondrocytes[283,285,286]. P1 regulates the Type II isoform, *Runx2*-II[281,287]. P2 is active in a range of tissues, such as the cartilage, thymus and calvarium and is

active earlier in development than P1[279,288]. P2 generates the Type I isoform of *Runx2*, *Runx2*-I. This was the first *Runx2* isoform, discovered in the thymi of adult mice[275,281]. A delicate balance of expression from these two promoters is required for effective bone formation and bone cell differentiation[281].

1.4.6 Roles of *Runx2*

Runx2 has contrasting roles in osteogenesis. It regulates mesenchymal stem cells to differentiate into osteoblasts[289,290], but regulates the proliferation and transdifferentiation of chondrocytes[291]. *Runx2* also has a role in neuronal regeneration and remyelination after injury, despite not being expressed in nerve development[290,292,293]. Indeed, many of the roles of *Runx2* involve regulation of cellular proliferation, differentiation and the cell cycle. In fibroblasts, osteoblasts and vascular endothelial cells, RUNX2 induces proliferation by repressing the p21 promoter[294–296]. The p21 promoter is a tumour suppressor thaf regulates the cell cycle[297,298].

Unlike *Runx1*, which has defined roles in developmental and adult haematopoiesis, *Runx2* is not as well-characterised. It is expressed in T-progenitor cells, HSPCs and NK cells[299–301]. Its expression in T-cell differentiation is limited to DN cells[301]. Overexpression of *Runx2* in mice causes a disruption in T-cell differentiation with an increased output of $CD8^+$ cells from the thymus[301,302]. In humans, *RUNX2* is required for tissue residency of NK cells[300]. *RUNX2* knockdown leads to reduction in NK cell differentiation and accordingly, overexpression results in reduction of HSC numbers and increased NK cell differentiation[300].

Runx2 has a critical role in migration and maturation of plasmacytoid dendritic cells (pDCs), an essential immune cell which produces Type I interferon[303]. *Runx2* loss results in an accumulation of pDCs in the bone marrow via a lack of chemokine signalling.

Overall, the roles of *Runx2* in haematopoiesis and beyond tend to be within proliferation, differentiation and migration. It has not yet been characterised in regulation of HSC activity.

1.4.7 Cleidocranial dysplasia

Haploinsufficiency of *RUNX2* in humans causes a condition called cleidocranial dysplasia (CCD)[304]. It was first formally characterised in 1898[305] as a bone development disorder, resulting in lack of clavicle formation, short stature, supernumerary teeth, unfused fontanelles, and other bone abnormalities. A systematic review of CCD cases identified an extensive range of *RUNX2* mutations in patients with a broad range of severities, with the majority of mutations located within the Runt domain[306]. Of the Runt domain mutations, missense mutations contribute to a more severe disease phenotype. A summary of the mutations found in this review can be found in **Figure 1.7**.

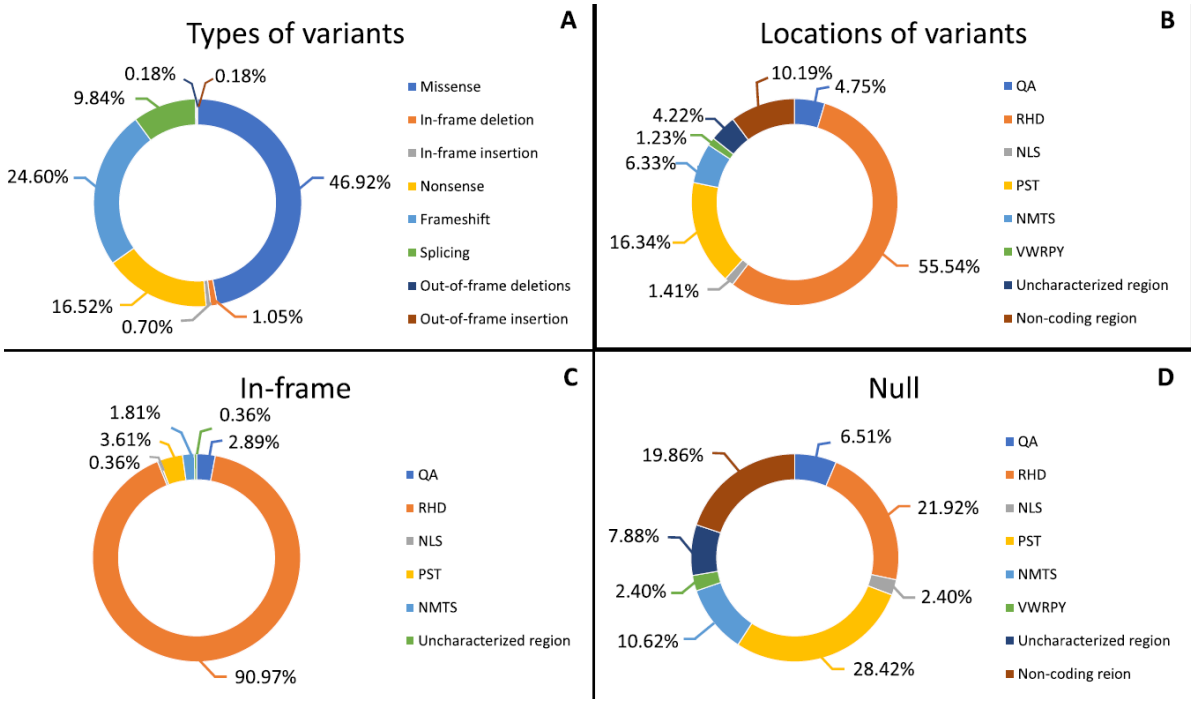

Figure 1.7: Characterisation of RUNX2 mutation variants in cleidocranial dysplasia patients, from a systematic review of the literature.

(A) Prevalence of types of RUNX2 variants.
(B) Location of variants across RUNX2 gene.
(C) In-frame locations of RUNX2 mutations.
(D) Locations of null RUNX2 mutations.

QA = polyalanine polyglutamine tract. RHD = Runt homology domain. NLS = nuclear localisation signal. PST = proline-serine-threonine C-terminal domain. NMTS = nuclear matrix targeting signal. VWRPY = C-terminal repressive domain. Adapted from Thaweesapphithak et al., 2024[306], under a CC BY 4.0 license.

Despite *RUNX2* being expressed in the haematopoietic system, CCD patients have no reported increased risk of haematological disorder development. It has been purported in the literature but as the incidence of CCD is only 1:1,000,000 in live births it is difficult to make meaningful associations. A clinical case report in 2012 discussed a case of a 3-year-old boy with CCD being diagnosed with ALL, suggesting that as the incidence of both conditions is so low this could be evidence of their comorbidity[307].

1.4.8 Disorders of *Runx2* dysregulation

Runx2 has a role in cancer progression in many contexts, usually through collaboration with other oncogenes and or via ectopic expression. *Runx2* has a role in the progression of AML in mice. Kuo and colleagues found that ectopic expression of *Runx2* disrupts myeloid differentiation via dysregulation of CBF target genes[299]. In CBFβ-MYH11 AML, ectopically expressed *RUNX2* can also synergise with the fusion protein to promote leukaemic progression and that this is dependent on the DNA-binding ability of RUNX2 protein[299]. Additionally, over-activation of the *Runx2* locus contributes to T-cell lymphoma development[287] in collaboration with c-MYC via increased tumour survival and overcoming of proliferation 'fail-safe' mechanisms[308]. Ectopic expression of even one allele of *RUNX2* promotes metastasis of human breast cancer cells to bone[309,310]. Thus, *Runx2* controls proliferation and homing in pathologies when overexpressed.

1.4.9 Overview of *Runx3*

Runx3 is the smallest of the *Runx* genes and was the first to emerge in evolution[311,312]. *Runx3* displays much lower expression levels in HSPCs than *Runx1* and *Runx2*[14]. In haematopoiesis, its role is regulation of lineage fate determination and commitment of lymphoid cells, specifically for formation of cytotoxic T-cells[313] and early T-progenitor cells [314–317]. It cooperates with *Runx1* for regulatory T-cell development and function[318]. It has also recently been shown to prime HSCs for lymphoid differentiation[319,320]. Homozygous conditional knockout (cKO) of

Runx3 showed a subtle expansion of the KSL compartment in aged mice, which then developed a myeloproliferative disorder[321(p3)].

In development, *Runx3* is indispensable for neurogenesis in the embryo, specifically of the dorsal root ganglia and muscle spindles - homozygous loss causes severe motor issues and a high rate of mortality[322,323]. It is also essential for the balance of apoptosis and proliferation in the gastric epithelium[324].

1.4.10 Overview of *Cbfb*

CBFβ is the RUNX family cofactor. It forms a heterodimer together with RUNX1, RUNX2 or RUNX3 with increased affinity for DNA binding than the RUNX factors alone[227,228]. Because of this, it is involved in all the roles of the other RUNX factors, summarised in Chapter 1.4.3, 1.4.6 and 1.4.9. It also has a role in mRNA stabilising, regulating transcription and translation initiation of a subset of genes[325].

Cbfb regulates HSPC differentiation and self-renewal in cooperation with *Runx1* and its mutation has been implicated in leukaemias[326]. Homozygous haematopoietic cKO in adult mice caused expansion of the KSL compartment in the bone marrow, differentiation blocks in myeloid and lymphoid lineages and subsequent stem cell exhaustion[327]. Despite this expansion phenotype, *Cbfb*$^{-/-}$ HSCs were unable to engraft when transplanted, suggesting they were functionally attenuated[327]. This was likely a result of the loss of RUNX function via decreased binding affinity for DNA.

1.4.11 Cooperation and compensation between RUNX proteins

Compensation between the three RUNX proteins has been observed in a leukaemic context. For example, shRNA-induced repression of *Runx1* resulted in overexpression of *Runx2* and *Runx3* in AML cells[328]. The mechanism of this was hypothesized to be repression of each gene by the other RUNX proteins through promoter binding[328]. Another study in *Runx1*-dependent AML cells showed that overexpression of *Runx2* restored the growth potential of

Runx1-depleted MLL-AF9 leukaemia cells[329]. Overexpression of *Runx1* in this context induced myeloid differentiation[329]. This hints at the expansion phenotype observed in *Runx1* and *Runx3* KOs being linked to the balance of expansion and differentiation. Another study showed that *Runx1* KO embryonic cells that normally fail to undergo definitive haematopoiesis can generate blood cells *in vitro* by overexpression of *Runx2* or *Runx3*[330].

Despite this compensation in development and leukaemia, compensation of the *Runx* family genes has not been fully investigated in the context of normal adult haematopoiesis. One study showed that double deletion of *Runx1* and *Runx3* blocks differentiation and causes bone marrow failure in mice, suggesting a redundant effect in haematopoiesis[321]. Another study presented a compensatory role for *Runx1* and *Runx2* in CAR niche cells. cKO of both *Runx1* and *Runx2* in CAR cells prevented HSC niche formation and reduced HSPC frequency, but loss of one of the factors permitted niche formation and normal frequencies of major haematopoietic cell types[331]. Taken together, these studies provide weight to the likelihood of compensation between all three genes.

Despite extensive study of TFs in HSC biology, the regulatory networks that control self-renewal and differentiation remain only partially understood. Developments in genetic tools such as CRISPR allow systematic interrogation of these factors and their downstream pathways with precision.

1.5 CRISPR-Cas9 technologies

1.5.1 CRISPR-Cas9 genome editing

CRISPR-Cas9 (Clustered Regularly Interspaced Short Palindromic Repeats) was discovered by Ishino and colleagues in 1987 as an unknown repetitive genomic sequence while analysing genes involved in phosphate metabolism in *Escherichia coli*[332,333]. It was subsequently found to act as a primitive prokaryotic immune system[334] and identified in many other organisms[335]. In 2012, Jinek and colleagues demonstrated its ability to target and cleave specific genomic

sites[336], and since then CRISPR-Cas9 has become a cornerstone of biological research and personalised medicine[337]. The CRISPR-Cas9 system consists of a Cas9 endonuclease, which produces double-stranded DNA breaks, and two short RNAs, tracrRNA and crRNA which provide targeting specificity[337]. These have since been combined into a sgRNA (single guide RNA)[338]. CRISPR has been engineered to alter various parts of its function but for the purposes of this thesis it was used to generate double stranded breaks for disruption of genes, to perturb their function and observe the effect on HSC activity.

CRISPR-Cas9-mediated gene KOs in HSCs can be performed using a variety of methodologies[339]. The first used in this thesis enlists lentivirus to package the sgRNA. Lentiviruses are simple retroviruses derived from HIV-1 which hijack host machinery to enter the nuclear membrane of cells and deliver their contents[340,341]. Unlike other viruses of this type, their action is independent of the cell cycle stage so can be used for non-dividing or terminally differentiated cells[340]. This, along with their ability to safely deliver the contents over a long period, has made them an attractive delivery system for CRISPR-based gene edits in HSCs for biological research and clinical purposes[342,343]. Selectable markers, such as fluorescent proteins or antibiotic resistance genes can be integrated into the lentiviral cassette, permitting selection of a purer population of transduced cells[344].

The second approach used is nucleofection, involving transfecting the CRISPR machinery into the HSCs via electroporation. This system does not require careful handling and containment like lentivirus and reduces the risk of immune effects caused by lentiviral transfection such as a primary immune response triggered by the presence of the virus[345,346]. There is no selectable marker however, so it can be more difficult to ascertain efficacy of gene edits and achieve a high proportion of edited cells.

1.5.2 CRISPR screening

CRISPR screening permits observation of the effects of many different single gene KOs in one assay[347,348]. Cells are transduced with a library of sgRNAs targeting many or all genes in

the genome. DNA is extracted from the cells at several timepoints to assess the frequency of the sgRNAs in the cell populations. From this, the effect of being transduced with one sgRNA over another can be interpreted, and therefore the putative role of the gene targeted in that context. Because of the number of different sgRNAs, to have enough 'coverage' (number of cells containing a particular sgRNA) to make meaningful biological conclusions, these screens require a high number of cells[349]. The coverage needed for sufficient depth in screens identifying negative regulators of a cell type can require 500-1000 cells carrying each sgRNA. This is because the cells with desired KOs drop out of the screen over time and may not be identified without sufficient depth.

Small-scale CRISPR screens have been used to investigate the roles of genes in haematopoiesis. Notable examples include Marson and colleagues, who used a CRISPR screen to target 400 putative regulators of FoxP3 TF to understand Treg function[350]. Carpenter and colleagues used a CRISPR screen in a macrophage cell line to identify genes key for macrophage viability to inform understanding of inflammatory responses[351].

As discussed above, and reviewed in Meaker et al.,[337] the CRISPR-Cas9 system may be modified for altered functionality which can be utilised for different types of CRISPR screening. For example, CRISPRi screening has been used to identify enhancer-gene relationships in haematopoietic cells, reviewed in Forsberg and Worthington, 2022[352].

Small-scale screening was used by Holmfeldt and colleagues to identify genes involved in haematopoietic reconstitution post-transplantation[353]. They targeted 51 candidate genes with shRNAs in KSL HSPCs and measured their repopulating potential in an HSC transplantation assay (described further in 1.6.5). They found 15 genes which, when knocked down, decreased HSPC engraftment and are therefore required for HSPC reconstitution potential[353]. Two genes (*Armcx1* and *Gprasp2*) were identified which, when knocked down, enhanced the reconstitution capacity. Many of these genes have a role in communication between HSPCs

and the niche, demonstrating the importance of niche conditioning for successful engraftment[353].

Lara-Astiaso and colleagues used a CRISPR screen to identify the roles of 680 chromatin factor genes in haematopoiesis, in regenerative and leukaemic contexts[354]. They transduced KSL HSPCs with the chromatin factor library, induced differentiation into myeloid, erythroid and megakaryocytic lineages and tracked the sgRNA enrichment or depletion in the various populations. This revealed lineage-specific requirements for different chromatin factors, for example the RNA elongation machinery genes promoted multipotency of progenitor cells whilst the cohesin and mediator complex genes were required for myeloid or mega-erythroid differentiation[354]. This *ex vivo* screen therefore provided many putative regulators of differentiation and proliferation which could be further investigated. To validate the putative roles of the chromatin factor genes *in vivo*, KSL HSPCs were transduced again with the library and transplanted into sublethally irradiated mice. They found disparate roles for the H3K4 methyltransferases, some novel and some previously described. The *ex vivo* screen was repeated in a Npm1c and Flt3-ITD model (a model for aggressive AML) and made the biological discovery that leukaemia misappropriates chromatin factors to produce aberrant differentiation and malignant haematopoiesis[354]. Importantly, they also found several potential therapeutic targets in their analyses.

Overall, the work discussed here demonstrates the biological and clinical value of using CRISPR screens in HSPCs and how they may lead to better understanding of normal and aberrant haematopoiesis. Careful experimental design and selection of candidate genes permits investigation of many key areas of haematopoietic biology. One caveat of these studies is the cell population chosen. KSL cells, as discussed, represent a highly heterogeneous cell population with a small fraction of functional HSCs. This means the findings may not truly reflect functional HSC biology. Additionally, selection of candidate genes limits the identification of novel genes which may be previously unexplored regulators of

haematopoiesis. A genome-wide approach in an immunophenotypic population of HSCs would be preferable for clearer insights into HSC biology, but this is limited by rarity of HSCs and limitations in *ex vivo* expansion approaches. The *ex vivo* expansion methodologies, and immunophenotyping of HSCs and other haematopoietic cells is explored below.

1.6 *Ex vivo* and *in vivo* methods to investigate HSC biology

This thesis focuses on HSC biology and is grounded in the many important techniques and technologies that have been developed to study these rare cells. Methods to isolate, track, discriminate, functionally evaluate, expand, and differentiate HSCs have been central to the field, and the work presented here builds directly on these foundations. HSC transplantation assays, immunophenotyping, and *ex vivo* expansion are key approaches that underpin the studies described in this thesis.

1.6.1 Immunophenotyping with flow cytometry

Cells of the immune system and beyond can be characterised and therefore defined by the cell surface markers they express. This is pertinent both *in vivo* and *ex vivo*, as haematopoietic populations of cells are very heterogeneous. The field has several definitions for immunophenotypic (p)HSCs – that is, a cell population with a high enrichment of functional HSCs, depending on the species, strain (of mouse) and origin of the cells. For example, a freshly isolated LT-HSC from a C57BL/6 mouse is defined as $CD150^{+}CD48^{-}CD34^{-}$c-$Kit^{+}$Sca-$1^{+}Lineage^{-}$. The most common definitions of pHSCs and other haematopoietic cell types described throughout this thesis are listed in **Table 1.1**. The other markers used in the literature to delineate HSCs and HSPCs are well reviewed in Challen et. al., 2021[25].

Table 1.1: Immunophenotypic cell definitions relevant to this thesis.

Cell type	Marker/s	Refs
Immunophenotypic LT-HSC, freshly isolated from C57BL/6 mouse	$CD150^{+}CD48^{-}CD34^{-}$c-$Kit^{+}$Sca-$1^{+}Lineage^{-}$	[355–359]

Haematopoietic stem and progenitor cell from C57BL/6 mouse	cKit$^+$Sca-1$^+$Lineage$^-$	357,359
Peripheral blood (or bone marrow/spleen) T-cell	CD4$^+$ (CD3$^+$)	360–362
Peripheral blood (or bone marrow/spleen) T-cell	CD8$^+$ (CD3$^+$)	360
T-cell	CD3$^+$	360,363
Thymic T-progenitor cell	CD25$^+$CD90$^+$CD4$^-$CD8$^-$	364,365
Thymic T-progenitor cell, double negative	CD4$^-$CD8$^-$	149,360
Granulocyte	Gr-1$^+$	366,367
Macrophage	CD11b$^+$	360,368
Natural killer cell	NK1.1$^+$	369,370
B-cell	B220/CD45R$^+$	360
Plasmacytoid dendritic cell	B220$^+$CD11b$^-$BST2$^+$	97,303,371
Ex vivo cultured (p)HSC from C57BL/6 mouse	CD201$^+$CD150$^+$c-Kit$^+$Sca-1$^+$Lineage$^-$	355–359,372,373
Common lymphoid progenitor cell	CD127$^+$KSL	25
Multipotent progenitor cell (MPP)	CD150$^-$CD48$^-$Flt3$^-$KSL	25
Lymphoid-biased MPP	CD150$^-$Flt3$^+$KSL	25
Granulocytic-monocyte-biased MPP	CD150$^+$CD48$^-$Flt3$^-$KSL	25
Megakaryocytic-erythroid-biased MPP	CD150$^+$CD48$^+$Flt3$^-$KSL	25

1.6.2 *Ex vivo* HSC expansion techniques

Due to the rarity of HSCs and their relevance in biology and the clinic, there is much interest in expanding HSCs *ex vivo*, to both understand the mechanisms regulating self-renewal and increase the feasibility of use for HSCT. Traditional culture methods use cytokines and serum albumin to support maintenance of the HSCs, but these cultures can only be used short-term and do not promote expansion[43,374]. Several approaches have been employed to increase the efficacy of these cultures, including small molecules, polymers and transgene overexpression (e.g. *Hoxb4*[375], *Notch*[376], *Dppa5*[377]).

The recent development of a polyvinyl alcohol (PVA)-based albumin-free culture system now permits long-term expansion of mouse HSPCs, including functional HSCs[378]. PVA is a synthetic polymer that increases experimental reproducibility compared to serum albumin which can introduce biological contaminants that promote HSC differentiation[378]. PVA's mechanism of action is currently hypothesized to mimic the function of albumin due to its amphiphilic nature[379]. PVA, in combination with the cytokines SCF and TPO, provides a selective environment for HSCs to expand *ex vivo* for several months. Within these cultures, transplantable HSCs reside within the $CD201^+CD150^+c\text{-}Kit^+Sca\text{-}1^+Lineage^-$ ($CD201^+CD150^+KSL$) compartment[380,381]. This culture system also enriches for HSCs when initiating with impure populations such as $c\text{-}Kit^+$ cells. After 1 month, the culture contains ~1:34 functional HSCs[378]. Under these conditions, several hundred-fold expansion of transplantable HSCs is possible, providing large numbers of cells for molecular and genetic methods that were previously limited due to the paucity of HSCs[378]. Examples include large-scale CRISPR screening and immunoprecipitation-based approaches e.g., chromatin immunoprecipitation (ChIP). This system therefore provides a tractable *ex vivo* approach for novel discoveries. Whilst CRISPR-Cas9 is often employed in collaboration with *ex vivo* HSC expansion to explore HSC biology[339], other approaches can interrogate the effects of gene perturbations on specific cell populations *in vivo* and *ex vivo*.

1.6.3 Human *ex vivo* HSC expansion techniques

Although this thesis focuses on murine HSCs, it is important to note the human *ex vivo* system, since clinical applications ultimately rely on human cells and insights from the mouse system may inform translational advances. Nicotinamide riboside, a small molecule, was approved for expansion of cord blood HSCs for HSCT by the FDA in 2023. It promotes human HSC expansion by inhibiting the deacetylase Sirtuin1 and by promoting the removal of dysfunctional mitochondria[43,382,383]. Another molecule, UM171, targets the LSD1 and CoREST epigenetic

regulators via the CULLIN3-E3 ubiquitin ligase complex for degradation[384,385]. *Ex vivo*, treatment with UM171 causes a 30-fold expansion of human functional HSCs over 10 days[386].

Alternative media compositions are also being explored, such as replacing serum albumin with synthetic polymers such as PVA or Soluplus (copolymer of polyvinyl-caprolactam, polyvinyl acetate and polyethylene glycol)[43]. To develop a serum-free *ex vivo* culture for human HSC expansion, Sakurai and colleagues used Soluplus instead of PVA and the small molecules 740-YP and butyzamide to replace SCF and TPO respectively[387]. These conditions promoted 70-fold expansion of human $CD34^+$ cord-blood derived HSPCs over 30 days and permits clonal expansion of human HSCs. A recent development by Bozhilov and colleagues reduced oxidative stress in the human HSC cultures and achieved ~400-fold expansion[388].

While *ex vivo* culture systems and small-molecule approaches provide powerful tools to expand and manipulate HSCs, *in vivo* genetic models remain essential for dissecting gene function with precision. One of the most widely used systems for this purpose is the conditional Cre/LoxP mouse model.

1.6.4 Cre/LoxP mouse models

The Cre/LoxP system evolved from a viral DNA recombination mechanism in bacteriophage P1, and since then has become a powerful genetic tool allowing cKOs, lineage tracing and genome engineering *in vivo*[389–391].

Conditional Cre/LoxP mouse models involve the insertion of a transgene flanked by LoxP recognition sites into the genomic locus of the gene of interest in the mouse (**Figure 1.8**). This mouse can then be crossed with another containing a transgene with Cre recombinase under the control of a promoter of choice, to permit induction under various experimental conditions. For example, treatment of cells or mice with certain molecules[392–394], changes in light levels[393], or design of the transgene to be under the control of a tissue-specific promoter[395]. The Cre recombinase has also been codon optimised, to minimise the chance of transgene silencing

– producing 'iCre'[396]. This system may also be used to study the effect of heterozygous vs homozygous loss of a gene of interest.

To study the effect of transgene expression on haematopoiesis, a Vav1-Cre system has been widely used. The Vav1 promoter is exclusively expressed in the haematopoietic system both in development and the adult[397] and, when controlling the expression of the Cre recombinase, permits exploration of genes where the pan-KO is fatal via haematopoiesis-specific targeting[398–400]. In this thesis, a *Runx2*^{flox} line developed by Qin and colleagues[395] was crossed with a line expressing Vav1-iCre recombinase[396]. This bred a mouse line with *Runx2* loss localised to the haematopoietic system.

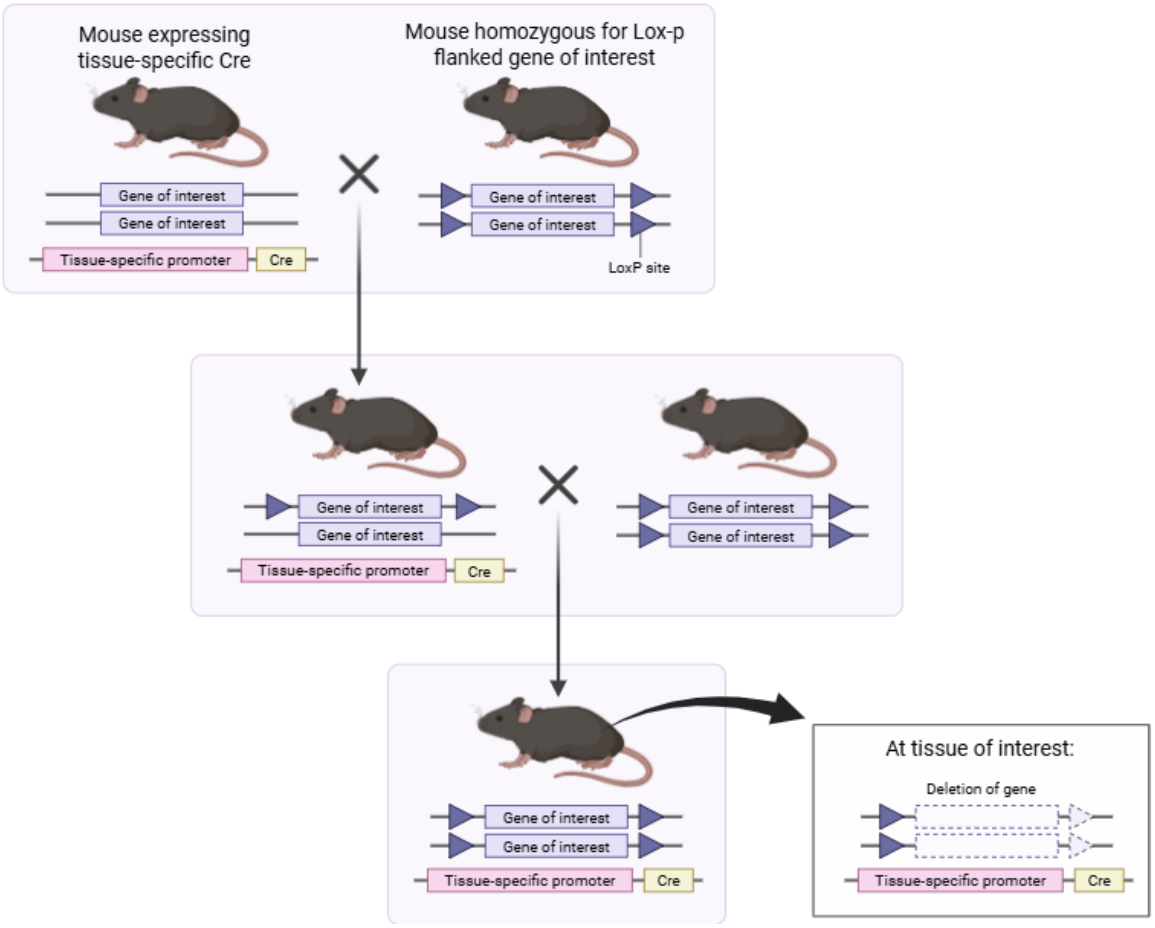

Figure 1.8: Summary of Cre-Lox knockout mouse models. Created in BioRender.

1.6.5 Competitive HSC transplantation assays

Competitive transplantation assays are the gold standard for evaluation of HSC activity. They involve transplantation of donor HSCs into irradiated recipient mice alongside WT competitor cells. The donor HSCs, recipient mice and WT competitor cells have differing CD45 surface marker alleles allowing their distinction by flow cytometry[31,401,402]. Chimerism or donor chimerism refers to the proportion of cells derived from the donor cells of interest as compared to the WT competitor cells[401]. Proportions of cells derived from the different sources are tracked over time in the peripheral blood, before harvesting tissues from the recipients at the endpoint to assess engraftment into the bone marrow and migration to the other haematopoietic organs. Secondary and tertiary transplants can then be performed by transplanting the whole bone marrow from the primary recipients into new recipient mice, to assess the long-term repopulation capacity of the HSCs via engraftment into the bone marrow and stable multilineage output[402].

HSCs are defined by their ability to durably reconstitute the blood system of recipient mice for 16 weeks or longer, whereas progenitor cells will deplete over the course of the experiment. Thus, in a primary transplantation assay, donor-derived engraftment beyond 3-4-months confirms the presence of functional HSCs. This reveals the fitness of the HSCs through their ability to engraft, as well as any lineage biases by observing the lymphoid and myeloid output of the donor HSCs *in vivo*. Considerations when using this assay include whether to transplant sorted HSCs or bulk culture, whether the treatment of HSCs (e.g. gene editing vectors/techniques) will affect their ability to engraft and whether the genetic background of the mice is more or less affected by the vector selection[401,402]. Additionally, the irradiation of the recipient mice is a fine balance – it must be sufficient to destroy the majority (~90%) of their native cells and would kill them if they did not receive an HSC transplant.

1.7 Aims of this thesis

The molecular factors regulating HSC self-renewal are incompletely understood. Identifying and characterising genes which regulate HSC expansion and self-renewal could help bolster HSC numbers in clinical applications. Additionally, understanding how these genes function provides fundamental biological insight into the mechanisms governing HSC expansion and self-renewal.

The overall aim of this work was to identify novel HSC regulators from the first genome-wide *ex vivo* HSPC CRISPR screen and investigate their role in haematopoiesis. The major focus of this thesis has been on the identification and characterisation of *Runx2* as a novel HSC regulator. The specific aims of this thesis were:

1. To investigate *Runx2* loss's effect on HSC expansion *ex vivo*
2. To assess how *Runx2* dosage affects haematopoiesis in the steady-state and transplantation settings
3. To determine the biological mechanism driving the increased HSC fitness with *Runx2* loss
4. To characterise the role that *Runx2* plays in T-cell commitment

To address these aims, I used a genome-wide *ex vivo* CRISPR screen in HSPCs, which identified many negative regulators and essential genes not previously characterised in HSCs. The RUNX transcription factor family emerged as candidates, with loss of *Runx1* or *Runx2* promoting HSC expansion *ex vivo* and increasing engraftment *in vivo*, but with different effects on haematopoietic reconstitution. *Runx2* was further validated using a *Runx2*^{flox} mouse, where even loss of one allele increased HSC expansion *ex vivo* and engraftment *in vivo*, showing a dosage-sensitive role in self-renewal but no role in steady-state haematopoiesis. *Runx2* loss also decreased T-cell output and partially blocked early T-cell differentiation, leading to an accumulation of lymphoid progenitors in the bone marrow and thymus. These findings identify

Runx2 as an important regulator of HSC fitness and T-cell commitment and reveal non-redundant roles for *Runx* family members in haematopoiesis.

Chapter 2: Methods

A full list of reagents used in this thesis can be found in **Appendix I**.

2.1 Mouse colony management

2.1.1 Overview of mouse usage

All experiments were initiated with 8-34-week-old mice and were approved by the UK Home Office (PP1874268). This study used a Cas9-expressing mouse line purchased from the Jackson Laboratory and bred in-house: the doxycycline-inducible Cas9-expressing line, C57BL/6-Gt(ROSA)26Sor$^{tm1(rtTA*M2)Jae}$ Col1a1$^{tm1(tetO-cas9)Sho}$ (JAX: 029415[403]). *Runx2*-KO mice were generated by crossing *Runx2*$^{tm1.1Tok}$ (MGI: 6874594[395]) with B6.Cg-*Commd10*$^{Tg(Vav1-icre)A2Kio}$/J (JAX: 008610[404]) for haematopoietic-specific *Runx2* deletion. C57BL/6-CD45.1^{+} and C57BL/6-CD45.1^{+}CD45.2^{+} were bred in-house while C57BL/6-CD45.2^{+} were purchased from Envigo.

2.1.2 Breeding strategy of *Runx2*^{flox} colony

Runx2^{flox} mice were bred and crossed with a Vav1-Cre, localising the loss of *Runx2* to the haematopoietic system primarily. It is important to note that Vav1 is also expressed in some endothelial cells[405]. Once the line had been established, the *Runx2*$^{fl/+}$ females were bred with CD45.2^{+} C57BL/6 males, then their offspring were bred until *Runx2*$^{fl/fl}$ mice were produced. These were then crossed with Tg$^{(Vav1-cre)1Graf}$ C57BL/6 mice to achieve heterozygous and homozygous loss in all nucleated blood cells.

2.1.3 Genotyping

PCR of ear notch DNA permitted genotyping as Vav1-iCre is not expressed in the skin. Ear notches were collected after weaning and lysed using 75 µL 25 mM NaOH and 2 mM EDTA ensuring they were submerged. They were then boiled at 98°C for 1 hour before being allowed

to cool down to 15 °C. 75 µL 40 mM Tris-HCl, 15 µL 3 M sodium acetate and 1 µL isopropanol was added before centrifuging at 9000 g for 15 minutes. The supernatant was then carefully removed, leaving ~10 µL liquid. 30 µL nuclease-free water was then added. 2 µL of this was used for each genotyping reaction.

For the genotyping PCR, two reactions were performed. The first used primers detecting the presence of the *Runx2*^{flox} region and the second used primers for the presence of Vav1-Cre. Mastermix components can be seen in **Table 2.1** and primer sequences in **Table 2.2**. Each reaction used a positive control of a known DNA sample and a negative control of mastermix with no DNA. Representative *Runx2* genotyping reaction shown in **Appendix II**. Presence of the flox insert site produced a band of 327 bp, the WT region produced a band of 173 bp.

Table 2.1: Reagents for genotyping PCR mastermix (1 reaction).

Component	**Volume (µL)**
2× Phusion Mastermix	12.5
Nuclease-free water	10.25
DNA template	2
10 µM primer mix	1.25

Table 2.2: Primer sequences for genotyping PCRs.

Name	**Sequence**	**Annealing temp. (°C)**	**Purpose**
oIMR9266	AGATGCCAGGACATCAGGAACCTG	69	Presence of Vav1-iCre for *Runx2*^{flox} mice
oIMR9267	ATCAGCCACACCAGACACAGAGATC	69	Presence of Vav1-iCre for *Runx2*^{flox} mice
runx2_geno_fwd	ACTTCGGTTGGTCAGAATAAACAG	60	Presence of *Runx2* flox site for *Runx2*^{flox} mice

runx2_geno_rev	CAAGCTAACGGGACTTGGAAGAG	60	Presence of *Runx2* flox site for *Runx2^{flox}* mice

1% agarose gels were made by adding 0.3 g agarose powder to 30 mL 1x TAE buffer and heating in the microwave for 2-3 minutes. 0.5 µL SYBR-Safe DNA stain was added once the gel had partially cooled, before pouring into the mould. Once solid, 4 µL of 1kb^{+} DNA ladder was added to the first well and 5 µL of the PCR reactions added to the subsequent wells. They were then run at 120 V for 25 minutes before imaging.

2.2 Mouse haematopoietic stem and progenitor cell (HSPC) isolation and *ex vivo* culture

2.2.1 Bone marrow isolation and c-Kit enrichment

8–12-week-old mice were euthanised and their femurs, tibias, hips and spine were dissected. The bones were crushed in a pestle and mortar with PBS and filtered in a 70 µm filter into a 15 mL falcon. Cells were then counted and spun down at 450 g for 5 minutes. Pellets were then resuspended in 350 µL phosphate-buffered saline (PBS) and 0.2 µL anti-c-Kit APC antibody added per 10 million cells. These were then incubated at 4 °C for 30 minutes. After incubation, 10 mL PBS was added and they were filtered through a 40 µm filter into a 15 mL falcon. They were then spun under the same conditions as before and resuspended in 350 µL PBS with 0.2 µL anti-APC microbeads per 10 million cells. They were incubated at 4 °C for 15 minutes. After this incubation, they were washed with 10 mL PBS, washed and resuspended in 2 mL PBS. They were then run through a 40 µm filter over a washed magnetic-activated cell sorting (MACS) column, followed by 9 mL PBS. The columns were then removed from the magnet and eluted with 5 mL PBS.

2.2.2 *Ex vivo* HSPC cultures

1 million c-Kit-enriched cells were plated per 1 mL of *ex vivo* HSC media (**Table 2.3**) in 24-well or 96-well CellBIND plates and kept in 37 °C incubators at 5% O^2. Media was changed every 2-3 days.

Table 2.3: Reagents for 1 mL of ex vivo HSC culture media. PSG = Penicillin-Streptomycin-Glutamine. HEPES = N-2-hydroxyethylpiperazine-N'-2-ethanesulfonic acid. PVA = polyvinyl alcohol. ITS-X = insulin-transferrin-selenium-X. TPO = thrombopoietin. SCF = stem cell factor.

Reagent	**Final concentration in F-12**	**Volume (µL)**
Ham's F-12 media	N/A	958
100X PSG	1X	10
1 M HEPES	10 mM	10
100 mg/mL PVA stock	1 mg/mL	10
100X ITS-X	1X	10
100 µg/mL TPO stock	100 ng/mL	1
10 µg/mL SCF stock	10 ng/mL	1

2.3 CRISPR gene knockouts and lentivirus production

2.3.1 Design of sgRNAs

sgRNA sequences were acquired from Bassik Lab CRISPR KO library[406] or designed using the Sanger WGE tool[407] and cloned into the pMCB306 lentiviral plasmid (Addgene #89360[408]), which had a puromycin cassette and GFP selectable markers. Vector schematic can be found in **Appendix III**. Sequences can be found in **Table 2.4**.

Table 2.4: sgRNA sequences used in this thesis.

sgRNA Name	Target Gene/Region	Sequence
Runx1 sgRNA 1	*Runx1*	GAGCGAGGCGCTGCCGCT
Runx1 sgRNA 2	*Runx1*	GTGAAGCGGCGGCTCGTGC
Runx2 sgRNA 1	*Runx2*	GTCGGTGCGGACCAGTT
Runx2 sgRNA 2	*Runx2*	GTGCGGCGGCCTCAATCG
Runx3 sgRNA 1	*Runx3*	GGCCCGAAGTGCGCTCGA
Runx3 sgRNA 2	*Runx3*	GCAGGGGAAGGCCGTGGA
Cbfb sgRNA 1	*Cbfb*	GTACACGGGCTTCAGGGAC
Cbfb sgRNA 2	*Cbfb*	GCGTGTCTGGCGCTCCTCGT
Rosa26	Safe harbour locus	GTGCCATGGTCCCCTGCCTA
Non-targeting control	N/A	GCACTACCAGAGCTAACTCA

2.3.2 HEK cell cultures

HEK293T cells between passages 2 and 25 were thawed in a water bath at 37 °C and washed with complete Dulbecco's modified Eagle medium (DMEM) (**Table 2.5**) before adding to fresh complete DMEM at a concentration of 50,000/mL in a sterile flask and put in a 5% CO_2 37 °C incubator. Cultures were split and trypsinised every 2-3 days.

Table 2.5: Complete DMEM for HEK293T cell culture. DMEM = Dulbecco's modified eagle medium. FBS = Foetal Bovine Serum. NEAA = non-essential amino acids.

Component	Volume for 10 mL	Final Concentration
DMEM	8.9	N/A
FBS	1	10%
Penicillin-Streptomycin	0.1	1%
L-Glutamine (200 mM stock)	0.1	2 mM

NEAA (100× stock)	0.1	1×

2.3.3 Lentivirus production using HEK cells

Porcine gelatine at 0.1% was used to coat 15 cm tissue culture plates which were then incubated at 37 °C for 2 hours. The gelatine was aspirated just before cells were plated. HEK293T cells at 80-90% confluence were washed gently with warm PBS and dissociated with 5 mL trypsin. The trypsin was then neutralised with 15 mL of complete DMEM, resuspended and pelleted at 300 g for 5 minutes. The cells were then resuspended in 20 mL complete DMEM, counted and viability assessed. Provided viability exceeded 95%, 12 million cells were added to 25 mL DMEM and plated. The plates were put into 5% CO_2 37 °C incubators overnight. For the transfection, 13.3 µg of sgRNA containing plasmid, 10 µg psPAX2 and 6.7 µg pMD2.G were required per plate. 970 µL Opti-MEM and 30 µL PEI-Pro were mixed per plate, briefly vortexed and incubated at room temperature for 5 minutes. These were added to an Eppendorf containing the 3 plasmids and mixed with a pipette. 9 mL of media was then removed from the plates, the cells were washed gently with 15 mL PBS. The PBS was then aspirated and replaced with 10-11 mL warm Ham's F12 (with 0.1% PVA, 1x ITS-X, 1x PSG and 1x HEPES), ensuring the plate was covered. The plates were then returned to the incubator for 48 hours. After this, 10 mL of supernatant was removed from the plates, added to a 50 mL falcon and spun down at 2000 g for 5 minutes in a pre-cooled 4 °C centrifuge. The supernatant was then filtered through a 0.45 µm cellulose acetate syringe filter, added to a Vivaspin 20 tube and centrifuged for 30 minutes at 4 °C. The centrifugation step was repeated until ~2 mL remained in the tube. The remaining supernatant was pipetted over the filter to resuspend any virus stuck to it, before aliquoting and storing at -80 °C.

2.3.4 Lentivirus titration

For the *Runx2* and *Rosa26* sgRNA-containing lentiviruses, the WIMM Virus Core provided the viral titre and produced the viruses, so titrations were not required. To achieve ~30%

transduction, a dose of 40 viral particles per cell was used[409]. For the *Runx1*, *Runx3* and *Cbfb* sgRNA-containing lentiviruses, the WIMM Virus Core cloned the sgRNAs into the pMCB306 lentiviral plasmid (Addgene #89360[408]), which had a puromycin cassette and GFP selectable markers.

To titrate the lentiviruses, volumes of 10 µl, 5 µl, 2 µL and 1 µL were used for the non-targeting control, *Runx1*, *Runx3*, and *Cbfb* sgRNA-containing lentiviruses in 200 µL HSC media with 100,000 c-Kit$^+$ cells. They were incubated for 16 hours at 5% O_2 and 37 °C, before removal of the virus and addition of fresh HSC media. The optimal volumes of each lentivirus were determined by the presence of 30-40% GFP$^+$ cells at day 0, 2 days after transduction by measurement via flow cytometry. 30-40% was the ideal transduction efficiency, as it gives the maximum likelihood that each cell receives one copy of the virus and permits observation of any competitive phenotypes the cells may have in the culture[409].

2.3.5 *Runx* family CRISPR knockouts in HSPCs

For *Runx1*, *Runx2*, *Runx3* and *Cbfb* CRISPR-based gene KOs, a doxycycline-inducible Cas9 expressing mouse was used (see 2.1.1 for details) to permit controlled expression of Cas9. HSPC cultures of these cells were initiated with c-Kit$^+$ cells in the PVA *ex vivo* system and grown for 14 days before transduction, so the pHSCs (CD201$^+$CD150$^+$c-Kit$^+$Sca-1$^+$Lineage$^-$) expanded to comprise ~30% of the live cells. Lentiviral transduction was performed overnight, 16-18 hours. For doxycycline treatment for experiments using dox-inducible Cas9 cells[403], Cas9 was induced by the addition of 500 ng/mL doxycycline for 48-hours at 48-hours post-transduction. For experiments using constitutive Cas9-expressing cells, lentivirally transduced cells were selected for with puromycin treatment for 48-hours, starting 48-hours post-transduction.

2.3.6 Ribonucleoprotein-based gene knockouts

sgRNAs were purchased from IDT. 3.2 µg of sgRNA and 0.6 µL of Alt-R Cas9 nuclease were used per reaction, added to a polymerase chain reaction (PCR) tube and complexed at 25 °C for 10 minutes. c-Kit$^+$ cells were counted and resuspended in nucleofection buffer from the Lonza P3 Primary Cell Nucleofector kit (~100k per reaction) before adding to the PCR tubes of complexed Cas9:sgRNA. The mixtures were gently added to the cuvettes and electroporated on the Lonza Nucleofector using the program for human CD34$^+$ cells. They were then quickly recovered in complete F12 media before plating at 1 million/mL in CellBIND plates and returning to the incubator. 80% of the media was changed 1 hour after electroporation and again the next day before continuing to the standard 2-3 days.

2.4 *Ex vivo* HSPC CRISPR screen

2.4.1 CRISPR screen methodology

Dr Adam Wilkinson performed this screen. Following an initial 17-day *ex vivo* expansion, constitutive Cas9-expressing HSCs were transduced with the Gouda genome-wide lentiviral sgRNA KO library (Addgene #136987[410]). High titre lentivirus library was generated from HEK 293T cells in DMEM supplemented with 10 mM sodium pyruvate, 2 mM GlutaMax, 4.5 mM sodium propionate, 2mM sodium butyrate, 1.5 mM caffeine, and 5% heat-inactivated FBS.

The genome-wide HSC KO library was split into two technical replicates at t7. It was then expanded another 21 days, with samples collected at t7, t14, and t21. At each timepoint, the cells were pooled from each replicate and split in half. Half was replated in fresh HSC media, and half were pelleted and kept at -80 °C for DNA extraction.

2.4.2 CRISPR library transduction

The cells were transduced in 24-well fibronectin-coated tissue culture plates at an MOI of 0.3 (volume of virus determined by droplet digital PCR, see 2.4.3). They were incubated for 16

hours at 5% O_2 and 37 °C, before removal of the virus and addition of fresh HSC media (**Table 2.3**). 48 hours after the transduction, they were puromycin selected at 1 µg/mL for 48-hours. The t0 timepoint was 48 hours after the puromycin selection.

2.4.3 Droplet digital PCR (ddPCR)

Probes for Zeb2 and puromycin (contained in the lentiviral construct) were used in the ddPCR reaction mixture (**Tables 2.6-7**) and added to a 96-well PCR plate with 25 ng DNA per sample. A non-template control well was used as a negative control. Droplets were generated before sealing the plate and running the PCR (reaction parameters in **Table 2.8**).

Table 2.6: Primers and probes used in ddPCR.

Name	Sequence	Annealing temp. (°C)	Purpose
Zeb2-P/5	TGATGGGTTGTGAAGGCAGCTGCACCT	N/A	Reference probe for ddPCR
PuroR-P/1	CACCGGCCCAAGGAGCCCG	N/A	Lentiviral integration probe for ddPCR
Zeb2-F/5	GGATGGGGAATGCAGCTCTT	64	ddPCR primer for reference gene
Zeb2-R/5.1	AGTGCGGCAGAATACAGCA	64	ddPCR primer for reference gene
PuroR-F/1	AGCAACAGATGGAAGGCCTC	64	ddPCR primer for lentiviral integration
PuroR-R/1	GACGGTGGCCAGGAACCA	64	ddPCR primer for lentiviral integration

Table 2.7: ddPCR reaction mixture.

Reagent	Volume for 1 reaction (25 µL)
ddPCR supermix	12.5
Puromycin probe (20X)	0.625
Zeb2 probe (20X)	0.625

Template DNA / H_2O	11.25

Table 2.8: ddPCR reaction conditions.

Step	Temperature	Time	Notes
1	95 °C	10 min	N/A
2	94 °C	30 sec	Ramp rate 2.5 °C/s
3	60 °C	1 min	Ramp rate 2.5 °C/s
4	Repeat 2-3	39 cycles	N/A
5	98 °C	10 min	N/A
6	4 °C	∞ (hold)	Maintain samples until retrieval

2.4.4 Genomic DNA extraction

The DNeasy Blood and Tissue Kit was used, following the procedure for 'cultured cells'. Pellets were resuspended in 200 µL PBS and 20 µL proteinase K added. 200 µL buffer AL was then added before vortexing and incubating at 56 °C for 10 minutes. After incubation, 200 µL 100% ethanol was added and the samples vortexed. Samples were then pipetted into DNeasy spin columns and centrifuged at 6000 g for 1 minute. The flow through was discarded and 500 µL buffer AW1 added, before centrifuging again at 6000 g for 1 minute. The flow through was discarded and 500 µL buffer AW2 added, before centrifuging at 20,000 g for 3 minutes. The waste tube and flow through was discarded and spin column moved to a 1.5 mL DNA lo-bind tube. DNA was eluted by addition of 50 µL buffer AE to the spin column membrane, incubating at room temperature for 4 minutes and centrifuging for 1 minute at 6000 G. DNA samples were stored at -20 °C.

2.4.5 Amplification of sgRNAs for Next Generation Sequencing

Following genomic DNA extraction, sgRNAs were PCR amplified for next generation sequencing. 4 parallel PCRs were set up for each sample in a 96-well PCR plate. Mastermix was made of reaction buffer, dNTP, P5 primer mix, Taq polymerase and water. A mix of P5 primers with stagger regions of different length is necessary to maintain sequence diversity, so 8 primers were used together in one P5 primer mix and used in all wells (**Table 2.9**). Reaction component volumes can be found in **Table 2.10**. A unique P7 primer was added to each reaction to allow demultiplexing. DNA was added last.

Table 2.9: Sequences of P5 primers. Bold indicates the staggered regions.

Name	**Sequence**
P5 0 nt stagger	AATGATACGGCGACCACCGAGATCTACACTCTTTCCCTACACGACGCTC TTCCGATCT**TT**GTGGAAAGGACGAAACACCG
P5 1 nt stagger	AATGATACGGCGACCACCGAGATCTACACTCTTTCCCTACACGACGCTC TTCCGATCT**CTT**GTGGAAAGGACGAAACACCG
P5 2 nt stagger	AATGATACGGCGACCACCGAGATCTACACTCTTTCCCTACACGACGCTC TTCCGATCT**GCTT**GTGGAAAGGACGAAACACCG
P5 3 nt stagger	AATGATACGGCGACCACCGAGATCTACACTCTTTCCCTACACGACGCTC TTCCGATCT**AGCTT**GTGGAAAGGACGAAACACCG
P5 4 nt stagger	AATGATACGGCGACCACCGAGATCTACACTCTTTCCCTACACGACGCTC TTCCGATCT**CAACTT**GTGGAAAGGACGAAACACCG
P5 6 nt stagger	AATGATACGGCGACCACCGAGATCTACACTCTTTCCCTACACGACGCTC TTCCGATCT**TGCACCTT**GTGGAAAGGACGAAACACCG
P5 7 nt stagger	AATGATACGGCGACCACCGAGATCTACACTCTTTCCCTACACGACGCTC TTCCGATCT**ACGCAACTT**GTGGAAAGGACGAAACACCG
P5 8 nt stagger	AATGATACGGCGACCACCGAGATCTACACTCTTTCCCTACACGACGCTC TTCCGATCT**GAAGACCCTT**GTGGAAAGGACGAAACACCG

Table 2.10: Reaction contents for library amplification.

Component	**Volume/Amount**
10x reaction buffer	10 µL
dNTP	8 µL
P5 primer mix (100 µM)	0.5 µL
ExTaq polymerase	1.5 µL
Genomic DNA	up to 10 µg
P7 primer (5 µM)	10 µL
Nuclease-free water	up to 100 µL (final volume adjustment)

Once the mastermix had been added to all wells (including a non-template negative control), the PCR was run using the reaction conditions detailed in **Table 2.11**.

Table 2.11: Reaction conditions for indexing PCR.

Step	**Temperature**	**Time**	**Description**	**Notes**
N/A	95 °C	N/A	Preheat block	Wait until block reaches 95 °C
1	95 °C	1 min	Initial denaturation	N/A
2	95 °C	30 sec	Denaturation	Cycle start
3	53 °C	30 sec	Annealing	N/A
4	72 °C	30 sec	Extension	N/A
N/A	Repeat 2–4	28 cycles	Main cycling	N/A
5	72 °C	10 min	Final extension	N/A

6	4 °C	∞ (hold)	Hold	Maintain samples until retrieval

PCR products were pooled (15–30 µL per well), and 100 µL of the pooled sample was transferred to a 96-well plate. An equal volume of resuspended AMPure XP beads was added, mixed, and incubated at room temperature for 5 minutes to bind DNA fragments ≥100 bp. Beads were captured on a magnetic stand, and the supernatant was removed. Samples were washed twice with 200 µL of 70% ethanol, air-dried for 1–4 minutes, and eluted in 50 µL of TE buffer. Eluates were collected and stored for downstream sequencing.

2.4.6 CRISPR screen analysis pipeline

The MAGeCK v0.5.9.2[411] pipeline was used by Ian Hsu to analyse the CRISPR-screen sequencing data. Raw sequencing reads were trimmed, aligned to the sgRNA library reference, and counted per sgRNA. Normalization across samples was performed to correct for library size and composition biases. Gene-level statistics were derived using the robust rank aggregation (RRA) algorithm. Beta scores were calculated via the MAGeCK MLE module to estimate effect size and direction of selection (positive = enrichment; negative = depletion). False discovery rates were used to adjust for multiple testing, and genes were prioritized based on beta scores, RRA scores, and adjusted p-values.

2.5 T-cell differentiation assays

Biotinylated recombinant human DLL4 was incubated with streptavidin-coated polystyrene particles for 30 minutes at room temperature to generate DLL4-µBeads. 1-20×10^3 HSPCs from 14-day HSC cultures were differentiated with 1×10^5 DLL4-µBeads in the media described in **Table 2.12.** After 7 days incubation at 37°C in 5% CO_2, cells were harvested for flow cytometry using the panel in **Table 2.13**. Gating schema can be found in **Appendix IV**.

Table 2.12: Lymphoid media for T-cell differentiation.

Reagent	**Final concentration**	**Volume for 5 mL**
IMDM with GlutaMAX Supplement	N/A	3.875 mL
BIT 15 9500 Serum Substitute	20%	1.0 mL
Penicillin/Streptomycin (100×)	1%	50 µL
mFLT3-L (10 µg/mL)	100 ng/mL	50 µL
SCF (10 µg/mL)	100 ng/mL	50 µL
mIL-7 (10 µg/mL)	100 ng/mL	50 µL
Recombinant Human CXCL12/SDF-1α (5 µg/mL)	25 ng/mL	25 µL

Table 2.13: T-cell differentiation analysis panel (100 µL/sample).

Antibody	**Volume (µL)**
CD44 BV605	8
CD25 BV785	2
CD90 PE	8
CD8a PE/Cy7	4
CD4 APC	4
Gr-1/Ly6C APC/Cy7	4
CD45R/B220 APC/Cy7	2
TER119 APC/Cy7	2
c-Kit BV421	2
CD24 FITC	2
PBS	766

2.6 Flow cytometry

HSPC cultures, peripheral blood, bone marrow, thymi, spleens and T-cell differentiations were stained using the relevant antibody cocktails for 30 minutes at 4 °C (unless otherwise indicated) and then analysed on a BD Fortessa or BD FACS Fusion. Where indicated, immunophenotypic cell populations were sorted using a BD FACS Fusion.

2.6.1 Characterisation of *Runx2^{flox}* mice

8–34-week-old mice were culled and their femurs, thymi, spleen and blood taken for analysis. c-Kit enrichment was performed on the bone marrow and ~10 million stained using 6 µL of the panel in **Table 2.14** with 100 µL PBS for 30 minutes at 4 °C. Samples were then washed with PBS/FBS, spun at 450 g for 5 minutes, resuspended in 100 µL of the panel in **Table 2.15** and incubated at 4 °C for 90 minutes, flicking the tubes every 20 minutes. Thymi and spleen were homogenised with syringes and filtered with a 15 µm filter before ~2 million stained using the panels in **Tables 2.16-17**. 50 µL peripheral blood was analysed using a complete blood count analyser. Bone marrow, thymi and spleen samples were then analysed, using the gating schema in **Appendices V-VII**.

Table 2.14: Biotin lineage panel (6 µL/sample in 100 µL PBS).

Antibody	**Volume (µL)**
Ly6G/Ly6C – biotin	100
Ter119 – biotin	100
CD4 – biotin	25
CD8a – biotin	25
CD45R/B220 – biotin	50
CD127 – biotin	50
Sterile PBS	350

Table 2.15: Fresh HSC analysis panel (100 µL/sample).

Antibody	**Volume (µL)**
CD34 FITC	4
c-Kit APC	1
Sca-1 PE	1
Streptavidin APC/Cy7	1
CD150 PE/Cy7	1
CD48 BV421	1
Sterile PBS	291

Table 2.16: Thymus analysis panel (100 µL/sample).

Antibody	**Volume (µL)**
CD11b FITC	1
Gr-1/ly6G FITC	1
NK1.1 FITC	2
CD19 FITC	2
CD4 APC	2
CD8 APC/Cy7	2
CD44 BV605	4
CD25 BV785	1
CD90 PE	4
PBS	781

Table 2.17: Spleen analysis panel (100 µL/sample).

Antibody	**Volume (µL)**
CD11b PE	1
Gr-1/Ly6G PE	1

CD4 APC	1
CD8 PB	2
CD45R/B220 APC/Cy7	2
NK1.1 FITC	2
CD3 PE/Cy7	2
PBS	389

2.6.2 *Ex vivo* cultured HSPC flow cytometry

50 µL of PVA-based *ex vivo* HSPC cultures (~50,000 cells) were taken and stained with 2 µL of the cultured HSC stain (**Table 2.18**) for 30 minutes at 4 °C. They were then washed with 200 µL PBS/FBS, spun at 450 g for 5 minutes and resuspended in 100 µL PBS/FBS with 1:1000 PI. They were then analysed on a BD Fortessa. Gating schema can be found in **Appendix VIII**.

Table 2.18: Ex vivo cultured HSPC panel (2 µL/sample in 50 µL PBS/media).

Antibody	**Volume (µL)**
c-Kit BV421	12.5
Sca-1 PE	12.5
CD150 PE/Cy7	12.5
CD4 APC/Cy7	5
CD8 APC/Cy7	5
Ter119 APC/Cy7	5
CD127 APC/Cy7	5
CD45R/B220 APC/Cy7	5
Ly6C/Ly6G APC/Cy7	5
CD201 APC	5
PBS	27.5

2.6.3 Fluorescence-activated cell sorting (FACS)

For fresh HSC/HPC sorting, bone marrow was first c-Kit enriched before staining with 6 µL of the panel in **Table 2.14** with 100 µL PBS. Samples were then washed with PBS/FBS, spun at 450 g for 5 minutes, resuspended in 100 µL of the panel in **Table 2.15** and incubated at 4 °C for 90 minutes, flicking the tubes every 20 minutes. Samples were then washed with PBS/FBS, spun at 450 g for 5 minutes, resuspended in 300 µL PBS/FBS with 1:1000 propidium iodide (PI) and sorted using a BD FACS Fusion. For single cell assays, the HSCs were sorted directly into U-bottom tissue culture plates containing 200 µL complete PVA media per well. For bulk cultures, HSCs were recovered in complete PVA media and plated at 1 million/mL in CellBIND plates. For RNA-seq, sorted cells were immediately pelleted at 450 g for 5 minutes and lysed in 100 µL Zymo Direct-zol RNA Lysis Buffer before RNA extraction or storing at -80 °C.

2.6.4 Intracellular flow cytometry

For intracellular flow cytometry, ~500,000-10 million cells were stained with relevant antibody panels (**Tables 2.19-21**), then fixed and permeabilised using the BD Pharmingen Transcription Factor Buffer Set per sample. They were then stained for 40 minutes with anti-RUNX2-PE or an isotype control. They were then washed with the provided wash buffer and run on the BD Fortessa. Cell number per sample was determined by the frequency of desired cell type, so that the final gate of interest would have at least 1,000 cells. Gating schema can be found in **Appendices IX-X**.

Table 2.19: Whole bone marrow HSC panel for intracellular flow cytometry (100 µL/sample).

Antibody	**Volume (µL)**
c-Kit APC	3
CD4 APC/Cy7	3
CD8a APC/Cy7	3
Gr-1 APC/Cy7	3
CD11b APC/Cy7	3

CD45R/B220 APC/Cy7	3
CD127 APC/Cy7	3
TER119 APC/Cy7	3
CD150 PE/Cy7	3
CD48 BV421	3
Sca-1 FITC	5
PBS	265

Table 2.20: Cultured HSC panel for intracellular flow cytometry (100 µL/sample).

Antibody	**Volume (µL)**
c-Kit BV421	12.5
Sca-1 FITC	12.5
CD150 PE/Cy7	12.5
CD4 APC/Cy7	5
CD8 APC/Cy7	5
Ter119 APC/Cy7	5
CD127 APC/Cy7	5
CD45R/B220 APC/Cy7	5
Ly6C/Ly6G APC/Cy7	5
CD201 APC	5
PBS	27.5

Table 2.21: Plasmacytoid dendritic cell panel for intracellular flow cytometry (100 µL/sample).

Antibody	**Volume (µL)**
CD45R/B220 APC/Cy7	2.5
CD11b APC	2.5
BST2 FITC	1.25

c-Kit BV421	6.25
PBS	287.5

2.7 HSC transplantation assays

2.7.1 Experimental overview

For the CRISPR-based *Runx2*-KO transplants, C57BL/6-CD45.1$^+$ mice were lethally irradiated (12 Gy) and injected in the tail vein with 2000 CD201$^+$CD150$^+$KSL pHSCs which had been cultured for 14 days after being transduced with either control sgRNAs or *Runx2*-targeting sgRNAs alongside 1 million CD45.1$^+$CD45.2$^+$ wild-type whole bone marrow competitor cells.

For the *Runx2^{flox}* transplants, lethally irradiated C57BL/6-CD45.1$^+$ mice received either 100 fresh bone marrow CD150$^+$CD34$^-$KSL HSCs of *Runx2*-wt, *Runx2*-het or *Runx2*-hom and 0.5 million CD45.1$^+$CD45.2$^+$ wild-type whole bone marrow competitor cells, or 10,000 day-14 cultured cells (initiated from CD150$^+$CD34$^-$KSL HSCs) and 1 million CD45.1$^+$CD45.2$^+$ wild-type whole bone marrow competitor cells.

2.7.2 Peripheral blood analysis

Peripheral blood was taken every 4 weeks and analysed via flow cytometry. 50 µL of peripheral blood was extracted from the tail vein of the recipient mice, then lysed in 1 mL Ammonium-Chloride-Potassium (ACK) buffer before incubating for 15 minutes at room temperature. Bloods were then spun at 450 g for 15 minutes and resuspended carefully in 1 mL ACK. They were again incubated at room temperature for 15 minutes. After this incubation, 900 µL was moved to FACS tubes with 100 µL from each sample used for single stains. They were all washed with 1 mL PBS, spun and resuspended in the peripheral blood stain (**Table 2.22**). The samples were stained at 4 °C for 30 minutes before washing with 1 mL PBS/FBS

and resuspending in 300 µL PBS/FBS with 1:1000 PI except the single stains, which were resuspended in 300 µL PBS/FBS. Gating schema can be found in **Appendix XI**.

Table 2.22: Peripheral blood analysis panel (100 µL/sample).

Antibody	**Volume (µL)**
CD11b PE	2
Gr-1/Ly6G PE	2
CD4 APC	2
CD8 APC	2
CD45R/B220 APC/Cy7	4
CD45.1 PE/Cy7	10
CD45.2 eBioscience	12
PBS	3972

2.7.3 Endpoint analysis

At 4-20-week endpoints of HSC transplantation assays, blood, bone marrow, spleen and thymi of recipient mice were collected after euthanasia and analysed via flow cytometry. The femurs and tibias were dissected, the ends cut off and flushed with PBS. The bone marrow suspension was then filtered through a 40 µm filter, counted and 10 million cells taken for flow cytometry. These were added to FACS tubes and washed with 1 mL PBS, spun down and resuspended in 6 µL antibody stain in **Table 2.14** with 100 µL PBS, before washing and staining with 100 µL of the panel in **Table 2.23** for 90 minutes at 4 °C, resuspending every 20 minutes. 10 million bone marrow cells were also stained with the lymphoid panel for CLP and LyMPPs in **Table 2.24**. The spleens and thymi were homogenised using a syringe and filtered with a 15 µm filter, with 2 million stained using the relevant antibody stains (**Tables 2.25-26**).

2 million bone marrow, spleen, thymus and peripheral blood cells were taken at the endpoint of the short-term HSPC transplantation assay in Chapter 5 and stained with the plasmacytoid dendritic cell (pDC) panel in **Table 2.27**.

Gating schema for thymi and HSC transplantation assay donor chimerism can be found in **Appendices VI** and **XI**, respectively. Gating schema for lymphoid panel for CLP and LyMPPs can be found in **Appendix XII**. Gating schema for pDCs can be found in **Appendix X**, and bone marrow **Appendix V**.

Table 2.23: Bone marrow panel for transplantation endpoint (100 µL/sample).

Antibody	**Volume (µL)**
CD34 FITC	100
CD45.1 PE/Cy7	75
CD45.2 eBioscience	75
Sca-1 PE	25
c-Kit APC	25
Streptavidin APC/Cy7	25
CD150 BV785	25
PBS	2150

Table 2.24: Lymphoid panel for CLP and LyMPPs in transplantation endpoint (100 µL/sample).

Antibody	**Volume (µL)**
CD45.2 BUV395	45
CD45.1 AF700	45
Streptavidin APC/Cy7	15
CD127 FITC	45
c-Kit APC	15
Sca-1 PE	15
CD150 PE/Cy7	15
CD48 BV785	30
Flt3 BV421	45
PBS	1230

Table 2.25: Thymus transplantation endpoint panel (100 µL/sample).

Antibody	**Volume (µL)**
B220 APC/Cy7	4
Gr-1/Ly6G APC/Cy7	4
TER119 APC/Cy7	4
CD24 FITC	4
c-Kit APC	4
CD8a PE/Cy7	4
CD44 BV605	8
CD25 BV785	4
CD90 PE	8
CD4 BV421	4
CD45.1 AF700	10
PBS	1558

Table 2.26: Spleen transplantation endpoint panel (100 µL/sample).

Antibody	**Volume (µL)**
CD11b PE	2.5
Gr-1/Ly6G PE	2.5
CD4 APC	2.5
CD8 FITC	10
B220 APC/Cy7	5
CD45.1 PE/Cy7	12.5
CD45.2 eFluor450	15
PBS/FBS	2450

Table 2.27: Plasmacytoid dendritic cell transplantation endpoint panel (100 µL/sample).

Antibody	**Volume (µL)**
B220 APC/Cy7	33
CD11b PE	33
BST2 FITC	16
CD45.2 eFluor450	79
CD45.1 PE/Cy7	66
PBS	3773

2.8 Molecular analyses

2.8.1 RNA extraction

RNA from FACS-isolated cells was extracted using the Zymo Direct-zol RNA Microprep kit. Samples lysed in 100 µL Tri Reagent had 100 µL 100% ethanol added and were thoroughly mixed by pipetting. The mixtures were then moved into Zymo-spin columns, centrifuged at 10,000 g for 30 seconds and flow through discarded. 400 µL RNA wash buffer was then added to the column, centrifuged at 10,000 g for 30 seconds before adding 5 µL DNase I and 35 µL DNA digestion buffer to the column matrix. The samples were then incubated at room temperature for 15 minutes. 400 µL Direct Zol RNA PreWash was then added and samples centrifuged at 10,000 g for 30 seconds. The flow through was discarded and this step repeated. 700 µL RNA Wash Buffer was then added and centrifuged for 1 minute at 10,000 G. The column was then transferred to a RNase free 1.5 mL Eppendorf tube. RNA was eluted with 15 µL of RNase-free water by incubation for 4 minutes followed by centrifugation at 10,000G for 2 minutes. Samples were stored at -80 °C.

2.8.2 RNA-sequencing

RNA-sequencing was performed by Novogene. Libraries were 150 bp paired-end sequenced with a NovaSeq (Illumina). Data analysis was performed by Catherine Chahrour. Quality

checking of FastQ files was performed using FastQC (v0.12.1)[412]. The reads were trimmed using Trim Galore (v0.6.10)[413]. STAR (v2.7.10b) was then used to map the trimmed reads to the mm39 reference genome[414]. Quantification of gene expression was performed using featureCounts (v2.0.3)[415]. Batch correction was carried out using RUVSeq (v1.36.0)[416] Differential gene analysis was performed using DESeq2 (v1.40.2)[417]. GO over-representation analysis was performed using Cluster Profiler (v4.10.1)[418]. GSEA analysis was performed using FGSEA (v1.28.0) with Molecular Signatures Database (MSigDB) Hallmarks collection for mouse[419–421].

2.8.3 CUT&Tag

CUT&Tag was performed by Dr Alastair Smith on sorted $CD201^{+}CD150^{+}$KSL pHSCs at day 14 of *ex vivo* culture, as previously described[422]. Briefly, pHSCs were immobilised on concanavalin A-coated magnetic beads and permeabilised. They were incubated with primary antibody against the target protein (RUNX2 or H3K4me3), followed by a secondary antibody to enhance tethering. pA-Tn5 transposase loaded with sequencing adapters was then added to the samples, allowing tagmentation at antibody-bound genomic loci. After activation of the transposase, DNA fragments were released, purified, and PCR-amplified using indexed primers from the NEB Next Ultra Library Prep Kit. Libraries were then quantified, pooled, and sequenced on an Illumina NovaSeq by Novogene.

Chapter 3: The *Runx* Family Have Novel Roles in Haematopoiesis

3.1 Introduction

In this chapter I interrogated a genome-wide *ex vivo* HSPC CRISPR screen to identify novel putative regulators of HSC expansion. I validated several hits from the screen as HSC regulators by performing CRISPR-based KOs of *Runx1*, *Runx2*, *Runx3* and *Cbfb* to investigate the effect of their loss on immunophenotypic HSCs (pHSCs) in the *ex vivo* expansion system. Post-translational RUNX protein inhibition was explored as a method to transiently promote HSC expansion *ex vivo* via several available chemical RUNX inhibitors. Finally, I investigated the functional consequences of loss of *Runx1* and *Runx2* in HSCs using transplantation assays.

3.2 *Ex vivo* CRISPR screen reveals *Runx* factors as putative negative regulators of HSC expansion

3.2.1 Genome-wide *ex vivo* CRISPR screen

Dr Adam Wilkinson performed the first genome-wide *ex vivo* CRISPR screen using the PVA-based HSPC expansion culture system[423,424] (**Figure 3.1A**). The library had a puromycin resistance cassette, allowing for selection of cells with successful viral integration. The mouse c-Kit$^+$ HSPCs had a constitutively expressed Cas9 (see Chapter 2 for details). After viral transduction and puromycin selection, gDNA was collected weekly at four timepoints (t0-t21) for sequencing. The data were analysed by Ian Hsu using the MAGeCK pipeline[411], which found that essentially all the sgRNAs were detectable throughout the 21-day screen, with the composition changing slightly over time (**Figure 3.1B**). MAGeCK-MLE[425] analysis was then performed for identification of statistically significant genes, either negatively regulating or

essential for HSPC expansion. From this analysis, the genes were assigned a beta score – putative essential genes had a negative score (sgRNA abundance decreased over time), and putative negative regulators had a positive score (sgRNA abundance increased over time) (**Figure 3.1C**, **Appendix XIII**).

3.2.2 CRISPR screening identifies new and established essential HSPC regulators

2305 statistically significant putative essential genes (false discovery rate, FDR<10%) were identified from this analysis. HSPC-specific essential genes were found by comparison to the Achilles common essential list. This list comprises 1552 genes found to be essential across many cancer cell lines[426]. 995 of the 2305 were present in the Achilles list, but 1310 appeared to be HSPC-specific (**Figure 3.1D**). Present in the HSPC-specific essential gene list were established regulators of HSPC activity e.g. *Gata2*[427,428] and *Lmo2*[429,430]. Some of the top hits were previously identified essential genes for various biological processes such as RNA processing (*C1d*, *Adar*[431–434]), genome regulation (*Men1, Hist1h4m*[435–437]) and translation (*Asna1, Ears2, Hars, Mrps25, Mrps33, Tars, Tars2*[438–442]).

3.2.3 CRISPR screening identifies new and established HSPC negative regulators

As established in Chapter 1, there is clinical and biological interest in expanding HSCs *ex vivo*. I therefore focussed on discovering novel negative regulators of HSC expansion – genes which, when knocked out, promote HSC expansion and self-renewal. The screen identified 92 statistically significant (FDR < 10%) putative negative regulators. Within these, some were previously established such as *Pten*[443] and *Trp53*[444] but others were novel putative negative regulators of HSC expansion (**Figure 3.1C**). To investigate the potential relationships between these genes, STRING analysis[445] was used to produce a putative interaction network (**Figure 3.1E**). STRING uses various sources to form connections between nodes, such as published experiments, text mining, co-expression data and others. Within this network of putative negative regulators, RUNX2 had many connections to the other nodes, which was interesting as it did not have an established role in regulation of HSC expansion. The sgRNA enrichment

over time for the other *Runx* family members was plotted (**Figure 3.1F**) and it was noted that *Runx2*-targeting sgRNAs increased ~4-fold over the course of the screen. *Runx1* and *Runx3* had an increase of ~3-fold but the FDR was not significant for these genes (**Figure 3.1F**). Because of the heterogeneous nature of these HSPC cultures, further validation was needed to ensure the hits identified were bona fide HSC regulators. Overall, the results from this screen prompted investigation of the RUNX family *ex vivo*, to see if their loss truly has an effect on HSC activity.

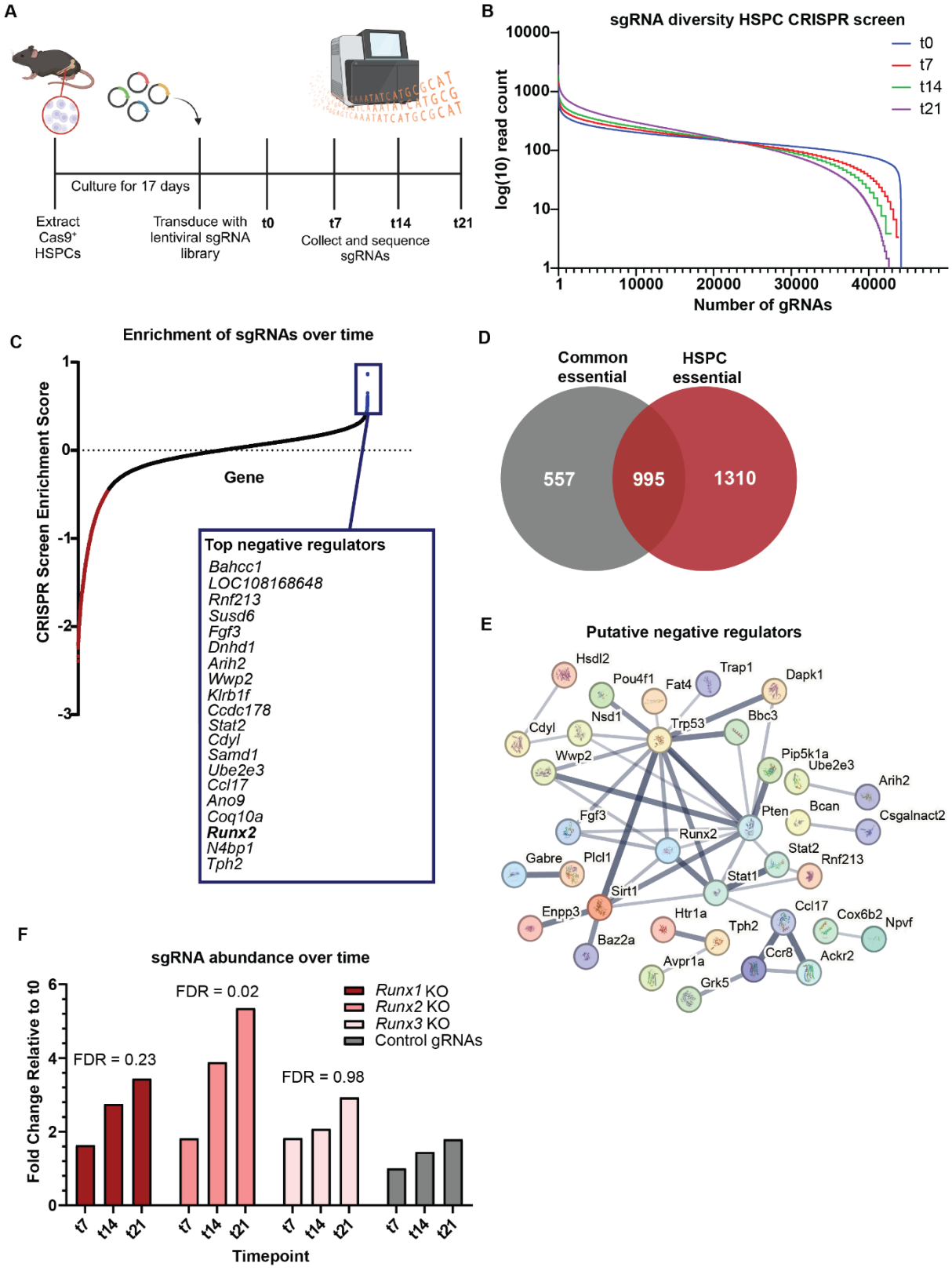

Figure 3.1: Genome-wide ex vivo HSPC CRISPR screen identifies putative regulators of expansion.

(A) Schematic overview of *ex vivo* HSPC CRISPR KO screen for top putative negative regulators. Created in BioRender.
(B) sgRNA diversity over time from *ex vivo* HSPC CRISPR screen.
(C) Beta score for the 21,601 genes targeted in the *ex vivo* HSPC expansion screen. Inset: Top 20 beta-score genes listed within insert.
(D) Venn diagram of the overlap in essential genes from Achilles common essential list[426] and the essential genes identified in our screen (mHSC).
(E) STRING analysis of protein-protein interactions of genes with positive beta score and FDR < 10%. Thicker line = stronger reported interaction. Interactions can be: from curated databases, experimentally determined, gene neighbourhood, gene fusions, gene co-occurrence, textmining, co-expression and protein homology.
(F) Timecourse of sgRNA-expressing cells over time for the three *Runx* genes and control sgRNAs, normalised to t0. FDR from the analysis shown in C are annotated above.

3.3 *Runx1*, *Runx2*, *Runx3* and *Cbfb* knockout HSCs have differing phenotypes *ex vivo*

3.3.1 CRISPR sgRNA design and implementation

As discussed, the CRISPR screen was performed in a heterogeneous population of HSPCs without tracking HSCs specifically. To elucidate whether the negative regulators identified were HSC-specific, single gene KOs were designed and performed in the HSPCs with the frequency of pHSCs ($CD201^+CD150^+KSL$) observed via flow cytometry over time. CRISPR-based KOs of *Runx1*, *Runx2*, *Runx3* and their binding partner *Cbfb* were performed with two sgRNAs for each gene. Two controls were used, a non-targeting control with no complement in the genome and a targeting control at the *Rosa26* safe harbour locus. As discussed in Chapter 2, the sgRNA-containing plasmid expressed EGFP, so this was used as a marker of lentiviral integration.

The *Runx1*, *Runx2*, *Runx3*, *Rosa26* and non-targeting control sgRNAs were from the Bassik Lab's sgRNA library[406] ensuring they targeted early in the gene to permit maximal disruption (**Figure 3.2A**). For effective disruption of *Runx* gene function, the sgRNAs targeted the coding sequence for the DNA-binding Runt domain. The Sanger WGE tool[407] was used to design the *Cbfb* sgRNAs, again early in the gene whilst also considering the number of off-targets for each sgRNA.

One batch of *Runx2*-targeting and *Rosa26*-targeting sgRNAs was produced and titrated by the WIMM Virus Core but *Runx1*, *Runx3*, *Cbfb* and subsequent *Runx2* and *Rosa26* batches were generated and titrated as detailed in Chapter 2.

3.3.2 CRISPR knockout *ex vivo* timecourse

To understand the effects of the single gene KOs on HSC expansion, an *ex vivo* timecourse was performed using both control sgRNAs and both targeting sgRNAs for each gene and tracking the frequency of pHSCs over time (**Figures 3.2A-C**).

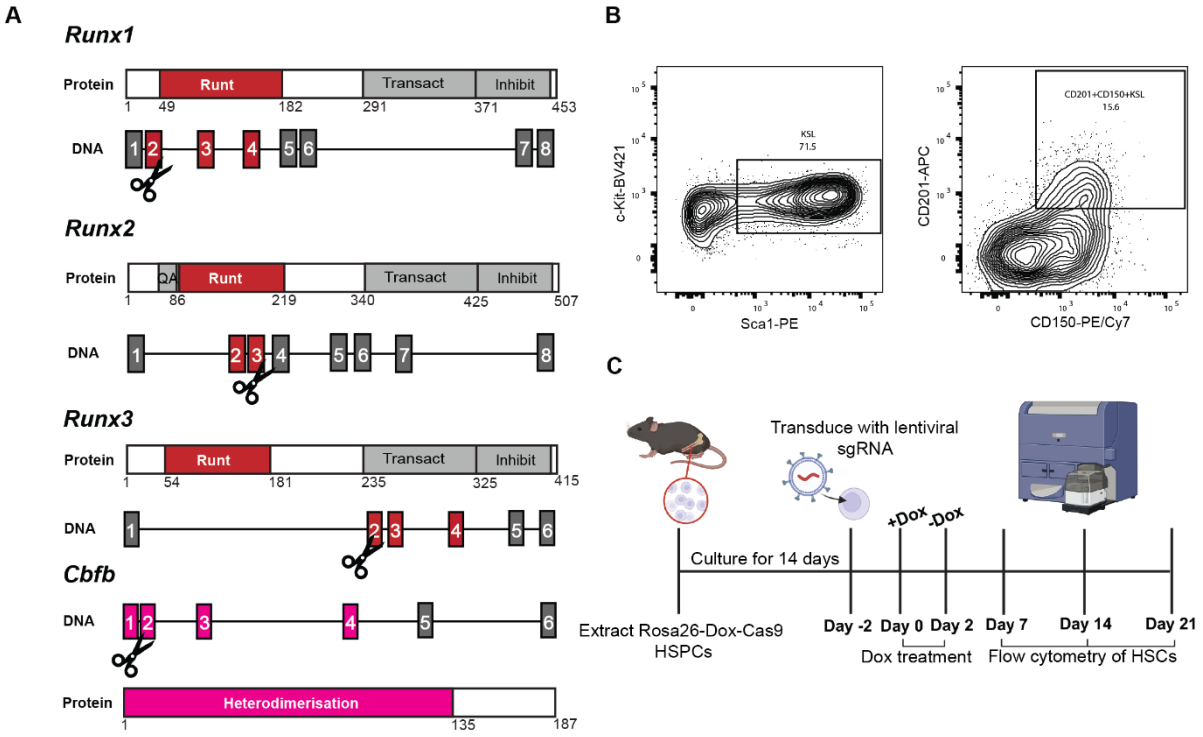

Figure 3.2: Experimental overview of CRISPR-mediated knockout of Runx genes.

(A) Schematic of *Runx* family gene targeting sgRNAs.
(B) Representative flow cytometry plots showing differences in pHSC ($CD201^+CD150^+c\text{-}Kit^+Sca\text{-}1^+Lineage^-$) populations *ex vivo* in *Runx2*-KO and control cultures.
(C) Schematic overview of the experiment. Two sgRNAs targeting *Runx* genes and two control sgRNAs (one non-targeting and one targeting the safe harbour locus *Rosa26*) were used. Created in BioRender.

Both *Runx1* and *Runx2* KOs promoted HSC expansion, up to 3-fold from day 0 to day 21 (**Figures 3.3A-B**). The effect of *Runx3* KO was less pronounced, with ~2-fold expansion from day 0 to day 21 (**Figure 3.3C**). This was only subtly more than the control sgRNAs, which

expanded from 10% pHSC to ~15% pHSC at day 21 as a result of the expansion-promoting PVA culture system.

Cbfb KO had a very different effect on the HSPC cultures, with a rapid ~4-fold expansion of pHSCs between days 0 and 7 then depletion to control sgRNA level for the remainder of the timecourse (**Figure 3.3D**). As *Cbfb* is an essential binding partner of the RUNX proteins, it is likely this phenotype is caused by a loss of function of the RUNX proteins[446–448]. This experiment therefore demonstrated the varying effects on HSC expansion of loss of the different *Runx* family members, and provided a basis for further investigation of the roles of *Runx1*, *Runx2* and the CBF:RUNX interaction in HSC expansion.

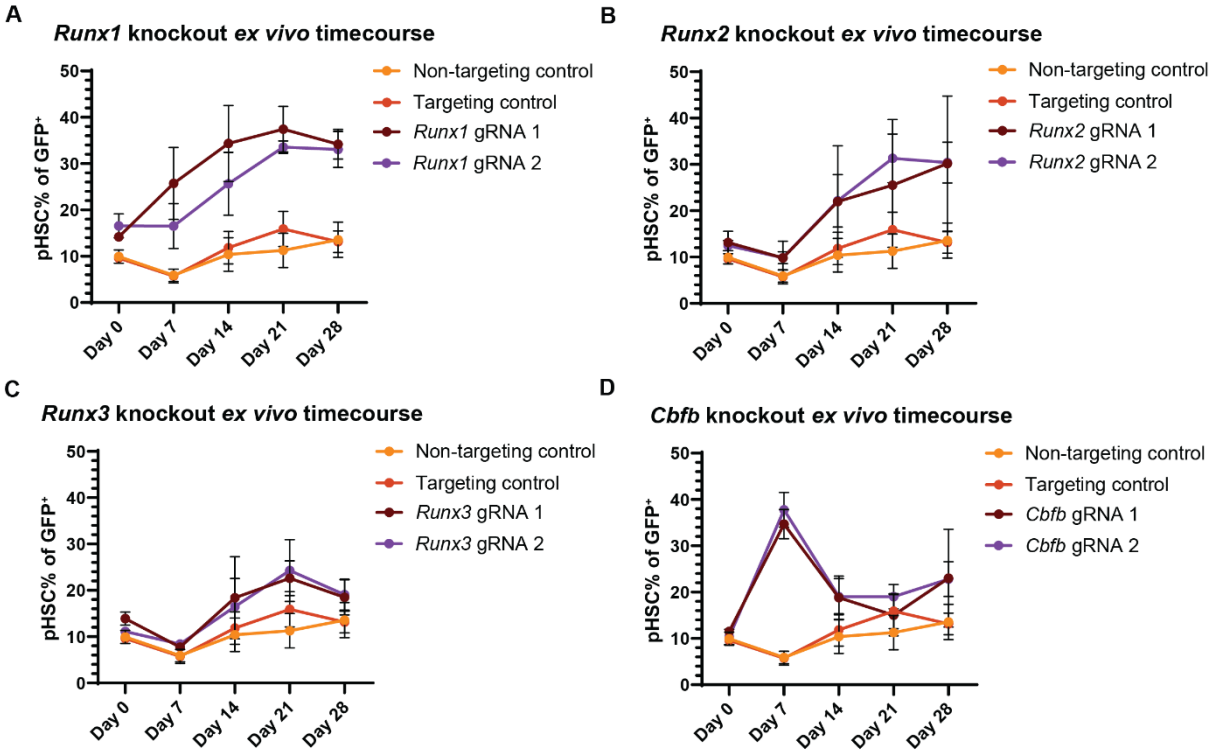

Figure 3.3: CRISPR-mediated knockout of Runx genes enhance HSC expansion, except for the binding partner Cbfb.

(A) *Runx1* knockout timecourse, with 2 control sgRNAs and 2 *Runx1*-targeting sgRNAs. pHSC = $CD201^+CD150^+KSL$. n = 4.
(B) *Runx2* knockout timecourse, with 2 control sgRNAs and 2 *Runx2*-targeting sgRNAs. pHSC = $CD201^+CD150^+KSL$. n = 4.
(C) *Runx3* knockout timecourse, with 2 control sgRNAs and 2 *Runx3*-targeting sgRNAs. pHSC = $CD201^+CD150^+KSL$. n = 4.
(D) *Cbfb* knockout timecourse, with 2 control sgRNAs and 2 *Cbfb*-targeting sgRNAs. pHSC = $CD201^+CD150^+KSL$. n = 4.

3.4 RUNX inhibitors partially recapitulate the *Runx*-deficient HSC phenotype

3.4.1 Inhibitors of RUNX-CBFβ have varying effects on *ex vivo* HSC expansion

As discussed in Chapter 1, there is clinical and biological interest in developing methods to expand HSCs *ex vivo*. Gene KOs may be used, but chemical inhibitors are far preferable as they can induce a transient loss of protein function. The *ex vivo Cbfb* KO experiments showed a rapid expansion of pHSCs, followed by their depletion (**Figure 3.3D**). It was therefore hypothesised that transient inhibition of CBFβ could promote HSC expansion *ex vivo* without depletion.

Several inhibitors of the RUNX-CBFβ interaction have been developed for treatment of human cancers[449–451]. Given the homology and similar roles of the RUNX family in both humans and mice, these inhibitors were tested in the mouse HSPC culture system[225]. Each inhibitor was tested at various concentrations (**Figure 3.4**) in cultures initiated with 100,000 c-Kit$^+$ HSPCs per replicate after 14 days of culture, except CADD522, which was only taken to 7 days of culture due to drug precipitation.

3.4.2 AI-10-47 is toxic to HSCs and depletes HSC purity *ex vivo*

Illendula and colleagues developed a range of small molecule inhibitors such as AI-10-47, which target and interfere with the CBFβ-RUNX interaction[450]. This work focussed on the RUNX1-CBFβ interaction, which in the case of RUNX1 fusion proteins in AML and ALL, represents an important clinical target[223,273,452]. AI-10-47 had an IC_{50} of 3.2 μM, with a concentration of 10 μM weakly inhibiting CBFβ-RUNX binding[450]. A range of concentrations were tested, 0, 2, 5, 10 μM (**Figures 3.4A-B**). The inhibitor was added during complete media changes every 2 days. The percentage of pHSCs and KSL in the culture along with the live cell count were used to understand the effect on the populations. AI-10-47 was toxic to the cells at 10 μM, with a 1000-fold decrease in the live cell count (**Figure 3.4A**). The other

concentrations were better tolerated by the cultures in terms of overall cell survival but resulted in a depletion of pHSC and HSPC (KSL) frequencies (**Figure 3.4B**).

3.4.3 Ro5-3335 can increase pHSC purity *ex vivo* with a toxicity trade-off

Ro5-3335 is another RUNX1-CBFβ, developed by Cunningham and colleagues to target human CBF leukaemia[449]. They found it to be effective in killing CBF leukaemic cell lines and decreasing leukaemic burden in a mouse model. The IC_{50} was between 1.1-21.7 μM in 3 different leukaemia cell lines[449], so 2 and 5 μM were tested with a DMSO control (**Figures 3.4C-D**). At both 2 μM and 5 μM the percentage of pHSCs was significantly increased, albeit subtly (**Figure 3.4D**). The percentage of KSL was decreased at 2 μM, suggesting this is not an HSPC but HSC-intrinsic effect. Both concentrations significantly depleted the number of live cells, with treatment of 2 μM inhibitor causing a 10-fold decrease in live cells and 5 μM a 100-fold decrease (**Figure 3.4C**). Therefore, despite an increase in HSC purity, there was an overall loss of HSC numbers in the culture as a result of Ro5-3335 treatment.

3.4.4 CADD522 is incompatible with the PVA-based HSC system at high concentration

The final inhibitor tested was CADD522, developed by Kim and colleagues as an inhibitor of DNA binding of the RUNX2 Runt domain[449] . RUNX2 activates genes which promote breast cancer progression, and treatment with CADD522 reduced tumour burden and volume in a mouse model and human patient derived xenograft model[451]. It has more recently been used in a primary bone cancer xenograft mouse model, with again promising results in increasing survival and reducing tumour volume and metastasis[453]. In the original paper the IC_{50} was given as 10 nM but was primarily used at 50 μM so 10, 25 and 50 μM concentrations were used in the experiments discussed here. On physical inspection of the wells, it was found that the inhibitor had precipitated in the media, meaning not all cells received the same dose of CADD522. The 50 μM concentration was therefore removed from the experiment. Treatment with 10 and 25 μM appeared to be toxic to the cells, as they promoted a 30 and 60-fold decrease in live cell numbers respectively as compared to the DMSO control (**Figure 3.4E**).

The frequency of KSL cells decreased with 10 μM and 25 μM relative to the DMSO control (**Figure 3.4F**).

In summary, RUNX:CBFβ inhibitors do not represent a suitable way to interrupt the RUNX:CBFβ interaction *ex vivo* in HSPC PVA cultures. Ro5-3353 can increase the HSC purity but has some toxicity to HSCs. Therefore, these RUNX drug treatment strategies were not pursued further within this thesis.

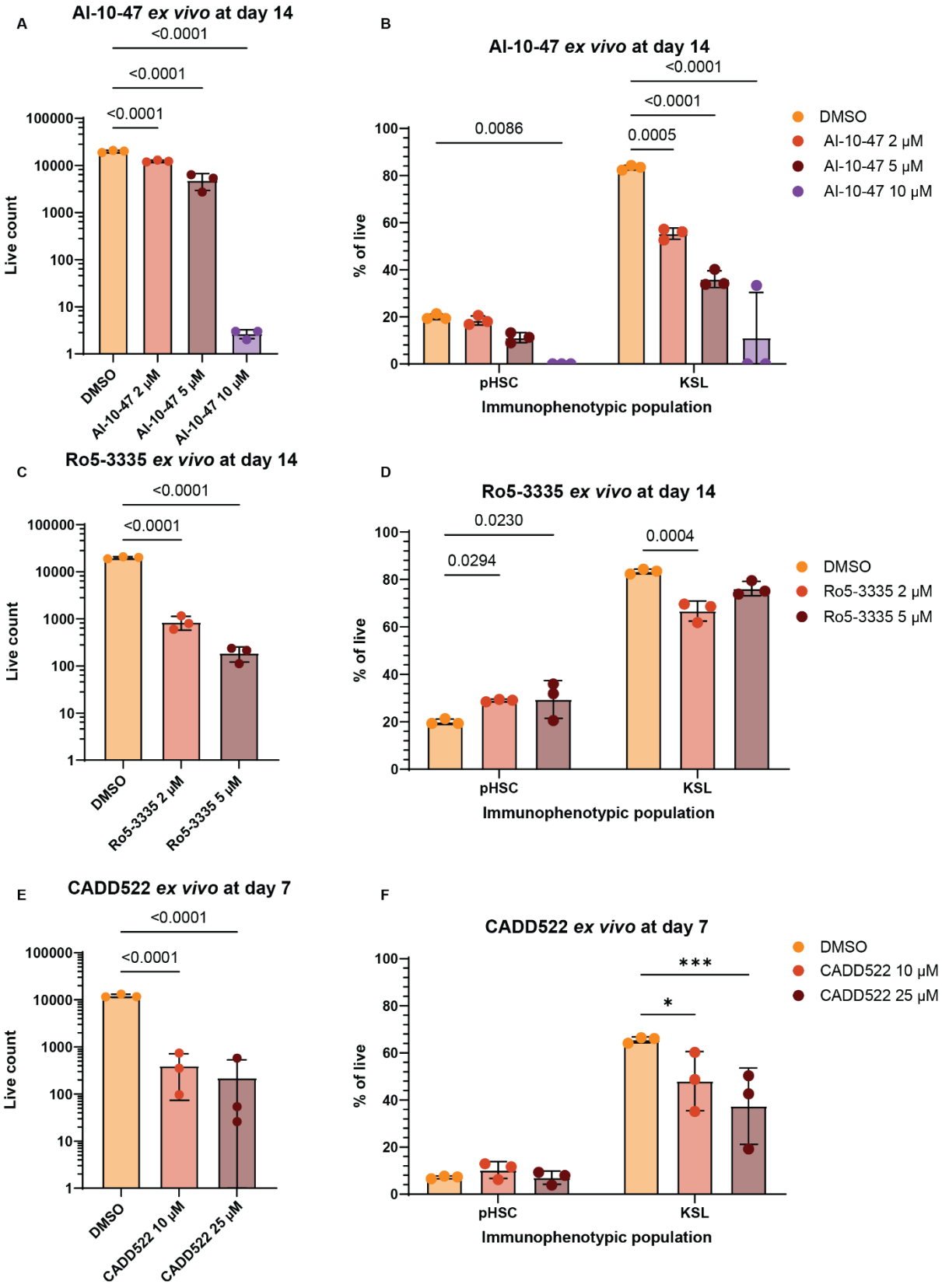

Figure 3.4: RUNX inhibitors partially recapitulate the ex vivo knockout phenotype but have toxic effects.

(A) Live cell numbers after AI-10-47 treatment in *ex vivo* HSC cultures at day 14. n = 3. 2-way ANOVA was performed.
(B) pHSC and KSL frequency in *ex vivo* HSC cultures after AI-10-47 treatment at day 14. n = 3. 2-way ANOVA was performed.
(C) Live cell numbers after Ro5-3335 treatment in *ex vivo* HSC cultures at day 14. n = 3. 2-way ANOVA was performed.
(D) pHSC and KSL frequency in *ex vivo* HSC cultures after Ro5-3335 treatment at day 14. n = 3. 2-way ANOVA was performed.
(E) Live cell numbers after CADD522 treatment in *ex vivo* HSC cultures at day 7. n = 3. 2-way ANOVA was performed.
(F) pHSC and KSL frequency in *ex vivo* HSC cultures after CADD522 treatment at day 7. n = 3. 2-way ANOVA was performed.

3.5 *Runx1* knockout HSCs have increased engraftment but reduced myeloid potential *in vivo*

The *Runx1* KO experiments revealed that *Runx1* is a negative regulator of pHSC expansion *ex vivo*. To observe the broader effects on HSPC function and activity, HSC transplantation assays were performed.

The *Runx1 in vivo* work was performed as part of the revisions for a manuscript from the lab[454], so used a slightly different methodology than the lentiviral CRISPR KO (**Figure 3.5A**). Electroporation was used to knock out *Runx1*, this time with sgRNAs targeting exon 2 rather than 3. The cells were expanded for 14 days post-electroporation before transplantation, with pHSC frequency observed using flow cytometry (**Figure 3.5B**). At day 14, the pHSC frequency was 0.5-fold more in the *Runx1* sgRNA 1 cells as compared to the Cas9-only and *Rosa26* controls, and *Runx1* sgRNA 2 contained 2.5-fold more pHSCs. 10,000 donor c-Kit$^+$ CD45.1$^+$ cells from either *Runx1* sgRNA 1 KO, *Runx1* sgRNA 2 KO or *Rosa26* were transplanted into lethally irradiated CD45.2$^+$ recipient mice alongside 1 million CD45.1$^+$CD45.2$^+$ whole bone marrow competitor cells (**Figure 3.5C**).

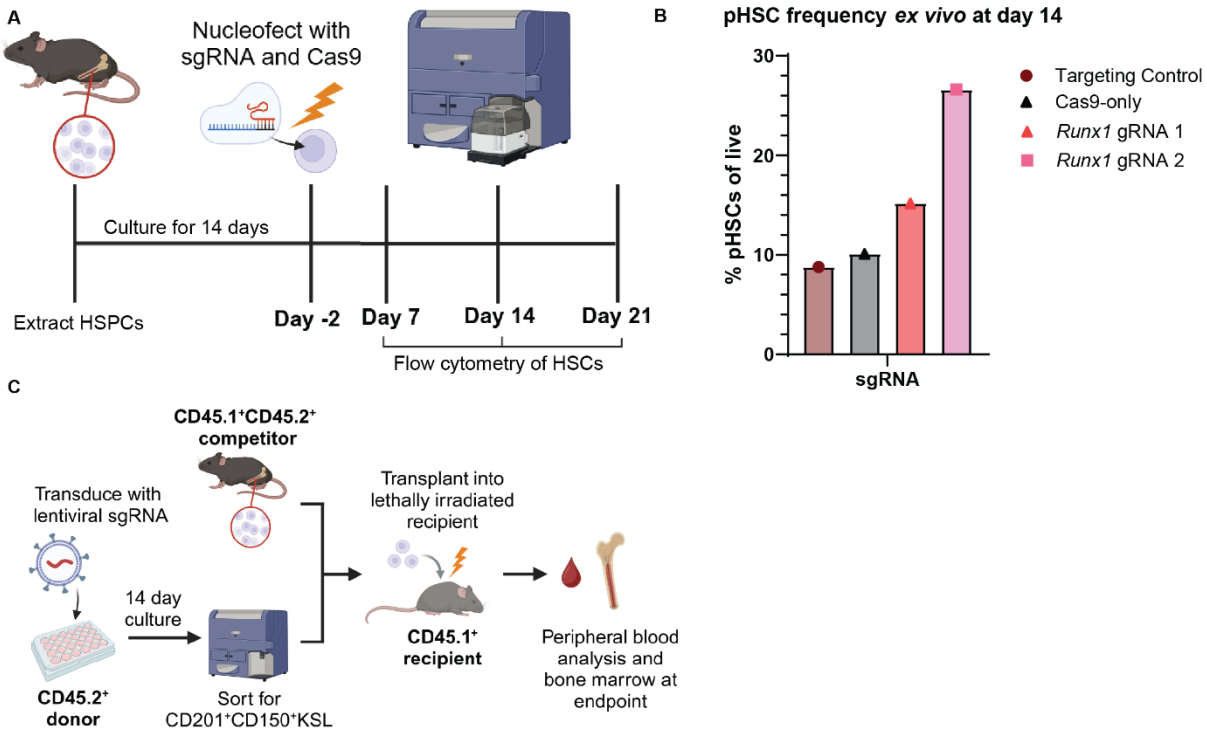

Figure 3.5: Experimental overview for CRISPR-mediated knockout of Runx1.

(A) Schematic overview of the experiment. Two sgRNAs targeting *Runx1* and a control sgRNA targeting the safe harbour locus *Rosa26* were used. Created in BioRender.
(B) *Ex vivo* pHSC frequency at 14 days. n = 1.
(C) Experimental overview of HSC transplantation assay following *ex vivo* culture of c-Kit$^+$ cells from doxycycline-inducible Cas9 mice. 10,000 donor CD45.1$^+$ c-Kit$^+$ cells alongside 1 million CD45.1$^+$CD45.2$^+$ whole bone marrow cells were transplanted into lethally irradiated CD45.2$^+$ recipient mice. Created in BioRender.

Both *Runx1* KO HSPCs displayed higher peripheral blood chimerism than the control cohort at the 4- and 8-week timepoints (**Figure 3.6A**). At the 12-week endpoint only sgRNA 2 had significantly more chimerism than the control. At the bone marrow level, both *Runx1* KOs engrafted significantly better than the control (**Figure 3.6B**). To ascertain the ability of these transplanted HSCs to reconstitute the blood system, the lineage output of the CD45.1$^+$ donor cells was determined (**Figures 3.6C-D**). It was found that the B-cell output was similar across all conditions, but the T-cell output was much lower in the two *Runx1* KO settings (**Figure 3.6C**). The myeloid output was also much higher in the *Runx1* KOs. Chimerism was then investigated across the compartments of the peripheral blood, with chimerism significantly lower than the overall blood chimerism in the B-cells and myeloid chimerism significantly

higher than the overall blood in both *Runx1*-deficient transplantation assays (**Figure 3.6D**). With *Runx1* sgRNA 2, the T-cell chimerism was significantly lower than the overall chimerism. In the control transplantation assay, chimerism of all compartments was not significantly different from the overall blood chimerism. Therefore, *Runx1*-deficient HSCs have an increased engraftment potential but a myeloid bias, resulting in a lymphoid defect.

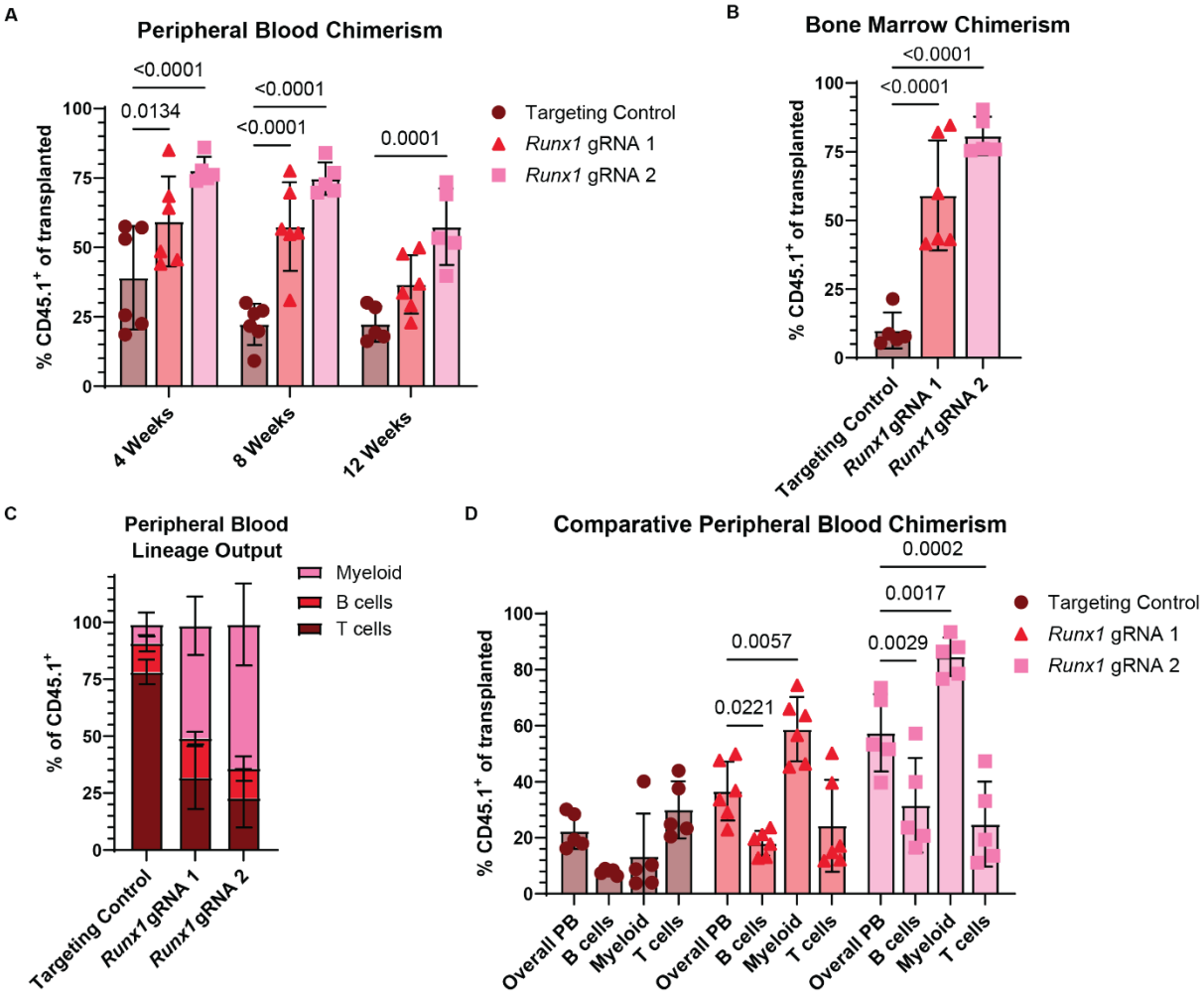

Figure 3.6: CRISPR-mediated knockout of Runx1 enhances HSC expansion and engraftment with a myeloid bias.

(A) Peripheral blood donor chimerism over 12 weeks following transplantation. n = 6. 2-way ANOVA was performed.
(B) Chimerism of overall bone marrow in recipient mice at 12-week endpoint. n = 6. 2-way ANOVA was performed.
(C) Proportion of myeloid, B and T-cells within the CD45.1$^+$ donor peripheral blood cell compartment at the 12-week endpoint. n = 6. 2-way ANOVA was performed.
(D) Peripheral blood donor chimerism of myeloid, T and B-cells at the 12-week endpoint compared to the overall peripheral blood. n = 6. 2-way ANOVA was performed.

Non-significance not labelled.

3.6 *Runx2* knockout HSCs have increased long-term engraftment potential *in vivo* and a T-cell differentiation defect

The *ex vivo* HSPC *Runx2* KO experiments revealed that *Runx2* is a negative regulator of pHSC expansion. To observe the broader effects on haematopoiesis and establish whether these pHSCs are functional HSCs which can engraft into an irradiated recipient to reconstitute haematopoiesis, HSC transplantation assays were performed.

For the *Runx2 in vivo* assay, $CD45.2^+$ Cas9 mice were used for the donor cells, $CD45.1^+CD45.2^+$ were again used for the competitor cells and $CD45.1^+$ for the recipient (**Figure 3.7A**). 14-day cultured HSPCs from these mice were transduced with lentiviral sgRNAs as before, either a non-targeting control, targeting control, or one of the 2 *Runx2*-targeting sgRNAs.

Ex vivo pHSC frequency was tracked over time and it was determined that day 21 was the optimal timepoint for transplantation as there was a 2-fold increase in pHSCs (**Figure 3.7B**). RUNX2 protein loss was confirmed using intracellular flow cytometry. Both sgRNAs had a similar loss of RUNX2, a 6-fold decrease (**Figure 3.7C**).

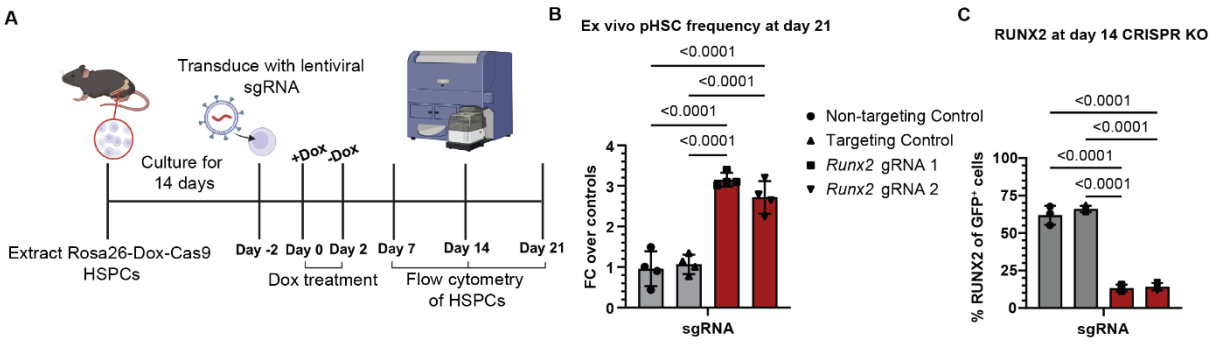

Figure 3.7: CRISPR-mediated knockout of Runx2 enhances HSC expansion.

(A) Schematic overview of the experiment. Two sgRNAs targeting *Runx2* and two control sgRNAs (one non-targeting and one targeting the safe harbour locus *Rosa26*) were used. Created in BioRender.

(B) *Ex vivo* pHSC frequency at 21 days. Data normalised to controls. n = 4.
(C) Intracellular flow cytometric analysis for RUNX2 in control and *Runx2*-KO HSPC cultures. n = 3.

To ensure the fold differences of pHSCs between the conditions did not affect the transplantation assay and therefore directly compare the activity of pHSCs within the HSPC cultures, 2000 CD45.2$^+$ pHSCs were sorted from the cultures and transplanted into lethally irradiated CD45.1$^+$ recipient mice alongside 1 million CD45.1$^+$CD45.2$^+$ whole bone marrow competitor cells (**Figure 3.8A**). There was a non-targeting control, to control for the effect of lentiviral transduction on the HSCs, and a targeting control, to control for the effect of CRISPR activity.

From the earliest timepoint of 4 weeks, peripheral blood CD45.2$^+$ chimerism was significantly higher in *Runx2*-deficient cells, 3-fold over the controls at ~75% relative to ~25% (**Figure 3.8B**). This high-level *Runx2*-deficient donor chimerism persisted throughout the assay, whilst the control donor chimerism dropped to ~15%. In the bone marrow at 20 weeks, the *Runx2*-KO HSCs had a strong competitive advantage, comprising up to 95% of the bone marrow (**Figure 3.8C**). Donor chimerism was plotted for different compartments of the bone marrow and it was consistent across all cell types analysed. This indicated an enhanced engraftment ability mediated by loss of *Runx2*.

Next, to understand the ability of the *Runx2*-deficient cells to reconstitute haematopoiesis, the lineage output of the CD45.2$^+$ donor cells was investigated (**Figure 3.8D**). Myeloid output was similar across all conditions, with *Runx2*-deficient cells producing fewer T-cells and more B-cells. To determine whether this was an increase in B-cell output or decrease in T-cell output, chimerism across all blood cell compartments was plotted (**Figure 3.8E**). It was found that in the two controls, ~50% of T-cells were derived from each cell source (donor and competitor) but in the *Runx2*-deficient transplantation assay, the majority (~75%) came from the wild-type competitor cells. Therefore, *Runx2*-deficient pHSCs were less able to produce T-cells.

The presence of a heightened white blood cell count in the blood can indicate immune-related or cancer pathologies, such as leukaemia or lymphoma[455–457]. Complete blood cell counts

were therefore taken from the recipient mice at the endpoint (**Figure 3.8F**) as an indicator of their overall haematopoietic health. These showed no significant differences between the transplanted cohorts, so the T-cell defect from the *Runx2*-deficient cells must resolve itself via haematopoietic homeostasis *in vivo*.

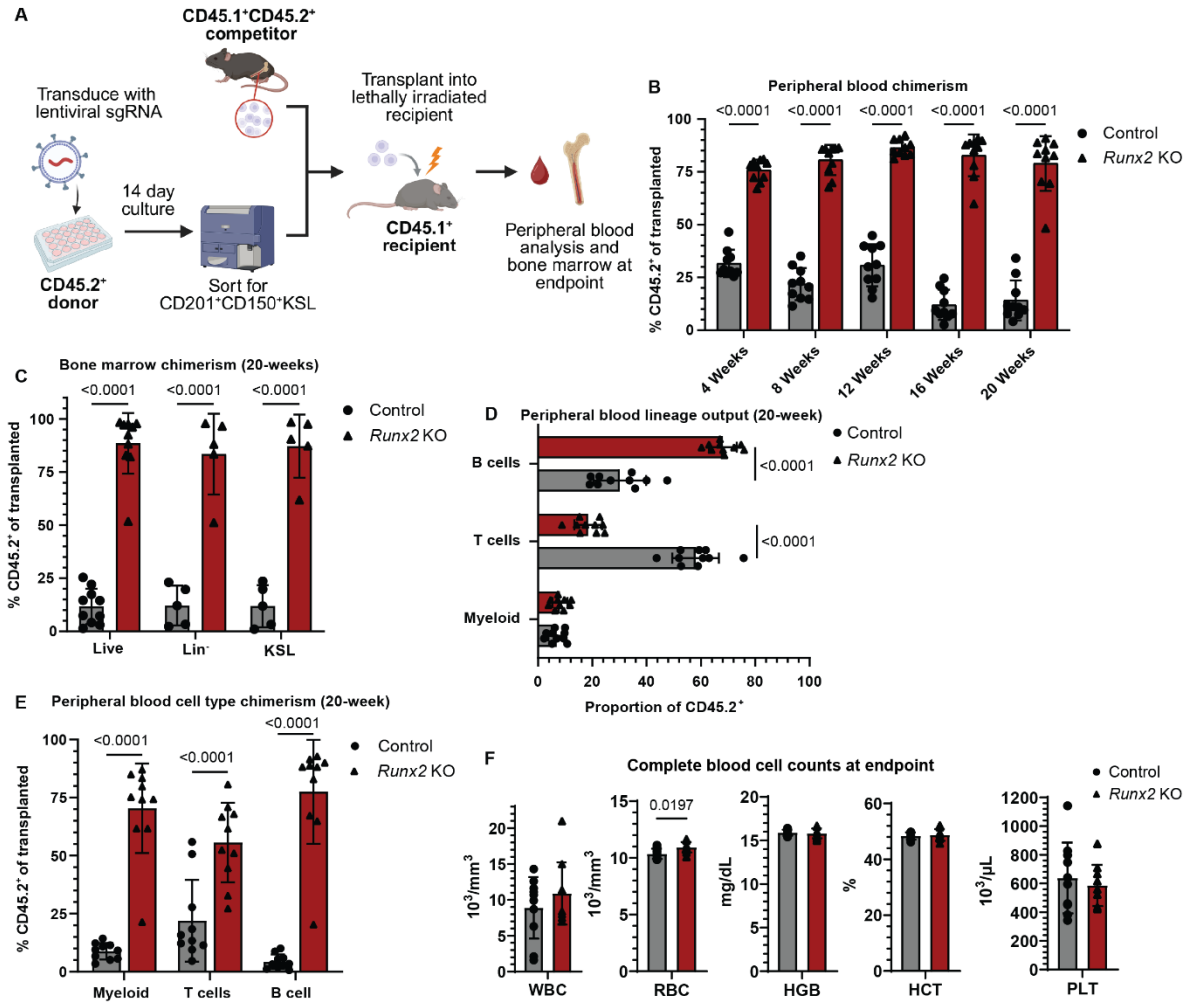

Figure 3.8: CRISPR-mediated knockout of Runx2 enhances HSC expansion and engraftment with a decrease in T-cell output.

(A) Experimental overview of HSC transplantation assay following *ex vivo* culture of c-Kit$^+$ cells from doxycycline-inducible Cas9 mice. 2,000 donor CD45.2$^+$ pHSCs alongside 1 million CD45.1$^+$CD45.2$^+$ were transplanted into lethally irradiated CD45.1$^+$ recipient mice. Created in BioRender.

(B) Peripheral blood donor chimerism over 20 weeks following transplantation. n = 10. 2-way ANOVA was performed.

(C) Chimerism of c-Kit$^+$Sca-1$^+$Lineage$^-$ (KSL), Lin$^-$ and overall bone marrow in recipient mice at 20-week endpoint. n = 5. 2-way ANOVA was performed.

(D) Proportion of myeloid, B and T-cells within the CD45.2$^+$ donor peripheral blood cell compartment at the 20-week endpoint. n = 10. 2-way ANOVA was performed.
(E) Peripheral blood donor chimerism of myeloid, T and B-cells at the 20-week endpoint. 2-way ANOVA was performed.
(F) Complete blood cell counts at 20 weeks post-transplantation in CRISPR transplantation assay recipients. WBC = white blood cells, RBC = red blood cells, HGB = haemoglobin, HCT = haematocrit, PLT = platelet counts. n = 10. Unpaired T test was performed.

Non-significance not labelled.

The ability of HSCs to support long-term haematopoiesis can be assessed by the transplantation of primary recipient bone marrow into secondary recipients[402]. Secondary transplantation assays were therefore performed to investigate the effect of the *Runx2*-deficiency on LT-HSC activity. Whole bone marrow of primary recipients was pooled for each condition and 10 million transplanted into lethally irradiated secondary recipients (**Figures 3.9A-B**). While donor chimerism from the controls was low (~10%), peripheral blood chimerism of the *Runx2*-KO cells remained high throughout this assay (~60%), indicating that loss of *Runx2* boosts LT-HSC activity or frequency.

To summarise, *Runx2*-deficient HSCs were better able to engraft than *Runx2*-wt HSCs, with a decreased T-cell output in the peripheral blood which had no effect on the presence of mature leukocytes. These HSCs were able to reconstitute long-term haematopoiesis and did not cause the recipients to develop leukaemia or other pathologies.

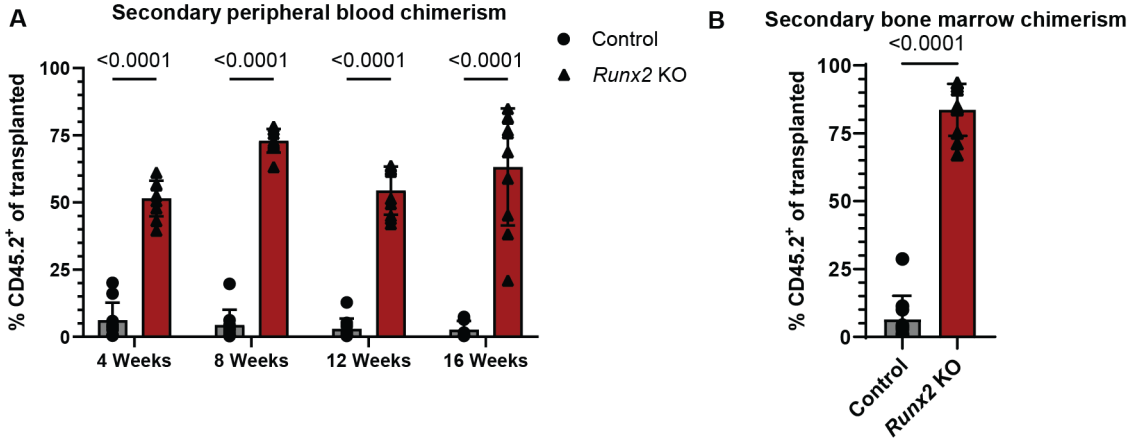

Figure 3.9: CRISPR-mediated knockout of Runx2 enhances LT-HSC engraftment.

(A) Donor peripheral blood chimerism for secondary transplantation assay, with 10 million whole bone marrow cells from primary recipients injected into irradiated secondary recipients. 2-way ANOVA was performed.
(B) Bone marrow chimerism for secondary transplantation assay at 16-week endpoint. 2-way ANOVA was performed.

Non-significance not labelled.

3.7 Conclusion and key findings

In this chapter, I investigated and validated the first genome-wide *ex vivo* HSPC CRISPR screen. 1,310 HSC-specific essential genes were identified, including known HSPC regulators as well as some novel hits. 92 putative negative regulators of HSPC expansion were identified, including the RUNX family of transcription factors. The screen provided a good basis for further investigation of putative negative regulators of HSC expansion, especially of the RUNX factors. Given the screen was performed in HSPCs, a heterogeneous population, experimental validation was required to establish whether these genes have an HSC-specific role.

CRISPR-based gene KOs were used to validate the screen, using the PVA-based *ex vivo* expansion culture. It was found that *Runx1* and *Runx2* KOs promoted pHSC expansion over time in this context, whereas *Runx3* KO did not. Loss of the RUNX family binding partner *Cbfb* causes a rapid but transient ~4-fold expansion of pHSCs which was then followed by depletion. This is consistent with the literature, wherein *Cbfb* cKO adult mice had an increased number of HSPCs but these were unable to engraft in transplantation assays, indicating their short-term nature[327]. Overall, the CRISPR screen was validated via these *ex vivo* KOs in that the *Runx* genes were found to be negative regulators of pHSC expansion. The increased expansion caused by the KOs warranted further investigation of *Runx1*, *Runx2* and *Cbfb* for the rest of this chapter. *Runx3* was not investigated further for several reasons. First, both in the screen and the *ex vivo* KOs *Runx3* had the weakest phenotype. Also, expression of *Runx3* in early haematopoiesis is lower than the other *Runx* genes, with its role generally considered

to be in lymphoid priming and differentiation[319,458] in the adult. For these reasons, it made sense to focus on *Runx1*, *Runx2* and *Cbfb* for their interest and novelty.

The drastic phenotype of the *Cbfb* KO HSPC cultures stimulated me to evaluate pharmacological targeting of RUNX-CBFβ interactions, as a potential approach to boost HSC numbers. The inhibitors tested showed efficacy in other contexts in the literature but had a variety of shortcomings in the *ex vivo* HSPC system. AI-10-47 was toxic and caused decrease of pHSC and HSPC (KSL) purity, Ro5-3335 increased pHSC purity at 5 μM but had a toxic trade-off with an 100-fold decrease in cell viability, and CADD522 precipitated in culture. Future work could test CADD522 in other culture systems, as well as lower concentrations of the other inhibitors or addition of other culture components which could mitigate the toxic effects. In summary, pharmacological inhibition of RUNX interactions represents a potentially interesting clinical avenue for expanding HSCs, but better tolerated compounds are required. The benzodiazepine Ro5-3335 used at 5 μM appeared to be the most viable method of using chemical inhibition to expand HSCs but given the very weak expansion, it was decided to focus on gene KOs for the rest of the thesis.

Runx1 KO promoted HSC expansion *ex vivo* and appeared to promote an increased engraftment ability, but as discussed, the certainty of this conclusion was reduced by the transplantation of a heterogenous cell population. It did appear that the peripheral blood chimerism was starting to decrease at the 12-week endpoint, which could support the literature where *Runx1* KOs have been reported to have a transient expansion of HSCs followed by exhaustion[327,459]. However, as HSPCs were transplanted and the assay only lasted 12 weeks, it is hard to conclude this as there may still have been progenitors contributing to the increased donor chimerism. The lineage output of the *Runx1* KO donor cells was biased to myeloid overproduction, with T-cell output drastically reduced. This myeloid bias is likely to be driving the increased peripheral blood chimerism, and indeed an over proliferation of myeloid progenitor cells in the bone marrow could be driving the increased bone marrow chimerism

but this was not evaluated in these experiments. Myeloid bias with *Runx1* loss has been well characterised in the literature, in both mouse models and human patients with *Runx1/RUNX1* mutations[265,271,273,460,461].

The *Runx2* KOs also promoted expansion *ex vivo*; to assess the phenotype *in vivo* a different experimental design was used with a pHSC sort to better equalise the numbers of HSCs transplanted. The transplanted *Runx2*-deficient pHSCs engrafted up to 10-fold more than the controls in the peripheral blood and bone marrow. The *Runx2*-deficient HSCs displayed a LT-HSC phenotype, as the chimerism persisted across a secondary transplantation assay. Given the reported myeloid depletion caused by *Runx2* overexpression, it is interesting to note that these transplantation assays did not identify any myeloproliferation[462]. These experiments also uncovered a T-cell defect, with a decreased T-cell output from the *Runx2*-KO donor cells. This prompted further investigation to determine whether this is linked to the increased HSC expansion or whether *Runx2* has another role in this context, in Chapters 4 and 5.

Chapter 4: *Runx2* is a previously underappreciated regulator of haematopoiesis

4.1 Introduction

In Chapter 3, I uncovered *Runx2* as a novel regulator of HSC activity in the context of *ex vivo* expansion and subsequent transplantation assays. In this chapter, I explored the effects of *Runx2* loss on steady-state and post-transplantation haematopoiesis, using a *Runx2*^{flox} mouse. This eliminated the confounding nature of the CRISPR-based *Runx2* KOs used in Chapter 3 which gave a mixture of heterozygous KO and homozygous KO (and wild type) alleles. I generated and characterised a previously established *Runx2*^{flox} mouse line bred with a Vav1-iCre recombinase line which localised the loss of *Runx2* to the haematopoietic system[395,400]. This permitted investigation of the phenotype of heterozygous loss of *Runx2* (hereby referred to as *Runx2*-het), complete loss of *Runx2* (hereby *Runx2*-hom) as compared to the wild-type (*Runx2*-wt). As discussed in Chapter 1, *RUNX2* developmental haploinsufficiency in humans causes cleidocranial dysplasia, a bone disorder, but has no significant effects on the adult haematopoietic system[279,304,463]. It could therefore represent an interesting clinical target if haploinsufficiency of *Runx2* gives a similar boost in HSC fitness as complete homozygous loss.

First, I examined *Runx2*-deficient haematopoietic systems at the steady-state by analysing immune cell populations in the bone marrow, thymus, and spleen of young adult and older mice, and by measuring complete blood counts to assess mature blood production.

Next, I tested whether the pHSC expansion seen with CRISPR-based *Runx2* KOs (Chapter 3) could be reproduced using a *Runx2*^{flox} system and investigated the effect of different *Runx2* dosages. To do this, I cultured *Runx2*-hom, *Runx2*-het, and *Runx2*-wt HSCs in the *ex vivo* PVA-based system and tracked pHSC expansion over time.

I then assessed how *Runx2* dosage in cultured pHSCs influences engraftment and blood system reconstitution by performing primary and secondary HSC transplantation assays with *Runx2*-hom, *Runx2*-het, and *Runx2*-wt pHSCs. To compare culture effects, I also transplanted freshly isolated pHSCs. I then endeavoured to understand the biological mechanism of increased HSC frequency in bulk *ex vivo* cultures so expanded the *Runx2*-hom and *Runx2*-wt pHSCs clonally.

Finally, in collaboration with Catherine Chahrour, I studied the molecular mechanisms underlying the increased expansion and engraftment. I performed RNA-seq on cultured $CD201^{+}CD150^{+}$KSL pHSCs to profile transcriptional changes in *Runx2*-hom, *Runx2*-het, and *Runx2*-wt cells. To identify genes directly regulated by RUNX2, I worked with Catherine Chahrour and Dr Alastair Smith to integrate these RNA-seq results with RUNX2 CUT&Tag data from *Runx2*-wt pHSCs. I also included CUT&Tag for H3K4me3 to map active promoters[464–466].

4.2 Adult *Runx2*-deficient mice have no haematopoietic defects at the steady-state

4.2.1 Young adult *Runx2*-deficient mice have no defects in haematopoiesis at the steady-state

To better understand the role *Runx2* plays in the regulation of HSC self-renewal and in the broader haematopoietic system, it was important to elucidate whether its loss affects haematopoiesis at the steady-state.

Thus, I bred $Runx2^{flox}$ mice with Vav1-Cre, localising the loss of *Runx2* to the haematopoietic system[395,400]. Immunophenotypic haematopoietic and immune cell populations within the bone marrow, spleen, thymus, and blood of young (8-12-week-old) *Runx2*-hom, *Runx2*-het and

Runx2-wt mice were compared via flow cytometry (**Figure 4.1**). Gating schema and antibodies used can be found in the Appendices and Chapter 2 respectively.

Firstly, I wanted to determine the effect of *Runx2* deletion on the development of LT-HSCs. These are most enriched in the $CD150^{+}CD48^{-}CD34^{-}$KSL population. Within the bone marrow, the frequency of LT-HSCs in the three genotypes were measured, with no significant differences between them (**Figure 4.1A**). There was a slight increase in the frequency of KSL HSPCs between the *Runx2*-hom and the *Runx2*-wt. This indicates that *Runx2* is likely to have a limited role in regulating developmental or steady-state HSC homeostasis.

For the spleen, the frequencies of three types of T-cells were measured. $CD3^{+}$ T-cells (TCR-expressing cells[360,363]), $CD4^{+}$ T-cells (subset of T-cells recognising MHC class II[360–362]), and $CD8^{+}$ T-cells (subset of T-cells recognising MHC class I[360,362]). There were no significant differences between the frequencies of these in the three genotypes. These results suggest that *Runx2* loss does not alter the steady-state distribution of these T-cell types in the spleen. Other mature cell type frequencies measured in the spleen were B-cells ($CD45R/B220^{+}$[360]), granulocytes ($Gr\text{-}1^{+}$[366,367]), and NK cells ($NK1.1^{+}$[369,370]). These cell types were measured with again no significant differences between the genotypes (**Figure 4.1B**). These findings suggest that *Runx2* loss does not alter the steady-state distribution of major mature immune cell populations in the spleen.

For the thymus, single positive T-cell output ($CD4^{+}$ and $CD8^{+}$) was measured, again with no significant differences between the three genotypes (**Figure 4.1C**). This indicates that *Runx2* is not required for mature T-cell output in the thymus at the steady-state. There were no significant differences in T-cell differentiation in the thymus, with T-progenitor cell frequencies, defined as $CD90^{+}CD25^{+}CD4^{-}CD8$[364,365] and $CD4^{-}CD8^{-}$[149] also measured (**Figure 4.1C**). T-progenitor cells were tracked from DN1-DN3, again with no significant difference in frequency between the genotypes (**Figure 4.1D**). *Runx2* loss therefore does not perturb thymic T-cell development at the steady-state.

Finally, the complete blood counts of the three genotypes were measured to determine any differences between the mature blood cells in the peripheral blood (**Figure 4.1E**). These were also not significantly different, indicating these mice have no overt abnormalities in peripheral blood composition at the steady-state as a result of *Runx2* loss.

Overall, there appears to be no effect of haploinsufficiency or full loss of *Runx2* on haematopoiesis at the steady-state in young adult mice.

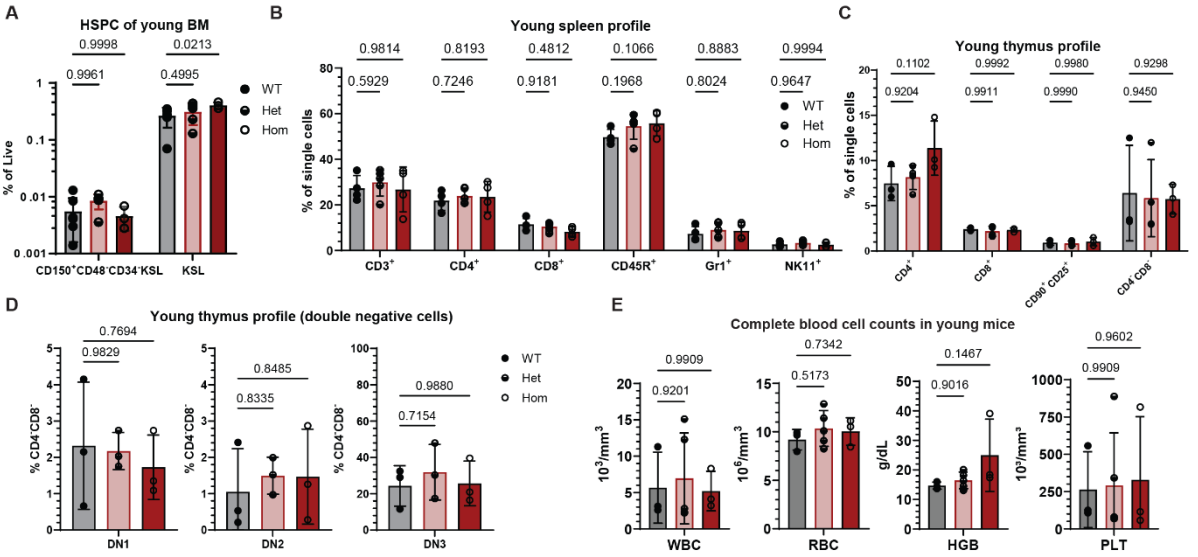

Figure 4.1: Characterisation of young adult Runx2^{flox} mice at the steady-state.

(A) Bone marrow cell frequencies in 8-12-week-old *Runx2*^{flox} mice. n = 3-5. 2-way ANOVA was performed.
(B) Spleen cell frequencies in 8-12-week-old *Runx2*^{flox} mice. n = 3-5. 2-way ANOVA was performed.
(C) Thymus cell frequencies in 8-12-week-old *Runx2*^{flox} mice. n = 3-5. 2-way ANOVA was performed.
(D) Double Negative (DN) cell proportions in the thymi of 8-12-week-old *Runx2*^{flox} mice. DN1 = CD44^{+}CD25^{-}, DN2 = CD44^{+}CD25^{+}, DN3 = CD44^{-}CD25^{+}, DN4 = CD44^{-}CD25^{-}. n = 3-5. 2-way ANOVA was performed.
(E) Complete blood cell counts for 8-12-week-old *Runx2*^{flox} mice. n = 3-5. WBC = white blood cells, RBC = red blood cells, HGB = haemoglobin, PLT = platelet counts. Unpaired T test was used.

Grey bars = *Runx2*-wt, pink bars = *Runx2*-het, red bars = *Runx2*-hom.

4.2.2 Older adult *Runx2*-deficient mice have no defects in haematopoiesis at the steady-state

To gain a more complete picture of the effect of *Runx2* loss in haematopoiesis, these assays were repeated with older mice between 25-34-weeks-old (**Figure 4.2**). Because of limitations in breeding, these were only performed on *Runx2*-het and *Runx2*-wt.

Within the bone marrow, the frequency of $CD150^{+}CD48^{-}CD34^{-}$KSL LT-HSCs had no significant differences between *Runx2*-het and *Runx2*-wt (**Figure 4.2A**). There was also no difference in the frequency of KSL HSPCs. There were 10-fold more LT-HSCs in the older mice than in the young adult regardless of genotype which is consistent with the literature[133,145,467]. This indicates that *Runx2* is likely to have a limited role in regulating developmental or steady-state HSC homeostasis in the older mouse setting.

For the spleen, frequencies of T-cells ($CD4^{+}$, $CD8^{+}$ and $CD3^{+}$) B-cells, granulocytes and NK cells were measured with again no significant differences between the genotypes (**Figure 4.2B**). For the thymus, frequencies of T-cells and T-progenitors ($CD90^{+}CD25^{+}CD4^{-}$CD8 and $CD4^{-}CD8^{-}$) were measured, again with no significant differences between them (**Figure 4.2C**). This implies that *Runx2* haploinsufficiency does not alter the steady-state distribution of major mature immune cell populations in the older spleen.

For the thymus, single positive T-cell output ($CD4^{+}$ and $CD8^{+}$) was measured, again with no significant differences between the two genotypes (**Figure 4.2C**). This indicates that *Runx2* is not required for mature T-cell output in the thymus at the steady-state. There were no significant differences in T-cell differentiation in the thymus, with T-progenitor cell frequencies, defined as $CD90^{+}CD25^{+}$[364,365] and $CD4^{-}CD8^{-}$[149] also measured (**Figure 4.2C**). T-progenitor cells were tracked from DN1-DN3 again with no significant difference in frequency between the genotypes (**Figure 4.2D**). *Runx2* therefore has no role in T-cell differentiation in the thymus in the older mouse steady-state context.

Finally, the complete blood counts of the two genotypes were measured to determine any differences between the mature blood cells in the peripheral blood (**Figure 4.2E**). These were also not significantly different, indicating these older mice have no clear haematological malignancies as a result of *Runx2* haploinsufficiency despite the increased risk for developing pathologies like leukaemia with age[62,145]. Overall, there appears to be no effect of haploinsufficiency of *Runx2* on haematopoiesis in the older mice.

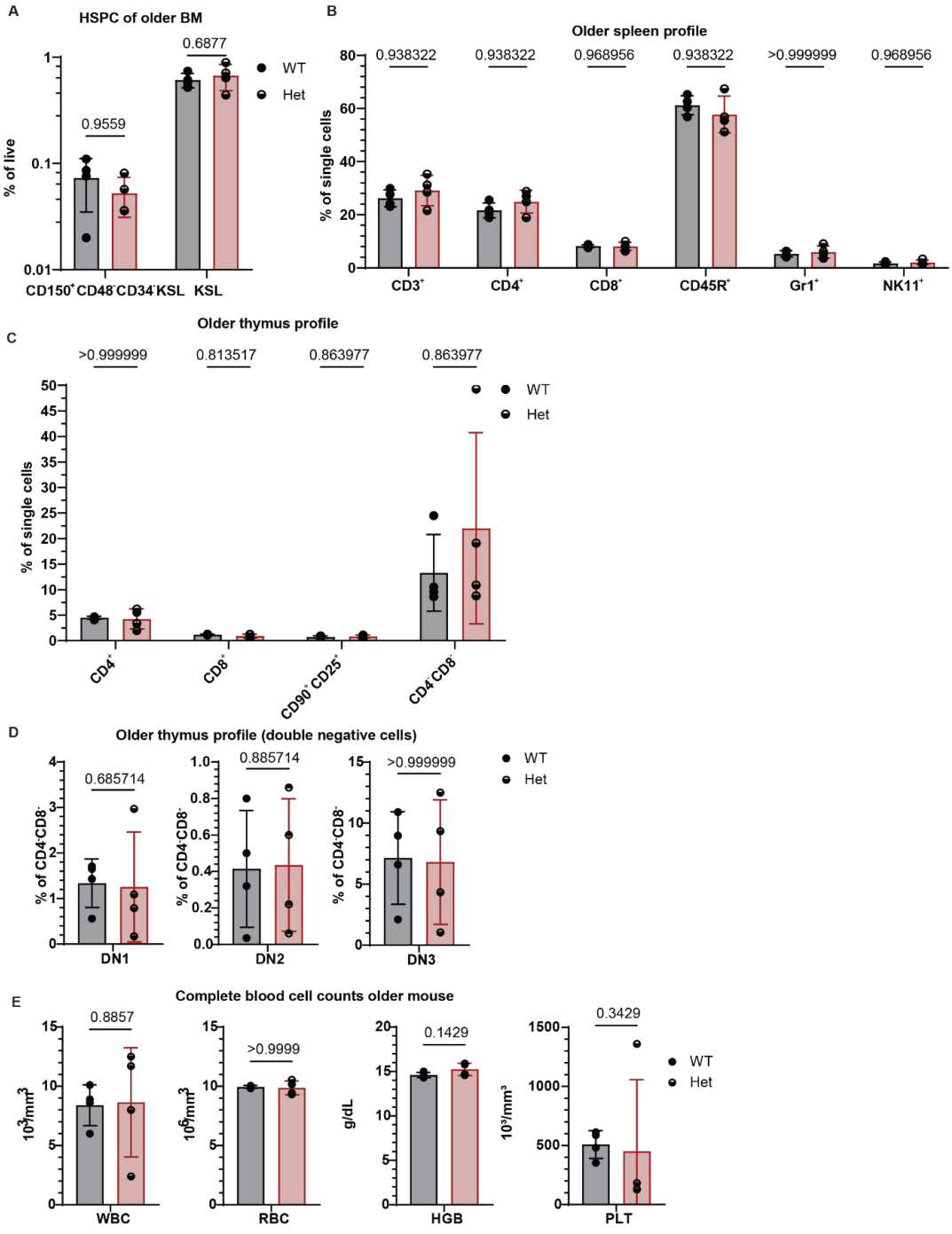

Figure 4.2: Characterisation of older Runx2^{flox} mice at the steady-state.

(A) Bone marrow cell frequencies in 26-34-week-old *Runx2*^{flox} mice. n = 4. 2-way ANOVA was performed.
(B) Spleen cell frequencies in 26-34-week-old *Runx2*^{flox} mice. n = 4. 1-way ANOVA was performed.
(C) Thymus cell frequencies in 26-34-week-old *Runx2*^{flox} mice. n = 4. 1-way ANOVA was performed.
(D) Double Negative (DN) cell proportions in the thymi of 26-34-week-old *Runx2*^{flox} mice. DN1 = CD44^{+}CD25^{-}, DN2 = CD44^{+}CD25^{+}, DN3 = CD44^{-}CD25^{+}, DN4 = CD44^{-}CD25^{-}. n = 4. Unpaired T test was used.

(E) Complete blood cell counts for 26-34-week-old *Runx2*^{flox} mice. n = 4. WBC = white blood cells, RBC = red blood cells, HGB = haemoglobin, PLT = platelet counts. Unpaired T test was used.

Grey bars = *Runx2*-wt, pink bars = *Runx2*-het.

4.3 *Runx2*-het and *Runx2*-hom pHSCs expand better *ex vivo* than WT pHSCs

Next, the investigation of the expansion ability of *Runx2*-het pHSCs and therefore the effect of *Runx2* dosage on *ex vivo* pHSC expansion was performed. Expansion of the *Runx2*-deficient (*Runx2*-hom and *Runx2*-het) CD150^{+}CD34^{-}KSL HSCs were tracked to see if they had an increased expansion as in the CRISPR-based *Runx2* KOs explored in Chapter 3.

CD150^{+}CD34^{-}KSL HSCs were sorted from *Runx2*-hom, *Runx2*-het and *Runx2*-wt bone marrow and expanded *ex vivo* for 21 days in the PVA-based culture system. They were then assayed via flow cytometry to determine the frequency of HSCs at weekly timepoints (**Figure 4.3A**). Both the *Runx2*-hom and *Runx2*-het expanded ~2-fold as compared to *Runx2*-wt by day 21. This is comparatively lower than the ~3-fold expansion seen in the CRISPR KOs at day 21 but still confirmed that loss of *Runx2* increased pHSC frequencies within these expansion cultures. This discrepancy could be due to the CRISPR KOs being performed in 14-day HSPC cultures, as well as other experimental differences like the cell type the cultures were initiated with.

4.3.1 *Ex vivo* expanded *Runx2*-het and *Runx2*-hom HSCs have increased engraftment *in vivo*

After establishing that both *Runx2*-het and *Runx2*-hom pHSCs have increased expansion ability *ex vivo*, the effect *Runx2* dosage has on the engraftment of cultured HSCs, and the long-term reconstitution of the blood system was explored using HSC transplantation assays (**Figure 4.3B**). 10,000 CD45.2^{+} 14-day cultured HSPCs were transplanted alongside 1 million whole bone marrow competitor cells (CD45.1^{+}CD45.2^{+}).

As in Chapter 3, the peripheral blood chimerism was tracked over time to assay the donor cells' ability to produce differentiated cells which migrate into the peripheral blood. The *Runx2*-deficient donor cells phenocopied the CRISPR *Runx2*-KO transplantation assays in Chapter 3, with ~60-80% chimerism in both the *Runx2*-hom and *Runx2*-het transplants as compared to ~10-20% in the *Runx2*-wt (**Figure 4.3C**). The bone marrow chimerism was also assayed at the 16-week endpoint to determine the ability of the donor cells to home to the bone marrow and engraft effectively. The *Runx2*-deficient HSPCs displayed donor bone marrow chimerism of 60-70% compared to ~20% in the *Runx2*-wt setting (**Figure 4.3D**), again phenocopying the increased engraftment ability seen in the CRISPR *Runx2*-KO transplantation assays. Heterozygous loss of *Runx2* is therefore sufficient for increased HSC engraftment ability.

To gain a broader understanding of the how *Runx2*-deficient HSPCs reconstitute haematopoiesis, the donor chimerism across the bone marrow, peripheral blood, spleen and thymi was determined. The donor chimerism across the organs was similar to the peripheral blood and bone marrow, with the *Runx2*-hom and *Runx2*-het HSPCs having significantly higher chimerism than the *Runx2*-wt (**Figure 4.3D**).

To ascertain the lineage potential of the donor cells, the myeloid, T-cell and B-cell output were plotted within the CD45.2^{+} compartment of the peripheral blood. The lineage output of the *Runx2*-het and *Runx2*-hom was again similar to the CRISPR *Runx2*-KO transplantation assays (**Figure 4.3E**), with similar myeloid output from CD45.2^{+} donor cells of all genotypes, increased B-cell output and decreased T-cell output from the *Runx2*-hom and *Runx2*-het donor cells.

To summarise, the *Runx2*-hom and *Runx2*-het HSCs derived from *Runx2*^{flox} mice are phenotypically similar to the CRISPR *Runx2* KOs, with an increased expansion *ex vivo*, increased engraftment *in vivo*, a decreased T-cell output and increased B-cell output in the peripheral blood.

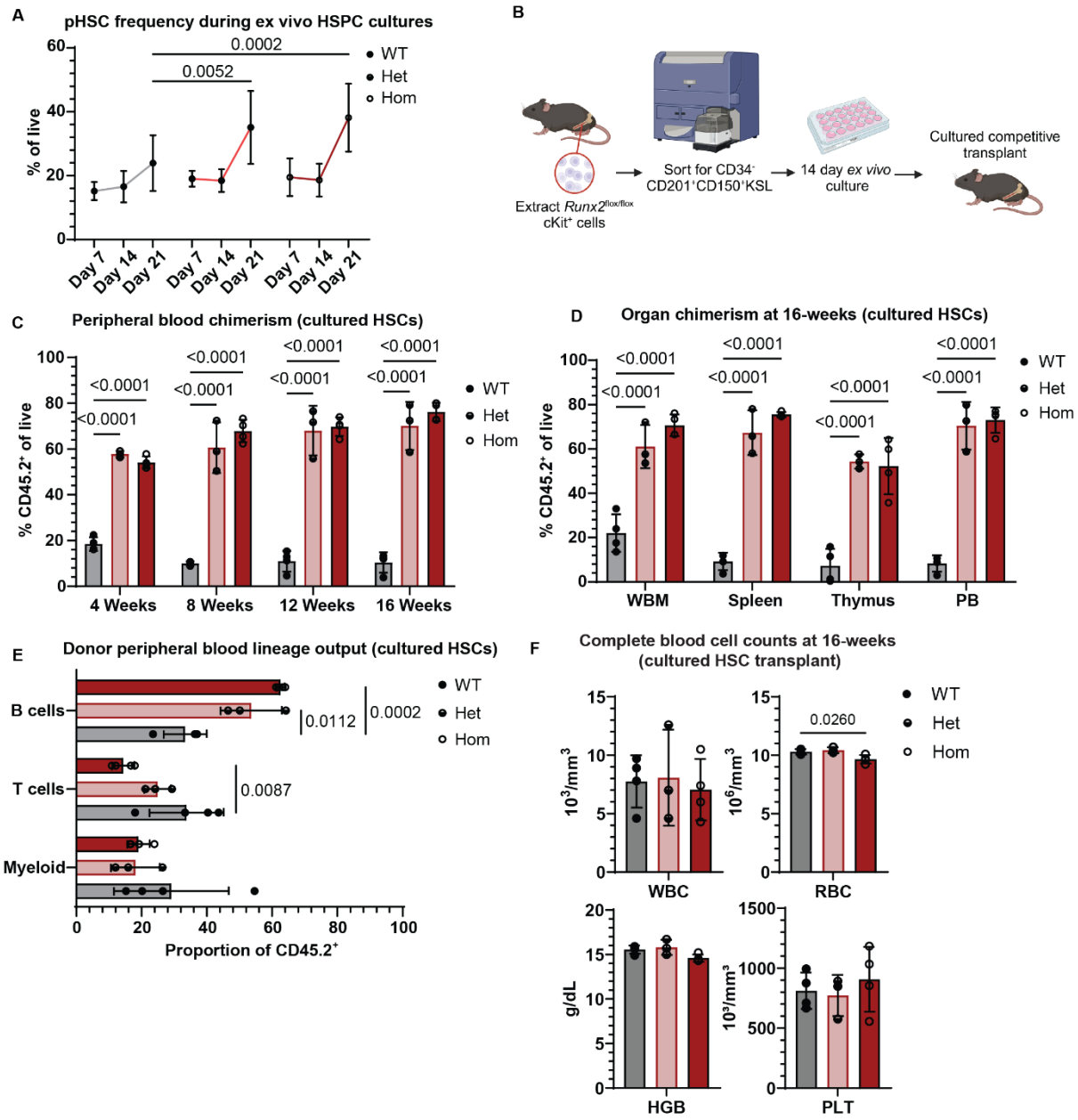

Figure 4.3: Heterozygous loss of Runx2 in cultured HSCs is sufficient to drive increased HSC expansion and reconstitution potential.

(A) Experimental overview for assays exploring the phenotypes of homozygous and heterozygous *Runx2* KO HSCs. Created in BioRender.

(B) *Ex vivo* pHSC frequency over three-week culture. n = 6.

(C) Peripheral blood chimerism of HSC transplantation assay using 10,000 $CD45.2^+$ cultured cells vs 1 million WBM competitor cells ($CD45.1^+CD45.2^+$) n = 3-4. 2-way ANOVA was performed.

(D) Overall bone marrow (WBM), spleen, thymus and peripheral blood (PB) of HSC transplantation assay using 10,000 $CD45.2^+$ cultured cells vs 1 million WBM competitor cells ($CD45.1^+CD45.2^+$). n = 3-4. 2-way ANOVA was performed.

(E) 16-week peripheral blood lineage output of HSC transplantation assay using 10,000 cultured cells vs 1 million WBM competitor cells ($CD45.1^+CD45.2^+$). n = 3-4. 2-way ANOVA was performed.

(F) Complete blood cell counts of 16-week endpoint recipient mice in cultured HSC transplantation assay. n = 3-4. WBC = white blood cells, RBC = red blood cells, HGB = haemoglobin, PLT = platelet counts. n = 10.

Grey bars = *Runx2*-wt, pink bars = *Runx2*-het, red bars = *Runx2*-hom. Non-significance not labelled.

4.3.2 *Runx2* loss improves secondary engraftment and long-term haematopoietic output of cultured HSCs

The primary HSC transplantation assays in **Figure 4.3** showed that cultured *Runx2*-deficient HSPCs have an increased engraftment ability. To test the potential of the *Runx2*-deficient HSCs for supporting long-term haematopoiesis, a secondary transplantation assay was performed (**Figure 4.4**). Here, 5 million whole bone marrow cells from the primary recipients were transplanted into lethally irradiated secondary recipients.

Both the *Runx2*-hom and *Runx2*-het secondary recipients had high peripheral blood chimerism and bone marrow chimerism at the endpoint. This indicates that these *Runx2*-deficient cultured HSCs are able to support long-term haematopoiesis better than the *Runx2*-wt, even with loss of one allele of *Runx2*.

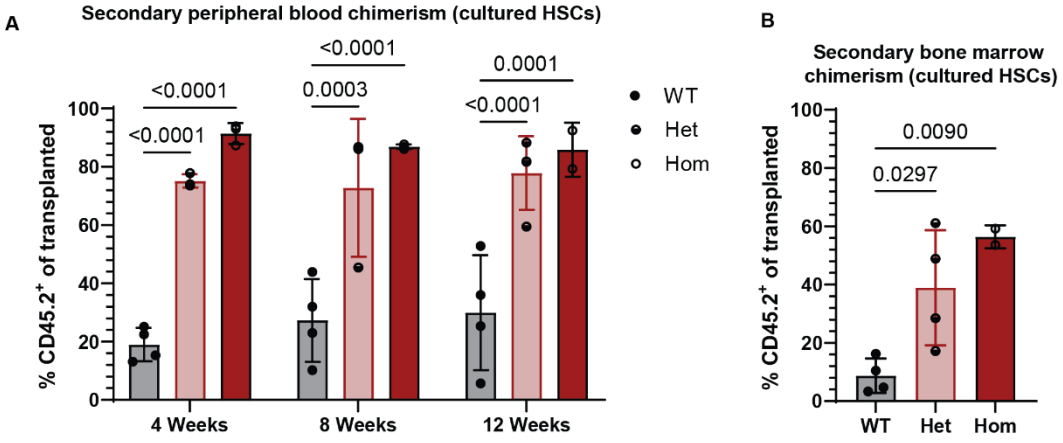

Figure 4.4: Heterozygous loss of Runx2 in cultured HSCs is sufficient to drive long-term haematopoietic reconstitution.

(A) Donor peripheral blood chimerism for cultured HSC secondary transplant, with 5 million whole bone marrow cells from primary recipients injected into irradiated secondary recipients. 2-way ANOVA was performed.

(B) Bone marrow chimerism for cultured HSC secondary transplantation assay at 12-week endpoint. 2-way ANOVA was performed.

Grey bars = *Runx2*-wt, pink bars = *Runx2*-het, red bars = *Runx2*-hom. Non-significance not labelled.

4.4 Fresh *Runx2* deficient HSCs have increased engraftment ability and decreased T-cell output

4.4.1 *Runx2*-deficient fresh HSCs engraft better than WT HSCs

Runx2-deficient HSCs from the CRISPR *Runx2*-KO transplantation assays and *Runx2*^{flox} mice had increased engraftment potential after *ex vivo* culture. To investigate whether the improved engraftment phenotype of the *Runx2*-KOs is dependent on pre-culture or an intrinsic property of the *Runx2*-KO HSCs, fresh *Runx2*-deficient HSCs were evaluated in an HSC transplantation assay (**Figure 4.5**). 100 fresh sorted CD45.2$^+$ LT-HSCs (CD150$^+$CD48$^-$CD34$^-$ c-Kit$^+$Sca-1$^+$Lin$^-$) were transplanted alongside 0.5 million whole bone marrow competitor cells (CD45.1$^+$CD45.2$^+$) (**Figure 4.5A**).

As in **Figure 4.3C**, the peripheral blood chimerism of both the *Runx2*-het and *Runx2*-hom derived CD45.2$^+$ cells was significantly higher than the *Runx2*-wt across the timecourse (**Figure 4.5B**). Fresh *Runx2*-deficient HSCs show a modest competitive advantage over competitor cells compared to cultured *Runx2*-deficient HSCs, with only ~20% higher chimerism over the *Runx2*-wt, versus the ~60% observed in cultured cells (**Figure 4.3C**).

This more subtle competitive advantage of the *Runx2*-deficient donor HSCs was also reflected in the bone marrow, with the overall bone marrow chimerism of *Runx2*-het HSCs achieving ~70% and *Runx2*-hom at ~80%, as compared to ~50% donor chimerism in the *Runx2*-wt setting (**Figure 4.5C**). This contrasted to the ~50% increase in donor chimerism of the *Runx2*-deficient bone marrow as compared to the *Runx2*-wt in the cultured transplants (**Figure 4.3D**).

Looking across the haematopoietic organs (**Figure 4.5C**), the *Runx2*-hom HSPCs had higher chimerism as compared to *Runx2*-wt in all organs except the thymus, which could be linked

to the decreased T-cell output seen in the peripheral blood (**Figure 4.5D**). The *Runx2*-het HSCs however only had a significant difference with the *Runx2*-wt at the bone marrow level.

In the peripheral blood, there was no difference in myeloid output across the genotypes (**Figure 4.5D**) but the *Runx2*-hom had a skew towards B and away from T-cell production as seen in the CRISPR *Runx2*-KO transplantation assays in Chapter 3 and the *Runx2*^{flox} cultured cell transplantation assays in this chapter. This skew was not observed in the *Runx2*-het peripheral blood output, which was similar to the *Runx2*-wt.

The complete blood cell counts were determined for the recipient mice at the endpoint, with no significant differences between the transplanted genotypes (**Figure 4.5E**). This is consistent with the CRISPR and cultured cell transplants **(Figures 3.7** and **4.3**) and suggests that although *Runx2*-deficient HSCs enhance engraftment, they still maintain mature blood cell production required for haematopoietic homeostasis.

In summary, these data show that *Runx2*-hom fresh HSCs have increased engraftment ability, decreased T-cell output and an increased B-cell output. The *Runx2*-het fresh HSCs had a similar, albeit more subtle increase in engraftment ability but a normal lineage output in the peripheral blood. The chimerism in the haematopoietic organs was similar between the *Runx2*-het and *Runx2*-wt, indicating no increased ability to fully reconstitute haematopoiesis by loss of one allele of *Runx2*. The increased engraftment ability of the HSCs upon *Runx2* loss is therefore not dependent on pre-treatment of the cells with *ex vivo* culturing.

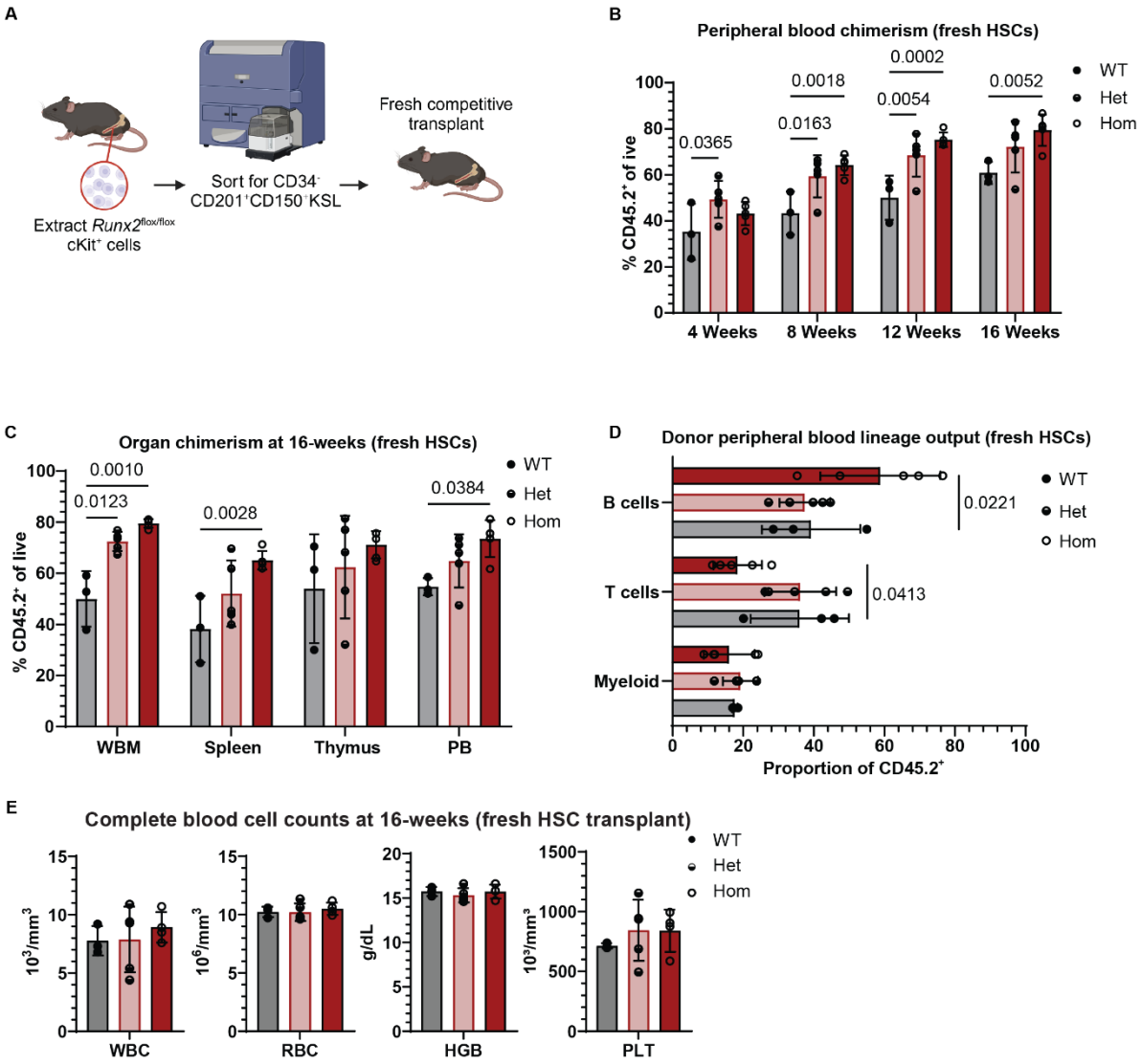

Figure 4.5: Heterozygous loss of Runx2 in fresh HSCs is sufficient to drive increased reconstitution potential.

(A) Experimental overview for assays exploring the phenotypes of homozygous and heterozygous *Runx2* HSCs. Created in BioRender.

(B) Peripheral blood chimerism of HSC transplantation assay using 100 fresh sorted CD45.2$^+$ HSCs vs 0.5 million WBM competitor cells (CD45.1$^+$CD45.2$^+$). n = 3-5. 2-way ANOVA was performed.

(C) Overall bone marrow (WBM), spleen, thymus and peripheral blood (PB) chimerism of HSC transplantation assay using 100 fresh sorted CD45.2$^+$ HSCs vs 0.5 million WBM competitor cells (CD45.1$^+$CD45.2$^+$). n = 3-5. 2-way ANOVA was performed.

(D) 16-week peripheral blood lineage output of HSC transplantation assay using 100 fresh sorted CD45.2$^+$ HSCs vs 0.5 million WBM competitor cells (CD45.1$^+$CD45.2$^+$). n = 3-5. 2-way ANOVA was performed.

(E) Complete blood cell counts at 16-week endpoint of fresh HSC transplantation assays. n = 3-5. WBC = white blood cells, RBC = red blood cells, HGB = haemoglobin, PLT = platelet counts.

Grey bars = *Runx2*-wt, pink bars = *Runx2*-het, red bars = *Runx2*-hom. Non-significance not labelled.

4.4.2 *Runx2* loss improves secondary engraftment and long-term haematopoietic output of fresh HSCs

The primary transplantation assays in **Figure 4.5** showed that *Runx2*-deficient, freshly isolated HSCs have an increased engraftment ability. To test the potential of the *Runx2*-deficient HSCs to support long-term haematopoiesis, a secondary transplantation assay was performed. Here, 5 million whole bone marrow cells from the primary recipients were transplanted into lethally irradiated secondary recipients (**Figure 4.6**).

It was found that the *Runx2*-deficient fresh HSCs can persist at high chimerism throughout the secondary transplantation assay, both in the peripheral blood and the bone marrow (**Figures 4.6A-B**). It is interesting to note that the peripheral blood chimerism of both the *Runx2*-hom and *Runx2*-het secondary transplants (**Figure 4.6A**) is higher than in the primary transplants (**Figure 4.5B**). It is also interesting that the chimerism is very similar between both the *Runx2*-hom and *Runx2*-het. This indicates that the loss of *Runx2* promotes HSC fitness over the long-term, regardless of *Runx2* dosage.

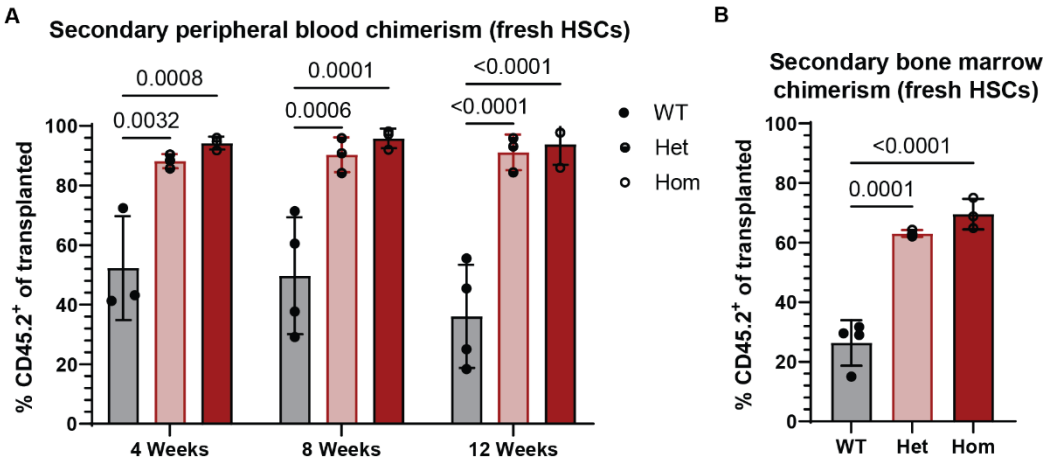

Figure 4.6: Heterozygous loss of Runx2 in HSCs is sufficient to drive long-term haematopoietic reconstitution.

(A) Peripheral blood chimerism from secondary transplantation assay of freshly isolated HSCs, with 5 million whole bone marrow cells from primary recipients injected into irradiated secondary recipients. 2-way ANOVA was performed.

(B) Bone marrow chimerism from secondary transplantation assay of freshly isolated HSCs at 12-week endpoint. 2-way ANOVA was performed.

Grey bars = *Runx2*-wt, pink bars = *Runx2*-het, red bars = *Runx2*-hom. Non-significance not labelled.

4.4.3 Single *Runx2*-deficient HSCs have no increased survival ability or cell division speed but increased self-renewal

Several biological mechanisms could explain the increased pHSC frequency observed in bulk *ex vivo* cultures. One possibility is that *Runx2* loss promotes HSC survival, leading to fewer cells dying compared to wild type. Another is an overall acceleration of cell division, resulting in greater cell numbers in *Runx2*-deficient cultures. Since these cultures favour expansion over differentiation, this would lead to a higher HSC frequency over time. Finally, *Runx2* loss could alter fate decisions: HSCs can divide asymmetrically (self-renewal plus progenitor), symmetrically into two progenitors (differentiation), or symmetrically into two HSCs (self-renewal)[1,30]. A shift towards symmetric self-renewal would expand the HSC pool in *Runx2*-deficient cultures.

To investigate the mechanism underlying the increased expansion of *Runx2*-deficient HSCs *ex vivo*, I performed a clonal assay comparing *Runx2*-hom and *Runx2*-wt cells **(Figure 4.7**). Single $CD150^{+}CD34^{-}$KSL HSCs were plated and cultured for 14 days, after which the entire contents of each well were harvested and analysed by flow cytometry (**Figure 4.7A**). If *Runx2* loss enhanced survival, we would expect more positive wells (wells containing at least one viable cell), but this was not observed (**Figure 4.7B**). Likewise, the total number of live cells per well did not differ significantly between genotypes (**Figure 4.7C**), suggesting that increased proliferation rate was not responsible for the phenotype. However, *Runx2*-hom cultures contained significantly more pHSCs ($CD201^{+}$KSL) per well (**Figure 4.7D**). This indicates that the expansion phenotype is at least partially driven by altered fate decisions, with *Runx2* loss increasing HSC self-renewal. An alternative explanation is that *Runx2* influences HSC cell-cycle regulation; its loss could promote increased cycling specifically in

HSCs, thereby expanding the HSC pool without affecting overall progenitor numbers.

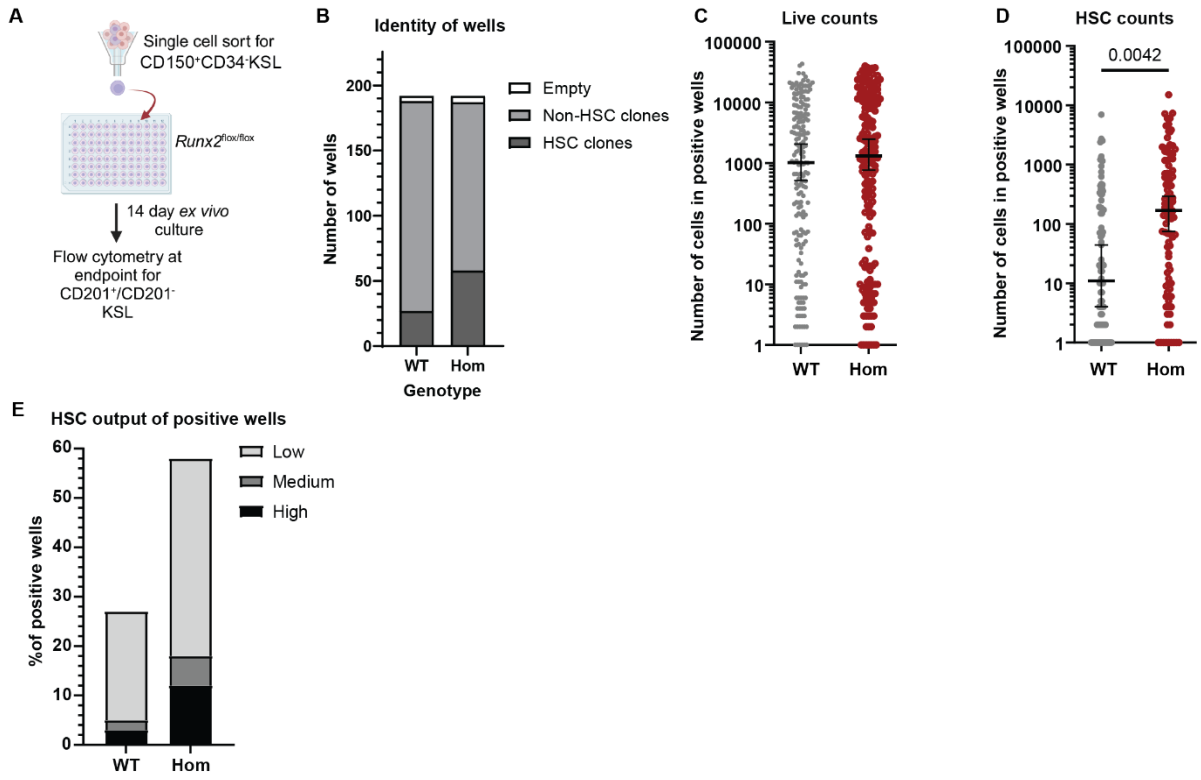

Figure 4.7: Runx2 loss causes an increase in self-renewal potential.

(A) Experimental overview for *ex vivo* clonal plating assays of *Runx2*-hom pHSCs. Created in BioRender.

(B) Clonal identities at 14 days after single HSC plating and number of wells with this identity. Empty = no live cells, HSC clones = clones containing CD201$^+$KSL cells, non-HSC clones = clones not containing CD201$^-$KSL cells.

(C) Number of live cells per positive well 14 days after single cell plating of CD150$^+$CD34$^-$KSL. n = 190. Numbers above data indicate number of positive wells for each genotype. Line at median with 95% CI. Unpaired T-test was performed.

(D) Number of CD201$^+$KSL live cells in wells 14 days after single cell plating of CD150$^+$CD34$^-$KSL. n = 190. Numbers below data indicate number of positive wells for each genotype. Line at median with 95% CI. Unpaired T-test was performed.

(E) Clonal identities at 14-days after single cell plating and percentage of wells with this identity. Low output clones = < 50% CD201$^+$KSL, Medium output clones = 50-75% CD201$^+$KSL, High output clones = > 76% CD201$^+$KSL.

Non-significance not labelled.

4.5 Gene expression profiles vary with *Runx2* dosage in haematopoiesis

4.5.1 *Runx2*-hom HSCs have a different transcriptional programme to *Runx2*-wt

Transcriptional control of HSC activity involves a myriad of genetic interactions and signalling pathways[468]. As RUNX2 is a TF, loss is highly likely to affect the HSC transcriptional programme. To understand the specific genes dysregulated in *Runx2*-deficient HSCs, RNA-seq was performed on 14-day cultured *Runx2*-hom, *Runx2*-het and *Runx2*-wt $CD201^{+}CD150^{+}$KSL pHSCs (**Figure 4.8A**). CUT&Tag was also performed on the same population of sorted cells, discussed in Chapter 4.6. The bioinformatic analysis was performed by Catherine Chahrour.

Initially, PCA analysis was performed on the *Runx2*-hom, *Runx2*-het and *Runx2*-wt samples. This analysis identified a clear separation between the three genotypes, indicating they have different transcriptional programmes as a result of the altered *Runx2* dosage (**Figure 4.8B**).

To understand the genes involved in the different transcriptional programmes between the three genotypes, differential gene expression analysis was next performed. Between the *Runx2*-hom and *Runx2*-wt HSCs, we identified 564 genes that were significantly differentially expressed (DEGs, padj<0.05). 317 were upregulated in the *Runx2*-hom and 247 downregulated (**Figure 4.8C**, **Appendix XIV**). Between the *Runx2*-het and *Runx2*-wt samples, 610 statistically significant DEGs were identified (**Appendix XV**). Of these, 326 were downregulated and 284 upregulated, indicating that *Runx2*-deficiency is associated with broad transcriptional changes that include both gene activation and repression (**Figure 4.8D**). These changes likely reflect a combination of direct and indirect effects of *Runx2* loss.

The DEGs with the highest log-fold change and statistical significance, and therefore the most disparate in expression between the genotypes were identified for the *Runx2*-hom and *Runx2*-het pHSCs (**Figures 4.8E-F**). As *Runx2* was the only overlapping DEG in the top 5 down and

upregulated genes plotted, it was decided to compare the DEGs in both datasets to see how many are consistent between the two cellular contexts.

Surprisingly, there were only 119 DEGs shared between the *Runx2*-het vs *Runx2*-wt and *Runx2*-hom vs *Runx2*-wt settings (**Figure 4.8G**). 53 of these were downregulated and 66 upregulated. One notable commonly downregulated gene was *Ccr7*, encoding a chemokine receptor which has many roles in the immune system such as lymphocyte trafficking, dendritic cell migration and maturation, and suppression of HSC proliferation[469–474]. The presence of this DEG in both the *Runx2*-hom and *Runx2*-het to *Runx2*-wt comparison shows that its downregulation is likely linked to the loss of *Runx2* in these cells.

From these data, it is clear that *Runx2* loss has a broad effect on the transcriptional programme of the pHSCs. This indicates a varied role of *Runx2* in HSCs, with gene activation and repression occurring with its loss which is consistent with its role in other contexts[281,475–477].

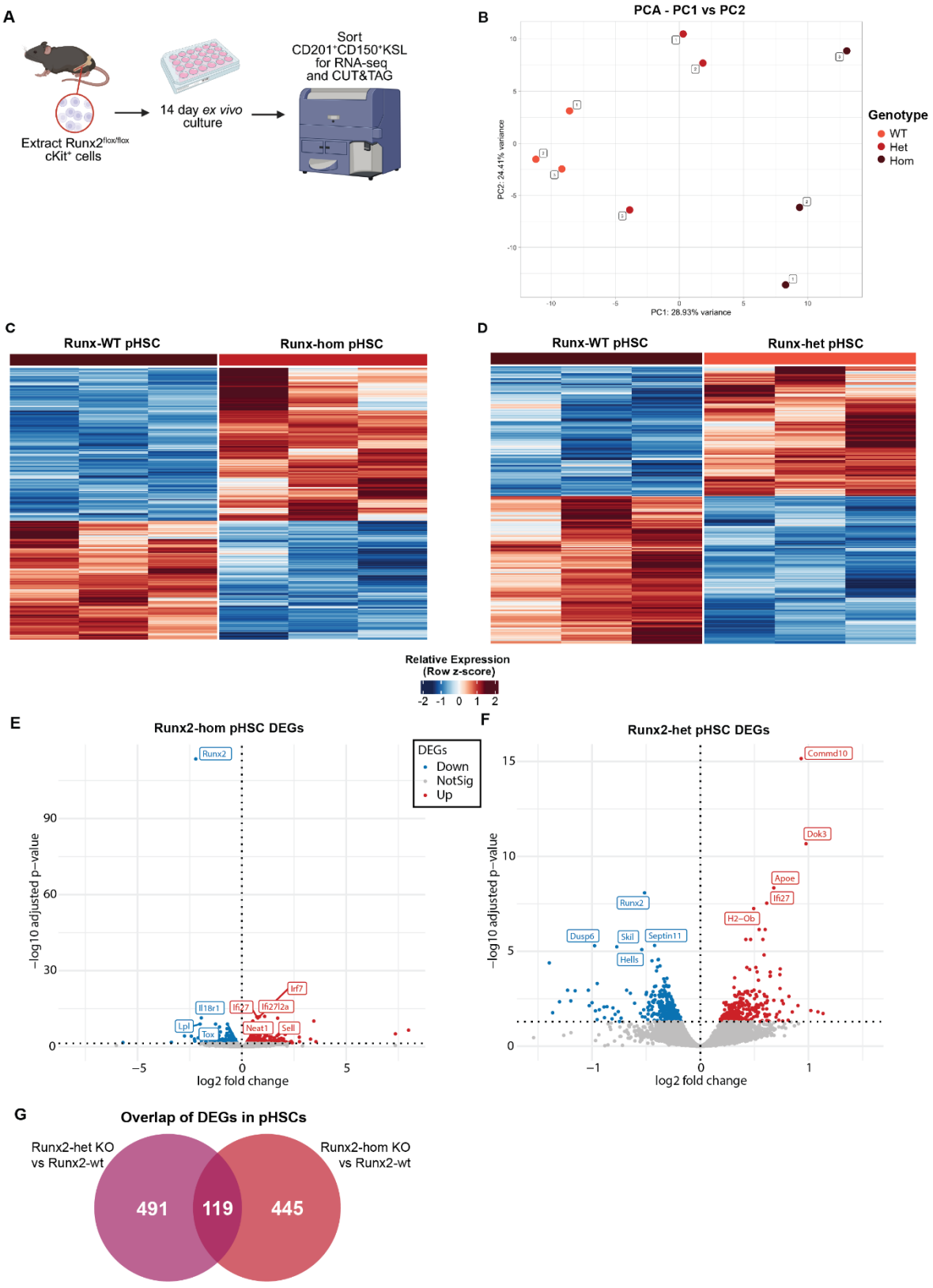

Figure 4.8: Runx2-deficient pHSCs have different transcriptional programmes to Runx2-wt.

(A) Experimental overview for RNA-seq on cultured pHSCs (CD201^{+}CD150^{+}KSL). Created in BioRender.

(B) Principal component analysis of CD201^{+}CD150^{+}KSL pHSC RNA-seq for *Runx2*-hom, *Runx2*-het and *Runx2*-wt
(C) Heatmap of all up and downregulated genes between *Runx2*-hom vs *Runx2*-wt in pHSCs.
(D) Heatmap of all up and downregulated genes between *Runx2*-het vs *Runx2*-wt in pHSCs.
(E) Volcano plot of differentially expressed genes (DEGs) for *Runx2*-hom KO vs *Runx2*-wt in pHSCs.
(F) Volcano plot of differentially expressed genes (DEGs) for *Runx2*-het KO vs *Runx2*-wt in pHSCs.
(G) Overlap of differentially expressed genes (DEGs) between *Runx2*-hom and *Runx2*-het in pHSCs.

4.5.2 *Runx2*-hom pHSCs have increased transcription of interferon-related genes and *Runx2*-deficient pHSCs have altered cell cycle regulation gene expression

As discussed in Chapter 4.5.1, the top DEGs for the *Runx2*-hom and *Runx2*-het pHSCs as compared to the *Runx2*-wt were not conserved between the two *Runx2* dosages. Therefore, to better understand the molecular mechanism driving the increased expansion of *Runx2*-deficient pHSCs, the specific biological pathways differentially expressed in the *Runx2*-hom and *Runx2*-het pHSCs were investigated using Gene Ontology: Biological Process, GO:BP (**Figure 4.9**) and Gene Set Enrichment Analysis, GSEA (**Figure 4.10**).

In the GO:BP analysis, *Runx2*-hom pathways involved with Type I interferon and innate immune response were the most upregulated which have been shown to promote HSC activation and proliferation[110] (**Figure 4.9A**), whereas in the *Runx2*-het it was the antigen processing and presentation and negative regulation of NK cell activity (**Figure 4.9B**). It is interesting to note the lack of overlap with these, despite their similar expansion phenotype *ex vivo*. The broad implication is that there are altered immune pathways in pHSCs with both *Runx2* dosages.

The downregulated pathways in the *Runx2*-hom pHSCs included regulation of the cell cycle and apoptosis (**Figure 4.9C**), which could link to the increased expansion *ex vivo* as there is an altered regulation of the balance of cell proliferation and division. Almost all of the pathways downregulated in the *Runx2*-het pHSCs related to this, such as regulation of mitosis and DNA replication.

Overall, the upregulation of interferon-related gene pathways was interesting given interferon's established role in HSC self-renewal and activation[109,110]. The alterations in

expression of cell cycle and proliferation genes in the *Runx2*-deficient pHSCs could link to the increased expansion seen *ex vivo*. However, further experimental validation would be needed to establish this.

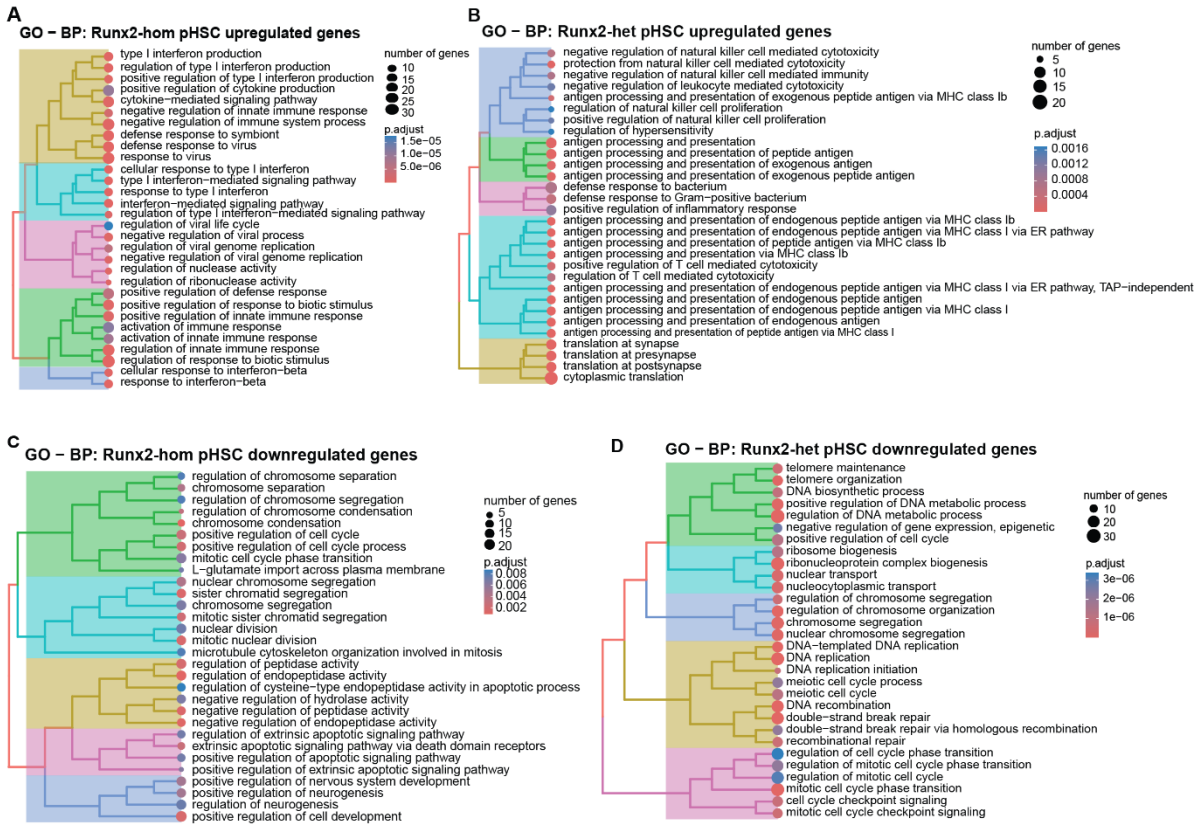

Figure 4.9: Homozygous loss of Runx2 causes increased transcription of interferon signalling genes in pHSCs and Runx2-deficient pHSCs have altered expression of cell cycle genes.

(A) Top 30 upregulated Gene Ontology Biological Process for *Runx2*-hom KO vs *Runx2*-wt pHSC RNA-seq.

(B) Top 30 upregulated Gene Ontology Biological Process for *Runx2*-het KO vs *Runx2*-wt pHSC RNA-seq.

(C) Top 30 downregulated Gene Ontology Biological Process for *Runx2*-hom KO vs *Runx2*-wt pHSC RNA-seq.

(D) Top 30 downregulated Gene Ontology Biological Process for *Runx2*-het KO vs *Runx2*-wt pHSC RNA-seq.

(E) Top 50 significant Gene Set Enrichment Analysis pathways for *Runx2*-hom KO vs *Runx2*-wt pHSC RNA-seq

4.5.3 *Runx2*-deficient pHSCs have upregulated hallmarks of interferon signalling and downregulated hallmarks of cellular proliferation

Examination of the DEGs in the *Runx2*-hom and *Runx2*-het pHSCs revealed little overlap in the top DEGs and upregulated GO:BP pathways. To investigate the molecular pathways dysregulated by *Runx2* loss, GSEA was used to build a picture of the regulatory networks involved in the increased HSC expansion *ex vivo* (**Figure 4.10**).

In the *Runx2*-hom pHSCs (**Figure 4.10A**), it was found that the top upregulated gene sets were the interferon alpha and gamma responses, along with IL6 signalling, which are all present in the *Runx2*-het upregulated pathways (**Figure 4.10B**). In both the *Runx2*-hom and *Runx2*-het, the top downregulated pathways include E2F targets, G2/M checkpoint, MYC targets and the mitotic spindle. The overlap of these gene sets suggests that common transcriptional programmes are altered in both *Runx2*-hom and *Runx2*-het pHSCs, highlighting pathways that may be influenced by *Runx2* deficiency.

The pathways up and downregulated in both contexts in the GSEA are very similar overall, contrasting to the lack of overlap seen in the GO:BP. Conclusions on whether these changes in gene expression are actively or passively effected by *Runx2* cannot be made, however, without identifying which genes RUNX2 binds and therefore regulates in this context.

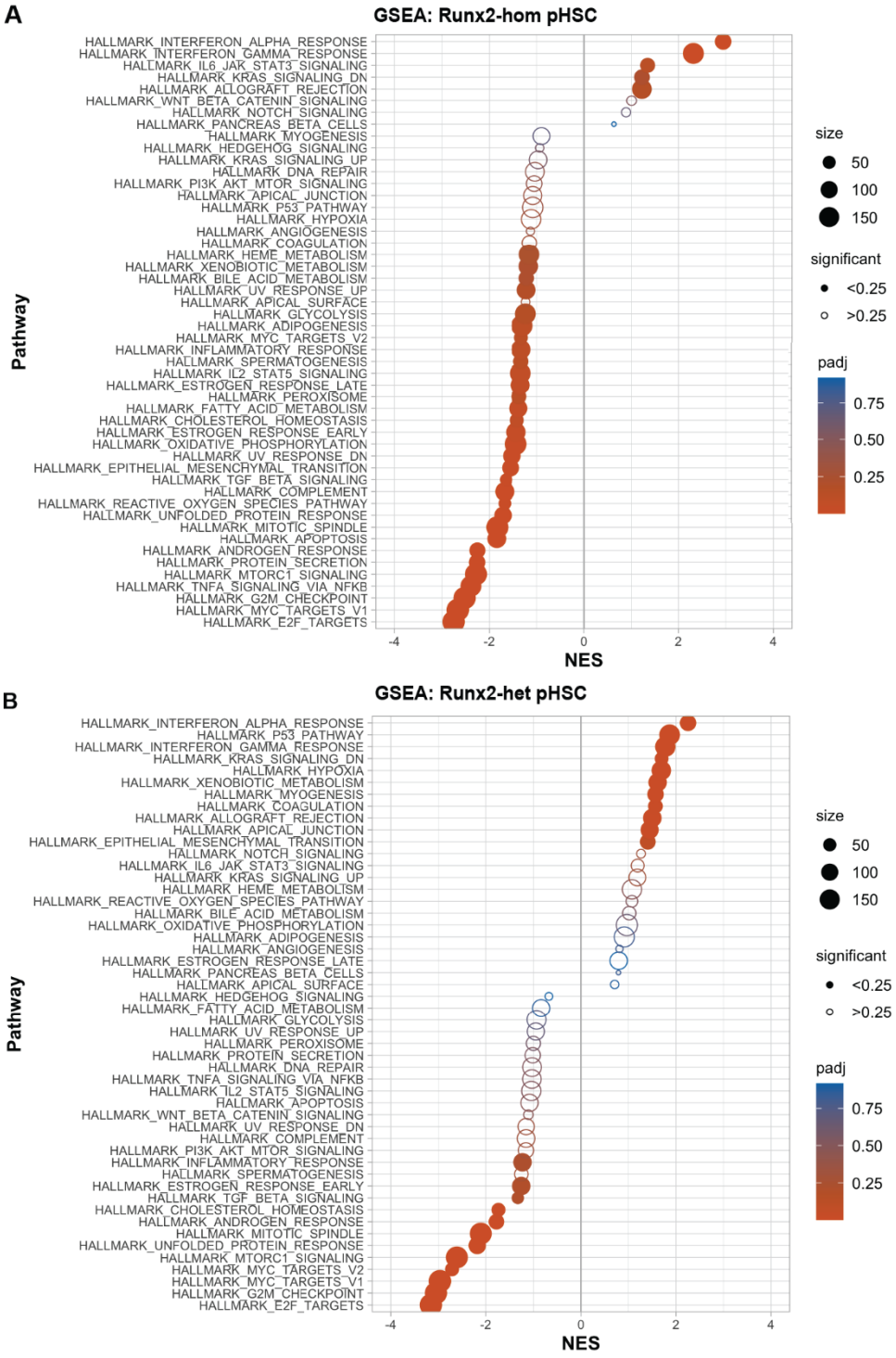

Figure 4.10: Runx2-deficient pHSCs have upregulation of interferon Type I pathways and downregulation of cellular proliferation pathways.

(A) Top 50 significant Gene Set Enrichment Analysis pathways for *Runx2*-hom vs *Runx2*-wt pHSC RNA-seq

(B) Top 50 significant Gene Set Enrichment Analysis pathways for *Runx2*-het vs *Runx2*-wt pHSC RNA-seq

4.6 RUNX2 binds mainly at promoters and is both an activator and repressor in pHSCs

To gain insight into how RUNX2 loss may be actively altering gene expression in pHSCs, CUT&Tag experiments were performed. CUT&Tag is a variation of chromatin immunoprecipitation which requires far fewer cells making it appropriate for usage in rare cell populations such as HSCs[422]. It also initiates with live cells, meaning they are closer to the native state which is important when studying TFs.

To identify putative RUNX2 binding sites in pHSCs, and therefore which genes are likely being regulated by RUNX2 in this context, RUNX2 CUT&Tag was used on sorted *Runx2*-wt $CD201^{+}CD150^{+}$KSL pHSCs after 14 days of culture (**Figure 4.11A**). The downstream processing of the cells was performed by Dr Alastair Smith and analysis performed by Catherine Chahrour. This is the first time RUNX2 binding has been characterized in this way as there is currently no published ChIP-seq or related technique of RUNX2 in HSCs. 15,649 statistically significant binding sites were found and profiled to find which genomic features RUNX2 binds to in HSCs (**Figure 4.11B**). Of these, 58% were gene promoters while ~13% were distal intergenic regions and the rest were within genes. This was different from RUNX2's established binding pattern in osteoblasts, where only 20% of binding was identified in gene promoters[476].

To identify potential binding partners for RUNX2 in pHSCs, motif analysis was then performed (**Figures 4.11C-D**). RUNX2 binding sites were filtered by genes expressed in *Runx2*-wt HSCs (from the RNA-seq in Chapter 4.5) to enrich for likelihood. The most frequent motif was ERF, followed by ELF4 and KLF9. The RUNX motif was also identified, which suggests that RUNX2 is likely to be binding to these sites directly via its DNA binding motif rather than indirectly.

The ERF transcriptional repressor regulates cellular proliferation by controlling the G0/G1 transition[478,479]. Work by Twigg and colleagues identified 130 overlapping transcriptional

targets between RUNX2 and ERF by comparing prostate cancer cells and mouse embryonic fibroblasts[480]. They later concluded that ERF antagonises RUNX2 activity in this context. The enrichment of ERF motifs in RUNX2 binding sites in pHSCs implies that genes controlling the cell cycle transition (as seen in the GSEA, **Figure 4.10**) are regulated by RUNX2.

To better understand the direct vs indirect regulatory role RUNX2 has on the DEGs identified in the RNA-seq, the gene promoter binding sites were integrated with the DEGs (**Figure 4.11E**). RUNX2 was found to be enriched at a similar number of sites in the up and downregulated genes, with a higher proportion of downregulated gene promoters not bound by RUNX2. This corroborates the finding that RUNX2 has both an activating and repressing role in the HSCs' transcriptional regulation.

At the *Runx2* locus, RUNX2 was enriched at the proximal promoter which indicates potential autoregulation (**Figure 4.11F**). Interestingly, there was no peak at the distal promoter site, implying the proximal promoter is preferentially used in HSCs[281,481]. This prompted H3K4me3 CUT&Tag to be performed on these cells, and it was found that there is indeed a peak at the proximal but not at the distal *Runx2* promoter in HSCs.

Overall, these results characterise RUNX2 as a promiscuous TF, with an active role in regulating cellular proliferation in pHSCs.

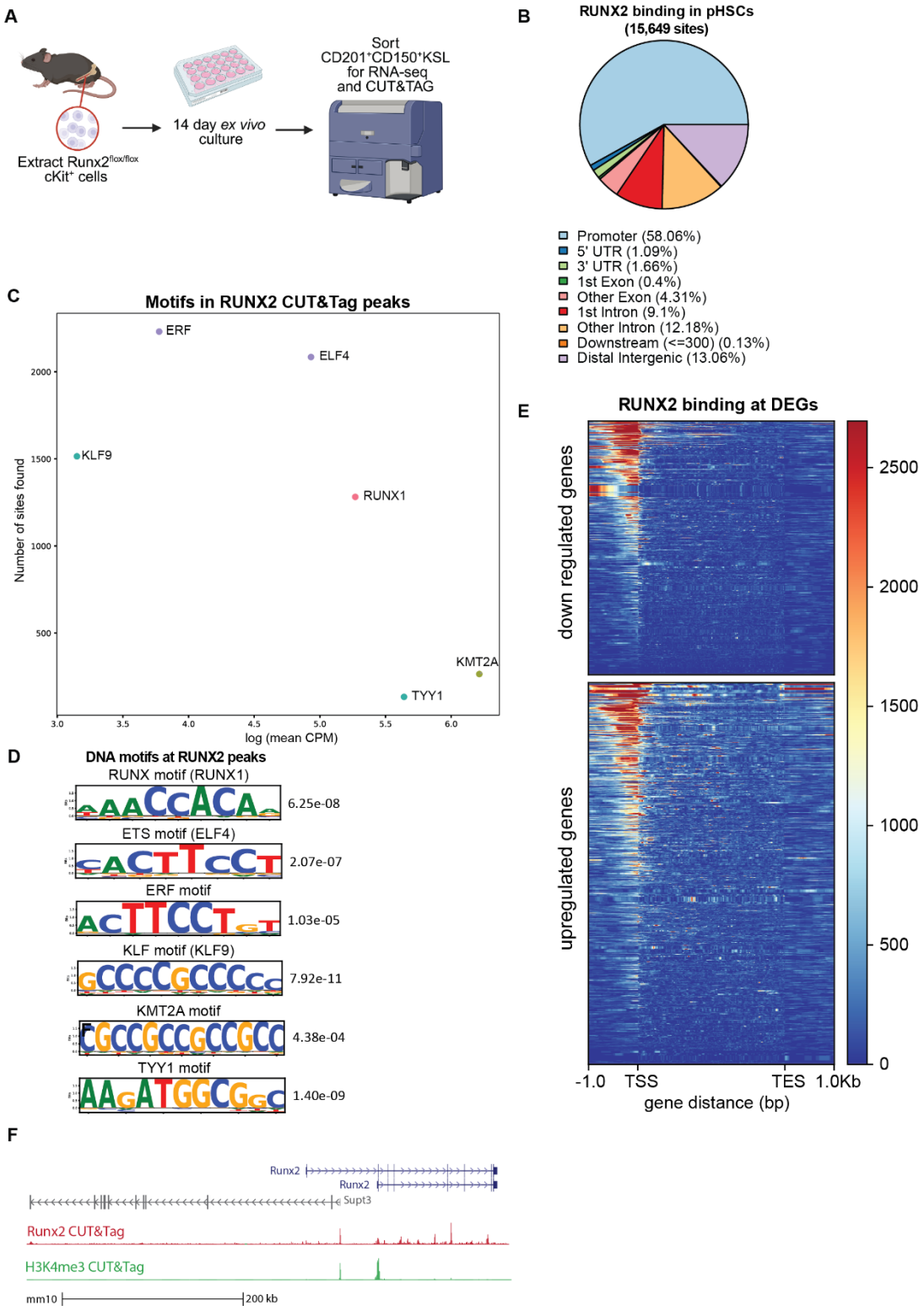

Figure 4.11: RUNX2 has a broad binding pattern in pHSCs and is an activator and repressor in this context.

(A) Experimental overview for CUT&Tag on cultured pHSCs ($CD201^{+}CD150^{+}KSL$). Created in BioRender.

(B) Genomic features present at RUNX2 peaks in *Runx2-wt* pHSCs.

(C) Motif analysis of RUNX2-bound promoter peaks after filtering by genes expressed in *Runx2*-wt pHSC RNA-seq.
(D) Top 6 motifs present in RUNX2-bound promoters after filtered by genes expressed in *Runx2*-wt pHSC RNA-seq. *p*-value was calculated using a null model consisting of sampling motif columns from all the columns in the set of target motifs.
(E) RUNX2 binding across promoters in DEGs from *Runx2*-hom KO vs *Runx2*-wt pHSC RNA-seq.
(F) UCSC Genome Browser[482–484] tracks at the *Runx2* gene locus showing RUNX2 and H3K4me3 CUT&Tag in *Runx2*-wt pHSCs.

4.7 Conclusion and key findings

This chapter aimed to explore the effects of complete and partial loss of *Runx2* on HSC self-renewal and engraftment in the context of steady-state haematopoiesis, *ex vivo* expansion, and haematopoietic reconstitution. I uncovered no discernible effects on the cell types present in any of the haematopoietic organs between the *Runx2*-hom, *Runx2*-het and *Runx2*-wt young adult mice (**Figure 4.1**). This suggests *Runx2* has no role in steady-state haematopoiesis or in formation of the haematopoietic system developmentally and could explain why it has not been characterised in the literature as a negative regulator of HSC activity. Decreased lymphoid output and increased HSC expansion (at least in the short-term) are hallmarks of aged HSCs, so it was important to characterise the older *Runx2*^{flox} mice to determine if *Runx2* loss was promoting an accelerated, aged-like phenotype. There were no discernible effects between the *Runx2*-het and *Runx2*-wt older mice in terms of the mature haematopoietic cells present in the spleen and thymi, or in the T-progenitor cells in the thymi or the frequency of HSCs in the bone marrow (**Figure 4.2**). A next step would be to assess aged cohorts (18-24 months) to understand if *Runx2* has a role in haematopoietic aging.

In a similar way to in this chapter, Growney and colleagues characterised a Mx1-Cre *Runx1* KO mouse and found decreased $CD4^+CD8^+$ thymocytes, decreased DN3 and DN4 thymic progenitor cells, decreased $CD4^+$ and $CD8^+$ circulating T-cells and decreased platelets and white blood cells in the blood[266]. Interestingly, they saw a 3-fold increase in HSCs (as defined by $IL\text{-}7R\alpha^-Lin^-Sca\text{-}1^{hi}$ $c\text{-}Kit^{hi}$) in the bone marrow. These findings are similar to those observed in the recipient mice of the *Runx2*-deficient donor cells (**Figures 4.3-4**). Additionally,

Matthijssens and colleagues demonstrated in Vav-iCre *Runx2* KO mice, both heterozygous and homozygous animals were viable, fertile, and showed no significant differences in blood counts, thymocyte numbers, or T-cell developmental subsets compared to controls[485]. These results indicate that steady-state haematopoiesis and T-cell development are largely unaffected by *Runx2* loss, despite its upregulation in early T-cell progenitors. Therefore, whilst *Runx1* loss affects steady-state haematopoiesis the *Runx2*-deficiency is only pertinent during haematopoietic reconstitution. This difference is important as a key question when discussing the possibility of RUNX2 inhibition for clinical applications is – does *Runx2* loss cause an increased chance of leukaemia in the same way *Runx1* loss/mutation does?[271,486] Clearly the deficiency of the two *Runx* genes is very different, which supports the finding that no *RUNX2* loss of function mutations have currently been linked to increased leukaemic risk. On the contrary, as discussed in Chapter 1, overexpression of *Runx2* drives leukaemic development in several contexts[308,462,477(p20)].

The purpose of using a *Runx2*^{flox} mouse model for these experiments was two-fold. Firstly, to validate the CRISPR *Runx2*-KO transplantation assays to see that the increased expansion *ex vivo* and increased engraftment seen were reproducible with a different system, which they were (**Figure 4.3**). Secondly, the usage of this model permitted investigation of heterozygous *Runx2* KO HSCs. Broadly the *Runx2*-het HSCs had a similar phenotype to the *Runx2*-hom, with increased *ex vivo* expansion and increased engraftment when freshly transplanted and when cultured (**Figures 4.3-4.6**). However, it is interesting to note that the lineage output of the fresh transplanted *Runx2*-het donor HSCs was similar to the *Runx2*-wt, with no defect in T-cell output, whilst still having increased engraftment in the primary and secondary transplantation assays (**Figure 4.5E**). This highlights how haploinsufficiency of *Runx2* could improve engraftment for transplantation therapies without loss of T-cell output.

The comparison of cultured HSPCs to fresh HSCs in HSC transplantation assays provided some interesting findings. Firstly, whilst both transplantation assays showed that *Runx2*-

deficient HSCs have increased engraftment as compared to the *Runx2*-wt, this effect is stronger in the cultured HSC transplantation assay (**Figures 4.3-4.4**). This could be because the PVA system promotes the most competitive HSCs to survive and proliferate throughout the 14-day expansion, in which case it is interesting that *Runx2* loss synergises with this to create a population of more competitive HSCs.

The RNA-seq in pHSCs indicated that as in other cell types (osteoblasts[476], chondrocytes[475], pre-malignant thymocytes[477]), *Runx2* is likely to have an activating and repressing role. It was interesting to note that the *Runx2*-hom and *Runx2*-het comparisons with *Runx2*-wt showed a different array of DEGs and GO:BP terms associated with these (**Figures 4.8-4.9**). The GSEA however had very similar up and downregulated gene sets in both *Runx2* dosages (**Figure 4.10**). This could indicate that while the specific transcriptional outputs of *Runx2* loss differ slightly with *Runx2* dosage, as seen in **Figures 4.3** and **4.5,** the broader pathway-level changes are similar.

Two such conserved upregulated gene sets in both *Runx2*-deficient settings were the IFN-α and IFN-γ signalling pathways, making it likely that increased interferon response is either a result of the *Runx2*-deficient phenotype or driving it. As discussed in Chapter 1, interferon has a complex role in haematopoiesis and response to infection. Stimulation of mouse HSPCs with interferon mobilised HSCs and promoted their proliferation at a cost to their long-term engraftment ability[109]. The effects of interferon vary depending on its chronic or acute treatment[110], and the dosages used in these studies were much higher than the physiological fluctuations present in the endogenous interferon response. Additionally, *Runx2* loss in pDCs led to altered expression of interferon-related regulators, including reduced IRF7 levels and disrupted control of CXCR4, linking RUNX2 to both interferon competence and cellular stress responses[487]. These findings suggest that RUNX2 normally helps fine-tune interferon signalling rather than switching it fully on or off. In HSCs, loss of Runx2 may similarly disturb this balance, resulting in inappropriate activation of ISGs. *Runx2* loss could therefore be

promoting increased interferon production at a level which increases HSC expansion but does not attenuate their long-term reconstitution potential.

RUNX2 CUT&Tag analysis revealed the canonical binding locations of RUNX2 in pHSCs. Using the UCSC Genome Browser and RUNX2 and H3K4me3 CUT&Tag, it was discovered that the proximal promoter is likely to be the primary active promoter in pHSCs (**Figure 4.11**). The proximal promoter is more broadly utilized and distal promoter more bone-specific[281]. A study by Wu and colleagues profiled RUNX2 binding during osteogenesis, its best characterised role in the literature[476]. They found that >70% of RUNX2 binding in osteoblast differentiation was at non-promoter sites, which contrasts to the finding here that 58% of RUNX2 binding in pHSCs is to occupy promoters. However, they used a different bioinformatic tool (and RUNX2 antibody) to characterise these functional sites, so this must be taken into account[476]. Another finding from the CUT&Tag was that the ERF transcriptional repressor motif was the most enriched at the RUNX2 peaks (**Figure 4.11C**). ERF's role is primarily to regulate the G0/G1 transition, which is key for HSC activity as HSCs are mostly quiescent and therefore reside in G0[31,459,488,489]. It also corroborates the finding of cell cycle and proliferation gene sets seen dysregulated in the *Runx2*-deficient pHSCs (**Figure 4.10**) and suggests RUNX2 loss affects cellular proliferation and potentially activation of HSCs.

The single cell clonal expansion assay permitted investigation of the biological mechanism of the increased pHSC frequency *ex vivo*. As discussed, there was no clear survival advantage of the plated pHSCs or an increase in overall numbers, just an increase in pHSC frequency (**Figure 4.7**). As the number of pHSCs was significantly different with *Runx2* loss, the pHSCs could be cycling faster which would link to the cell cycle genes seen dysregulated in the molecular analyses. However, single cell tracking would be needed to validate this.

Extrapolating to the *in vivo* setting, the increased engraftment observed in the bone marrow is unlikely to be explained solely by enhanced HSC robustness or faster cell-cycle progression. This interpretation is supported by the persistence of *Runx2*-deficient HSCs in secondary

transplantation assays (**Figures 4.4** and **4.6**). Short-term HSCs typically cycle more actively but cannot sustain long-term reconstitution, whereas long-term HSCs divide less frequently yet maintain durable haematopoiesis. The ability of *Runx2*-deficient HSCs to support secondary haematopoietic reconstitution therefore suggests that they retain LT-HSC properties, with any changes in cell-cycle dynamics likely to be subtle and compatible with long-term engraftment.

To summarise, this chapter revealed that *Runx2* dosage has context-specific effects on haematopoiesis, with *Runx2*-het and *Runx2*-hom HSCs having similar functional activities *in vivo* and *ex vivo*. *Runx2* loss bolsters *ex vivo* pHSC expansion and long-term engraftment but appears to have no role in steady-state haematopoiesis. Thus, patients with haploinsufficiency of *RUNX2* (CCD) may have HSCs with a better ability to reconstitute haematopoiesis. From the molecular data combined with the single cell expansion assay, it appears *Runx2* has a complex role in cell cycle progression and proliferation which could be linked to interferon production and response.

Chapter 5: *Runx2* has a role in T-cell commitment

5.1 Introduction

5.1.1 Summary of findings in Chapter 4

In Chapter 4, I found that loss of one or two alleles of *Runx2* in HSCs increased long-term engraftment and reconstitution of the haematopoietic system, with the caveat of decreased T-cell output.

There were several unanswered questions arising from these experiments. First, how does the loss of *Runx2* affect T-cell output, and what stage of T-cell differentiation does it affect?

Second, what is the effect of *Runx2* dosage on T-cell output? *Runx2*-het HSCs had different outputs of T-cells in the peripheral blood depending on whether the HSCs had been cultured *ex vivo* prior to transplantation.

Third, what are the molecular regulators of this decreased T-cell output? Is it related to the increased self-renewal phenotype or effected by *Runx2* in another way?

5.1.2 Introduction to Chapter 5

In this chapter, I focussed on the role of *Runx2* in T-cell commitment and differentiation. First, I summarised the findings of HSC transplantation assays performed in Chapter 4, as I then analysed the thymi of the recipient mice, focussing on the production of early T-progenitor cells. I also assessed how *Runx2* affects early reconstitution of the thymus, as well as the contribution to lymphoid precursor populations in the bone marrow by performing short-term transplantation assays. I then investigated the effect *Runx2* loss has on the cells' intrinsic ability to pass through the phases of early T-cell commitment by using *ex vivo* T-cell differentiation assays in collaboration with Matthew Nicholls. Finally, in collaboration with Catherine Chahrour, I explored the transcriptional consequences of *Runx2* loss in

haematopoietic progenitor cells (pHPCs) by comparing the transcriptional profile of *Runx2*-hom and *Runx2*-het cells with *Runx2*-wt.

5.2 *Runx2*-deficient HSCs have a decreased T-cell output

5.2.1 Fresh *Runx2*-deficient HSCs have fewer circulating T-cells

To further characterise the altered T-cell output seen in the transplantation assays in Chapter 4.4, the thymi and peripheral blood compartments of the recipient mice were investigated. The experimental overview is shown in **Figure 5.1A** and lineage output of the CD45.2$^+$ cells in the peripheral blood for reference in **Figure 5.1B**.

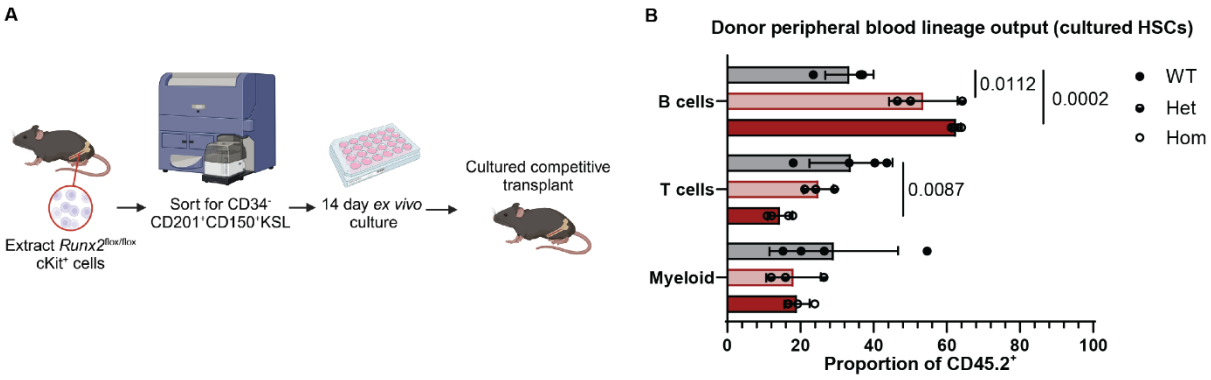

Figure 5.1: Summary of relevant findings from Chapter 4.

(A) Experimental overview for assays exploring the phenotypes of fresh homozygous and heterozygous *Runx2* KO HSCs. Created in BioRender.

(B) 16-week peripheral blood lineage output of HSC transplantation assay using 100 fresh sorted CD45.2$^+$ pHSCs vs 0.5 million WBM competitor cells (CD45.1$^+$CD45.2$^+$). n = 3-5. 2-way ANOVA was performed.

Grey = *Runx2*-wt, pink = *Runx2*-het and red = *Runx2*-hom. Non-significance not labelled.

To investigate this phenotype further, the donor chimerism of individual cell types was tracked across the peripheral blood (**Figure 5.2A**). Compartments of the peripheral blood were compared for each donor genotype to observe which blood cell type was more affected by the loss of *Runx2*. If the chimerism of a cell type is similar to the overall peripheral blood chimerism in the *Runx2*-deficient setting, it is likely this cell type is not affected by the loss of *Runx2*. If

the chimerism is lower than the overall peripheral blood however, it is likely that loss of *Runx2* reduces the HSPCs' ability to produce this cell type in the peripheral blood. The B-cell and myeloid chimerism in both *Runx2*-deficient transplantation assays had no significant difference to the *Runx2*-wt, indicating that loss of *Runx2* does not affect output of these cells in the peripheral blood. This suggests that the increase in B-cell output seen in **Figure 5.1B** is likely to be a lineage switch from T to B-cell in lymphoid differentiation caused by the loss of *Runx2*. In both the *Runx2*-hom and *Runx2*-het transplantation assays, donor peripheral blood T-cells had lower chimerism than the overall peripheral blood (**Figure 5.2A**). In the *Runx2*-het both $CD4^+$ and $CD8^+$ T-cells had significantly decreased chimerism and in the *Runx2*-hom, only the $CD8^+$ T-cells displayed a significant decrease. This suggested *Runx2* loss decreases T-cell output. This is interesting given the *Runx2*-het derived donor cells had a comparable lineage output to the *Runx2*-wt (**Figure 5.1B**).

5.2.2 Fresh *Runx2*-deficient HSCs have a buildup of early T-cells in thymus

Given the decreased T-cell output observed in the peripheral blood, the thymi were analysed at the endpoint to investigate the effect of loss of *Runx2* in the stages of T-cell differentiation (**Figures 5.2B-D**). The T-cell output in the $CD45.2^+$ compartment of the thymi showed *Runx2*-hom producing a higher proportion of double positive (DP) $CD4^+CD8^+$ cells than *Runx2*-wt and a lower proportion of $CD4^+$ (**Figure 5.2B**). The double negative stages (DN, **Figure 5.2C**) had no significant differences between genotypes, but the *Runx2*-hom displayed a modest increase in DN1 cells (**Figure 5.2D**). $CD90^+CD25^+$ cells represent pro-T-cells, a T-progenitor cell stage which sit between DN1 and DN4 in the differentiation[364,365]. The proportion of $CD25^+CD90^+$ progenitor cells was similar across the genotypes (**Figure 5.2E**).

Overall, this suggests a potential role for *Runx2* in the normal progression through the DN stages but that any defect in the *Runx2*-deficient setting can be compensated, perhaps by proliferation later in T-cell differentiation. As there was no decrease in single positive T-cells

in the thymus, it appears that *Runx2* is not required for the later stages of T-cell development or selection in the thymus but could have a role in T-cell egress into the peripheral blood.

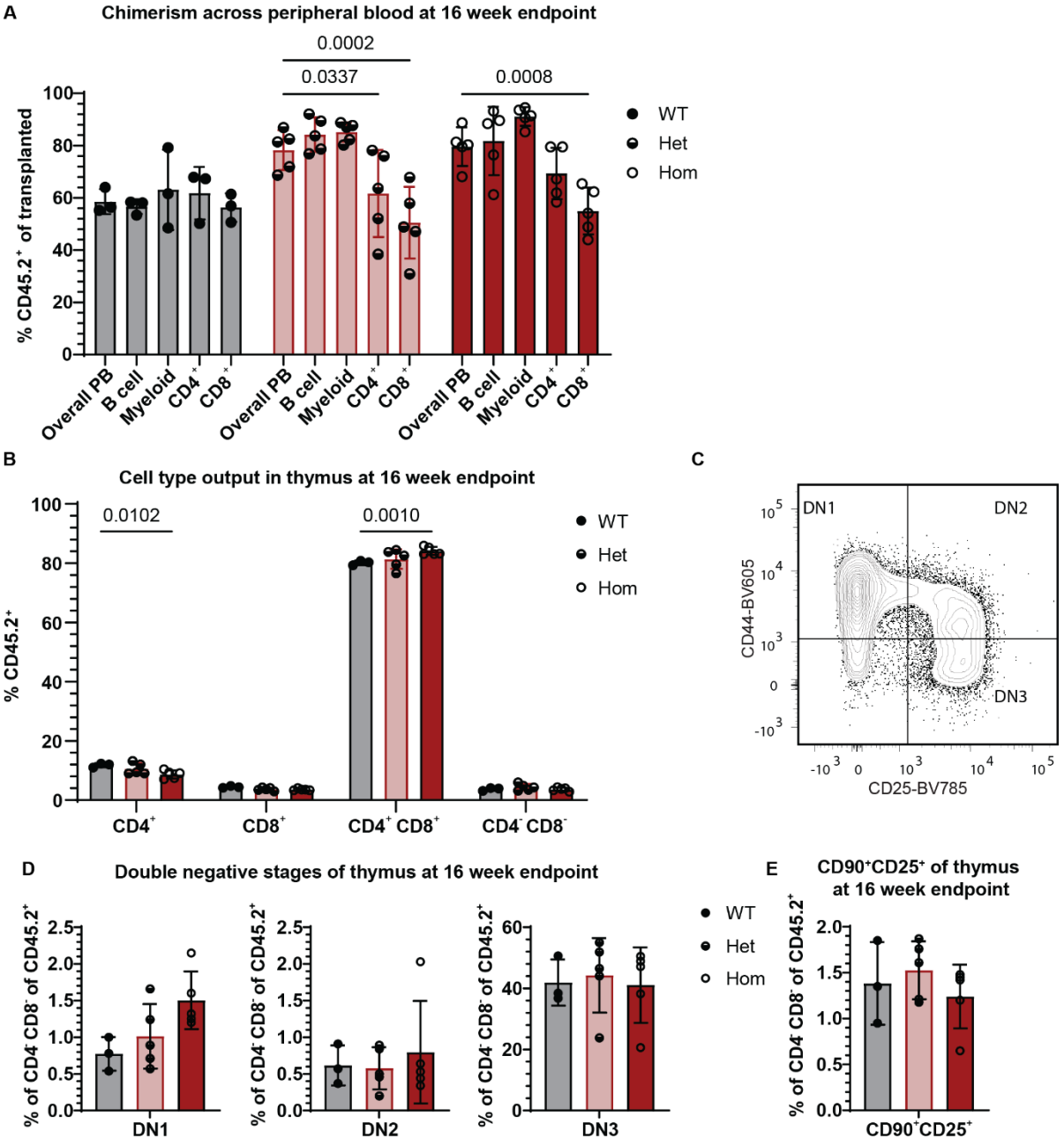

Figure 5.2: Runx2-deficient fresh HSCs have decreased CD4⁺ and CD8⁺ cell output in peripheral blood and altered thymic T-cell output.

(A) Chimerism of B-cells, myeloid cells, CD4⁺ and CD8⁺ cells as compared to overall peripheral blood. n = 3-5. 2-way ANOVA was performed.

(B) Single positive (CD4⁺ and CD8⁺), double positive (CD4⁺CD8⁺) and double negative (CD4⁻CD8⁻) cell output of CD45.2⁺ donor cells in thymi of recipient mice at 16-week endpoint. n = 3-5. 2-way ANOVA was performed.

(C) Representative flow plot for progression through the DN stages.

(D) Double negative cell stage output of CD45.2$^+$ donor cells in thymi of recipient mice at 16-week endpoint. DN1 = CD44$^+$CD25$^-$, DN2 = CD44$^+$CD25$^+$, DN3 = CD44$^-$CD25$^+$, DN4 = CD44$^-$CD25$^-$. n = 3-5. 1-way ANOVA was performed.

(E) CD90$^+$CD25$^+$CD4$^-$CD8$^-$ cell output of CD45.2$^+$ donor cells in thymi of recipient mice at 16-week endpoint. n = 3-5. 1-way ANOVA was performed.

Grey = *Runx2*-wt, pink = *Runx2*-het and red = *Runx2*-hom. Non-significance not labelled.

5.2.3 Cultured *Runx2*-deficient HSPCs produce fewer circulating T-cells

I next investigated the T-cell phenotype in the cultured HSC transplantation assay in Chapter 4.3, by again analysing the peripheral blood and thymi of these recipient mice. Experimental overview and lineage output are again provided for reference (**Figures 5.3A-B**).

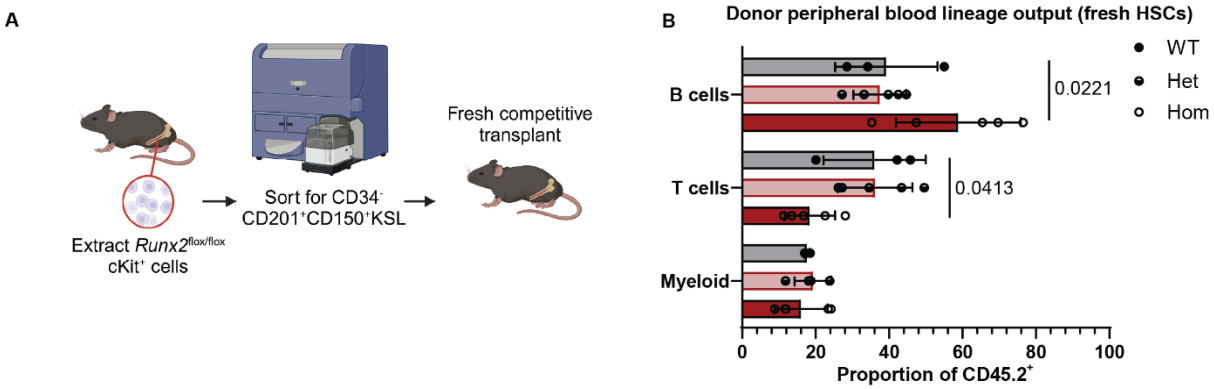

Figure 5.3: Summary of relevant findings from Chapter 4.

(A) Experimental overview for assays exploring the phenotypes of cultured homozygous and heterozygous *Runx2* KO HSCs. Created in BioRender.

(B) 16-week peripheral blood lineage output of HSC transplantation assay using 10,000 cultured cells vs 1 million WBM competitor cells (CD45.1$^+$CD45.2$^+$). n = 3-4. 2-way ANOVA was performed.

Grey = *Runx2*-wt, pink = *Runx2*-het and red = *Runx2*-hom. Non-significance not labelled.

The *Runx2*-deficient donor cells' ability to contribute to compartments of the peripheral blood was investigated by plotting chimerism across the peripheral blood. Again, as in the fresh HSC transplantation assay (**Figure 5.2**), the chimerism across all the blood compartments derived from the *Runx2*-wt donor cells was consistent (**Figure 5.4A**). However, both the *Runx2*-hom

and *Runx2*-het derived peripheral blood had a decrease in $CD8^+$ cell chimerism. The *Runx2*-hom also had a significant decrease in $CD4^+$ chimerism.

The cell type output of the thymi at the endpoint is consistent across the genotypes, despite the decrease in T-cell output in the peripheral blood (**Figure 5.4B**). This contrasts to the modest increase in $CD4^-CD8^-$ seen in the *Runx2*-hom fresh transplantation assay (**Figure 5.2B**). The *Runx2*-hom derived progenitor cells did display a slight increase in DN1 (and DN2) cell frequencies compared to the *Runx2*-wt, however this was not significant (**Figure 5.4C**). This could be because of thymic homeostasis reached at the endpoint of this transplantation assay, which would also explain why there was no difference in the mature cells in the thymus. There was also no difference in the $CD90^+CD25^+$ progenitor cells between the genotypes (**Figure 5.4D**).

Overall, *Runx2* loss decreases the single positive T-cells circulating in the peripheral blood and appears to cause an accumulation of progenitor cells in the thymus, but it is hard to conclude the downstream effects on progenitor production due to the confounding nature of thymic and T-cell homeostasis reached during the transplantation assays. To further investigate this, the thymi must be collected at an earlier endpoint while thymic reconstitution is still ongoing.

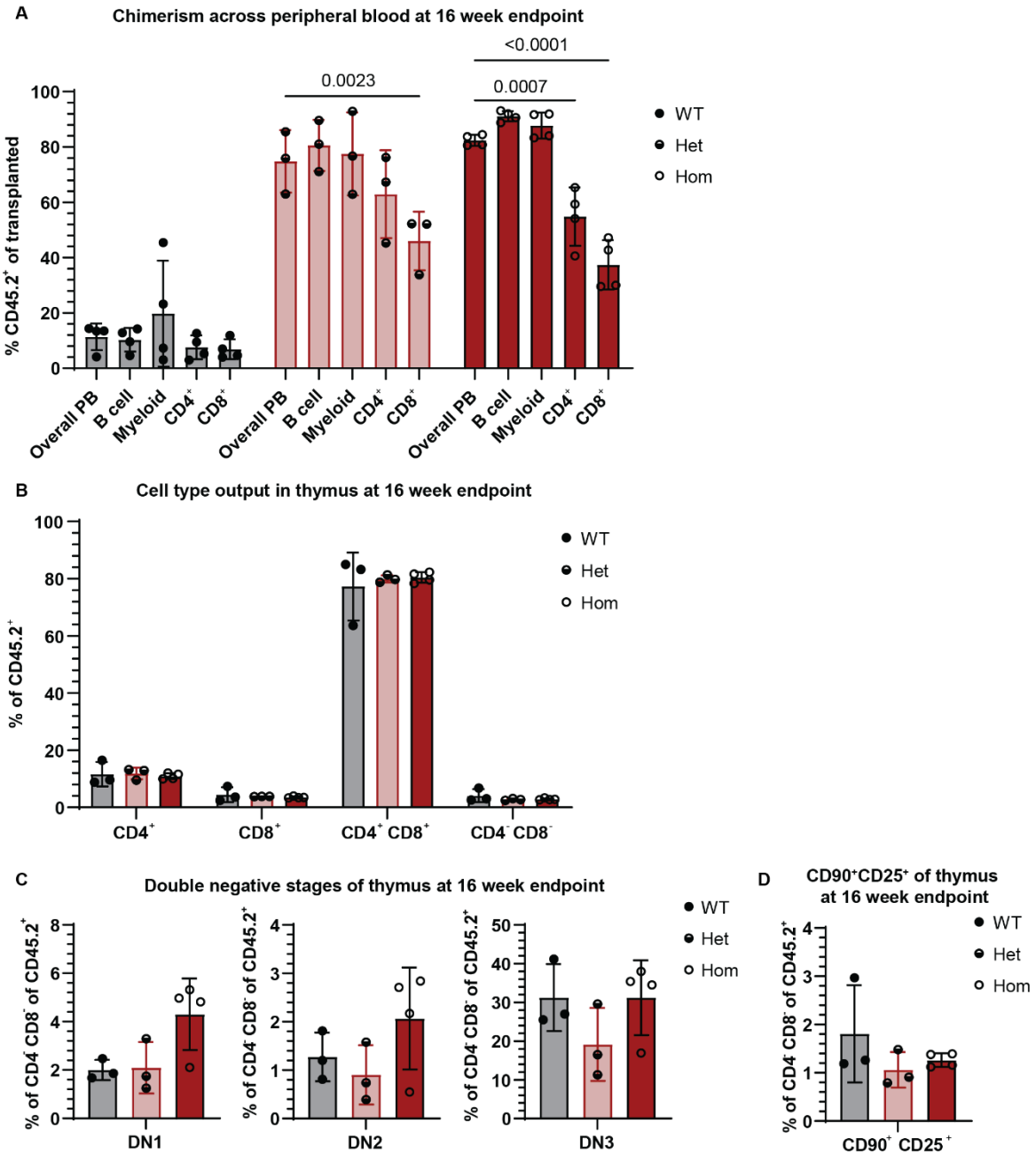

Figure 5.4: Runx2 cultured HSPCs have decreased CD4⁺ and CD8⁺ cell output in peripheral blood but not the thymus.

(A) Chimerism of B-cells, myeloid cells, $CD4^+$ and $CD8^+$ cells as compared to overall peripheral blood. n = 3-4. 2-way ANOVA was performed.

(B) Single positive ($CD4^+$ and $CD8^+$), double positive ($CD4^+CD8^+$) and double negative ($CD4^-CD8^-$) cell output of $CD45.2^+$ donor cells in thymi of recipient mice at 16-week endpoint.

(C) Double negative cell stage output of $CD45.2^+$ donor cells in thymi of recipient mice at 16-week endpoint. DN1 = $CD44^+CD25^-$, DN2 = $CD44^+CD25^+$, DN3 = $CD44^-CD25^+$, DN4 = $CD44^-CD25^-$. n = 3-4. 1-way ANOVA was performed.

(D) $CD90^+CD25^+CD4^-CD8^-$ cell output of $CD45.2^+$ donor cells in thymi of recipient mice at 16-week endpoint. n = 3-4. 1-way ANOVA was performed.

Grey = *Runx2*-wt, pink = *Runx2*-het and red = *Runx2*-hom. Non-significance not labelled.

5.3 *Runx2*-deficient HSCs have a reduced T-cell commitment

5.3.1 *Runx2*-deficiency reduces T-cell commitment *in vivo*

To better assess the effect *Runx2* loss has on early thymic reconstitution and T-cell commitment, a 4-week HSC transplantation assay was performed using cultured *Runx2*-hom, *Runx2*-het and *Runx2*-wt HSPCs (**Figure 5.5A**). There were slightly higher DN1 frequencies in the *Runx2*-hom and *Runx2*-het as compared to the *Runx2*-wt, but this was not significant (**Figure 5.5B**). There was also no significant difference across the DN2 and DN3 stages regardless of genotype, as in the longer-term transplantation assays (**Chapter 4.3**).

As there was no difference at DN2-DN3, but an apparent increase in DN1 progenitor cells, the DN1 compartment was further investigated. The subsets within DN1 can be separated using c-Kit and CD24[490]. Once cells pass DN1 (and are expressing CD25) they become a more homogeneous population, but DN1 has distinct subsets with different proliferative abilities. DN1 cells expressing low or no CD24 (DN1b and DN1a, respectively) are canonical T-cell precursors, but DN1 $CD24^+$ (DN1c) have less proliferative ability and can give rise to B-cells[490]. *Runx2*-hom progenitor cells had an increase in DN1a frequency as compared to *Runx2*-wt, while *Runx2*-het had a non-significant increase (**Figure 5.5C**).

To summarise, *Runx2* loss causes an increase in the frequency of DN1a cells but has no effect on the progression of DN2-DN4 stages in the thymus at this timepoint of thymic reconstitution. This could be linked to the reduced egress of *Runx2*-deficient single positive T-cells into the peripheral blood, as progression from DN1 to DN2 requires migration through the thymic cortex[471,491].

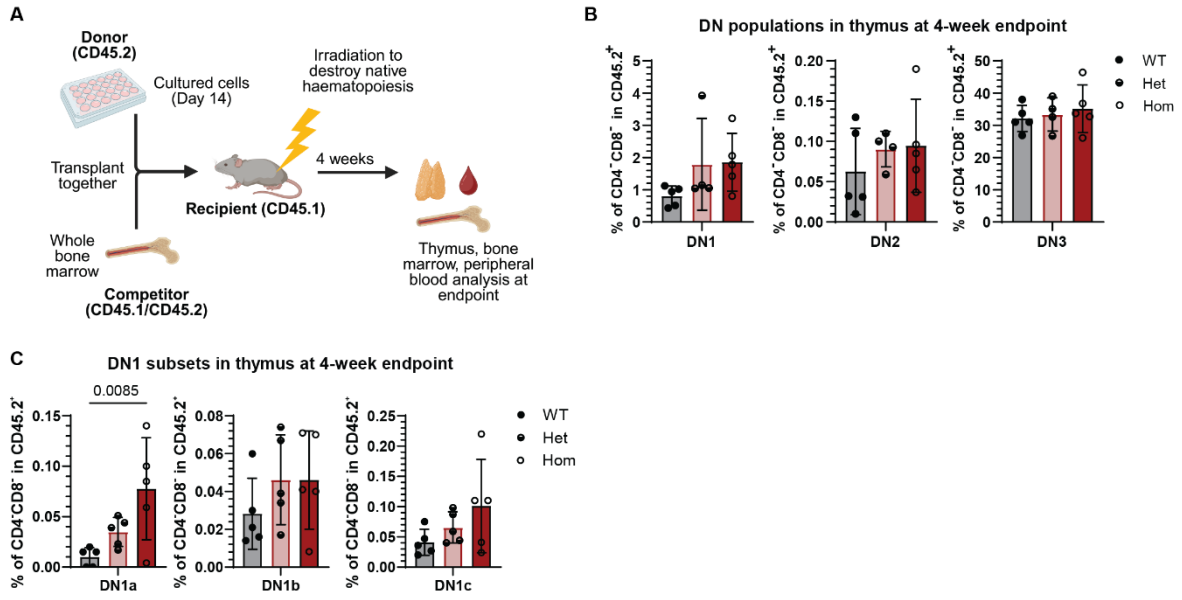

Figure 5.5: Runx2 loss causes an accumulation of DN1 cells in the thymus.

(A) Experimental overview for 4-week HSC transplantation assay. Created in BioRender.
(B) Frequency of DN1 to DN3 stage cells in CD45.2$^+$ donor-derived CD8$^-$CD8$^-$ cells in the thymus of recipient mice at 4-week endpoint. n = 5, one way ANOVA was performed.
(C) Frequency of CD24$^-$c-Kit$^+$ CD44$^+$CD25$^-$CD4$^-$CD8$^-$Lin$^-$ (DN1a), CD24^{lo}c-Kit$^+$CD44$^+$CD25$^-$CD4$^-$CD8$^-$Lin$^-$ (DN1b), and CD24^{hi}c-Kit$^+$CD44$^+$CD25$^-$CD4$^-$CD8$^-$Lin$^-$ (DN1c) cell subsets in thymic donor cells at 4-weeks post-transplantation. n = 5, one way ANOVA was performed.

Grey = *Runx2*-wt, pink = *Runx2*-het and red = *Runx2*-hom. Non-significance not labelled.

The increased frequency of DN1a cells in the thymus of recipient mice seen in the transplantation assay in **Figure 5.5** suggested that the block in differentiation might occur earlier, prompting an investigation of bone marrow lymphoid precursors.

Multipotent progenitor cells (MPPs) and lymphoid progenitor cell subsets were next investigated in the recipient bone marrow, as the upstream precursors to T-cells (**Figure 5.6**). The lineages were referred to using CD127$^+$KSL to resolve common lymphoid progenitor cell populations (CLPs) and recently defined MPP immunophenotypes[25], summarised in **Figure 5.6A**. It was found that the *Runx2*-hom HSPCs had significantly more immunophenotypic MPPs, granulocytic-monocytic MPPs (MPP$^{G/M}$), lymphoid-primed MPPs (LyMPPs) and CLPs than the *Runx2*-wt (**Figure 5.6B**). This suggests *Runx2*-hom HSPCs have an increased ability

to reconstitute multilineage haematopoiesis as compared to *Runx2*-wt. However, the *Runx2*-hom population had a decreased frequency of lineage positive cells (**Figure 5.6B**). This reduction in lineage positive cell output coupled with the higher frequencies of progenitor cells, especially the lymphoid progenitor cells, alludes to two potential drivers. First, there could be a block further along differentiation, or second, a decrease in the cells' ability to migrate to the thymus that causes an accumulation of progenitor cells in the bone marrow. The increased frequency of DN1 cells seen in **Figure 5.5** suggests the latter.

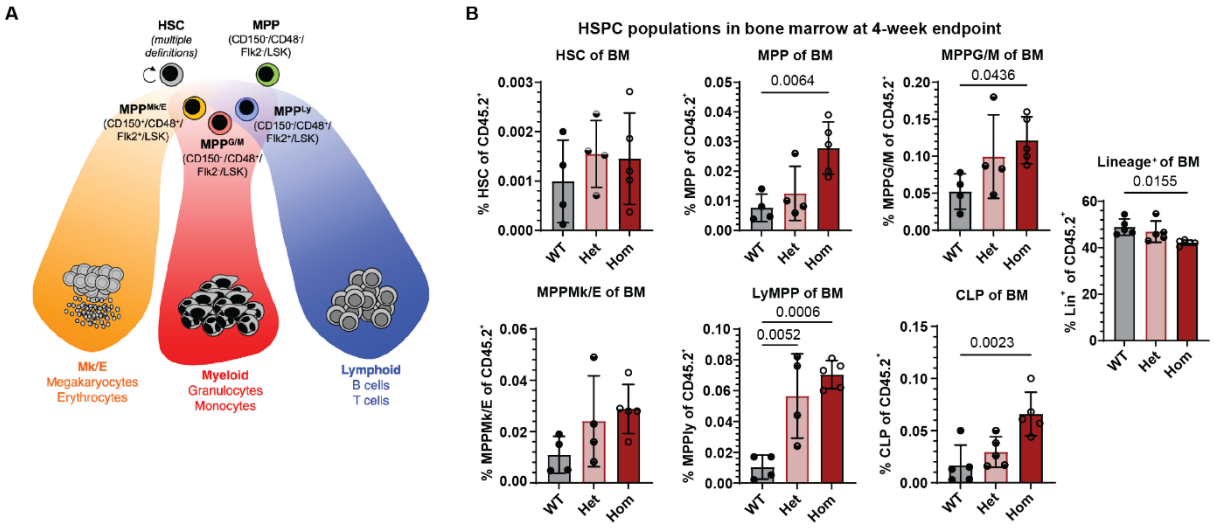

Figure 5.6: Runx2 loss causes an increase in multipotent progenitor cells in the bone marrow of recipient mice.

(A) Revised model of haematopoiesis. Reprinted from Challen and colleagues[25] with permission from Elsevier.

(B) Frequency of immunophenotypic HSPC populations in donor derived bone marrow of recipient mice at 4-week endpoint. n = 5, unpaired T-test was performed. HSC = $CD150^{+}CD48^{-}KSL$, MPP = $CD150^{-}CD48^{-}Flt3^{-}KSL$, $MPP^{G/M}$ = $CD150^{+}CD48^{-}Flt3^{-}KSL$, $MPP^{Mk/E}$ = $CD150^{+}CD48^{+}Flt3^{-}KSL$, MPP^{Ly} = $CD150^{-}Flt3^{+}KSL$, CLP = $CD127^{+}KSL$.

Grey = *Runx2*-wt, pink = *Runx2*-het and red = *Runx2*-hom. Non-significance not labelled.

To understand further the potential mechanism for the build-up of lymphoid progenitor cells in the bone marrow, the frequency of an established *Runx2*-regulating cell type was measured in the bone marrow, thymus and peripheral blood of these recipient mice; plasmacytoid dendritic cells (pDCs)[303] (**Figure 5.7**).

The frequency of pDCs in the bone marrow of the *Runx2*-hom recipient mice was increased compared to the *Runx2*-wt but drastically decreased in the peripheral blood and thymi (**Figure 5.7**). This supports the idea that whilst the *Runx2*-deficient HSCs are more active in production of progenitor cells such as lymphoid progenitor cells and pDCs, in this case, these are less able to leave the bone marrow to enter the other haematopoietic organs which is consistent with the established role for *Runx2* in pDC migration[303]. pDCs have a well-characterised role in interferon production, and it is possible that an increased frequency of pDCs elevates interferon levels in the bone marrow. Such an effect could, at least in part, contribute to the enhanced activation of *Runx2*-deficient HSCs, given interferon's known role in HSC stimulation[97,109,110,492].

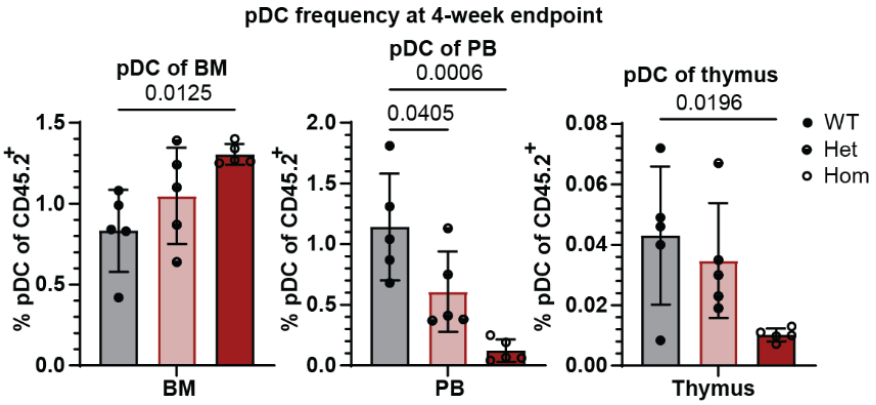

Figure 5.7: Runx2 loss causes an increase in plasmacytoid dendritic cells (pDCs) in the bone marrow and a decrease in peripheral organs. Frequency of $BST2^{+}B220^{+}CD11b^{-}$ pDCs in the donor cells from the peripheral blood (PB), bone marrow (BM), and thymus at 4-weeks post-transplantation. n = 5, one way ANOVA was performed. Grey = *Runx2*-wt, pink = *Runx2*-het and red = *Runx2*-hom. Non-significance not labelled.

5.3.2 *Runx2*-deficient T-cell progenitor cells are less able to make DN2 and DN3 cells via a block at DN1 *ex vivo*

Given the effect of *Runx2* loss on donor cell mature T-cell output in the peripheral blood (**Figures 5.1** and **5.3**), and an increase in DN1a progenitor frequency in the thymus (**Figure 5.5)**, it was important to directly test T-cell differentiation potential. To do this, an *ex vivo* T-cell differentiation assay was used as a tractable system that also avoids the confounding effects

of thymic homing and compensatory mechanisms *in vivo*. There are a few ways to mimic the complex milieu of factors present in the thymic environment *ex vivo*, with most techniques relying on Notch signalling to stimulate production of stages DN1-DP[149,364].

Matthew Nicholls performed an *ex vivo* DLL4-microbead T-cell differentiation assay to test the T-cell commitment potential from cultured HSPCs. Because the *Runx2*-deficient progenitor cells do not have a complete block in T-cell production, it was decided to measure the output of these assays at an early timepoint of 7 days to capture the early stages of DN1-DN3 commitment (**Figure 5.8A**).

At the 7-day endpoint, there were no significant differences between the genotypes in DN1, but both *Runx2*-hom and *Runx2*-het progenitor cells generated lower frequencies of DN2 and DN3 cells than *Runx2*-wt (**Figure 5.8B**). This indicates that the *Runx2*-deficient HSPCs have an intrinsically reduced potential to progress from DN1-DN3.

DN1 subsets were also investigated, with an increased frequency of *Runx2*-hom DN1a and DN1b as compared to the *Runx2*-wt but DN1c unaffected by *Runx2* loss (**Figure 5.8C**). The frequency of DN1a progenitor cells in the *Runx2*-hom mirrors the frequency seen in the thymi of the short-term transplantation assay recipients (**Figure 5.5C**), but unlike *in vivo*, DN2 and DN3 stages had significantly lower frequencies than the *Runx2*-wt. The *Runx2*-hom also displayed a significant decrease in the frequency of $CD90^{+}CD25^{+}$ pre-T-cells (**Figure 5.8D**)

These data demonstrate a reduced intrinsic ability of the *Runx2*-hom cells to produce T-progenitor cells which is likely compensated for *in vivo* to produce DN2 and DN3 and subsequently more mature cell types. This compensation could be driven by the presence of a constant stream of lymphoid progenitor cells entering the thymus *in vivo*, whereas this assay seeded an initial fixed number of HSPCs (and analysed at an early timepoint).

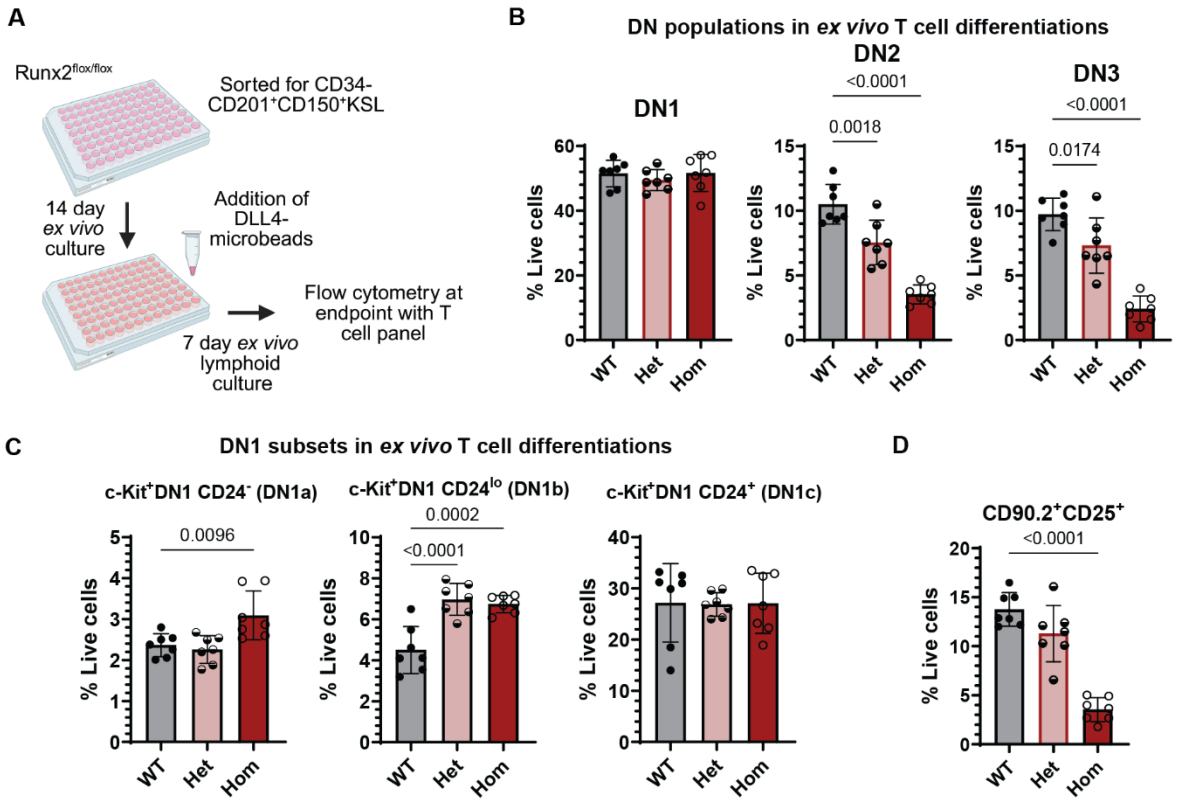

Figure 5.8: Runx2 loss causes a T-cell differentiation block at DN1.

(A) Experimental overview for *ex vivo* T-cell differentiation assays of *Runx2*-hom, *Runx2*-het and *Runx2*-wt HSPCs. Created in BioRender.
(B) Frequency of DN1 to DN3 stage cells generated in *ex vivo* T-cell differentiation assays. n = 5-10, unpaired T-test was performed.
(C) Frequency of $CD24^{-}$c-Kit^{+} $CD44^{+}CD25^{-}CD4^{-}CD8^{-}Lin^{-}$ (DN1a), $CD24^{lo}$c-$Kit^{+}CD44^{+}CD25^{-}CD4^{-}CD8^{-}Lin^{-}$ (DN1b), and $CD24^{hi}$c-$Kit^{+}CD44^{+}CD25^{-}CD4^{-}CD8^{-}Lin^{-}$ (DN1c) cell subsets generated in *ex vivo* T-cell differentiation assays. n = 5-10, unpaired T-test was performed.
(D) Frequency of $CD90.2^{+}CD25^{+}CD4^{-}CD8^{-}Lin^{-}$ T-cell precursor cells generated in *ex vivo* T-cell differentiation assays. n = 5-10, unpaired T-test was performed.

Grey = *Runx2*-wt, pink = *Runx2*-het and red = *Runx2*-hom. Non-significance not labelled.

5.3.3 *Runx2*-hom pHPCs have a different transcriptional programme to *Runx2*-het and *Runx2*-wt

So far in this chapter, the effect of *Runx2* loss on T-cell development has been hypothesised to be a reduction in the migration potential of lymphoid progenitor cells, evidenced by accumulation of progenitor cells at various stages of T-cell differentiation, as well as an intrinsic decrease in T-cell commitment. To understand the genes dysregulated in this setting,

RNA-seq was performed on the *Runx2*-hom, *Runx2*-het and *Runx2*-wt haematopoietic progenitor cells (pHPCs), by sorting $CD201^{-}CD150^{-}$KSL pHPCs at day 14 of culture to explore the transcriptional effects of *Runx2* loss on downstream progenitor cells (**Figure 5.9A**).

RNA-seq data was analysed by Catherine Chahrour. PCA analysis of the *Runx2*-hom, *Runx2*-het and *Runx2*-wt samples showed good clustering of the *Runx2*-wt samples and clear separation between the three genotypes (**Figure 5.9B**). This identified that the three genotypes display different transcriptional programmes as a result of the varied *Runx2* dosage.

Using DESeq2, 14921 genes were identified within the *Runx2*-hom and *Runx2*-wt, with 1095 significant DEGs (**Appendix XVI**). Of the DEGs, 508 were downregulated and 587 upregulated. Between the *Runx2*-het and *Runx2*-wt, 12884 genes were identified with 2016 statistically significant (**Appendix XVII**). Of these, 894 were upregulated and 1122 were downregulated. This again demonstrates the loss of *Runx2* is associated with broad transcriptional changes that include both gene activation and repression. These changes likely reflect a combination of direct and indirect effects of *Runx2* loss.

The DEGs with the highest log-fold change and statistical significance, and therefore the most disparate in expression between the genotypes were identified for the *Runx2*-hom and *Runx2*-het pHPCs (**Figures 5.9E-F**). Similar to what was observed in the pHSCs, there were no overlapping genes of the top 5 up and downregulated DEGs, again showing how *Runx2* dosage causes differential transcriptional effects. However, there were 643 DEGs conserved between the *Runx2*-het vs *Runx2*-wt and *Runx2*-hom vs *Runx2*-wt in the pHPCs (**Figure 5.9E**).

Overall, these data show that *Runx2* loss causes transcriptional changes in pHPCs which vary depending on *Runx2* dosage. The DEGs most significantly up or downregulated in the *Runx2*-hom and *Runx2*-het pHPCs as compared to the *Runx2*-wt are different. Therefore, to understand the molecular mechanism for the alterations in T-cell development and potentially

migration, the biological pathways dysregulated in the pHPCs by *Runx2* must be investigated instead of the specific genes.

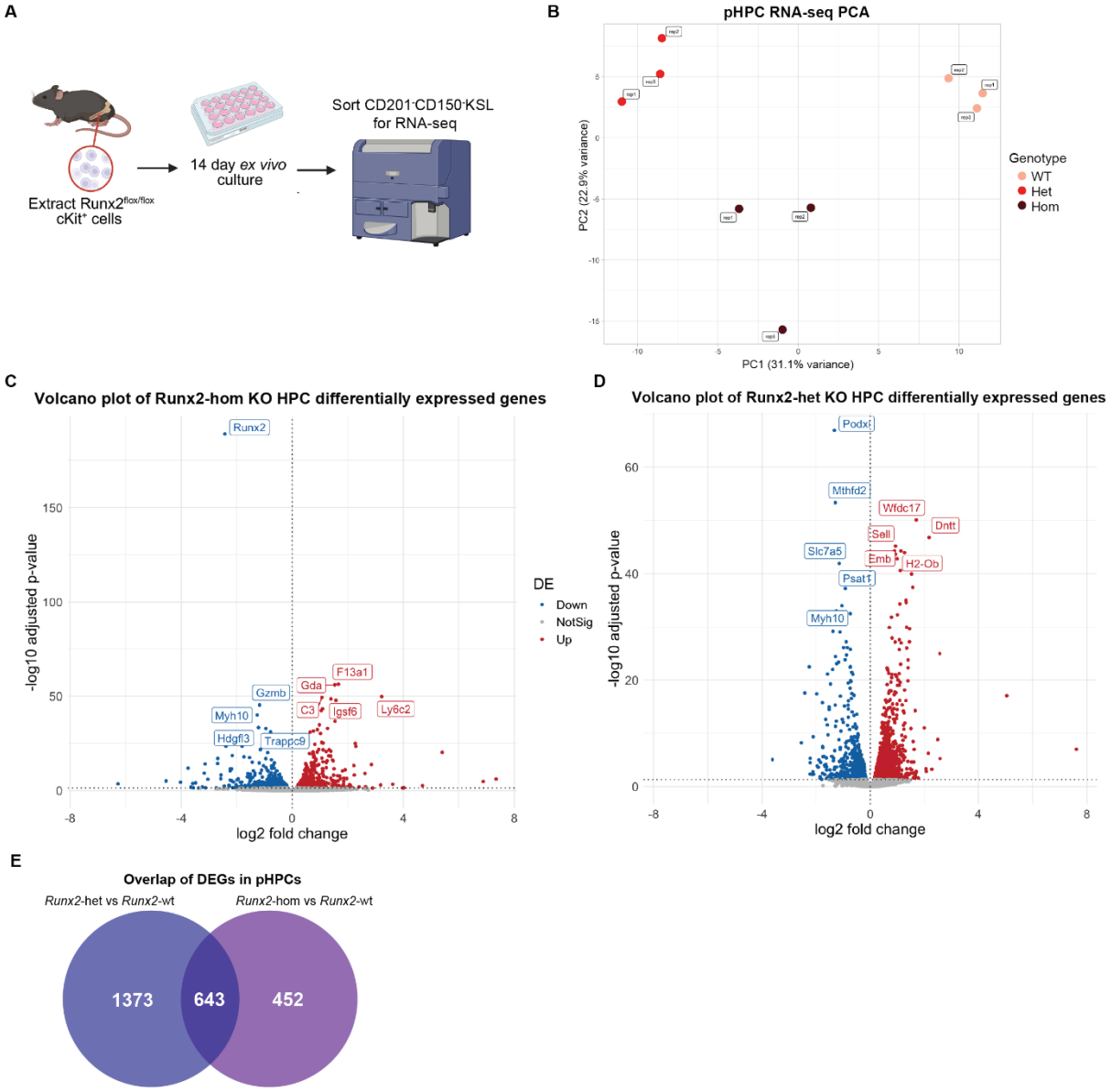

Figure 5.9: Runx2-deficient pHSCs have different transcriptional programmes to Runx2-wt.

(A) Experimental overview for RNA-seq on cultured pHPCs (CD201$^-$CD150$^-$KSL). Created in BioRender.
(B) Principal component analysis of CD201$^-$CD150$^-$KSL pHPC RNA-seq for *Runx2*-hom, *Runx2*-het and *Runx2*-wt
(C) Volcano plot of differentially expressed genes (DEGs) for *Runx2*-hom vs *Runx2*-wt in pHPCs.
(D) Volcano plot of differentially expressed genes (DEGs) for *Runx2*-het vs *Runx2*-wt in pHPCs.
(E) Gene overlap for *Runx2*-hom vs *Runx2*-wt and *Runx2*-het vs *Runx2*-wt in pHPC RNA-seq.

5.3.4 *Runx2*-deficient pHPCs have increased expression of interferon response genes

As discussed in Chapter 5.3.3, the top DEGs for the *Runx2*-hom and *Runx2*-het pHPCs as compared to the *Runx2*-wt were not conserved between the two *Runx2* dosages. Therefore, to better understand the molecular mechanism driving the potentially decreased migration ability of *Runx2*-deficient pHPCs, the specific biological pathways differentially expressed in the *Runx2*-hom and *Runx2*-het pHPCs were investigated using GO:BP (**Figure 5.10**) and GSEA (**Figure 5.11**).

In the *Runx2*-hom, upregulated pathways in the GO:BP analysis (**Figure 5.10A**) included the immune and inflammatory responses, consistent with the pathways seen upregulated in the pHSC *Runx2*-hom vs *Runx2*-wt (Chapter 4.5). In the *Runx2*-het, the upregulated pathways also included immune and inflammatory responses as well as cytokine signalling (**Figure 5.10B**). The broad implication is that there are altered immune pathways in pHPCs with both *Runx2* dosages, as in the *Runx2* pHSCs. Interestingly, the leukocyte proliferation pathway is upregulated in the *Runx2*-het vs *Runx2*-wt comparison which could link to the more subtle T-cell output defect seen in the *Runx2*-het recipient peripheral blood (**Figures 5.1** and **5.3**).

Regulation of T-cell activation and differentiation pathways were downregulated in the *Runx2*-hom pHPCs which is consistent with the T-cell output defect seen in *Runx2*-deficient progenitor cells (**Figure 5.10C**). In contrast, the *Runx2*-het had pathways related to DNA replication and cell cycle regulation downregulated (**Figure 5.10D**).

Overall, the upregulation of interferon-related gene pathways was consistent with both *Runx2* dosages as compared to the *Runx2*-wt pHPCs. Type I IFN is essential for T-cell activity, so it is unclear how this upregulation could link to the decreased T-cell output of *Runx2*-deficient cells described in this chapter[493–496]. Interferon is an important stimulant of HSC proliferation in times of injury or stress, so could be involved in the regeneration of the early lymphoid lineage. This could help to explain the increased MPP frequency seen in the bone marrow of *Runx2*-deficient HSC recipient mice (**Figure 5.6**). As mentioned in Chapter 5.3.1, the

increased frequency of interferon-producing pDCs in the bone marrow could contribute to the increased engraftment seen *in vivo*, but it is unclear how interferon behaves in the *ex vivo* cultures.

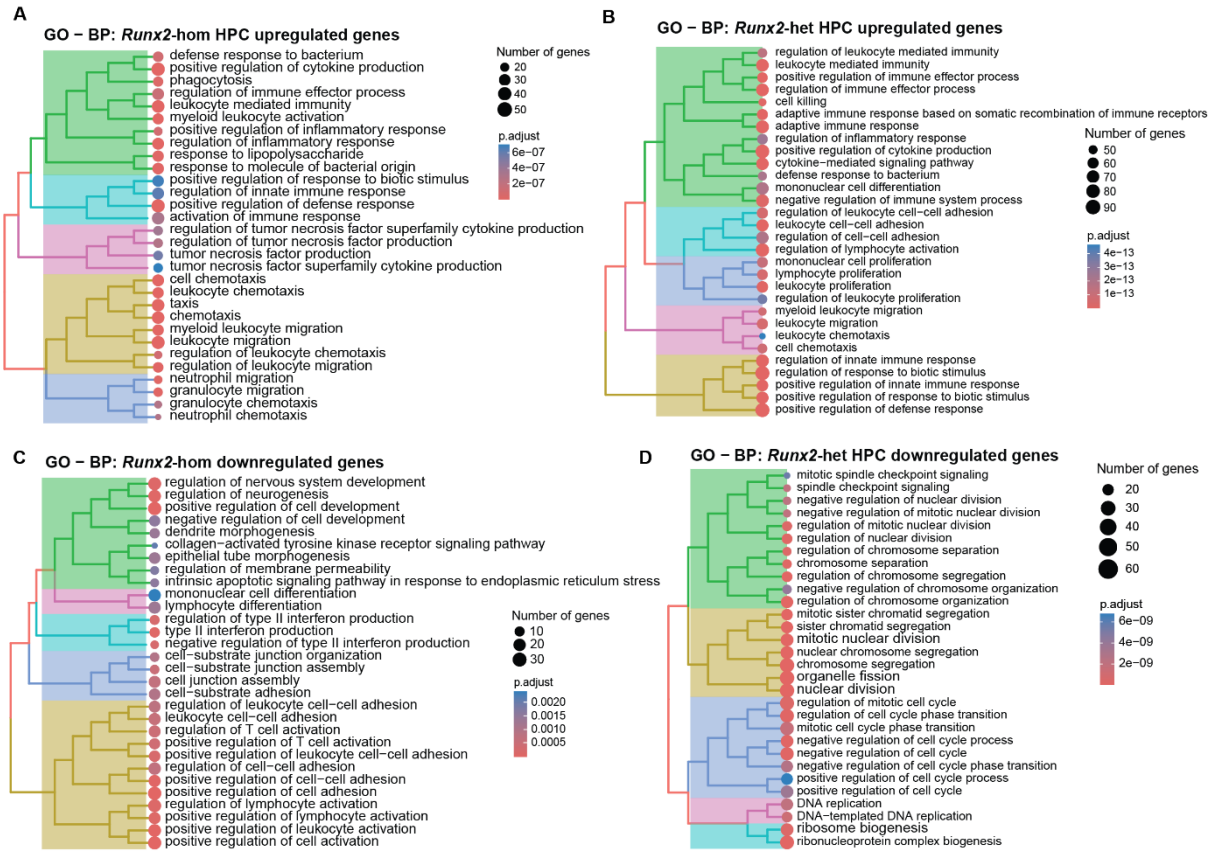

Figure 5.10: Loss of Runx2 causes increased transcription of interferon signalling genes in pHPCs.

(A) Top 30 upregulated Gene Ontology Biological Process for *Runx2*-hom vs *Runx2*-wt pHPC RNA-seq.
(B) Top 30 upregulated Gene Ontology Biological Process for *Runx2*-het vs *Runx2*-wt pHPC RNA-seq.
(C) Top 30 downregulated Gene Ontology Biological Process for *Runx2*-hom vs *Runx2*-wt pHPC RNA-seq.
(D) Top 30 downregulated Gene Ontology Biological Process for *Runx2*-het vs *Runx2*-wt pHPC RNA-seq.

5.3.5 *Runx2*-deficient pHPCs have decreased expression of mTORC1, E2F and MYC signalling gene sets

Examination of the DEGs in the *Runx2*-hom and *Runx2*-het pHPCs revealed some overlap in the top DEGs and GO:BP pathways, particularly the interferon and inflammatory signalling. To investigate the molecular pathways dysregulated by *Runx2* loss, GSEA was used to build

a picture of the regulatory networks involved in the loss of T-cell output and potentially their migration (**Figure 5.11**).

GSEA of the *Runx2*-het vs *Runx2*-wt DEGs in pHPCs (**Figure 5.11A**) showed an upregulation of the inflammatory response, IFN-α and IFN-γ responses. These hallmarks were also upregulated in the *Runx2*-hom vs *Runx2*-wt GSEA (**Figure 5.11B**). Alterations in the interferon response genes were also observed in the GO:BP analysis as discussed in Chapter 5.3.4.

The downregulated hallmark pathways included MYC targets, mTORC1 and E2F targets in both the *Runx2*-het vs *Runx2*-wt and the *Runx2*-hom vs *Runx2*-wt pHPCs. This shows that despite the specific DEGs being different between the *Runx2* dosages, many of the pathways altered transcriptionally in these cells are conserved in pHPCs. MYC is a TF with a myriad of roles in proliferation and apoptosis and is essential for production of single positive T-cells in the thymus[497]. mTORC1 has a role in T-effector cell lineage commitment via regulation of cytokine signalling[498]. E2F1, a cell cycle regulator in the E2F family is important for T-cell development via regulation of apoptosis in the negative selection stage in the thymus[499–501]. Whilst these are molecular regulators with a wide range of biological roles, their downregulation in the *Runx2*-deficient pHPCs does fit with the loss of T-cell output. For example, cytokine signalling is key for communication between the thymocytes and the thymic niche, and the negative selection stage controls the number of thymocytes progressing through T-cell development[502]. Without further investigation into the specific genes involved however, it is difficult to conclude that these gene families are contributing to the loss of T-cell output in *Runx2*-deficient haematopoietic reconstitution.

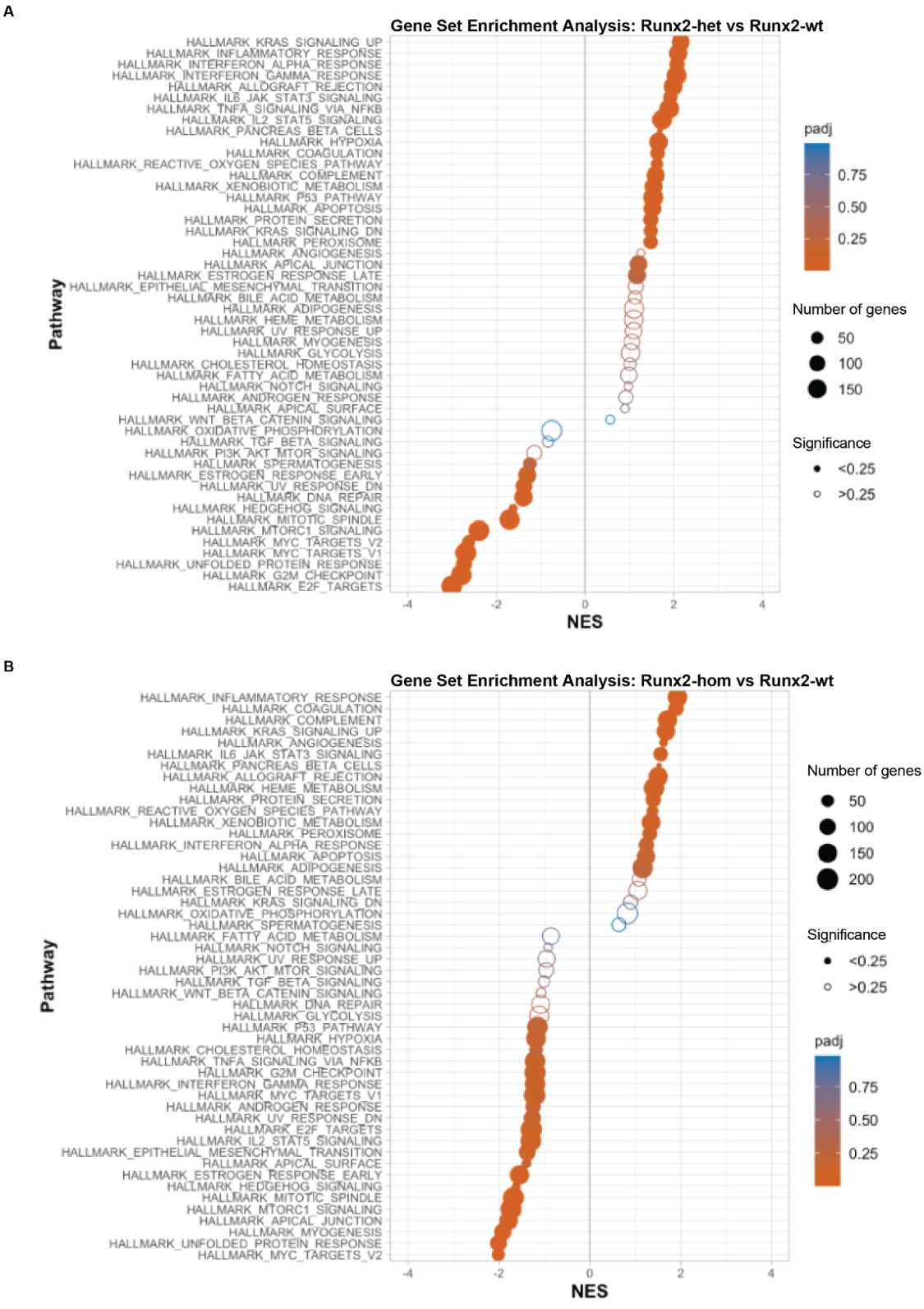

Figure 5.11: Runx2-deficient pHPCs have dysregulated interferon response gene pathways, inflammatory pathways and cell signalling regulators.

(A) Top 50 Gene Set Enrichment Analysis for *Runx2*-het vs *Runx2*-wt pHPC RNA-seq.
(B) Top 50 Gene Set Enrichment Analysis for *Runx2*-hom vs *Runx2*-wt pHPC RNA-seq

5.3.6 Comparison of *Runx2*-hom vs *Runx2*-wt in pHPCs and pHSCs

The transcriptional changes in *Runx2*-deficient pHPCs were conserved between the *Runx2* dosages in terms of the molecular hallmarks and biological processes. Given some of these, particularly the interferon response, were also present in the pHSC RNA-seq discussed in Chapter 4.5, the two datasets were compared to find which genes might be shared between these cellular contexts and provide insight into potential mediators of *Runx2*'s role in the haematopoietic system.

Runx2-hom vs *Runx2*-wt DEGs were compared between the pHPC and pHSC datasets. It was found that only 186 DEGs were conserved between these settings (**Figure 5.12**), and the GO:BP identified no significantly enriched pathways. Despite this, there were shared upregulated pathways between both comparisons with *Runx2*-wt, such as cytokine production and regulation of the innate immune response. There were no downregulated pathways shared between the two, though this is likely to be because a majority of the downregulated pathways in the *Runx2*-hom pHPC RNA-seq related to T-cell differentiation and activities (**Figure 5.10C**), and these genes are likely not expressed at the HSC level. Also, these data are showing the downstream effects of loss of *Runx2*, which are likely to be diverse in cell types at different stages of differentiation.

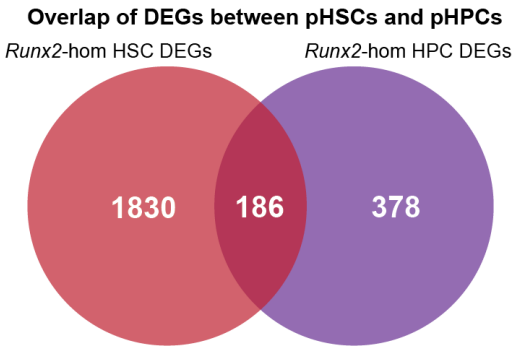

Figure 5.12: Gene overlap for Runx2-hom vs Runx2-wt pHSC and Runx2-hom vs Runx2-wt pHPC RNA-seq.

Because of the shared gene sets upregulated in both cell types, a different approach was taken to identify their biological roles. Enrichr was used to characterize the 186 shared DEGs,

with the Reactome Pathways 2024 and MSigDB Hallmark 2020 used[503–505]. After filtering for significance, just 6 pathways were present in the Reactome gene set (**Table 5.1**). These were primarily signalling/response pathways of cytokines, interleukins and interferons. This fits with the hypothesis that *Runx2* loss affects the interferon and inflammatory responses, which may be a driver of increased HSC expansion and self-renewal as well as potentially impacting lymphoid differentiation[506].

Table 5.1: Reactome Pathways 2024 Enrichr analysis of 186 shared differentially expressed genes between the Runx2-hom vs Runx2-wt RNA-seq in the pHSCs and pHPCs[503–505].

Term	Gene overlap	padj	Genes
Cytokine Signaling in Immune System	24/776	0.00015	*Dusp4, Ccl22, Cish, Flt3, Stat2, Camk2a, Mx1, Fn1, Ptgs2, Tnf, Ccnd1, Ifi27, Oas3, Ccl5, Il3ra, Bcl2, Irf7, Trim25, Sdc1, Irf5, Xaf1, Il18r1, Mcl1, Ccr2*
Interferon Alpha Beta Signaling	7/78	0.00241	*Ifi27, Oas3, Stat2, Mx1, Irf7, Irf5, Xaf1*
Signaling by Interleukins	15/452	0.00446	*Dusp4, Ccl22, Cish, Stat2, Fn1, Ptgs2, Tnf, Ccnd1, Ccl5, Il3ra, Bcl2, Sdc1, Il18r1, Mcl1, Ccr2*
Immune System	39/2150	0.00476	*Arhgap9, Nckap1, Flt3, Camk2a, Pld4, Kif11, Ptgs2, Tnf, Plac8, Ccnd1, Ccl5, Trim25, Itgb7, Cd33, Mcl1, Ccr2, Dusp4, Ccl22, Cish, Stat2, Mx1, Tap2, Fn1, Tap1, Lat2, Tyrobp, Dok3, Ifi27, Sell, Oas3, Il3ra, Bcl2, Irf7, Tax1bp1, Sdc1, Tlr7, Irf5, Xaf1, Il18r1*
Interleukin-10 Signaling	5/46	0.00785	*Ccl22, Ccl5, Ptgs2, Tnf, Ccr2*
Interleukin-4 and Interleukin-13 Signaling	7/112	0.00844	*Ccl22, Ccnd1, Fn1, Bcl2, Ptgs2, Tnf, Mcl1*

After filtering, 12 significant MSigDB gene set pathways were identified (**Table 5.2**). These, as in the Reactome analysis, included IFN-α and IFN-γ response pathways as well as TNF-α and STAT signalling. TNF-α has a complex role in T-cell commitment[507]. JAK-STAT signalling is an important effector of immune homeostasis[508]. These could therefore be involved in the *Runx2* T-cell commitment phenotype seen in this chapter. The G2/M checkpoint was also notable with key cell cycle regulators and DNA replication genes present in the gene list (**Table 5.2**). The function of checkpoint cell cycle regulation genes is to prevent DNA damage accumulation as cells pass through the cell cycle, which is important for proliferating HSCs[90,509,510]. This could therefore be a hallmark of an activated HSC, either directly or indirectly effected by the loss of *Runx2*.

In summary, both the *Runx2*-hom pHPCs and *Runx2*-hom pHSCs share altered expression of genes involved in the Type I and II interferon responses and progression through the cell cycle. These could therefore be passively correlated with *Runx2* loss or effectors of the increased self-renewal of *Runx2*-deficient cells.

Table 5.2*: *MSigDB Hallmark 2020 Enrichr analysis of 186 shared differentially expressed genes between the Runx2-hom vs Runx2-wt RNA-seq in the pHSCs and pHPCs*[503–505]*.

Term	Gene overlap	padj	Genes
Interferon Gamma Response	17/200	2.44E-10	*Stat2, Mx1, Tnfaip2, Tap1, Ifi44, Pla2g4a, Ddx60, Ptgs2, Znfx1, Ifi27, Oas3, Ccl5, Irf7, Trim25, Itgb7, Irf5, Xaf1*
Interferon Alpha Response	10/97	4.98E-07	*Ifi27, Sell, Stat2, Mx1, Irf7, Trim25, Tap1, Ifi44, Tent5a, Ddx60*
Mitotic Spindle	9/199	1.15E-03	*Top2a, Marcks, Cttn, Itsn1, Arhgap29, Kif11, Arhgap5, Myh10, Bub1*
TNF-alpha Signaling via NF-kB	9/200	1.15E-03	*Dusp4, Marcks, Ccnd1, Ccl5, Tnfaip2, Tap1, Ptgs2, Tnf, Mcl1*
Inflammatory Response	8/200	4.07E-03	*Gabbr1, Ccl22, Sell, Ccl5, Irf7,*

			Ccr7, Acvr1b, Il18r1
Allograft Rejection	8/200	4.07E-03	*Ccl22, Ccl5, Tap2, Irf7, Tap1, Thy1, Tnf, Ccr2*
Apoptosis	7/161	4.72E-03	*Top2a, Ccnd1, Tap1, Pmaip1, Timp3, Tnf, Mcl1*
IL-6/JAK/STAT3 Signaling	7/199	6.91E-03	*Stat2, Il3ra, Acvr1b, Tnf, Il18r1*
IL-2/STAT5 Signaling	7/199	1.04E-02	*Cdcp1, Cish, Sell, Il3ra, Bcl2, Tlr7, Il18r1*
G2-M Checkpoint	7/200	1.04E-02	*Top2a, Ccna2, Marcks, Ccnd1, Kif11, Bub1, Smc2*
Oestrogen Response Early	7/200	1.04E-02	*Gja1, Ccnd1, Cish, Podxl, Stc2, Bcl2, Pmaip1*
Epithelial Mesenchymal Transition	6/200	3.91E-02	*Gja1, Serpinh1, Fn1, Sdc1, Timp3, Thy1*

5.3.7 *Runx2*-hom pHPCs and pHSCs have altered cytokine response gene expression

Because many of the genes present in the Reactome and MSigDB significant hallmarks were conserved, the 63 genes were analysed using STRING to produce a potential interaction network[445] (**Figure 5.13**). RUNX2 was added to see how it would cluster with these proteins. The network had more interactions than expected for a random set of proteins, suggesting these proteins are likely to be biologically connected. RUNX2 was present in the central cluster, with the chemokines CCL22[511–513] and CCL5[514,515], as well as the chemokine receptors CCR7[469] and CCR2[516].

Chemokine and chemokine receptor expression differed between pHPCs and pHSCs: *Ccl5* was downregulated in both, *Ccl22* was upregulated in pHSCs but downregulated in pHPCs, and *Ccr7* and *Ccr2* were upregulated in pHPCs but downregulated in pHSCs (**Appendices XIII-XVI**). Previous studies report that *Ccr7*$^{-/-}$ mice have increased numbers of HSCs with an increased engraftment ability[472] and that *Ccr7*$^{-/-}$ HSCs display enhanced long-term self-renewal capacity as compared to WT[517]. However, *Ccr7*$^{-/-}$ mice also display severe T-cell

defects due to a differentiation block localised to progression between DN1-DN2[469,471], resulting in immunodeficiencies. CCR7 is therefore implicated in lymphoid migration in haematopoiesis. The upregulation of *Ccr7* observed in *Runx2*-hom pHPCs is difficult to reconcile with this. CCR7 mediates directed migration in response to its ligands CCL19 and CCL21; however, expression of these ligands was not altered, suggesting that impaired migration could be from reduced receptor availability rather than changes in chemokine gradients. Additionally, given the heterogeneity of the pHPC population, variation in the frequency of *Ccr7*-expressing cells between samples could have influenced the RNA-seq results. Taken together, these data raise the possibility that CCR7 may contribute both to altered HSC self-renewal and to impaired lymphoid development in *Runx2*-deficient settings, but whether it is a direct RUNX2 target remains unclear and will require further investigation.

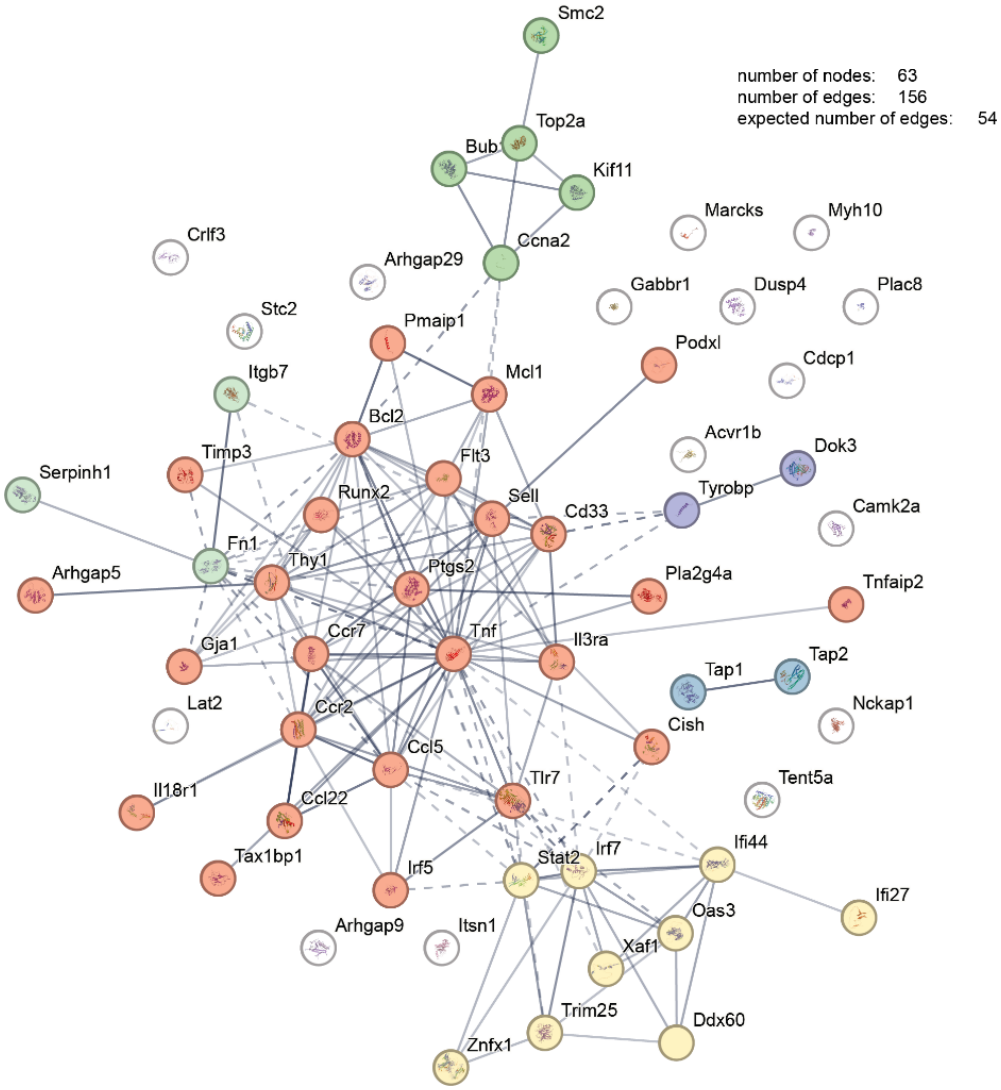

Figure 5.13: STRING analysis of protein-protein interactions of 63 proteins present in the Enrichr analysis of Runx2-hom vs Runx2-wt pHPC and pHSC RNA-seq differentially expressed genes[445]***.*** Thicker line = stronger reported interaction. Interactions can be: from curated databases, experimentally determined, gene neighbourhood, gene fusions, gene co-occurrence, textmining, co-expression and protein homology.

5.4 Conclusion and key findings

In this chapter, the role of *Runx2* dosage in T-cell commitment was investigated using HSC transplantation assays, *ex vivo* assays, and molecular techniques. Elucidation of the key genes and pathways correlating with the phenotype of *Runx2* loss in haematopoiesis was performed via comparison of RNA-seq from different *Runx2*-deficient cell types (pHPCs and pHSCs).

5.4.1 *Runx2*-deficient HSCs have decreased T-cell output in peripheral blood, despite no changes in thymic T-cell differentiation

Fresh, non-cultured *Runx2*-deficient HSCs showed reduced T-cell output in the peripheral blood following transplantation. Despite this, there were no differences in mature T-cell output within the thymus, suggesting either thymic homeostasis had been established or that these cells were unable to exit the thymus. An increased frequency of *Runx2*-deficient DN1 and DN2 cells was observed in the thymus compared to *Runx2*-wt, although this was not significant. Similar effects were seen in the cultured HSC transplantation assays, indicating that they are not due to pre-transplantation culture conditions but are intrinsic to *Runx2* loss. These findings prompted a short-term transplantation assay to investigate thymic repopulation at an earlier time point, as well as an expanded thymic analysis panel to more finely resolve the DN1 subpopulations.

5.4.2 *Runx2*-deficient HSPCs display a build-up of DN1a progenitor cells during early thymic reconstitution

The short-term HSPC transplantation assay permitted a closer look at thymic reconstitution. While the *Runx2*-deficient DN1-DN3 subsets had no significant differences in cell frequency, *Runx2*-hom DN1a cell frequency was significantly increased compared to *Runx2*-wt. This alludes to an accumulation of DN1a progenitor cells due to impaired progression, potentially compensated in the later stages of differentiation by proliferation. Notably, DN1a cells retain B-cell potential[490], which may help to explain the apparent increase in peripheral blood B-cell output. These findings prompted investigation of T-cell differentiation *ex vivo*, to characterise the progenitor cells' intrinsic T-cell commitment potential without the confounding effects of thymic homeostasis.

5.4.3 *Runx2*-deficient HSPCs have a differentiation block at DN1 *ex vivo*

Ex vivo, the *Runx2*-deficient T-progenitor cells accumulated at DN1a and DN1b, suggesting a partial block at the DN1-DN2 transition as compared to the *Runx2*-wt. There was also a significant decrease in the frequency of *Runx2*-deficient $CD90^{+}CD25^{+}$ progenitor cells. This contrasts with my *in vivo* results, in that the *Runx2*-deficient HSPCs were able to contribute to DN2, DN3 and $CD90^{+}CD25^{+}$ progenitor cell production at a similar frequency to the *Runx2*-wt. One possibility is that *in vivo*, the continuous influx of lymphoid progenitors from the bone marrow drives thymic differentiation despite the block. Alternatively, thymic homeostasis may be restored through compensatory mechanisms that are absent in the simplified *ex vivo* assay.

5.4.4 *Runx2*-hom HSCs have a higher output of progenitor cells in the bone marrow

Runx2-hom donor bone marrow populations demonstrated a significant increase in the frequency of MPPs, $MPP^{G/M}$, LyMPPs and CLPs as compared to the *Runx2*-wt. There was no significant difference in the frequency of pHSCs between the *Runx2*-deficient and *Runx2*-wt settings, likely because of the early endpoint and the fact HSCs cycle less frequently than progenitor cells[24,518]. These data suggest that while *Runx2*-hom HSPCs retain the capacity to generate progenitor cells of multiple lineages, these progenitors may have reduced migratory potential, leading to their accumulation in the bone marrow and early thymic stages. Such a migration defect would be expected to impact T-cell development most strongly, given the multiple stages at which progenitors must physically interact with distinct cells and tissues to progress[491].

It is interesting to note that the committed, lineage positive haematopoietic cells were significantly decreased in the *Runx2*-hom donor bone marrow as compared to the *Runx2*-wt, but as the panel included many different antibodies no conclusions can be made about which lineages this affects. pDC frequency of donor populations were also investigated across the haematopoietic organs, a cell type known to be regulated by *Runx2*. Interestingly, there was a significantly higher frequency of pDCs in the bone marrow in the *Runx2*-hom donor setting

but significantly lower in the peripheral blood and thymi compared to *Runx2*-wt. This finding, as discussed above, is consistent with *Runx2*'s role in pDC migration and could indicate a further role for *Runx2* in lymphoid cell migration, perhaps explaining the normal mature cell output of the thymi in the transplantation assays in **Figures 5.2** and **5.4**, but decreased T-cell egress into the peripheral blood.

5.4.5 *Runx2* has a dosage-dependent effect on transcription in pHPCs

Transcriptomic analysis of the *Runx2*-hom, *Runx2*-het and *Runx2*-wt pHPCs revealed the differing transcriptional programmes resulting from homozygous and heterozygous *Runx2* loss. Despite the differences in the specific DEGs identified, several notable pathways were conserved in their upregulation between both zygosities as compared to the *Runx2*-wt. Specifically, the IFN-α response pathways and inflammatory response pathways. IFN-α promotes HSC proliferation and decreases quiescence when transiently present, however chronic IFN-α signalling decreases functional capacity of HSCs over the long-term[110,492]. These findings suggest that interferon signalling must be finely balanced in this context, since the long-term reconstitution capacity of *Runx2*-deficient HSCs was maintained in the secondary transplantation assays described in Chapter 4. The build-up of pDCs in the bone marrow of transplanted mice, seen in **Figure 5.7**, could be promoting this *in vivo* as they produce interferon[97]. This is a potential mechanism for the increased engraftment potential observed in *Runx2*-deficient HSCs.

5.4.6 *Runx2*-deficient pHSCs and pHPCs share common transcriptional pathways

Despite the relatively low number of conserved DEGs between the two *Runx2*-deficient cell types, those present in Enrichr pathway analysis clustered well in a protein interaction network, indicating the presence of a causal biological link between them. The main cluster, which included RUNX2, included chemokine signalling genes which have a broad range of roles within haematopoiesis and immune regulation. As discussed, RNA-seq alone is not sufficient to derive conclusions about molecular mechanisms driving the *Runx2*-deficient phenotypes

but it can be concluded that loss of *Runx2* has wide-spread effects on immune signalling, inflammatory signalling and interferon response, likely contributing to the loss of T-cell commitment and potentially their migration.

5.4.7 Chapter summary

In summary, *Runx2* loss perturbs T-cell development in the context of thymic reconstitution, but this can be compensated for *in vivo* to maintain T-cell homeostasis. The partial block in T-lineage potential is the likely cause of lymphoid progenitor cell accumulation in the bone marrow and thymus. Given these observations, and the reduced output of *Runx2*-deficient T-cells in the peripheral blood, it can be hypothesised that *Runx2* has a role in regulating haematopoietic cell migration. Only limited overlap was observed in the DEGs between *Runx2*-deficient pHSCs and pHPCs, suggesting that the transcriptional role of RUNX2 could differ between these cell types. Notably, the interferon response pathway was upregulated in *Runx2*-hom cells in both contexts, and changes in chemokine signalling gene expression were also detected, pointing to possible molecular contributors to the increased HSC expansion and altered T-cell development.

Chapter 6: Discussion

In this chapter, I will discuss the key findings of the thesis, the limitations of the experimental strategies used, implications for the wider field and future directions this work could take.

6.1 Key findings

6.1.1 *Ex vivo* CRISPR screen reveals *Runx* factors as negative regulators of HSPC expansion

In my first results chapter, I presented my analysis of the first genome-wide *ex vivo* HSPC CRISPR screen and identification of novel regulators of HSPC expansion. Of the essential genes identified in the screen, 1310 were not present in the Achilles Common Essential Gene list and were therefore likely to be more HSPC-specific genes. Some of these were known essential genes for HSPC activity, but many were new putative regulators which could be further investigated. The screen also identified 92 putative negative regulators, of which this thesis focussed on *Runx2*. The STRING analysis revealed RUNX2 as a well-connected node, so it would be worth following up on those interactions to understand whether some may be upstream regulators of *Runx2*. There are therefore also many other negative regulators which could be further explored in the context of increased HSC expansion for clinical applications.

The validation of *Runx2* as a hit from this screen throughout this thesis demonstrates the value of broad, genome-wide approaches to identify new regulators of HSC expansion and activity. The *Runx* family single-gene KOs revealed diverse effects of *Runx* gene loss on *ex vivo* pHSC expansion. *Runx1* and *Runx2* loss promoted an increased expansion of pHSCs over time, while *Runx3* loss only displayed a subtle effect. *Cbfb* loss promoted a large transient increase in frequency of pHSCs, rapidly followed by depletion. Given CBFβ's role as an essential binding partner for efficient DNA-binding of RUNX family members, this indicates there may be a minimum and maximum *Runx* dosage required for increased HSC expansion governed

by the CBFβ:RUNX ratio. This ratio being altered by the loss of RUNX2 via increased availability for other RUNX protein binding may therefore contribute to the *Runx2*-deficient phenotypes. Any clinical approaches utilising the loss of *Runx* factors must consider this.

6.1.2 *Runx1* and *Runx2* have differing roles in haematopoiesis

The *ex vivo* expanded *Runx1* and *Runx2* CRISPR KO pHSCs both displayed increased engraftment *in vivo* but had differing abilities to reconstitute the haematopoietic lineages. Whereas *Runx1*-deficient HSCs displayed a myeloid-biased output, *Runx2*-deficient HSCs reconstituted all lineages with a mild defect in T-cell output in the peripheral blood. The *Runx2*-deficient transplanted recipient mice displayed normal mature blood cell counts and had no alterations in $CD4^+$ or $CD8^+$ T-cell production in the thymi. It therefore appears that the T-cell output defect can be compensated for *in vivo* to produce sufficient T-cells for homeostasis. This could be by proliferation of committed T-cells that manage to pass through this partial block. To mount effective immune responses, there must be a high diversity of TCRs present in the body. This could be relevant to patients with *Runx2* haploinsufficiency in CCD[279,304,463] as if they have a decreased TCR repertoire diversity as a result of clonal proliferation they may have reduced immunity to infections, for example[519].

Despite similar roles for *Runx1* and *Runx2* in repressing HSC expansion *ex vivo* and engraftment *in vivo*, they have contrasting roles in regulation of haematopoietic reconstitution and development of the haematopoietic system. This could help to clarify the contrasting roles *Runx1* and *Runx2* mutations have in haematopoietic malignancies. *RUNX1* haploinsufficiency causes familial platelet disorder[268,270], giving a predisposition to myeloid malignancies such as AML and myelodysplastic syndrome and lymphoid malignancies such as ALL and lymphomas[271,272]. The increased risk of myeloid malignancies in *RUNX1*-deficient patients correlates with the data presented in Chapter 3, with *Runx1*-deficient transplanted HSPCs displaying a myeloid-biased output. *RUNX2* haploinsufficiency on the other hand causes CCD[279,304,463], a bone development disorder which is not currently causally linked to an

increased risk of haematological malignancies[307]. This supports the finding that *Runx2*-deficient transplanted HSPCs stably reconstituted all lineages and had a partial defect in T-cell output, likely resolved by downstream T-cell proliferation. *RUNX2* loss has not been causally linked to haematological malignancies, however as discussed in Chapter 1, overexpression of *Runx2/RUNX2* has been observed in multiple pathologies. In AML, ectopically expressed *RUNX2* promotes leukaemic progression, and its heterozygous loss was predicted to delay leukaemia development in mice[299,520]. *RUNX2* is also highly expressed in high-risk T-acute lymphoblastic leukaemia and has a role in its progression[521]. Additionally, overactivation of the *Runx2* locus contributes to development of T-cell lymphoma[308]. These observations, combined with the results presented in this thesis, suggest that ablation of RUNX2 could represent a viable therapeutic strategy in the haematopoietic system.

6.1.3 *Runx2* haploinsufficiency has no effect on steady-state haematopoiesis but generates increased HSC expansion and engraftment potential

Chapter 4 utilised a *Runx2*^{flox} mouse line to understand the role of *Runx2* in steady-state haematopoiesis. At the steady-state, adult *Runx2*-deficient mice had no alterations in frequency of haematopoietic cell types assessed. Six-month-old mice with heterozygous loss of *Runx2* were investigated in the same way and there were again no alterations in cell frequencies despite displaying a typical hallmark of the aged haematopoietic system across both genotypes - an increased frequency of LT-HSCs in the bone marrow. Therefore, these experiments had no evidence to support a role for *Runx2* in steady-state haematopoiesis. However, it would be interesting to assess aged *Runx2*-het and *Runx2*-hom mice for haematopoietic defects, as well as following haematopoietic stress (e.g. infection, chemotherapy, etc). This is significant for the field, as genes previously considered irrelevant in steady-state haematopoiesis may nonetheless enhance *ex vivo* HSC expansion and engraftment, two important components in improving clinical applications of HSC-derived products.

The distinct phenotypes observed with *Runx2* loss in the steady-state and transplantation settings can be contextualised by the differences in the mechanism of haematopoiesis in both contexts. Steady-state haematopoiesis is driven by many clones with HSC self-renewal occurring very slowly[522]. Progenitor cells maintain much of the blood production, with some cells derived from fetal HSCs as discussed in Chapter 1[523]. In transplantation, a few highly proliferative clones are responsible for repopulating the haematopoietic system rapidly, causing strong selective pressure and bottlenecks for self-renewal and homing[522]. Given these differences, it could be that *Runx2* loss gives a proliferative advantage to HSCs which is only apparent in this highly competitive, regenerative context.

Comparisons were performed between the behaviour of the fresh, uncultured *Runx2*-deficient HSCs and the cultured *Runx2*-deficient HSCs. Chapter 4 described how fresh HSCs had more similar chimerism between *Runx2*-wt and *Runx2*-deficient cohorts than cultured HSCs, which showed a strong advantage of the *Runx2*-deficient HSCs. This could be because *Runx2*-deficiency becomes more biologically relevant under stress conditions, as the *ex vivo* culture is stressful to the cells. Alternatively, there could be clonal selection occurring during *ex vivo* culture, resulting in transplantation of a larger proportion of highly proliferative clones. From the data in this thesis, the cause of this discrepancy cannot be determined.

Runx2 dosage was investigated in the context of pHSC expansion *ex vivo* and reconstitution of the haematopoietic system in HSC transplantation assays. It was found that both the *Runx2*-hom and *Runx2*-het pHSCs displayed increased expansion potential *ex vivo* compared to the *Runx2*-wt. Both *Runx2*-hom and *Runx2*-het cultured HSCs displayed ~4-fold increased engraftment *in vivo* which persisted long-term in primary and secondary recipients. The increase in engraftment ability of the fresh, uncultured *Runx2*-deficient HSCs was less pronounced at just under ~2-fold, but *Runx2* loss still significantly boosted chimerism in the peripheral blood and bone marrow. The similarity between the phenotype of homozygous loss and haploinsufficiency of *Runx2* suggests that knockdown of *Runx2* rather than KO may be

sufficient to stimulate increased HSC expansion, with fewer risks in promoting DNA damage or off-target or unintended effects. This means the increased expansion and engraftment is potentially achievable with clinically relevant systems of *Runx2* perturbation. Examples of such systems include siRNAs or targeted protein degraders, both of which have been used for FDA-approved therapies[524,525].

As mentioned in 6.1.1, as the RUNX proteins have a common cofactor, loss of one RUNX protein will increase availability of CBFβ binding sites to the others. This could, therefore, contribute to the *Runx2*-deficient phenotypes. Loss of one allele of *Runx2* is sufficient to drive increased expansion and has a similar phenotype to the loss of both alleles, this suggests that RUNX2 levels have little impact on the phenotype as long as they are less than WT. This could suggest that the *ex vivo* HSC expansion phenotype was more influenced by the increased availability of CBFβ binding sites than the *in vivo* phenotype, where RUNX2 dosage had more of an impact on the cells' behaviour.

These findings demonstrate that loss of a previously uncharacterised haematopoietic TF, RUNX2, can enhance HSC activity. This could be used clinically to bolster engraftment of donor HSCs during HSCT but would require careful consideration of the strategy employed.

6.1.4 Full loss or haploinsufficiency of *Runx2* promotes upregulation of interferon response pathways

Runx2-deficient pHSCs and pHPCs displayed upregulation of IFN-γ and IFN-α response pathways. IFN-γ stimulates HSCs to leave quiescence but can lead to exhaustion and myeloid bias *in vivo*[109]. IFN-α has a similar effect in reducing dormancy and promoting proliferation with a functional trade-off of reduced engraftment ability and eventual exhaustion[109,110]. This exhaustion was not observed in the *Runx2*-deficient HSCs, given they could engraft into secondary recipients and reconstitute haematopoiesis with no myeloid bias. These studies used much larger doses of interferon than are physiologically present, so a subtle alteration in interferon signalling could potentially boost HSC engraftment potential without attenuating

HSC function. *Runx2*-deficient pHSCs and pHPCs also displayed downregulation of MYC and E2F target genes, both of which are regulated by interferons and, in turn, influence interferon production[526–529]. Based on the findings in this thesis, it is therefore currently challenging to determine which aspects of these complex regulatory networks are a direct consequence of *Runx2* loss and which are secondary effects.

6.1.5 *Runx2* loss potentially affects T-progenitor cell migration and homing

The effect of *Runx2* loss on T-cell output was explored in various ways to build an overall picture of the altered lymphopoiesis. The *Runx2*-deficient HSPCs contributed to a decreased $CD4^+$ and $CD8^+$ T-cell output in the peripheral blood but similar $CD4^+$ and $CD8^+$ T-cell frequencies in the thymus as compared to the wild-type. There was an increase in frequency of DN1 cells in the recipients' thymi *in vivo* and an increase in lymphoid progenitor cell frequency in the bone marrow. T-cell differentiation requires many stages of precursor cell migration, first from the bone marrow to the blood, then from the blood to the thymus, through the regions of the thymus and into the peripheral blood[149]. Given the accumulation of progenitor cells preceding these stages in the *Runx2*-deficient context, it can be postulated that loss of *Runx2* dampens the migration ability of lymphoid progenitor cells and hence affects their ability to enter the subsequent stage of T-cell development. This is supported by the role of *Runx2* in plasmacytoid dendritic cells (pDCs) in regulating their development and migration - both discussed in the literature[303] and demonstrated in the decreased ability of *Runx2*-deficient pDCs to migrate into the peripheral blood and thymus as presented in Chapter 5.

Runx2-deficient HSPCs displayed an intrinsic T-cell commitment defect, with a reduced ability to produce DN2-DN3 progenitor cells *ex vivo*. The restoration of T-cell differentiation in the DN2-DN3 stages in the transplantation assay could be due to T-cell proliferation to balance output of the thymus, or a constant influx of lymphoid progenitor cells from the bone marrow overcoming the block. *Ex vivo*, the numbers of lymphoid progenitor cells are limited to the HSPC numbers initially seeded, so this could be why the DN2-DN3 stages are restricted. The

timepoint may also have affected the comparison, if sampling of the *ex vivo* assay had taken place later the DN2-DN3 stages may have increased in frequency.

The mechanism of *Runx2* loss affecting T-cell development both *ex vivo* and *in vivo* could be attributed to alteration in the expression of cytokines and cytokine receptor genes. Both *Runx2*-deficient HSCs and HPCs displayed differential expression of genes involved in cytokine signalling, interleukin signalling and chemokine signalling. These peptides act as chemical messengers for immune function, especially for cellular migration[92]. Of the mature immune cells, T-cells require many migrations for effective development, which could be why *Runx2* loss did not affect development of the other lineages and that the B-cell and myeloid cell output of *Runx2*-deficient progenitor cells was normal. Additionally, the alterations in expression of these key cellular signalling pathways could explain the increased *ex vivo* expansion ability of the *Runx2*-deficient cultured HSCs as they could have a different response to the cytokines in the *ex vivo* culture system.

To summarise, the data presented in this thesis revealed a potential new role for RUNX2 in progression from DN1 to DN2 cell stages during T-cell differentiation, as well as promotion of progenitor cell migration across lymphopoiesis. The tentative model for these hypotheses is summarised in **Figure 6.1**. However, we cannot currently rule out additional functions of *Runx2* in committed T-cells that may contribute to the observed reduction in T-cell reconstitution *in vivo*. This model demonstrates the value in using a haematopoiesis-wide approach when validating novel regulators of HSC expansion and provides considerations for any clinical usages of *Runx2*-deficient HSCs.

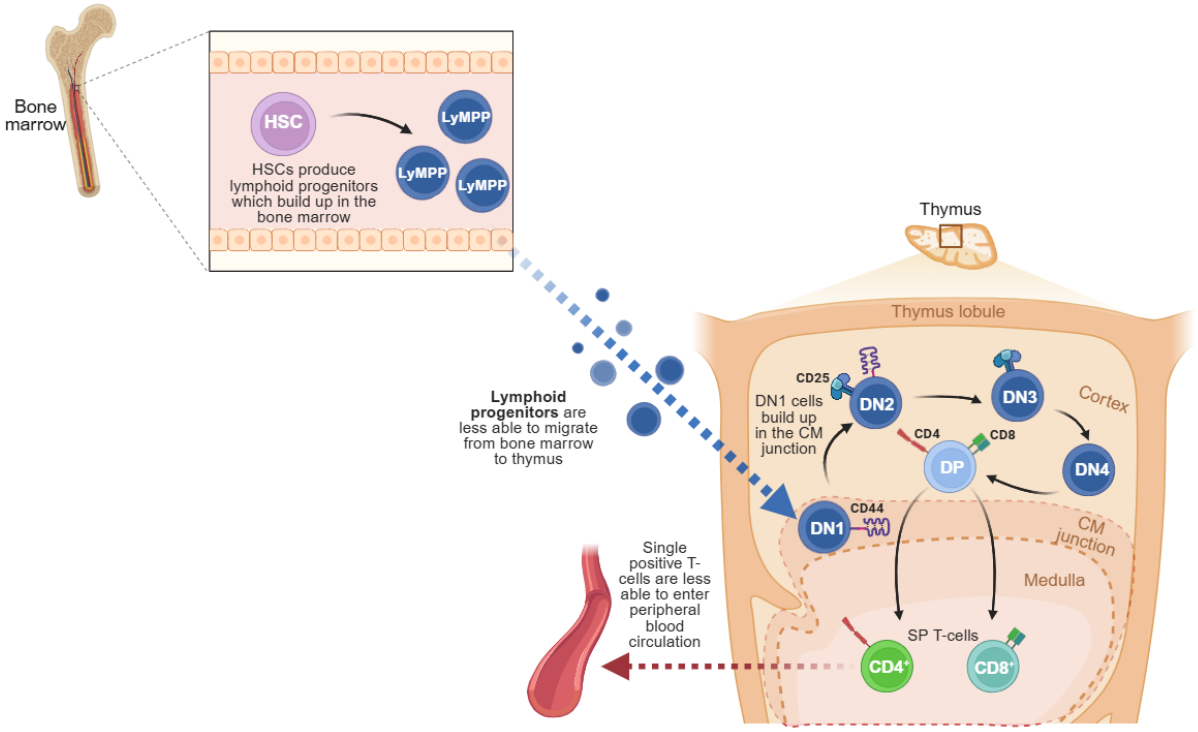

Figure 6.1: Proposed model for the role of Runx2 in reconstituting lymphopoiesis. *Runx2*-deficient HSCs produce lymphoid-primed multipotent progenitor cells (LyMPPs) in the bone marrow, which build up due to a defect in migration. The LyMPPs which reach the thymus pass into DN1 but build up due to defective migration across the cortex. They then pass through DN3-SP stages and experience reduced thymic egress, resulting in decreased single positive (SP) T-cell output in the peripheral blood. Mac = macrophage. MF = mesenchymal fibroblast. cTEC = cortical epithelial cell. mTEC = medullary epithelial cell. CM junction = cortico-medullary junction. Figure adapted from Zúñiga-Pflücker and Carlos, 2004[149]. Reproduced with permission from Springer Nature. Created in BioRender.

6.2 Future work

6.2.1 Dissecting *Runx2* function and compensation in haematopoiesis

The CRISPR-based *Runx1* and *Runx2* KOs explored in Chapter 3 targeted the Runt domain, the DNA-binding domain well-conserved within the RUNX family. This was because it is early in the gene, maximising the chance of full gene disruption, as well as being an important domain for RUNX activity. Many previous studies on *Runx* family genes target this domain[530,531] but it would be interesting to target a different region to explore the different consequences of *Runx2* mutations. An experiment to explore this could be an arrayed screen across the whole *Runx2* gene, to compete many sgRNAs against each other and hence find

which region of the gene, when targeted, permits the most competitive expansion phenotype *ex vivo*. This could also inform mechanistic characterisation of the increased expansion and engraftment phenotype, as regions of the RUNX2 protein interact with different cofactors[446].

As discussed in Chapter 1, many studies have explored full or partial compensation of *Runx* family members, especially in cancer. For example, repression of *RUNX1* resulted in overexpression of *RUNX2* and *RUNX3* in AML[328], and overexpression of *RUNX2* in *RUNX1*-depleted MLL-AF9 restored the growth potential of these *RUNX1*-dependent cells[329]. RUNX2 was also identified as a highly expressed gene in RUNX1-dependent MLL-rearranged leukaemias[532]. It would therefore be valuable to further these studies with investigation of *Runx* compensation in haematopoiesis. For example, tracking the expression levels of the *Runx* family genes when one is knocked out would shed light on their compensation during haematopoiesis. Given the drastic phenotype of *Cbfb* loss (a proxy for full *Runx* family inactivation), combinations of *Runx* family KOs could be performed to ascertain *Runx* dosage requirements in haematopoiesis. However, *Runx1* or *Runx3* were not significantly differentially expressed in the *Runx2*-hom pHSCs or pHPCs, so it would likely be a post-translational effect, if any. An experiment to investigate this could be RUNX1 (and RUNX3) CUT&Tag in a *Runx2*-hom or *Runx2*-het background, to identify and characterise common and distinct binding sites between the two factors. Given the compensation seen in haematological malignancies, investigating the compensation (or lack of) in *Runx* family members in haematopoietic reconstitution could be clinically relevant.

6.2.2 Genome-wide and single-cell approaches to resolve *Runx2*-dependent mechanisms

Molecular investigation of *Runx2* loss in Chapters 4 and 5 revealed some putative mechanistic pathways for the altered behaviours of HSCs and progenitor cells. However, there was no definitive answer for how *Runx2* loss increases HSC expansion, engraftment and effects changes in lymphoid differentiation. To gain insight into the genes directly altered by *Runx2*

loss in the context of HSC expansion, an *ex vivo* genome-wide counter screen could be performed. This would involve two parallel screens, one with *Runx2* KO via electroporation and one receiving electroporation of a control-region-targeting sgRNA, such as *Rosa26*. Both cell populations would receive the same genome-wide library and follow the same experimental procedures as used in Chapter 3 (and described in Chapter 2), to identify genes correlated with and directly affected by loss of *Runx2* in HSC expansion.

An additional experiment to bolster mechanistic understanding is single-cell RNA-sequencing to resolve cellular heterogeneity seen in bulk RNA-sequencing. Even the most refined immunophenotypic definition of an HSC only contains ~1:3 functional HSCs[533], so to gain understanding of how *Runx2* loss affects transcription in HSCs, a single-cell approach must be considered. In line with this, *in vivo* gene expression changes should be investigated by performing RNA-seq in a *Runx2*-deficient transplantation assay to transcriptionally characterise the engrafted HSCs and track genes of interest over lineage development.

The increased expansion and engraftment of *Runx2*-deficient HSCs correlated with upregulation of interferon response genes; this could be validated by testing interferon levels in the *ex vivo* HSPC culture media and mouse bone marrow. Following this, KOs of interferon response genes could be performed in the *Runx2*-deficient HSPCs to determine which genes are involved in interferon-mediated HSC expansion.

6.2.3 Mechanistic investigation into RUNX2 regulation of T-cell development and output

The RUNX2 CUT&Tag combined with the RNA-seq allowed exploration of genomic RUNX2 binding in wild-type HSCs. This could be performed on a more committed T-progenitor cell population to find direct targets of RUNX2 in this context, assisting with molecular characterisation of the alterations in T-cell commitment seen in *Runx2*-deficient cells. Additionally, Chapter 5 discussed the indication that the T-cell commitment phenotype could

be an effect of altered cytokine or chemokine signalling, this could be elucidated using ELISA assays.

From the exploration of the recipient thymi in Chapter 5, it appears that the T-cell commitment defect can resolve itself to produce sufficient T-cells for homeostasis. To mount effective immune responses, there must be a high diversity of TCRs present in the body. Proliferation of T-cell clones to compensate for the lack of T-cell output from the *Runx2*-deficient progenitor cells could be assayed using bulk-TCR sequencing. A low TCR diversity would not only inform how the *Runx2*-deficient haematopoietic system reaches T-cell homeostasis but also may be valuable for patients with CCD as they may experience reduced immunity as a result of *RUNX2* haploinsufficiency. A further experiment to track T-progenitor cell output and any clonality developing in the bone marrow could use lineage tracing. For example, the LARRY lentiviral barcode library, which permits tracking of HSC output at a clonal level throughout haematopoietic reconstitution[534].

6.2.4 *Runx2*-deficiency and HSC function in aging and haematopoietic reconstitution

As discussed in Chapter 4, there were breeding and time limitations which prevented loss of *Runx2* being investigated in aged mice. Given *Runx2* dosage gives a pronounced or moderate phenotype with homozygous or heterozygous loss respectively, future work should investigate the effect of full *Runx2* loss on the aged haematopoietic system. Again, because of breeding and time limitations, the oldest mice investigated were only 26-34 weeks old. They did display some hallmarks of aging, with increased size and increased frequencies of HSCs in the bone marrow. However, 2-year-old mice are generally considered to be equivalent to 70-year-old humans, so whilst the mice used for this experiment were relatively old compared to the 8–12-week-old mice used in the rest of the experiments, 2-year-old mice would be a better representation of old age. These experiments would allow more confident assertions about the role of *Runx2* in haematopoietic aging. Additionally, as *Runx2* loss had no effect on steady-state haematopoiesis in the young adult mice but did increase engraftment potential once

transplanted, it would be interesting to use aged *Runx2*-deficient HSCs in HSC transplantation assays. If these aged *Runx2*-deficient HSCs have greater capability to recapitulate haematopoiesis than the wild-type, it could provide an interesting clinical avenue for HSC rejuvenation.

6.2.5 *Runx2*-deficiency in haematopoietic stress and clinical potential for HSC expansion

In Chapter 4, secondary transplantation assays were used to characterise the long-term reconstitution potential of *Runx2*-hom, *Runx2*-het and *Runx2*-wt HSCs. To more confidently ascertain the long-term potential of these HSCs, a tertiary transplantation assay could be performed, with the bone marrow of secondary recipients transplanted into irradiated tertiary recipients, but time constraints prevented this. This would bolster the finding that *Runx2*-deficient HSCs have long-term reconstitution potential. Another interesting comparison would be between the tertiary transplants of the fresh-derived HSCs and the cultured HSCs, to see how similar the chimerism is at the endpoint. This would test the hypothesis that extended presence in a regenerative context increases the potential of *Runx2* loss to affect HSC activity.

To validate the finding that *Runx2* loss boosts HSC activity under stress, lipopolysaccharide (LPS) injections could be used to simulate infections[535]. The *Runx2*^{flox} mice could be treated with LPS and their haematopoietic recovery tracked. If *Runx2* loss indeed boosts HSC activity in a stress condition, the *Runx2*-deficient mice should recover more quickly.

The single *Runx* KOs revealed diverse phenotypes of *Runx* family loss on *ex vivo* HSC expansion, from little effect from loss of *Runx3* to a transient expansion followed by depletion from *Cbfb* loss. Despite the RUNX:CBFβ inhibitors having limited success in reproducing this phenotype, it would be beneficial to implement them in other HSC expansion techniques such as using Soluplus instead of PVA (given the precipitation of CADD522 in PVA)[381]. It would also be interesting to assess a transient knockdown of *Cbfb* using siRNA or shRNA[536] to

observe potential recapitulation of this phenotype. These could have clinical value in promoting HSC expansion without genetic perturbations.

Chapter 4 investigated the effect of heterozygous loss of *Runx2* on the haematopoietic system. As discussed, *Runx2*-deficient young adult 8-12-week-old mice (and 6-month *Runx2*-het) did not display any identifiable haematopoietic system perturbations. If there is a conservation of *Runx2* activity in the haematopoietic systems of mouse and humans, this would be an interesting finding for the approximately 8,000 people worldwide who have *RUNX2* mutations in CCD[304].

Whilst using mouse HSC studies to understand the biology of haematopoiesis is a standard preliminary technique for extrapolating findings to human biology, the clinical potential for the conclusions lies in the conservation between human and mouse biology. Given this, a key follow-up experiment of this thesis would be to investigate the effect of *RUNX2* loss in human HSPCs. The human HSPC expansion system is less well-developed than the mouse, with ~400-fold expansion over 28 days as compared to ~10,000-fold[378,381,387]. It is also a more heterogeneous population of cells, with less well-established immunophenotypic definitions of pHSCs[43]. Despite these limitations, it will be important to understand if transient knockdown of *RUNX2* can promote an HSC with improved self-renewal and engraftment potential, as this would be extremely valuable for clinical HSC transplantation therapies. The effects on T-cell commitment must also be closely observed.

6.2.6 Concluding remarks

In this thesis, I presented my identification and validation of *Runx2* as a novel negative regulator of HSC expansion and its role in haematopoiesis. I have demonstrated that *Runx2* loss has no effect on steady-state haematopoiesis; however, *Runx2*-deficient HSCs display an increased ability to expand *ex vivo* and engraft *in vivo*. My work also highlighted a second haematopoietic role for *Runx2* in T-cell commitment. These findings will help us to better

understand the molecular regulation of blood production and have potential therapeutic implications for HSC-based therapies.

Bibliography

1. Laurenti E, Göttgens B. From haematopoietic stem cells to complex differentiation landscapes. *Nature*. 2018;553(7689):418-426. doi:10.1038/nature25022

2. Seita J, Weissman IL. Hematopoietic Stem Cell: Self-renewal versus Differentiation. *Wiley Interdiscip Rev Syst Biol Med*. 2010;2(6):640-653. doi:10.1002/wsbm.86

3. Patel AA, Ginhoux F, Yona S. Monocytes, macrophages, dendritic cells and neutrophils: an update on lifespan kinetics in health and disease. *Immunology*. 2021;163(3):250-261. doi:10.1111/imm.13320

4. Pillay J, den Braber I, Vrisekoop N, et al. In vivo labeling with 2H2O reveals a human neutrophil lifespan of 5.4 days. *Blood*. 2010;116(4):625-627. doi:10.1182/blood-2010-01-259028

5. Yona S, Kim KW, Wolf Y, et al. Fate mapping reveals origins and dynamics of monocytes and tissue macrophages under homeostasis. *Immunity*. 2013;38(1):79-91. doi:10.1016/j.immuni.2012.12.001

6. Murphy J, Summer R, Wilson AA, Kotton DN, Fine A. The Prolonged Life-Span of Alveolar Macrophages. *Am J Respir Cell Mol Biol*. 2008;38(4):380-385. doi:10.1165/rcmb.2007-0224RC

7. Mossadegh-Keller N, Gentek R, Gimenez G, Bigot S, Mailfert S, Sieweke MH. Developmental origin and maintenance of distinct testicular macrophage populations. *J Exp Med*. 2017;214(10):2829-2841. doi:10.1084/jem.20170829

8. Molawi K, Wolf Y, Kandalla PK, et al. Progressive replacement of embryo-derived cardiac macrophages with age. *J Exp Med*. 2014;211(11):2151-2158. doi:10.1084/jem.20140639

9. Schepper SD, Verheijden S, Aguilera-Lizarraga J, et al. Self-Maintaining Gut Macrophages Are Essential for Intestinal Homeostasis. *Cell*. 2018;175(2):400-415.e13. doi:10.1016/j.cell.2018.07.048

10. Seita J, Weissman IL. Hematopoietic Stem Cell: Self-renewal versus Differentiation. *Wiley Interdiscip Rev Syst Biol Med*. 2010;2(6):640-653. doi:10.1002/wsbm.86

11. Kondo M, Weissman IL, Akashi K. Identification of Clonogenic Common Lymphoid Progenitors in Mouse Bone Marrow. *Cell*. 1997;91(5):661-672. doi:10.1016/S0092-8674(00)80453-5

12. Matsuzaki Y, Gyotoku J, Ogawa M, et al. Characterization of c-kit positive intrathymic stem cells that are restricted to lymphoid differentiation. *J Exp Med*. 1993;178(4):1283-1292. doi:10.1084/jem.178.4.1283

13. Wu L, Antica M, Johnson GR, Scollay R, Shortman K. Developmental potential of the earliest precursor cells from the adult mouse thymus. *J Exp Med*. 1991;174(6):1617-1627. doi:10.1084/jem.174.6.1617

14. Allman D, Sambandam A, Kim S, et al. Thymopoiesis independent of common lymphoid progenitors. *Nat Immunol*. 2003;4(2):168-174. doi:10.1038/ni878

15. Cabezas-Wallscheid N, Klimmeck D, Hansson J, et al. Identification of Regulatory Networks in HSCs and Their Immediate Progeny via Integrated Proteome, Transcriptome, and DNA Methylome Analysis. *Cell Stem Cell*. 2014;15(4):507-522. doi:10.1016/j.stem.2014.07.005

16. Pietras EM, Reynaud D, Kang YA, et al. Functionally distinct subsets of lineage-biased multipotent progenitors control blood production in normal and regenerative conditions. *Cell Stem Cell*. 2015;17(1):35-46. doi:10.1016/j.stem.2015.05.003

17. Ferchen K, Zhang X, Thakkar K, et al. A unified multimodal single-cell framework reveals a discrete state model of hematopoiesis in mice. *Nat Immunol*. 2025;26(11):2086-2099. doi:10.1038/s41590-025-02307-3

18. Cheng H, Zheng Z, Cheng T. New paradigms on hematopoietic stem cell differentiation. *Protein Cell*. 2020;11(1):34-44. doi:10.1007/s13238-019-0633-0

19. Yang L, Bryder D, Adolfsson J, et al. Identification of Lin–Sca1+kit+CD34+Flt3– short-term hematopoietic stem cells capable of rapidly reconstituting and rescuing myeloablated transplant recipients. *Blood*. 2005;105(7):2717-2723. doi:10.1182/blood-2004-06-2159

20. Yamamoto R, Morita Y, Ooehara J, et al. Clonal Analysis Unveils Self-Renewing Lineage-Restricted Progenitors Generated Directly from Hematopoietic Stem Cells. *Cell*. 2013;154(5):1112-1126. doi:10.1016/j.cell.2013.08.007

21. Benveniste P, Frelin C, Janmohamed S, et al. Intermediate-Term Hematopoietic Stem Cells with Extended but Time-Limited Reconstitution Potential. *Cell Stem Cell*. 2010;6(1):48-58. doi:10.1016/j.stem.2009.11.014

22. Wilson A, Laurenti E, Oser G, et al. Hematopoietic Stem Cells Reversibly Switch from Dormancy to Self-Renewal during Homeostasis and Repair. *Cell*. 2008;135(6):1118-1129. doi:10.1016/j.cell.2008.10.048

23. Sanjuan-Pla A, Macaulay IC, Jensen CT, et al. Platelet-biased stem cells reside at the apex of the haematopoietic stem-cell hierarchy. *Nature*. 2013;502(7470):232-236. doi:10.1038/nature12495

24. Laurenti E, Göttgens B. From haematopoietic stem cells to complex differentiation landscapes. *Nature*. 2018;553(7689):418-426. doi:10.1038/nature25022

25. Challen GA, Pietras EM, Wallscheid NC, Signer RAJ. Simplified murine multipotent progenitor isolation scheme: Establishing a consensus approach for multipotent progenitor identification. *Exp Hematol*. 2021;104:55-63. doi:10.1016/j.exphem.2021.09.007

26. Paul F, Arkin Y, Giladi A, et al. Transcriptional Heterogeneity and Lineage Commitment in Myeloid Progenitors. *Cell*. 2015;163(7):1663-1677. doi:10.1016/j.cell.2015.11.013

27. Grün D, Muraro MJ, Boisset JC, et al. De Novo Prediction of Stem Cell Identity using Single-Cell Transcriptome Data. *Cell Stem Cell*. 2016;19(2):266-277. doi:10.1016/j.stem.2016.05.010

28. Mitchell E, Spencer Chapman M, Williams N, et al. Clonal dynamics of haematopoiesis across the human lifespan. *Nature*. 2022;606(7913):343-350. doi:10.1038/s41586-022-04786-y

29. Wilkinson AC, Igarashi KJ, Nakauchi H. Haematopoietic stem cell self-renewal in vivo and ex vivo. *Nat Rev Genet*. 2020;21(9):541-554. doi:10.1038/s41576-020-0241-0

30. Olson OC, Kang YA, Passegué E. Normal Hematopoiesis Is a Balancing Act of Self-Renewal and Regeneration. *Cold Spring Harb Perspect Med*. 2020;10(12):a035519. doi:10.1101/cshperspect.a035519

31. Till JE, McCULLOCH EA. A direct measurement of the radiation sensitivity of normal mouse bone marrow cells. *Radiat Res*. 1961;14:213-222.

32. Purification and Characterization of Mouse Hematopoietic Stem Cells. doi:10.1126/science.2898810

33. Caocci G, Greco M, La Nasa G. Bone Marrow Homing and Engraftment Defects of Human Hematopoietic Stem and Progenitor Cells. *Mediterr J Hematol Infect Dis*. 2017;9(1):e2017032. doi:10.4084/MJHID.2017.032

34. Hasan T, Pasala AR, Hassan D, Hanotaux J, Allan DS, Maganti HB. Homing and Engraftment of Hematopoietic Stem Cells Following Transplantation: A Pre-Clinical Perspective. *Curr Oncol*. 2024;31(2):603-616. doi:10.3390/curroncol31020044

35. Sugiyama T, Kohara H, Noda M, Nagasawa T. Maintenance of the Hematopoietic Stem Cell Pool by CXCL12-CXCR4 Chemokine Signaling in Bone Marrow Stromal Cell Niches. *Immunity*. 2006;25(6):977-988. doi:10.1016/j.immuni.2006.10.016

36. Ibbotson GC, Doig C, Kaur J, et al. Functional α4-integrin: A newly identified pathway of neutrophil recruitment in critically ill septic patients. *Nat Med*. 2001;7(4):465-470. doi:10.1038/86539

37. Peled A, Kollet O, Ponomaryov T, et al. The chemokine SDF-1 activates the integrins LFA-1, VLA-4, and VLA-5 on immature human CD34+ cells: role in transendothelial/stromal migration and engraftment of NOD/SCID mice. *Blood*. 2000;95(11):3289-3296. doi:10.1182/blood.V95.11.3289

38. Thomas ED, Lochte HL, Lu WC, Ferrebee JW. Intravenous Infusion of Bone Marrow in Patients Receiving Radiation and Chemotherapy. *N Engl J Med*. 1957;257(11):491-496. doi:10.1056/NEJM195709122571102

39. Khaddour K, Hana CK, Mewawalla P. Hematopoietic Stem Cell Transplantation. In: *StatPearls*. StatPearls Publishing; 2025. Accessed September 12, 2025. http://www.ncbi.nlm.nih.gov/books/NBK536951/

40. Balassa K, Danby R, Rocha V. Haematopoietic stem cell transplants: principles and indications. *Br J Hosp Med*. 2019;80(1):33-39. doi:10.12968/hmed.2019.80.1.33

41. Copelan EA. Hematopoietic Stem-Cell Transplantation. *N Engl J Med*. 2006;354(17):1813-1826. doi:10.1056/NEJMra052638

42. Zhu X, Tang B, Sun Z. Umbilical cord blood transplantation: Still growing and improving. *Stem Cells Transl Med*. 2021;10(Suppl 2):S62-S74. doi:10.1002/sctm.20-0495

43. Meaker GA, Wilkinson AC. Ex vivo hematopoietic stem cell expansion technologies: recent progress, applications, and open questions. *Exp Hematol*. 2023;0(0). doi:10.1016/j.exphem.2023.12.001

44. Schofield R. The relationship between the spleen colony-forming cell and the haemopoietic stem cell. *Blood Cells*. 1978;4(1-2):7-25.

45. Dexter TM, Allen TD, Lajtha LG. Conditions controlling the proliferation of haemopoietic stem cells in vitro. *J Cell Physiol*. 1977;91(3):335-344. doi:10.1002/jcp.1040910303

46. Human osteoblasts support hematopoiesis through the production of granulocyte colony-stimulating factor. *J Exp Med*. 1994;179(5):1677-1682. doi:10.1084/jem.179.5.1677

47. Park D, Spencer JA, Koh BI, et al. Endogenous Bone Marrow MSCs Are Dynamic, Fate-Restricted Participants in Bone Maintenance and Regeneration. *Cell Stem Cell*. 2012;10(3):259-272. doi:10.1016/j.stem.2012.02.003

48. Zhang J, Niu C, Ye L, et al. Identification of the haematopoietic stem cell niche and control of the niche size. *Nature*. 2003;425(6960):836-841. doi:10.1038/nature02041

49. Morrison SJ, Scadden DT. The bone marrow niche for haematopoietic stem cells. *Nature*. 2014;505(7483):327-334. doi:10.1038/nature12984

50. Blair HC, Dong SS, Julian BA. Expression of stem cell factor by osteoblasts in normal and hyperparathyroid bone: relation to ectopic mast cell differentiation. *Virchows Arch*. 1999;435(1):50-57. doi:10.1007/s004280050394

51. Dolgalev I, Tikhonova AN. Connecting the Dots: Resolving the Bone Marrow Niche Heterogeneity. *Front Cell Dev Biol*. 2021;9:622519. doi:10.3389/fcell.2021.622519

52. Fröbel J, Landspersky T, Percin G, et al. The Hematopoietic Bone Marrow Niche Ecosystem. *Front Cell Dev Biol*. 2021;9:705410. doi:10.3389/fcell.2021.705410

53. Nelson P, Masel J. Intercellular competition and the inevitability of multicellular aging. *Proc Natl Acad Sci U S A*. 2017;114(49):12982-12987. doi:10.1073/pnas.1618854114

54. Kiel MJ, Yilmaz ÖH, Iwashita T, Yilmaz OH, Terhorst C, Morrison SJ. SLAM Family Receptors Distinguish Hematopoietic Stem and Progenitor Cells and Reveal Endothelial Niches for Stem Cells. *Cell*. 2005;121(7):1109-1121. doi:10.1016/j.cell.2005.05.026

55. Kiel MJ, Radice GL, Morrison SJ. Lack of Evidence that Hematopoietic Stem Cells Depend on N-Cadherin-Mediated Adhesion to Osteoblasts for Their Maintenance. *Cell Stem Cell*. 2007;1(2):204-217. doi:10.1016/j.stem.2007.06.001

56. Greenbaum A, Hsu YMS, Day RB, et al. CXCL12 Production by Early Mesenchymal Progenitors is Required for Hematopoietic Stem Cell Maintenance. *Nature*. 2013;495(7440):227-230. doi:10.1038/nature11926

57. Ding L, Saunders TL, Enikolopov G, Morrison SJ. Endothelial and perivascular cells maintain haematopoietic stem cells. *Nature*. 2012;481(7382):457-462. doi:10.1038/nature10783

58. O'Neill A, Chin D, Tan D, Majeed ABBA, Nakamura-Ishizu A, Suda T. Thrombopoietin maintains cell numbers of hematopoietic stem and progenitor cells with megakaryopoietic potential. *Haematologica*. 2020;106(7):1883-1891. doi:10.3324/haematol.2019.241406

59. Decker M, Leslie J, Liu Q, Ding L. Hepatic thrombopoietin is required for bone marrow hematopoietic stem cell maintenance. *Science*. 2018;360(6384):106-110. doi:10.1126/science.aap8861

60. Zhang J, Wu Q, Johnson CB, et al. In situ mapping identifies distinct vascular niches for myelopoiesis. *Nature*. 2021;590(7846):457-462. doi:10.1038/s41586-021-03201-2

61. Comazzetto S, Shen B, Morrison SJ. Niches that regulate stem cells and hematopoiesis in adult bone marrow. *Dev Cell*. 2021;56(13):1848-1860. doi:10.1016/j.devcel.2021.05.018

62. Latchney SE, Calvi LM. The aging hematopoietic stem cell niche: Phenotypic and functional changes and mechanisms that contribute to hematopoietic aging. *Semin Hematol*. 2017;54(1):25-32. doi:10.1053/j.seminhematol.2016.10.001

63. Moore MAS, Metcalf D. Ontogeny of the Haemopoietic System: Yolk Sac Origin of In Vivo and In Vitro Colony Forming Cells in the Developing Mouse Embryo. *Br J Haematol*. 1970;18(3):279-296. doi:10.1111/j.1365-2141.1970.tb01443.x

64. Palis J, Robertson S, Kennedy M, Wall C, Keller G. Development of erythroid and myeloid progenitors in the yolk sac and embryo proper of the mouse. *Development*. 1999;126(22):5073-5084. doi:10.1242/dev.126.22.5073

65. Tober J, Koniski A, McGrath KE, et al. The megakaryocyte lineage originates from hemangioblast precursors and is an integral component both of primitive and of definitive hematopoiesis. *Blood*. 2007;109(4):1433-1441. doi:10.1182/blood-2006-06-031898

66. SWIERS G, DE BRUIJN M, SPECK NA. Hematopoietic stem cell emergence in the conceptus and the role of Runx1. *Int J Dev Biol*. 2010;54(0):1151-1163. doi:10.1387/ijdb.103106gs

67. Ciau-Uitz A, Monteiro R, Kirmizitas A, Patient R. Developmental hematopoiesis: Ontogeny, genetic programming and conservation. *Exp Hematol*. 2014;42(8):669-683. doi:10.1016/j.exphem.2014.06.001

68. Dzierzak E, Speck NA. Of lineage and legacy – the development of mammalian hematopoietic stem cells. *Nat Immunol*. 2008;9(2):129-136. doi:10.1038/ni1560

69. Brotherton TW, Chui DH, Gauldie J, Patterson M. Hemoglobin ontogeny during normal mouse fetal development. *Proc Natl Acad Sci U S A*. 1979;76(6):2853-2857. doi:10.1073/pnas.76.6.2853

70. Medvinsky A, Dzierzak E. Definitive Hematopoiesis Is Autonomously Initiated by the AGM Region. *Cell*. 1996;86(6):897-906. doi:10.1016/S0092-8674(00)80165-8

71. Müller AM, Medvinsky A, Strouboulis J, Grosveld F, Dzierzakt E. Development of hematopoietic stem cell activity in the mouse embryo. *Immunity*. 1994;1(4):291-301. doi:10.1016/1074-7613(94)90081-7

72. Boisset JC, van Cappellen W, Andrieu-Soler C, Galjart N, Dzierzak E, Robin C. In vivo imaging of haematopoietic cells emerging from the mouse aortic endothelium. *Nature*. 2010;464(7285):116-120. doi:10.1038/nature08764

73. McGrath KE, Frame JM, Fegan KH, et al. Distinct Sources of Hematopoietic Progenitors Emerge before HSCs and Provide Functional Blood Cells in the Mammalian Embryo. *Cell Rep*. 2015;11(12):1892-1904. doi:10.1016/j.celrep.2015.05.036

74. Batsivari A, Rybtsov S, Souilhol C, et al. Understanding Hematopoietic Stem Cell Development through Functional Correlation of Their Proliferative Status with the Intra-aortic Cluster Architecture. *Stem Cell Rep*. 2017;8(6):1549-1562. doi:10.1016/j.stemcr.2017.04.003

75. Bowie MB, McKnight KD, Kent DG, McCaffrey L, Hoodless PA, Eaves CJ. Hematopoietic stem cells proliferate until after birth and show a reversible phase-specific engraftment defect. *J Clin Invest*. 2006;116(10):2808-2816. doi:10.1172/JCI28310

76. Agrawal H, Mehatre SH, Khurana S. The hematopoietic stem cell expansion niche in fetal liver: Current state of the art and the way forward. *Exp Hematol*. 2024;136:104585. doi:10.1016/j.exphem.2024.104585

77. Bowie MB, McKnight KD, Kent DG, McCaffrey L, Hoodless PA, Eaves CJ. Hematopoietic stem cells proliferate until after birth and show a reversible phase-specific engraftment defect. *J Clin Invest*. 2006;116(10):2808-2816. doi:10.1172/JCI28310

78. Christensen JL, Wright DE, Wagers AJ, Weissman IL. Circulation and Chemotaxis of Fetal Hematopoietic Stem Cells. *PLoS Biol*. 2004;2(3):e75. doi:10.1371/journal.pbio.0020075

79. Morrison SJ, Hemmati HD, Wandycz AM, Weissman IL. The purification and characterization of fetal liver hematopoietic stem cells. *Proc Natl Acad Sci U S A*. 1995;92(22):10302-10306. doi:10.1073/pnas.92.22.10302

80. Patel SH, Christodoulou C, Weinreb C, et al. Lifelong multilineage contribution by embryonic-born blood progenitors. *Nature*. 2022;606(7915):747-753. doi:10.1038/s41586-022-04804-z

81. Bowie MB, Kent DG, Dykstra B, et al. Identification of a new intrinsically timed developmental checkpoint that reprograms key hematopoietic stem cell properties. *Proc Natl Acad Sci*. 2007;104(14):5878-5882. doi:10.1073/pnas.0700460104

82. Chen C, Yu W, Tober J, et al. Spatial Genome Re-organization between Fetal and Adult Hematopoietic Stem Cells. *Cell Rep*. 2019;29(12):4200-4211.e7. doi:10.1016/j.celrep.2019.11.065

83. Holyoake TL, Nicolini FE, Eaves CJ. Functional differences between transplantable human hematopoietic stem cells from fetal liver, cord blood, and adult marrow. *Exp Hematol*. 1999;27(9):1418-1427. doi:10.1016/S0301-472X(99)00078-8

84. Yuan J, Nguyen CK, Liu X, Kanellopoulou C, Muljo SA. Lin28b reprograms adult bone marrow hematopoietic progenitors to mediate fetal-like lymphopoiesis. *Science*. 2012;335(6073):1195-1200. doi:10.1126/science.1216557

85. Darr H, Benvenisty N. Genetic Analysis of the Role of the Reprogramming Gene LIN-28 in Human Embryonic Stem Cells. *Stem Cells*. 2009;27(2):352-362. doi:10.1634/stemcells.2008-0720

86. Copley MR, Babovic S, Benz C, et al. The Lin28b–let-7–Hmga2 axis determines the higher self-renewal potential of fetal haematopoietic stem cells. *Nat Cell Biol*. 2013;15(8):916-925. doi:10.1038/ncb2783

87. Wang D, Tanaka-Yano M, Meader E, et al. Developmental maturation of the hematopoietic system controlled by a Lin28b-let-7-Cbx2 axis. *Cell Rep*. 2022;39(1):110587. doi:10.1016/j.celrep.2022.110587

88. Wilson A, Laurenti E, Oser G, et al. Hematopoietic Stem Cells Reversibly Switch from Dormancy to Self-Renewal during Homeostasis and Repair. *Cell*. 2008;135(6):1118-1129. doi:10.1016/j.cell.2008.10.048

89. Foudi A, Hochedlinger K, Van Buren D, et al. Defining Hematopoietic Stem and Progenitor Cell Turnover by Analysis of Histone 2B-GFP Dilution. *Nat Biotechnol*. 2009;27(1):84-90. doi:10.1038/nbt.1517

90. Flach J, Bakker ST, Mohrin M, et al. Replication stress is a potent driver of functional decline in ageing haematopoietic stem cells. *Nature*. 2014;512(7513):198-202. doi:10.1038/nature13619

91. Isaacs A, Lindenmann J. Pillars Article: Virus Interference. I. The Interferon. Proc R Soc Lond B Biol Sci. 1957. 147: 258-267. *J Immunol Baltim Md 1950*. 2015;195(5):1911-1920.

92. Pestka S, Krause CD, Walter MR. Interferons, interferon-like cytokines, and their receptors. *Immunol Rev*. 2004;202(1):8-32. doi:10.1111/j.0105-2896.2004.00204.x

93. Kotenko SV, Gallagher G, Baurin VV, et al. IFN-λs mediate antiviral protection through a distinct class II cytokine receptor complex. *Nat Immunol*. 2003;4(1):69-77. doi:10.1038/ni875

94. Sheppard P, Kindsvogel W, Xu W, et al. IL-28, IL-29 and their class II cytokine receptor IL-28R. *Nat Immunol*. 2003;4(1):63-68. doi:10.1038/ni873

95. Kumagai Y, Takeuchi O, Kato H, et al. Alveolar Macrophages Are the Primary Interferon-α Producer in Pulmonary Infection with RNA Viruses. *Immunity*. 2007;27(2):240-252. doi:10.1016/j.immuni.2007.07.013

96. Colonna M, Trinchieri G, Liu YJ. Plasmacytoid dendritic cells in immunity. *Nat Immunol*. 2004;5(12):1219-1226. doi:10.1038/ni1141

97. Ngo C, Garrec C, Tomasello E, Dalod M. The role of plasmacytoid dendritic cells (pDCs) in immunity during viral infections and beyond. *Cell Mol Immunol*. 2024;21(9):1008-1035. doi:10.1038/s41423-024-01167-5

98. Blasius AL, Beutler B. Intracellular Toll-like Receptors. *Immunity*. 2010;32(3):305-315. doi:10.1016/j.immuni.2010.03.012

99. Green DS, Young HA, Valencia JC. Current prospects of type II interferon γ signaling and autoimmunity. *J Biol Chem*. 2017;292(34):13925-13933. doi:10.1074/jbc.R116.774745

100. Manivasagam S, Klein RS. Type III Interferons: Emerging Roles in Autoimmunity. *Front Immunol*. 2021;12. doi:10.3389/fimmu.2021.764062

101. Darnell JE. STATs and gene regulation. *Science*. 1997;277(5332):1630-1635. doi:10.1126/science.277.5332.1630

102. Uzé G, Schreiber G, Piehler J, Pellegrini S. The receptor of the type I interferon family. *Curr Top Microbiol Immunol*. 2007;316:71-95. doi:10.1007/978-3-540-71329-6_5

103. MacNamara KC, Oduro K, Martin O, et al. Infection-Induced Myelopoiesis during Intracellular Bacterial Infection Is Critically Dependent upon IFN-γ Signaling. *J Immunol Baltim Md 1950*. 2011;186(2):1032-1043. doi:10.4049/jimmunol.1001893

104. Zhao X, Ren G, Liang L, et al. Brief Report: Interferon-γ Induces Expansion of Lin−Sca-1+C-Kit+ Cells. *Stem Cells*. 2010;28(1):122-126. doi:10.1002/stem.252

105. Chen J, Feng X, Desierto MJ, Keyvanfar K, Young NS. IFN-γ-mediated hematopoietic cell destruction in murine models of immune-mediated bone marrow failure. *Blood*. 2015;126(24):2621-2631. doi:10.1182/blood-2015-06-652453

106. Matatall KA, Shen CC, Challen GA, King KY. Type II Interferon Promotes Differentiation of Myeloid-Biased Hematopoietic Stem Cells. *Stem Cells Dayt Ohio*. 2014;32(11):3023-3030. doi:10.1002/stem.1799

107. Young HA, Klinman DM, Reynolds DA, et al. Bone Marrow and Thymus Expression of Interferon-γ Results in Severe B-Cell Lineage Reduction, T-Cell Lineage Alterations, and Hematopoietic Progenitor Deficiencies. *Blood*. 1997;89(2):583-595. doi:10.1182/blood.V89.2.583

108. Shiohara M, Koike K, Nakahata T, Komiyama A. Hematopoietic Progenitors and Synergism of Interferon-γ and Stem Cell Factor. *Leuk Lymphoma*. 1994;14(3-4):203-211. doi:10.3109/10428199409049670

109. Baldridge MT, King KY, Boles NC, Weksberg DC, Goodell MA. Quiescent hematopoietic stem cells are activated by IFNγ in response to chronic infection. *Nature*. 2010;465(7299):793-797. doi:10.1038/nature09135

110. Essers MAG, Offner S, Blanco-Bose WE, et al. IFNα activates dormant haematopoietic stem cells in vivo. *Nature*. 2009;458(7240):904-908. doi:10.1038/nature07815

111. Xu Y, Lee MKS, de Weerd NA, et al. Type I interferon signaling controls the early hematopoietic expansion in response to β-glucan. *iScience*. 2025;28(5):112347. doi:10.1016/j.isci.2025.112347

112. Villa NY, Bais S, Meacham AM, et al. Ex Vivo Virotherapy With Myxoma Virus Does Not Impair Hematopoietic Stem and Progenitor Cells. *Cytotherapy*. 2016;18(3):465-480. doi:10.1016/j.jcyt.2015.12.007

113. Hong XX, Carmichael GG. Innate Immunity in Pluripotent Human Cells. *J Biol Chem*. 2013;288(22):16196-16205. doi:10.1074/jbc.M112.435461

114. Wu X, Thi VLD, Huang Y, et al. Intrinsic Immunity Shapes Viral Resistance of Stem Cells. *Cell*. 2018;172(3):423-438.e25. doi:10.1016/j.cell.2017.11.018

115. López-Otín C, Blasco MA, Partridge L, Serrano M, Kroemer G. The Hallmarks of Aging. *Cell*. 2013;153(6):1194-1217. doi:10.1016/j.cell.2013.05.039

116. Kenyon CJ. The genetics of ageing. *Nature*. 2010;464(7288):504-512. doi:10.1038/nature08980

117. Kasbekar M, Mitchell CA, Proven MA, Passegué E. Hematopoietic Stem Cells Through the Ages: A Lifetime of Adaptation to Organismal Demands. *Cell Stem Cell*. 2023;30(11):1403-1420. doi:10.1016/j.stem.2023.09.013

118. Mitchell CA, Verovskaya EV, Calero-Nieto FJ, et al. Stromal niche inflammation mediated by IL-1 signaling is a targetable driver of hematopoietic aging. *Nat Cell Biol*. 2023;25(1):30-41. doi:10.1038/s41556-022-01053-0

119. Bogeska R, Mikecin AM, Kaschutnig P, et al. Inflammatory exposure drives long-lived impairment of hematopoietic stem cell self-renewal activity and accelerated aging. *Cell Stem Cell*. 2022;29(8):1273-1284.e8. doi:10.1016/j.stem.2022.06.012

120. Bernitz JM, Kim HS, MacArthur B, Sieburg H, Moore K. Hematopoietic Stem Cells Count and Remember Self-Renewal Divisions. *Cell*. 2016;167(5):1296-1309.e10. doi:10.1016/j.cell.2016.10.022

121. Sudo K, Ema H, Morita Y, Nakauchi H. Age-Associated Characteristics of Murine Hematopoietic Stem Cells. *J Exp Med*. 2000;192(9):1273-1280. doi:10.1084/jem.192.9.1273

122. de Haan G, Van Zant G. Dynamic Changes in Mouse Hematopoietic Stem Cell Numbers During Aging. *Blood*. 1999;93(10):3294-3301. doi:10.1182/blood.V93.10.3294.410k07_3294_3301

123. de Haan G, Nijhof W, Van Zant G. Mouse Strain-Dependent Changes in Frequency and Proliferation of Hematopoietic Stem Cells During Aging: Correlation Between Lifespan and Cycling Activity. *Blood*. 1997;89(5):1543-1550. doi:10.1182/blood.V89.5.1543

124. Lichtman MA, Rowe JM. The relationship of patient age to the pathobiology of the clonal myeloid diseases1. *Semin Oncol*. 2004;31(2):185-197. doi:10.1053/j.seminoncol.2003.12.029

125. Beghé C, Wilson A, Ershler WB. Prevalence and outcomes of anemia in geriatrics: a systematic review of the literature. *Am J Med*. 2004;116(7):3-10. doi:10.1016/j.amjmed.2003.12.009

126. Linton PJ, Dorshkind K. Age-related changes in lymphocyte development and function. *Nat Immunol*. 2004;5(2):133-139. doi:10.1038/ni1033

127. Hirokawa K, Kubo S, Utsuyama M, Kurashima C, Sado T. Age-related change in the potential of bone marrow cells to repopulate the thymus and splenic T cells in mice. *Cell Immunol*. 1986;100(2):443-451. doi:10.1016/0008-8749(86)90043-2

128. Rossi DJ, Jamieson CHM, Weissman IL. Stems Cells and the Pathways to Aging and Cancer. *Cell*. 2008;132(4):681-696. doi:10.1016/j.cell.2008.01.036

129. Jang G, Contreras Castillo S, Esteva E, et al. Stem cell decoupling underlies impaired lymphoid development during aging. *Proc Natl Acad Sci U S A*. 120(22):e2302019120. doi:10.1073/pnas.2302019120

130. George AJT, Ritter MA. Thymic involution with ageing: obsolescence or good housekeeping? *Immunol Today*. 1996;17(6):267-272. doi:10.1016/0167-5699(96)80543-3

131. Taub DD, Longo DL. Insights into thymic aging and regeneration. *Immunol Rev*. 2005;205(1):72-93. doi:10.1111/j.0105-2896.2005.00275.x

132. Palmer DB. The Effect of Age on Thymic Function. *Front Immunol*. 2013;4:316. doi:10.3389/fimmu.2013.00316

133. Rossi DJ, Bryder D, Zahn JM, et al. Cell intrinsic alterations underlie hematopoietic stem cell aging. *Proc Natl Acad Sci U S A*. 2005;102(26):9194-9199. doi:10.1073/pnas.0503280102

134. Morrison SJ, Wandycz AM, Akashi K, Globerson A, Weissman IL. The aging of hematopoietic stem cells. *Nat Med*. 1996;2(9):1011-1016. doi:10.1038/nm0996-1011

135. Thurman RE, Rynes E, Humbert R, et al. The accessible chromatin landscape of the human genome. *Nature*. 2012;489(7414):75-82. doi:10.1038/nature11232

136. Chambers SM, Shaw CA, Gatza C, Fisk CJ, Donehower LA, Goodell MA. Aging Hematopoietic Stem Cells Decline in Function and Exhibit Epigenetic Dysregulation. *PLoS Biol*. 2007;5(8):e201. doi:10.1371/journal.pbio.0050201

137. Rando TA, Chang HY. Aging, Rejuvenation, and Epigenetic Reprogramming: Resetting the Aging Clock. *Cell*. 2012;148(1-2):46-57. doi:10.1016/j.cell.2012.01.003

138. Genovese G, Kähler AK, Handsaker RE, et al. Clonal Hematopoiesis and Blood-Cancer Risk Inferred from Blood DNA Sequence. *N Engl J Med*. 2014;371(26):2477-2487. doi:10.1056/NEJMoa1409405

139. Rossi DJ, Bryder D, Seita J, Nussenzweig A, Hoeijmakers J, Weissman IL. Deficiencies in DNA damage repair limit the function of haematopoietic stem cells with age. *Nature*. 2007;447(7145):725-729. doi:10.1038/nature05862

140. Zimmermann S, Martens UM. Telomeres, senescence, and hematopoietic stem cells. *Cell Tissue Res*. 2008;331(1):79-90. doi:10.1007/s00441-007-0469-4

141. Blasco MA, Lee HW, Hande MP, et al. Telomere Shortening and Tumor Formation by Mouse Cells Lacking Telomerase RNA. *Cell*. 1997;91(1):25-34. doi:10.1016/S0092-8674(01)80006-4

142. Fagagna F d'Adda di, Reaper PM, Clay-Farrace L, et al. A DNA damage checkpoint response in telomere-initiated senescence. *Nature*. 2003;426(6963):194-198. doi:10.1038/nature02118

143. Verovskaya E, Broekhuis MJC, Zwart E, et al. Heterogeneity of young and aged murine hematopoietic stem cells revealed by quantitative clonal analysis using cellular barcoding. *Blood*. 2013;122(4):523-532. doi:10.1182/blood-2013-01-481135

144. Dykstra B, Olthof S, Schreuder J, Ritsema M, de Haan G. Clonal analysis reveals multiple functional defects of aged murine hematopoietic stem cells. *J Exp Med*. 2011;208(13):2691-2703. doi:10.1084/jem.20111490

145. Beerman I, Maloney WJ, Weissmann IL, Rossi DJ. Stem cells and the aging hematopoietic system. *Curr Opin Immunol*. 2010;22(4):500-506. doi:10.1016/j.coi.2010.06.007

146. Ergen AV, Boles NC, Goodell MA. Rantes/Ccl5 influences hematopoietic stem cell subtypes and causes myeloid skewing. *Blood*. 2012;119(11):2500-2509. doi:10.1182/blood-2011-11-391730

147. Gorentla BK, Zhong XP. T cell Receptor Signal Transduction in T lymphocytes. *J Clin Cell Immunol*. 2012;2012(Suppl 12):005. doi:10.4172/2155-9899.S12-005

148. Germain RN. T-cell development and the CD4–CD8 lineage decision. *Nat Rev Immunol*. 2002;2(5):309-322. doi:10.1038/nri798

149. Zúñiga-Pflücker JC. T-cell development made simple. *Nat Rev Immunol*. 2004;4(1):67-72. doi:10.1038/nri1257

150. Godfrey DI, Kennedy J, Suda T, Zlotnik A. A developmental pathway involving four phenotypically and functionally distinct subsets of CD3-CD4-CD8- triple-negative adult mouse thymocytes defined by CD44 and CD25 expression. *J Immunol Baltim Md 1950*. 1993;150(10):4244-4252.

151. Scollay RG, Butcher EC, Weissman IL. Thymus cell migration: Quantitative aspects of cellular traffic from the thymus to the periphery in mice. *Eur J Immunol*. 1980;10(3):210-218. doi:10.1002/eji.1830100310

152. Klein L, Kyewski B, Allen PM, Hogquist KA. Positive and negative selection of the T cell repertoire: what thymocytes see and don't see. *Nat Rev Immunol*. 2014;14(6):377-391. doi:10.1038/nri3667

153. Charles A Janeway J, Travers P, Walport M, Shlomchik MJ. The major histocompatibility complex and its functions. In: *Immunobiology: The Immune System in Health and Disease. 5th Edition*. Garland Science; 2001. Accessed September 17, 2025. https://www.ncbi.nlm.nih.gov/books/NBK27156/

154. Andersen MH, Schrama D, thor Straten P, Becker JC. Cytotoxic T Cells. *J Invest Dermatol*. 2006;126(1):32-41. doi:10.1038/sj.jid.5700001

155. Bao X, Qin Y, Lu L, Zheng M. Transcriptional Regulation of Early T-Lymphocyte Development in Thymus. *Front Immunol*. 2022;13. doi:10.3389/fimmu.2022.884569

156. von Boehmer H, Aifantis I, Feinberg J, et al. Pleiotropic changes controlled by the pre-T-cell receptor. *Curr Opin Immunol*. 1999;11(2):135-142. doi:10.1016/S0952-7915(99)80024-7

157. Borowski C, Martin C, Gounari F, et al. On the brink of becoming a T cell. *Curr Opin Immunol*. 2002;14(2):200-206. doi:10.1016/S0952-7915(02)00322-9

158. Krangel MS. Mechanics of T cell receptor gene rearrangement. *Curr Opin Immunol*. 2009;21(2):133-139. doi:10.1016/j.coi.2009.03.009

159. Tan JB, Visan I, Yuan JS, Guidos CJ. Requirement for Notch1 signals at sequential early stages of intrathymic T cell development. *Nat Immunol*. 2005;6(7):671-679. doi:10.1038/ni1217

160. Rothenberg EV. Transcriptional Drivers of the T-cell Lineage Program. *Curr Opin Immunol*. 2012;24(2):132-138. doi:10.1016/j.coi.2011.12.012

161. Rothenberg EV, Moore JE, Yui MA. Launching the T-Lineage Developmental Programme. *Nat Rev Immunol*. 2008;8(1):9-21. doi:10.1038/nri2232

162. Taghon T, Yui MA, Pant R, Diamond RA, Rothenberg EV. Developmental and molecular characterization of emerging beta- and gammadelta-selected pre-T cells in the adult mouse thymus. *Immunity*. 2006;24(1):53-64. doi:10.1016/j.immuni.2005.11.012

163. Hock H, Hamblen MJ, Rooke HM, et al. Intrinsic requirement for zinc finger transcription factor Gfi-1 in neutrophil differentiation. *Immunity*. 2003;18(1):109-120. doi:10.1016/s1074-7613(02)00501-0

164. Yücel R, Karsunky H, Klein-Hitpass L, Möröy T. The Transcriptional Repressor Gfi1 Affects Development of Early, Uncommitted c-Kit+ T Cell Progenitors and CD4/CD8 Lineage Decision in the Thymus. *J Exp Med*. 2003;197(7):831-844. doi:10.1084/jem.20021417

165. David-Fung ES, Yui MA, Morales M, et al. PROGRESSION OF REGULATORY GENE EXPRESSION STATES IN FETAL AND ADULT PRO-T CELL DEVELOPMENT. *Immunol Rev*. 2006;209:212-236. doi:10.1111/j.0105-2896.2006.00355.x

166. Varas A, Hager-Theodorides AL, Sacedón R, Vicente A, Zapata AG, Crompton T. The role of morphogens in T-cell development. *Trends Immunol*. 2003;24(4):197-206. doi:10.1016/s1471-4906(03)00033-4

167. Hager-Theodorides AL, Outram SV, Shah DK, et al. Bone morphogenetic protein 2/4 signaling regulates early thymocyte differentiation. *J Immunol Baltim Md 1950*. 2002;169(10):5496-5504. doi:10.4049/jimmunol.169.10.5496

168. El Andaloussi A, Graves S, Meng F, Mandal M, Mashayekhi M, Aifantis I. Hedgehog signaling controls thymocyte progenitor homeostasis and differentiation in the thymus. *Nat Immunol*. 2006;7(4):418-426. doi:10.1038/ni1313

169. Chann AS, Russell SM. An integrated transcriptional switch at the β-selection checkpoint determines T cell survival, development and leukaemogenesis. *Biochem Soc Trans*. 2019;47(4):1077-1089. doi:10.1042/BST20180414

170. Dutta A, Zhao B, Love PE. New insights into TCR β-selection. *Trends Immunol*. 2021;42(8):735-750. doi:10.1016/j.it.2021.06.005

171. Chann AS, Charnley M, Newton LM, et al. Stepwise progression of β-selection during T cell development involves histone deacetylation. *Life Sci Alliance*. 2022;6(1):e202201645. doi:10.26508/lsa.202201645

172. Ciofani M, Schmitt TM, Ciofani A, et al. Obligatory Role for Cooperative Signaling by Pre-TCR and Notch during Thymocyte Differentiation1. *J Immunol*. 2004;172(9):5230-5239. doi:10.4049/jimmunol.172.9.5230

173. Kreslavsky T, Gleimer M, Miyazaki M, et al. β-Selection-Induced Proliferation Is Required for αβ T Cell Differentiation. *Immunity*. 2012;37(5):840-853. doi:10.1016/j.immuni.2012.08.020

174. Positive selection of T cells: rescue from programmed cell death and differentiation require continual engagement of the T cell receptor. *J Exp Med*. 1995;181(6):1975-1984. doi:10.1084/jem.181.6.1975

175. Kyewski B, Klein L. A CENTRAL ROLE FOR CENTRAL TOLERANCE. *Annu Rev Immunol*. 2006;24(Volume 24, 2006):571-606. doi:10.1146/annurev.immunol.23.021704.115601

176. Klein L, Kyewski B, Allen PM, Hogquist KA. Positive and negative selection of the T cell repertoire: what thymocytes see and don't see. *Nat Rev Immunol*. 2014;14(6):377-391. doi:10.1038/nri3667

177. Sun L, Su Y, Jiao A, Wang X, Zhang B. T cells in health and disease. *Signal Transduct Target Ther*. 2023;8(1):235. doi:10.1038/s41392-023-01471-y

178. Alberts B, Johnson A, Lewis J, Raff M, Roberts K, Walter P. Helper T Cells and Lymphocyte Activation. In: *Molecular Biology of the Cell. 4th Edition*. Garland Science; 2002. Accessed September 17, 2025. https://www.ncbi.nlm.nih.gov/books/NBK26827/

179. Abbas AK, Murphy KM, Sher A. Functional diversity of helper T lymphocytes. *Nature*. 1996;383(6603):787-793. doi:10.1038/383787a0

180. Koh CH, Lee S, Kwak M, Kim BS, Chung Y. CD8 T-cell subsets: heterogeneity, functions, and therapeutic potential. *Exp Mol Med*. 2023;55(11):2287-2299. doi:10.1038/s12276-023-01105-x

181. Raphael I, Nalawade S, Eagar TN, Forsthuber TG. T cell subsets and their signature cytokines in autoimmune and inflammatory diseases. *Cytokine*. 2015;74(1):5-17. doi:10.1016/j.cyto.2014.09.011

182. Vignali DAA, Collison LW, Workman CJ. How regulatory T cells work. *Nat Rev Immunol*. 2008;8(7):523-532. doi:10.1038/nri2343

183. Hori S, Nomura T, Sakaguchi S. Control of Regulatory T Cell Development by the Transcription Factor Foxp3. *Science*. 2003;299(5609):1057-1061. doi:10.1126/science.1079490

184. Fontenot JD, Gavin MA, Rudensky AY. Foxp3 programs the development and function of CD4+CD25+ regulatory T cells. *Nat Immunol*. 2003;4(4):330-336. doi:10.1038/ni904

185. Nagata S. Fas-Mediated Apoptosis. In: Gupta S, Cohen JJ, eds *Mechanisms of Lymphocyte Activation and Immune Regulation VI*. Vol 406. Advances in Experimental Medicine and Biology. Springer US; 1996:119-124. doi:10.1007/978-1-4899-0274-0_12

186. Ju ST, Panka DJ, Cui H, et al. Fas(CD95)/FasL interactions required for programmed cell death after T-cell activation. *Nature*. 1995;373(6513):444-448. doi:10.1038/373444a0

187. Mogil RJ, Radvanyi L, Gonzalez-Quintial R, et al. Fas (CD95) participates in peripheral T cell deletion and associated apoptosis in vivo. *Int Immunol*. 1995;7(9):1451-1458. doi:10.1093/intimm/7.9.1451

188. Trapani JA, Smyth MJ. Functional significance of the perforin/granzyme cell death pathway. *Nat Rev Immunol*. 2002;2(10):735-747. doi:10.1038/nri911

189. Stinchcombe JC, Griffiths GM. Secretory Mechanisms in Cell-Mediated Cytotoxicity. *Annu Rev Cell Dev Biol*. 2007;23(Volume 23, 2007):495-517. doi:10.1146/annurev.cellbio.23.090506.123521

190. Tau GZ, Cowan SN, Weisburg J, Braunstein NS, Rothman PB. Regulation of IFN-γ Signaling Is Essential for the Cytotoxic Activity of CD8+ T Cells. *J Immunol Baltim Md 1950*. 2001;167(10):5574-5582. doi:10.4049/jimmunol.167.10.5574

191. Zheng L, Fisher G, Miller RE, Peschon J, Lynch DH, Lenardo MJ. Induction of apoptosis in mature T cells by tumour necrosis factor. *Nature*. 1995;377(6547):348-351. doi:10.1038/377348a0

192. Ahmed R, Gray D. Immunological Memory and Protective Immunity: Understanding Their Relation. *Science*. 1996;272(5258):54-60. doi:10.1126/science.272.5258.54

193. Kaech SM, Cui W. Transcriptional control of effector and memory CD8+ T cell differentiation. *Nat Rev Immunol*. 2012;12(11):749-761. doi:10.1038/nri3307

194. Sallusto F, Lenig D, Förster R, Lipp M, Lanzavecchia A. Two subsets of memory T lymphocytes with distinct homing potentials and effector functions. *Nature*. 1999;401(6754):708-712. doi:10.1038/44385

195. Gattinoni L, Speiser DE, Lichterfeld M, Bonini C. T memory stem cells in health and disease. *Nat Med*. 2017;23(1):18-27. doi:10.1038/nm.4241

196. Yang J, Brook MO, Carvalho-Gaspar M, et al. Allograft rejection mediated by memory T cells is resistant to regulation. *Proc Natl Acad Sci U S A*. 2007;104(50):19954-19959. doi:10.1073/pnas.0704397104

197. Kornberg RD. The molecular basis of eukaryotic transcription. *Proc Natl Acad Sci U S A*. 2007;104(32):12955-12961. doi:10.1073/pnas.0704138104

198. Thomas MC, Chiang CM. The general transcription machinery and general cofactors. *Crit Rev Biochem Mol Biol*. 2006;41(3):105-178. doi:10.1080/10409230600648736

199. Spitz F, Furlong EEM. Transcription factors: from enhancer binding to developmental control. *Nat Rev Genet*. 2012;13(9):613-626. doi:10.1038/nrg3207

200. Mazina MYu, Vorobyeva NE. Chromatin Modifiers in Transcriptional Regulation: New Findings and Prospects. *Acta Naturae*. 2021;13(1):16-30. doi:10.32607/actanaturae.11101

201. Banerji J, Rusconi S, Schaffner W. Expression of a beta-globin gene is enhanced by remote SV40 DNA sequences. *Cell*. 1981;27(2 Pt 1):299-308. doi:10.1016/0092-8674(81)90413-x

202. Lambert SA, Jolma A, Campitelli LF, et al. The Human Transcription Factors. *Cell*. 2018;172(4):650-665. doi:10.1016/j.cell.2018.01.029

203. Orkin SH, Zon LI. Hematopoiesis: An Evolving Paradigm for Stem Cell Biology. *Cell*. 2008;132(4):631-644. doi:10.1016/j.cell.2008.01.025

204. Kim SI, Bresnick EH. Transcriptional control of erythropoiesis: emerging mechanisms and principles. *Oncogene*. 2007;26(47):6777-6794. doi:10.1038/sj.onc.1210761

205. Orkin SH. Diversification of haematopoietic stem cells to specific lineages. *Nat Rev Genet*. 2000;1(1):57-64. doi:10.1038/35049577

206. Göttgens B, Nastos A, Kinston S, et al. Establishing the transcriptional programme for blood: The SCL stem cell enhancer is regulated by a multiprotein complex containing Ets and GATA factors. *EMBO J*. 2002;21(12):3039-3050. doi:10.1093/emboj/cdf286

207. Wilson NK, Foster SD, Wang X, et al. Combinatorial Transcriptional Control In Blood Stem/Progenitor Cells: Genome-wide Analysis of Ten Major Transcriptional Regulators. *Cell Stem Cell*. 2010;7(4):532-544. doi:10.1016/j.stem.2010.07.016

208. Hsu T, Schulz RA. Sequence and functional properties of Ets genes in the model organism Drosophila. *Oncogene*. 2000;19(55):6409-6416. doi:10.1038/sj.onc.1204033

209. Ciau-Uitz A, Wang L, Patient R, Liu F. ETS transcription factors in hematopoietic stem cell development. *Blood Cells Mol Dis*. 2013;51(4):248-255. doi:10.1016/j.bcmd.2013.07.010

210. Hart AH, Reventar R, Bernstein A. Genetic analysis of ETS genes in C. elegans. *Oncogene*. 2000;19(55):6400-6408. doi:10.1038/sj.onc.1204040

211. Liu F, Patient R. Genome-wide analysis of the zebrafish ets family identifies three genes required for hemangioblast differentiation or angiogenesis. *Circ Res*. 2008;103(10):1147-1154. doi:10.1161/CIRCRESAHA.108.179713

212. Hoogenkamp M, Krysinska H, Ingram R, et al. The Pu.1 Locus Is Differentially Regulated at the Level of Chromatin Structure and Noncoding Transcription by Alternate Mechanisms at Distinct Developmental Stages of Hematopoiesis. *Mol Cell Biol*. 2007;27(21):7425-7438. doi:10.1128/MCB.00905-07

213. Yokomizo T, Ogawa M, Osato M, et al. Requirement of Runx1/AML1/PEBP2αB for the generation of haematopoietic cells from endothelial cells. *Genes Cells*. 2001;6(1):13-23. doi:10.1046/j.1365-2443.2001.00393.x

214. Nottingham WT, Jarratt A, Burgess M, et al. Runx1-mediated hematopoietic stem-cell emergence is controlled by a Gata/Ets/SCL-regulated enhancer. *Blood*. 2007;110(13):4188-4197. doi:10.1182/blood-2007-07-100883

215. Arman M, Aguilera-Montilla N, Mas V, et al. The human *CD6* gene is transcriptionally regulated by RUNX and Ets transcription factors in T cells. *Mol Immunol*. 2009;46(11):2226-2235. doi:10.1016/j.molimm.2009.04.018

216. Fowler M, Borazanci E, McGhee L, et al. RUNX1 (AML-1) and RUNX2 (AML-3) cooperate with prostate-derived Ets factor to activate transcription from the PSA upstream regulatory region. *J Cell Biochem*. 2006;97(1):1-17. doi:10.1002/jcb.20664

217. Ng AP, Loughran SJ, Metcalf D, et al. Erg is required for self-renewal of hematopoietic stem cells during stress hematopoiesis in mice. *Blood*. 2011;118(9):2454-2461. doi:10.1182/blood-2011-03-344739

218. Nijnik A, Woodbine L, Marchetti C, et al. DNA repair is limiting for haematopoietic stem cells during ageing. *Nature*. 2007;447(7145):686-690. doi:10.1038/nature05875

219. Satoh Y, Yokota T, Sudo T, et al. The Satb1 Protein Directs Hematopoietic Stem Cell Differentiation toward Lymphoid Lineages. *Immunity*. 2013;38(6):1105-1115. doi:10.1016/j.immuni.2013.05.014

220. He X, Hawkins C, Lawley L, et al. Loss of G-protein coupled receptor 68 in hematopoietic tissues enhances long-term hematopoietic stem cell function upon aging. *Stem Cell Res Ther*. 2025;16:408. doi:10.1186/s13287-025-04506-z

221. Zhang S, Ayemoba CE, Di Staulo AM, et al. Platelet Factor 4 (PF4) Regulates Hematopoietic Stem Cell Aging. *Blood*. Published online 8 September 2025:blood.2024027432. doi:10.1182/blood.2024027432

222. Xu P, Zhang X, Li D, et al. Loss of DCAF8 impairs hematopoietic stem cell function with cellular senescence via the DOCK11-CDC42 axis. *Blood*. Published online 10 July 2025:blood.2024027335. doi:10.1182/blood.2024027335

223. Blyth K, Cameron ER, Neil JC. The runx genes: gain or loss of function in cancer. *Nat Rev Cancer*. 2005;5(5):376-387. doi:10.1038/nrc1607

224. de Bruijn M, Dzierzak E. Runx transcription factors in the development and function of the definitive hematopoietic system. *Blood*. 2017;129(15):2061-2069. doi:10.1182/blood-2016-12-689109

225. Rennert J, Coffman JA, Mushegian AR, Robertson AJ. The evolution of Runx genes I. A comparative study of sequences from phylogenetically diverse model organisms. *BMC Evol Biol*. 2003;3(1):4. doi:10.1186/1471-2148-3-4

226. Gergen JP, Wieschaus E. Dosage requirements for runt in the segmentation of Drosophila embryos. *Cell*. 1986;45(2):289-299. doi:10.1016/0092-8674(86)90393-4

227. Ogawa E, Inuzuka M, Maruyama M, et al. Molecular Cloning and Characterization of PEBP2β, the Heterodimeric Partner of a Novel *Drosophila runt*-Related DNA Binding Protein PEBP2α. *Virology*. 1993;194(1):314-331. doi:10.1006/viro.1993.1262

228. Wang S, Wang Q, Crute BE, Melnikova IN, Keller SR, Speck NA. Cloning and Characterization of Subunits of the T-Cell Receptor and Murine Leukemia Virus Enhancer Core-Binding Factor. *Mol Cell Biol*. 1993;13(6):3324-3339. doi:10.1128/mcb.13.6.3324-3339.1993

229. Ito Y, Bae SC, Chuang LSH. The RUNX family: developmental regulators in cancer. *Nat Rev Cancer*. 2015;15(2):81-95. doi:10.1038/nrc3877

230. Strippoli P, D'Addabbo P, Lenzi L, et al. Segmental paralogy in the human genome: a large-scale triplication on 1p, 6p, and 21q. *Mamm Genome*. 2002;13(8):456-462. doi:10.1007/s00335-001-2157-0

231. Newton AH, Pask AJ. Evolution and expansion of the RUNX2 QA repeat corresponds with the emergence of vertebrate complexity. *Commun Biol*. 2020;3(1):1-9. doi:10.1038/s42003-020-01501-3

232. Morrison NA, Stephens AA, Osato M, et al. Glutamine Repeat Variants in Human RUNX2 Associated with Decreased Femoral Neck BMD, Broadband Ultrasound Attenuation and Target Gene Transactivation. *PLOS ONE*. 2012;7(8):e42617. doi:10.1371/journal.pone.0042617

233. Thirunavukkarasu K, Mahajan M, McLarren KW, Stifani S, Karsenty G. Two Domains Unique to Osteoblast-Specific Transcription Factor Osf2/Cbfa1 Contribute to Its Transactivation Function and Its Inability To Heterodimerize with Cbfβ. *Mol Cell Biol*. 1998;18(7):4197-4208.

234. Tahirov TH, Inoue-Bungo T, Morii H, et al. Structural Analyses of DNA Recognition by the AML1/Runx-1 Runt Domain and Its Allosteric Control by CBFβ. *Cell*. 2001;104(5):755-767. doi:10.1016/S0092-8674(01)00271-9

235. Krishnan V. The RUNX Family of Proteins, DNA Repair, and Cancer. *Cells*. 2023;12(8):1106. doi:10.3390/cells12081106

236. Levanon D, Goldstein RE, Bernstein Y, et al. Transcriptional repression by AML1 and LEF-1 is mediated by the TLE/Groucho corepressors. *Proc Natl Acad Sci*. 1998;95(20):11590-11595. doi:10.1073/pnas.95.20.11590

237. Aronson BD, Fisher AL, Blechman K, Caudy M, Gergen JP. Groucho-dependent and -independent repression activities of Runt domain proteins. *Mol Cell Biol*. 1997;17(9):5581-5587. doi:10.1128/mcb.17.9.5581

238. Durst KL, Hiebert SW. Role of RUNX family members in transcriptional repression and gene silencing. *Oncogene*. 2004;23(24):4220-4224. doi:10.1038/sj.onc.1207122

239. Lutterbach B, Westendorf JJ, Linggi B, Isaac S, Seto E, Hiebert SW. A Mechanism of Repression by Acute Myeloid Leukemia-1, the Target of Multiple Chromosomal Translocations in Acute Leukemia *. *J Biol Chem*. 2000;275(1):651-656. doi:10.1074/jbc.275.1.651

240. Laherty CD, Yang WM, Sun JM, Davie JR, Seto E, Eisenman RN. Histone Deacetylases Associated with the mSin3 Corepressor Mediate Mad Transcriptional Repression. *Cell*. 1997;89(3):349-356. doi:10.1016/S0092-8674(00)80215-9

241. Durst KL, Lutterbach B, Kummalue T, Friedman AD, Hiebert SW. The inv(16) Fusion Protein Associates with Corepressors via a Smooth Muscle Myosin Heavy-Chain Domain. *Mol Cell Biol*. 2003;23(2):607-619. doi:10.1128/MCB.23.2.607-619.2003

242. Aikawa Y, Nguyen L, Isono K, et al. Roles of HIPK1 and HIPK2 in AML1- and p300-dependent transcription, hematopoiesis and blood vessel formation. *EMBO J*. 2006;25:3955-3965. doi:10.1038/sj.emboj.7601273

243. Sierra J, Villagra A, Paredes R, et al. Regulation of the Bone-Specific Osteocalcin Gene by p300 Requires Runx2/Cbfa1 and the Vitamin D3 Receptor but Not p300 Intrinsic Histone Acetyltransferase Activity. *Mol Cell Biol*. 2003;23(9):3339-3351. doi:10.1128/MCB.23.9.3339-3351.2003

244. Westendorf JJ, Yamamoto CM, Lenny N, Downing JR, Selsted ME, Hiebert SW. The t(8;21) Fusion Product, AML-1–ETO, Associates with C/EBP-α, Inhibits C/EBP-α-Dependent Transcription, and Blocks Granulocytic Differentiation. *Mol Cell Biol*. 1998;18(1):322-333. doi:10.1128/mcb.18.1.322

245. Giese K, Kingsley C, Kirshner JR, Grosschedl R. Assembly and function of a TCR alpha enhancer complex is dependent on LEF-1-induced DNA bending and multiple protein-protein interactions. *Genes Dev*. 1995;9(8):995-1008. doi:10.1101/gad.9.8.995

246. Shrivastava T, Mino K, Babayeva ND, I.Baranovskaya O, Rizzino A, Tahirov TH. Structural basis of Ets1 activation by Runx1. *Leukemia*. 2014;28(10):2040-2048. doi:10.1038/leu.2014.111

247. Gu TL, Goetz TL, Graves BJ, Speck NA. Auto-Inhibition and Partner Proteins, Core-Binding Factor β (CBFβ) and Ets-1, Modulate DNA Binding by CBFα2 (AML1). *Mol Cell Biol*. 2000;20(1):91-103. doi:10.1128/mcb.20.1.91-103.2000

248. Zaidi SK, Sullivan AJ, van Wijnen AJ, Stein JL, Stein GS, Lian JB. Integration of Runx and Smad regulatory signals at transcriptionally active subnuclear sites. *Proc Natl Acad Sci*. 2002;99(12):8048-8053. doi:10.1073/pnas.112664499

249. Yao F, Xiao Z, Sun Y, Ma L. SKP2 and OTUD1 govern non-proteolytic ubiquitination of YAP that promotes YAP nuclear localization and activity. *Cell Stress*. 2(9):233-235. doi:10.15698/cst2018.09.153

250. Korinfskaya S, Parameswaran S, Weirauch MT, Barski A. Runx Transcription Factors in T Cells—What Is Beyond Thymic Development? *Front Immunol*. 2021;12. doi:10.3389/fimmu.2021.701924

251. Huang G, Zhang P, Hirai H, et al. PU.1 is a major downstream target of AML1 (RUNX1) in adult mouse hematopoiesis. *Nat Genet*. 2008;40(1):51-60. doi:10.1038/ng.2007.7

252. Mevel R, Draper JE, Lie-a-Ling M, Kouskoff V, Lacaud G. RUNX transcription factors: orchestrators of development. *Development*. 2019;146(17):dev148296. doi:10.1242/dev.148296

253. Chen MJ, Yokomizo T, Zeigler B, Dzierzak E, Speck NA. Runx1 is required for the endothelial to hematopoietic cell transition but not thereafter. *Nature*. 2009;457(7231):887-891. doi:10.1038/nature07619

254. Mangan JK, Speck NA. RUNX1 mutations in clonal myeloid disorders: from conventional cytogenetics to next generation sequencing, a story 40 years in the making. *Crit Rev Oncog*. 2011;16(1-2):77-91.

255. North T, Gu TL, Stacy T, et al. Cbfa2 is required for the formation of intra-aortic hematopoietic clusters. *Development*. 1999;126(11):2563-2575. doi:10.1242/dev.126.11.2563

256. Yzaguirre AD, de Bruijn MFTR, Speck NA. The role of Runx1 in embryonic blood cell formation. *Adv Exp Med Biol*. 2017;962:47-64. doi:10.1007/978-981-10-3233-2_4

257. Lacaud G, Gore L, Kennedy M, et al. Runx1 is essential for hematopoietic commitment at the hemangioblast stage of development in vitro. *Blood*. 2002;100(2):458-466. doi:10.1182/blood-2001-12-0321

258. Miyoshi H, Ohira M, Shimizu K, et al. Alternative splicing and genomic structure of the AML1 gene involved in acute myeloid leukemia. *Nucleic Acids Res*. 1995;23(14):2762-2769.

259. Telfer JC, Rothenberg EV. Expression and Function of a Stem Cell Promoter for the Murine CBFα2 Gene: Distinct Roles and Regulation in Natural Killer and T Cell Development. *Dev Biol*. 2001;229(2):363-382. doi:10.1006/dbio.2000.9991

260. Martinez M, Hinojosa M, Trombly D, et al. Transcriptional Auto-Regulation of RUNX1 P1 Promoter. *PLoS ONE*. 2016;11(2):e0149119. doi:10.1371/journal.pone.0149119

261. Lorsbach RB, Moore J, Ang SO, Sun W, Lenny N, Downing JR. Role of RUNX1 in adult hematopoiesis: analysis of RUNX1-IRES-GFP knock-in mice reveals differential lineage expression. *Blood*. 2004;103(7):2522-2529. doi:10.1182/blood-2003-07-2439

262. North TE, Stacy T, Matheny CJ, Speck NA, de Bruijn MFTR. Runx1 Is Expressed in Adult Mouse Hematopoietic Stem Cells and Differentiating Myeloid and Lymphoid Cells, But Not in Maturing Erythroid Cells. *Stem Cells*. 2004;22(2):158-168. doi:10.1634/stemcells.22-2-158

263. Motoda L, Osato M, Yamashita N, et al. Runx1 Protects Hematopoietic Stem/Progenitor Cells from Oncogenic Insult. *Stem Cells*. 2007;25(12):2976-2986. doi:10.1634/stemcells.2007-0061

264. Cai X, Gaudet JJ, Mangan JK, et al. Runx1 Loss Minimally Impacts Long-Term Hematopoietic Stem Cells. *PLoS ONE*. 2011;6(12):e28430. doi:10.1371/journal.pone.0028430

265. Cai X, Gao L, Teng L, et al. Runx1 deficiency decreases ribosome biogenesis and confers stress resistance to hematopoietic stem and progenitor cells. *Cell Stem Cell*. 2015;17(2):165-177. doi:10.1016/j.stem.2015.06.002

266. Growney JD, Shigematsu H, Li Z, et al. Loss of Runx1 perturbs adult hematopoiesis and is associated with a myeloproliferative phenotype. *Blood*. 2005;106(2):494-504. doi:10.1182/blood-2004-08-3280

267. Ichikawa M, Asai T, Saito T, et al. AML-1 is required for megakaryocytic maturation and lymphocytic differentiation, but not for maintenance of hematopoietic stem cells in adult hematopoiesis. *Nat Med*. 2004;10(3):299-304. doi:10.1038/nm997

268. Sun W, Downing JR. Haploinsufficiency of AML1 results in a decrease in the number of LTR-HSCs while simultaneously inducing an increase in more mature progenitors. *Blood*. 2004;104(12):3565-3572. doi:10.1182/blood-2003-12-4349

269. Ng KP, Hu Z, Ebrahem Q, Negrotto S, Lausen J, Saunthararajah Y. Runx1 deficiency permits granulocyte lineage commitment but impairs subsequent maturation. *Oncogenesis*. 2013;2(11):e78. doi:10.1038/oncsis.2013.41

270. Song WJ, Sullivan MG, Legare RD, et al. Haploinsufficiency of CBFA2 causes familial thrombocytopenia with propensity to develop acute myelogenous leukaemia. *Nat Genet*. 1999;23(2):166-175. doi:10.1038/13793

271. Deuitch N, Broadbridge E, Cunningham L, Liu P. RUNX1 Familial Platelet Disorder with Associated Myeloid Malignancies. In: Adam MP, Feldman J, Mirzaa GM, Pagon RA, Wallace SE, Amemiya A, eds *GeneReviews®*. University of Washington, Seattle; 1993. Accessed March 13, 2025. http://www.ncbi.nlm.nih.gov/books/NBK568319/

272. Schlegelberger B, Heller PG. RUNX1 deficiency (familial platelet disorder with predisposition to myeloid leukemia, FPDMM). *Semin Hematol*. 2017;54(2):75-80. doi:10.1053/j.seminhematol.2017.04.006

273. Metzeler KH, Bloomfield CD. Clinical Relevance of RUNX1 and CBFB Alterations in Acute Myeloid Leukemia and Other Hematological Disorders. In: Groner Y, Ito Y, Liu P, Neil JC, Speck NA, van Wijnen A, eds *RUNX Proteins in Development and Cancer*. Springer; 2017:175-199. doi:10.1007/978-981-10-3233-2_12

274. Sood R, Kamikubo Y, Liu P. Role of RUNX1 in hematological malignancies. *Blood*. 2017;129(15):2070-2082. doi:10.1182/blood-2016-10-687830

275. Satake M, Nomura S, Yamaguchi-Iwai Y, et al. Expression of the Runt Domain-Encoding PEBP2α Genes in T cells during Thymic Development. *Mol Cell Biol*. 1995;15(3):1662-1670. doi:10.1128/MCB.15.3.1662

276. Ogawa E, Maruyama M, Kagoshima H, et al. PEBP2/PEA2 represents a family of transcription factors homologous to the products of the Drosophila runt gene and the human AML1 gene. *Proc Natl Acad Sci U S A*. 1993;90(14):6859-6863. doi:10.1073/pnas.90.14.6859

277. Komori T. Roles of Runx2 in Skeletal Development. In: Groner Y, Ito Y, Liu P, Neil JC, Speck NA, van Wijnen A, eds *RUNX Proteins in Development and Cancer*. Springer; 2017:83-93. doi:10.1007/978-981-10-3233-2_6

278. Komori T, Yagi H, Nomura S, et al. Targeted Disruption of Cbfa1 Results in a Complete Lack of Bone Formation owing to Maturational Arrest of Osteoblasts. *Cell*. 1997;89(5):755-764. doi:10.1016/S0092-8674(00)80258-5

279. Otto F, Thornell AP, Crompton T, et al. Cbfa1, a Candidate Gene for Cleidocranial Dysplasia Syndrome, Is Essential for Osteoblast Differentiation and Bone Development. *Cell*. 1997;89(5):765-771. doi:10.1016/S0092-8674(00)80259-7

280. Komori T. Runx2, an inducer of osteoblast and chondrocyte differentiation. *Histochem Cell Biol*. 2018;149(4):313-323. doi:10.1007/s00418-018-1640-6

281. Liu JC, Lengner CJ, Gaur T, et al. Runx2 Protein Expression Utilizes the Runx2 P1 Promoter to Establish Osteoprogenitor Cell Number for Normal Bone Formation. *J Biol Chem*. 2011;286(34):30057-30070. doi:10.1074/jbc.M111.241505

282. Banerjee C, Javed A, Choi JY, et al. Differential Regulation of the Two Principal Runx2/Cbfa1 N-Terminal Isoforms in Response to Bone Morphogenetic Protein-2 during Development of the Osteoblast Phenotype. *Endocrinology*. 2001;142(9):4026-4039. doi:10.1210/endo.142.9.8367

283. Banerjee C, McCabe LR, Choi JY, et al. Runt homology domain proteins in osteoblast differentiation: AML3/CBFA1 is a major component of a bone-specific complex. *J Cell Biochem*. 1997;66(1):1-8. doi:10.1002/(SICI)1097-4644(19970701)66:1%3C1::AID-JCB1%3E3.0.CO;2-V

284. Ducy P, Zhang R, Geoffroy V, Ridall AL, Karsenty G. Osf2/Cbfa1: A Transcriptional Activator of Osteoblast Differentiation. *Cell*. 1997;89(5):747-754. doi:10.1016/S0092-8674(00)80257-3

285. Enomoto H, Enomoto-Iwamoto M, Iwamoto M, et al. Cbfa1 Is a Positive Regulatory Factor in Chondrocyte Maturation *. *J Biol Chem*. 2000;275(12):8695-8702. doi:10.1074/jbc.275.12.8695

286. Fujiwara M, Tagashira S, Harada H, et al. Isolation and characterization of the distal promoter region of mouse *Cbfa1*1. *Biochim Biophys Acta BBA - Gene Struct Expr*. 1999;1446(3):265-272. doi:10.1016/S0167-4781(99)00113-X

287. Stewart M, Terry A, Hu M, et al. Proviral insertions induce the expression of bone-specific isoforms of PEBP2αA (CBFA1): Evidence for a new myc collaborating oncogene. *Proc Natl Acad Sci U S A*. 1997;94(16):8646-8651.

288. Otto F, Kanegane H, Mundlos S. Mutations in the RUNX2 gene in patients with cleidocranial dysplasia. *Hum Mutat*. 2002;19(3):209-216. doi:10.1002/humu.10043

289. Hartmann C, Yang Y. Chapter 1 - Molecular and cellular regulation of intramembranous and endochondral bone formation during embryogenesis. In: Bilezikian JP, Martin TJ, Clemens TL, Rosen CJ, eds *Principles of Bone Biology (Fourth Edition)*. Academic Press; 2020:5-44. doi:10.1016/B978-0-12-814841-9.00001-4

290. Azarkina K, Gromova E, Malashicheva A. “A Friend Among Strangers” or the Ambiguous Roles of Runx2. *Biomolecules*. 2024;14(11):1392. doi:10.3390/biom14111392

291. Komori T. Whole Aspect of Runx2 Functions in Skeletal Development. *Int J Mol Sci*. 2022;23(10):5776. doi:10.3390/ijms23105776

292. Chen B, Banton MC, Singh L, Parkinson DB, Dun X peng. Single Cell Transcriptome Data Analysis Defines the Heterogeneity of Peripheral Nerve Cells in Homeostasis and Regeneration. *Front Cell Neurosci*. 2021;15. doi:10.3389/fncel.2021.624826

293. Hu R, Dun X, Singh L, Banton MC. Runx2 regulates peripheral nerve regeneration to promote Schwann cell migration and re-myelination. *Neural Regen Res*. 2024;19(7):1575. doi:10.4103/1673-5374.387977

294. Westendorf JJ, Zaidi SK, Cascino JE, et al. Runx2 (Cbfa1, AML-3) Interacts with Histone Deacetylase 6 and Represses the p21CIP1/WAF1 Promoter. *Mol Cell Biol*. 2002;22(22):7982-7992. doi:10.1128/MCB.22.22.7982-7992.2002

295. Sun L, Vitolo MI, Qiao M, Anglin IE, Passaniti A. Regulation of TGFβ1-mediated growth inhibition and apoptosis by RUNX2 isoforms in endothelial cells. *Oncogene*. 2004;23(27):4722-4734. doi:10.1038/sj.onc.1207589

296. Qiao M, Shapiro P, Fosbrink M, Rus H, Kumar R, Passaniti A. Cell Cycle-dependent Phosphorylation of the RUNX2 Transcription Factor by cdc2 Regulates Endothelial Cell Proliferation *. *J Biol Chem*. 2006;281(11):7118-7128. doi:10.1074/jbc.M508162200

297. Kreis NN, Louwen F, Yuan J. Less understood issues: p21Cip1 in mitosis and its therapeutic potential. *Oncogene*. 2015;34(14):1758-1767. doi:10.1038/onc.2014.133

298. El-Deiry WS, Tokino T, Velculescu VE, et al. *WAF1*, a potential mediator of p53 tumor suppression. *Cell*. 1993;75(4):817-825. doi:10.1016/0092-8674(93)90500-P

299. Kuo YH, Zaidi SK, Gornostaeva S, Komori T, Stein GS, Castilla LH. Runx2 induces acute myeloid leukemia in cooperation with Cbfβ-SMMHC in mice. *Blood*. 2009;113(14):3323-3332. doi:10.1182/blood-2008-06-162248

300. Wahlen S, Matthijssens F, Van Loocke W, et al. The transcription factor RUNX2 drives the generation of human NK cells and promotes tissue residency. *eLife*. 11:e80320. doi:10.7554/eLife.80320

301. Vaillant F, Blyth K, Andrew L, Neil JC, Cameron ER. Enforced Expression of Runx2 Perturbs T Cell Development at a Stage Coincident with β-Selection1. *J Immunol*. 2002;169(6):2866-2874. doi:10.4049/jimmunol.169.6.2866

302. Vaillant F, Blyth K, Terry A, et al. A full-length Cbfa1 gene product perturbs T-cell development and promotes lymphomagenesis in synergy with MYC. *Oncogene*. 1999;18(50):7124-7134. doi:10.1038/sj.onc.1203202

303. Sawai CM, Sisirak V, Ghosh HS, et al. Transcription factor Runx2 controls the development and migration of plasmacytoid dendritic cells. *J Exp Med*. 2013;210(11):2151-2159. doi:10.1084/jem.20130443

304. Mundlos S. Cleidocranial dysplasia: clinical and molecular genetics. *J Med Genet*. 1999;36(3):177-182.

305. The classic: Marie, P., and Sainton P.: Sur la dysostose cleido-cranienne herediataire, Rev. neurol. 6:835, 1898. On hereditary cleido-cranial dysostosis. *Clin Orthop*. 1968;58:5-7.

306. Thaweesapphithak S, Termteerapornpimol K, Wongsirisuwan S, Chantarangsu S, Porntaveetus T. The impact of RUNX2 gene variants on cleidocranial dysplasia phenotype: a systematic review. *J Transl Med*. 2024;22:1099. doi:10.1186/s12967-024-05904-2

307. Gardham A, Forsythe E, Goulden N. One in 10 million: a case of cleidocranial dysplasia and acute lymphoblastic leukaemia – more than just a coincidence? *Clin Dysmorphol*. 2012;21(3):170. doi:10.1097/MCD.0b013e32835431fd

308. Blyth K, Vaillant F, Hanlon L, et al. Runx2 and MYC Collaborate in Lymphoma Development by Suppressing Apoptotic and Growth Arrest Pathways In vivo. *Cancer Res*. 2006;66(4):2195-2201. doi:10.1158/0008-5472.CAN-05-3558

309. Barnes GL, Javed A, Waller SM, et al. Osteoblast-related transcription factors Runx2 (Cbfa1/AML3) and MSX2 mediate the expression of bone sialoprotein in human metastatic breast cancer cells. *Cancer Res*. 2003;63(10):2631-2637.

310. Barnes GL, Hebert KE, Kamal M, et al. Fidelity of Runx2 Activity in Breast Cancer Cells Is Required for the Generation of Metastases-Associated Osteolytic Disease. *Cancer Res*. 2004;64(13):4506-4513. doi:10.1158/0008-5472.CAN-03-3851

311. Bangsow C, Rubins N, Glusman G, et al. The *RUNX3* gene – sequence, structure and regulated expression. *Gene*. 2001;279(2):221-232. doi:10.1016/S0378-1119(01)00760-0

312. Levanon D, Glusman G, Bettoun D, et al. Phylogenesis and regulated expression of the RUNT domain transcription factors RUNX1 and RUNX3. *Blood Cells Mol Dis*. 2003;30(2):161-163. doi:10.1016/S1079-9796(03)00023-8

313. Woolf E, Xiao C, Fainaru O, et al. Runx3 and Runx1 are required for CD8 T cell development during thymopoiesis. *Proc Natl Acad Sci*. 2003;100(13):7731-7736. doi:10.1073/pnas.1232420100

314. Ebihara T, Song C, Ryu SH, et al. Runx3 specifies lineage commitment of innate lymphoid cells. *Nat Immunol*. 2015;16(11):1124-1133. doi:10.1038/ni.3272

315. Egawa T, Littman DR. The transcription factor ThPOK acts late in helper T cell lineage specification and suppresses Runx-mediated commitment to the cytotoxic T cell lineage. *Nat Immunol*. 2008;9(10):1131-1139. doi:10.1038/ni.1652

316. Shin B, Zhou W, Wang J, Gao F, Rothenberg EV. Runx factors launch T cell and innate lymphoid programs via direct and gene network-based mechanisms. *Nat Immunol*. 2023;24(9):1458-1472. doi:10.1038/s41590-023-01585-z

317. Wang D, Diao H, Getzler AJ, et al. The Transcription Factor Runx3 Establishes Chromatin Accessibility of *cis*-Regulatory Landscapes that Drive Memory Cytotoxic T Lymphocyte Formation. *Immunity*. 2018;48(4):659-674.e6. doi:10.1016/j.immuni.2018.03.028

318. Klunker S, Chong MMW, Mantel PY, et al. Transcription factors RUNX1 and RUNX3 in the induction and suppressive function of Foxp3+ inducible regulatory T cells. *J Exp Med*. 2009;206(12):2701-2715. doi:10.1084/jem.20090596

319. Meng Y, Carrelha J, Drissen R, et al. Epigenetic programming defines haematopoietic stem cell fate restriction. *Nat Cell Biol*. 2023;25(6):812-822. doi:10.1038/s41556-023-01137-5

320. Shin B, Zhou W, Wang J, Gao F, Rothenberg EV. Runx factors launch T cell and innate lymphoid programs via direct and gene network-based mechanisms. *Nat Immunol*. 2023;24(9):1458-1472. doi:10.1038/s41590-023-01585-z

321. Wang CQ, Krishnan V, Tay LS, et al. Disruption of Runx1 and Runx3 Leads to Bone Marrow Failure and Leukemia Predisposition due to Transcriptional and DNA Repair Defects. *Cell Rep*. 2014;8(3):767-782. doi:10.1016/j.celrep.2014.06.046

322. Levanon D, Bettoun D, Harris-Cerruti C, et al. The Runx3 transcription factor regulates development and survival of TrkC dorsal root ganglia neurons. *EMBO J*. 2002;21(13):3454-3463. doi:10.1093/emboj/cdf370

323. Levanon D, Brenner O, Negreanu V, et al. Spatial and temporal expression pattern of Runx3 (Aml2) and Runx1 (Aml1) indicates non-redundant functions during mouse embryogenesis. *Mech Dev*. 2001;109(2):413-417. doi:10.1016/S0925-4773(01)00537-8

324. Li QL, Ito K, Sakakura C, et al. Causal Relationship between the Loss of RUNX3 Expression and Gastric Cancer. *Cell*. 2002;109(1):113-124. doi:10.1016/S0092-8674(02)00690-6

325. Malik N, Yan H, Moshkovich N, et al. The transcription factor CBFB suppresses breast cancer through orchestrating translation and transcription. *Nat Commun*. 2019;10(1):2071. doi:10.1038/s41467-019-10102-6

326. Link KA, Chou FS, Mulloy JC. Core Binding Factor at the Crossroads: Determining the Fate of the HSC. *J Cell Physiol*. 2010;222(1):50-56. doi:10.1002/jcp.21950

327. Wang CQ, Chin DWL, Chooi JY, et al. Cbfb deficiency results in differentiation blocks and stem/progenitor cell expansion in hematopoiesis. *Leukemia*. 2015;29(3):753-757. doi:10.1038/leu.2014.316

328. Morita K, Suzuki K, Maeda S, et al. Genetic regulation of the RUNX transcription factor family has antitumor effects. *J Clin Invest*. 127(7):2815-2828. doi:10.1172/JCI91788

329. Goyama S, Schibler J, Cunningham L, et al. Transcription factor RUNX1 promotes survival of acute myeloid leukemia cells. *J Clin Invest*. 2013;123(9):3876-3888. doi:10.1172/JCI68557

330. Goyama S, Yamaguchi Y, Imai Y, et al. The transcriptionally active form of AML1 is required for hematopoietic rescue of the AML1-deficient embryonic para-aortic splanchnopleural (P-Sp) region. *Blood*. 2004;104(12):3558-3564. doi:10.1182/blood-2004-04-1535

331. Omatsu Y, Aiba S, Maeta T, et al. Runx1 and Runx2 inhibit fibrotic conversion of cellular niches for hematopoietic stem cells. *Nat Commun*. 2022;13(1):2654. doi:10.1038/s41467-022-30266-y

332. Ishino Y, Shinagawa H, Makino K, Amemura M, Nakata A. *Nucleotide Sequence of the Iap Gene, Responsible for Alkaline Phosphatase Isozyme Conversion in Escherichia Coli, and Identification of the Gene Product*. Vol 169.; 1987:5429-5433. Accessed May 4, 2020. http://jb.asm.org/

333. Ishino Y, Krupovic M, Forterre P. History of CRISPR-Cas from encounter with a mysterious repeated sequence to genome editing technology. *J Bacteriol*. 2018;200(7). doi:10.1128/JB.00580-17

334. Mojica FJM, Díez-Villaseñor C, García-Martínez J, Soria E. Intervening sequences of regularly spaced prokaryotic repeats derive from foreign genetic elements. *J Mol Evol*. 2005;60(2):174-182. doi:10.1007/s00239-004-0046-3

335. Jansen Ruud, Embden JanDA van, Gaastra Wim, Schouls LeoM. Identification of genes that are associated with DNA repeats in prokaryotes. *Mol Microbiol*. 2002;43(6):1565-1575. doi:10.1046/j.1365-2958.2002.02839.x

336. Jinek M, Chylinski K, Fonfara I, Hauer M, Doudna JA, Charpentier E. A programmable dual-RNA-guided DNA endonuclease in adaptive bacterial immunity. *Science*. 2012;337(6096):816-821. doi:10.1126/science.1225829

337. Meaker GA, Hair EJ, Gorochowski TE. Advances in engineering CRISPR-Cas9 as a molecular Swiss Army knife. *Synth Biol*. 2020;5(ysaa021). doi:10.1093/synbio/ysaa021

338. Cong L, Ran FA, Cox D, et al. Multiplex genome engineering using CRISPR/Cas systems. *Science*. 2013;339(6121):819-823. doi:10.1126/science.1231143

339. Khoo HM, Meaker GA, Wilkinson AC. Ex Vivo Expansion and Genetic Manipulation of Mouse Hematopoietic Stem Cells in Polyvinyl Alcohol-Based Cultures. *JoVE J Vis Exp*. 2023;(192):e64791. doi:10.3791/64791

340. Dong W, Kantor B. Lentiviral Vectors for Delivery of Gene-Editing Systems Based on CRISPR/Cas: Current State and Perspectives. *Viruses*. 2021;13(7):1288. doi:10.3390/v13071288

341. Lewis PF, Emerman M. Passage through mitosis is required for oncoretroviruses but not for the human immunodeficiency virus. *J Virol*. 1994;68(1):510-516.

342. Dever DP, Bak RO, Reinisch A, et al. CRISPR/Cas9 Beta-globin Gene Targeting in Human Hematopoietic Stem Cells. *Nature*. 2016;539(7629):384-389. doi:10.1038/nature20134

343. DeWitt MA, Magis W, Bray NL, et al. Selection-free genome editing of the sickle mutation in human adult hematopoietic stem/progenitor cells. *Sci Transl Med*. 2016;8(360):360ra134-360ra134. doi:10.1126/scitranslmed.aaf9336

344. Tolmachov O, Tolmachova T, Al-Allaf FA, Tolmachov O, Tolmachova T, Al-Allaf FA. Designing Lentiviral Gene Vectors. In: *Viral Gene Therapy*. IntechOpen; 2011. doi:10.5772/17361

345. Gresch O, Engel FB, Nesic D, et al. New non-viral method for gene transfer into primary cells. *Methods*. 2004;33(2):151-163. doi:10.1016/j.ymeth.2003.11.009

346. ABORDO-ADESIDA E, FOLLENZI A, BARCIA C, et al. Stability of Lentiviral Vector-Mediated Transgene Expression in the Brain in the Presence of Systemic Antivector Immune Responses. *Hum Gene Ther*. 2005;16(6):741-751. doi:10.1089/hum.2005.16.741

347. Koike-Yusa H, Li Y, Tan EP, Velasco-Herrera MDC, Yusa K. Genome-wide recessive genetic screening in mammalian cells with a lentiviral CRISPR-guide RNA library. *Nat Biotechnol*. 2014;32(3):267-273. doi:10.1038/nbt.2800

348. Shalem O, Sanjana NE, Zhang F. High-throughput functional genomics using CRISPR–Cas9. *Nat Rev Genet*. 2015;16(5):299-311. doi:10.1038/nrg3899

349. Bock C, Datlinger P, Chardon F, et al. High-content CRISPR screening. *Nat Rev Methods Primer*. 2022;2(1):1-23. doi:10.1038/s43586-021-00093-4

350. Cortez JT, Montauti E, Shifrut E, et al. CRISPR Screen in Regulatory T Cells Reveals Modulators of Foxp3. *Nature*. 2020;582(7812):416-420. doi:10.1038/s41586-020-2246-4

351. Covarrubias S, Cortez Vollmers A, Capili A, et al. High-Throughput CRISPR Screening Identifies Genes Involved in Macrophage Viability and Inflammatory Pathways. *Cell Rep*. 2020;33(13):108541. doi:10.1016/j.celrep.2020.108541

352. Worthington AK, Forsberg EC. A CRISPR view of hematopoietic stem cells: Moving innovative bioengineering into the clinic. *Am J Hematol*. 2022;97(9):1226-1235. doi:10.1002/ajh.26588

353. Holmfeldt P, Ganuza M, Marathe H, et al. Functional screen identifies regulators of murine hematopoietic stem cell repopulation. *J Exp Med*. 2016;213(3):433-449. doi:10.1084/jem.20150806

354. Lara-Astiaso D, Goñi-Salaverri A, Mendieta-Esteban J, et al. In vivo screening characterizes chromatin factor functions during normal and malignant hematopoiesis. *Nat Genet*. 2023;55(9):1542-1554. doi:10.1038/s41588-023-01471-2

355. Zhang Q, Olofzon R, Konturek-Ciesla A, Yuan O, Bryder D. Ex vivo expansion potential of murine hematopoietic stem cells is a rare property only partially predicted by phenotype. *eLife*. 12:RP91826. doi:10.7554/eLife.91826

356. Gazit R, Mandal PK, Ebina W, et al. Fgd5 identifies hematopoietic stem cells in the murine bone marrow. *J Exp Med*. 2014;211(7):1315-1331. doi:10.1084/jem.20130428

357. van de Rijn M, Heimfeld S, Spangrude GJ, Weissman IL. Mouse hematopoietic stem-cell antigen Sca-1 is a member of the Ly-6 antigen family. *Proc Natl Acad Sci U S A*. 1989;86(12):4634-4638. doi:10.1073/pnas.86.12.4634

358. Kiel MJ, Yilmaz ÖH, Iwashita T, Yilmaz OH, Terhorst C, Morrison SJ. SLAM Family Receptors Distinguish Hematopoietic Stem and Progenitor Cells and Reveal Endothelial Niches for Stem Cells. *Cell*. 2005;121(7):1109-1121. doi:10.1016/j.cell.2005.05.026

359. Challen GA, Boles N, Lin KK, Goodell MA. Mouse Hematopoietic Stem Cell Identification And Analysis. *Cytom Part J Int Soc Anal Cytol*. 2009;75(1):14-24. doi:10.1002/cyto.a.20674

360. Barclay AN, Brown MH, Law SKAKA, McKnight AJ, Tomlinson MG, Merwe PA van der. *The Leucocyte Antigen Factsbook*. Elsevier; 1997.

361. Bierer BE, Sleckman BP, Ratnofsky SE, Burakoff SJ. The biologic roles of CD2, CD4, and CD8 in T-cell activation. *Annu Rev Immunol*. 1989;7:579-599. doi:10.1146/annurev.iy.07.040189.003051

362. Zamoyska R. The CD8 coreceptor revisited: One chain good, two chains better. *Immunity*. 1994;1(4):243-246. doi:10.1016/1074-7613(94)90075-2

363. Davis MM. T cell receptor gene diversity and selection. *Annu Rev Biochem*. 1990;59:475-496. doi:10.1146/annurev.bi.59.070190.002355

364. Trotman-Grant AC, Mohtashami M, De Sousa Casal J, et al. DL4-µbeads induce T cell lineage differentiation from stem cells in a stromal cell-free system. *Nat Commun*. 2021;12(1):5023. doi:10.1038/s41467-021-25245-8

365. Carrelha J, Meng Y, Kettyle LM, et al. Hierarchically related lineage-restricted fates of multipotent haematopoietic stem cells. *Nature*. 2018;554(7690):106-111. doi:10.1038/nature25455

366. Hestdal K, Ruscetti FW, Ihle JN, et al. Characterization and regulation of RB6-8C5 antigen expression on murine bone marrow cells. *J Immunol Baltim Md 1950*. 1991;147(1):22-28.

367. Gigon L, Yousefi S, Karaulov A, Simon HU. Mechanisms of toxicity mediated by neutrophil and eosinophil granule proteins. *Allergol Int*. 2021;70(1):30-38. doi:10.1016/j.alit.2020.11.003

368. Christensen JE, Andreasen SØ, Christensen JP, Thomsen AR. CD11b expression as a marker to distinguish between recently activated effector CD8+ T cells and memory cells. *Int Immunol*. 2001;13(4):593-600. doi:10.1093/intimm/13.4.593

369. Koo GC, Dumont FJ, Tutt M, Hackett J Jr, Kumar V. The NK-1.1(-) mouse: a model to study differentiation of murine NK cells. *J Immunol*. 1986;137(12):3742-3747. doi:10.4049/jimmunol.137.12.3742

370. Lanier LL. Natural Killer Cells: From No Receptors to Too Many. *Immunity*. 1997;6(4):371-378. doi:10.1016/S1074-7613(00)80280-0

371. Liu YJ. IPC: Professional Type 1 Interferon-Producing Cells and Plasmacytoid Dendritic Cell Precursors. *Annu Rev Immunol*. 2005;23(Volume 23, 2005):275-306. doi:10.1146/annurev.immunol.23.021704.115633

372. Kent DG, Copley MR, Benz C, et al. Prospective isolation and molecular characterization of hematopoietic stem cells with durable self-renewal potential. *Blood*. 2009;113(25):6342-6350. doi:10.1182/blood-2008-12-192054

373. Balazs AB, Fabian AJ, Esmon CT, Mulligan RC. Endothelial protein C receptor (CD201) explicitly identifies hematopoietic stem cells in murine bone marrow. *Blood*. 2006;107(6):2317-2321. doi:10.1182/blood-2005-06-2249

374. Rubio-Lara JA, Igarashi KJ, Sood S, et al. Expanding hematopoietic stem cell ex vivo: recent advances and technical considerations. *Exp Hematol*. 2023;125-126:6-15. doi:10.1016/j.exphem.2023.07.006

375. Antonchuk J, Sauvageau G, Humphries RK. HOXB4-Induced Expansion of Adult Hematopoietic Stem Cells Ex Vivo. *Cell*. 2002;109(1):39-45. doi:10.1016/S0092-8674(02)00697-9

376. Kunisato A, Chiba S, Nakagami-Yamaguchi E, et al. HES-1 preserves purified hematopoietic stem cells ex vivo and accumulates side population cells in vivo. *Blood*. 2003;101(5):1777-1783. doi:10.1182/blood-2002-07-2051

377. Miharada K, Sigurdsson V, Karlsson S. Dppa5 Improves Hematopoietic Stem Cell Activity by Reducing Endoplasmic Reticulum Stress. *Cell Rep*. 2014;7(5):1381-1392. doi:10.1016/j.celrep.2014.04.056

378. Wilkinson AC, Ishida R, Kikuchi M, et al. Long-term ex vivo hematopoietic stem cell expansion affords nonconditioned transplantation. *Nature*. 2019;571(7763):117-121. doi:10.1038/s41586-019-1244-x

379. Nishimura T, Hsu I, Martinez-Krams DC, et al. Use of polyvinyl alcohol for CAR T cell expansion. *Exp Hematol*. 2019;80:16-20. doi:10.1016/j.exphem.2019.11.007

380. Che JLC, Bode D, Kucinski I, et al. Identification and characterization of in vitro expanded hematopoietic stem cells. *EMBO Rep*. 2022;23(10):e55502. doi:10.15252/embr.202255502

381. Becker HJ, Ishida R, Wilkinson AC, et al. A Single Cell Cloning Platform for Gene Edited Functional Murine Hematopoietic Stem Cells. *bioRxiv*. Preprint posted online 23 March 2022:2022.03.23.485423. doi:10.1101/2022.03.23.485423

382. Peled T, Shoham H, Aschengrau D, et al. Nicotinamide, a SIRT1 inhibitor, inhibits differentiation and facilitates expansion of hematopoietic progenitor cells with enhanced bone marrow homing and engraftment. *Exp Hematol*. 2012;40(4):342-355.e1. doi:10.1016/j.exphem.2011.12.005

383. Vannini N, Campos V, Girotra M, et al. The NAD-Booster Nicotinamide Riboside Potently Stimulates Hematopoiesis through Increased Mitochondrial Clearance. *Cell Stem Cell*. 2019;24(3):405-418.e7. doi:10.1016/j.stem.2019.02.012

384. Subramaniam A, Žemaitis K, Talkhoncheh MS, et al. Lysine-specific demethylase 1A restricts ex vivo propagation of human HSCs and is a target of UM171. *Blood*. 2020;136(19):2151-2161. doi:10.1182/blood.2020005827

385. Chagraoui J, Girard S, Spinella JF, et al. UM171 Preserves Epigenetic Marks that Are Reduced in Ex Vivo Culture of Human HSCs via Potentiation of the CLR3-KBTBD4 Complex. *Cell Stem Cell*. 2021;28(1):48-62.e6. doi:10.1016/j.stem.2020.12.002

386. Fares I, Chagraoui J, Gareau Y, et al. Pyrimidoindole derivatives are agonists of human hematopoietic stem cell self-renewal. *Science*. 2014;345(6203):1509-1512. doi:10.1126/science.1256337

387. Sakurai M, Ishitsuka K, Ito R, et al. Chemically defined cytokine-free expansion of human haematopoietic stem cells. *Nature*. 2023;615(7950):127-133. doi:10.1038/s41586-023-05739-9

388. Bozhilov Y, Brown E, Hsu I, et al. Reducing oxidative stress improves ex vivo polymer-based human haematopoietic stem and progenitor cell culture and gene editing. *bioRxiv*. Preprint posted online 18 September 2024:2024.09.17.613552. doi:10.1101/2024.09.17.613552

389. Ghosh K, Van Duyne GD. Cre–*loxP* biochemistry. *Methods*. 2002;28(3):374-383. doi:10.1016/S1046-2023(02)00244-X

390. Sternberg N, Hamilton D. Bacteriophage P1 site-specific recombination: I. Recombination between loxP sites. *J Mol Biol*. 1981;150(4):467-486. doi:10.1016/0022-2836(81)90375-2

391. McLellan MA, Rosenthal NA, Pinto AR. Cre-loxP-Mediated Recombination: General Principles and Experimental Considerations. *Curr Protoc Mouse Biol*. 2017;7(1):1-12. doi:10.1002/cpmo.22

392. Indra AK, Warot X, Brocard J, et al. Temporally-controlled site-specific mutagenesis in the basal layer of the epidermis: comparison of the recombinase activity of the tamoxifen-inducible Cre-ER(T) and Cre-ER(T2) recombinases. *Nucleic Acids Res*. 1999;27(22):4324-4327. doi:10.1093/nar/27.22.4324

393. Vizoso M, E. J. Pritchard C, Bombardelli L, et al. A doxycycline- and light-inducible Cre recombinase mouse model for optogenetic genome editing. *Nat Commun*. 2022;13:6442. doi:10.1038/s41467-022-33863-z

394. Minamino T, Gaussin V, DeMayo FJ, Schneider MD. Inducible Gene Targeting in Postnatal Myocardium by Cardiac-Specific Expression of a Hormone-Activated Cre Fusion Protein. *Circ Res*. 2001;88(6):587-592. doi:10.1161/01.RES.88.6.587

395. Qin X, Jiang Q, Nagano K, et al. Runx2 is essential for the transdifferentiation of chondrocytes into osteoblasts. *PLOS Genet*. 2020;16(11):e1009169. doi:10.1371/journal.pgen.1009169

396. Shimshek D r., Kim J, Hübner M r., et al. Codon-improved Cre recombinase (iCre) expression in the mouse. *genesis*. 2002;32(1):19-26. doi:10.1002/gene.10023

397. Bustelo XR, Dosil M. Vav Family. In: *Encyclopedia of Signaling Molecules*. Springer, Cham; 2018:5892-5906. doi:10.1007/978-3-319-67199-4_513

398. Almarza E, Segovia JC, Guenechea G, Gómez SG, Ramírez Á, Bueren JA. Regulatory elements of the vav gene drive transgene expression in hematopoietic stem cells from adult mice. *Exp Hematol*. 2004;32(4):360-364. doi:10.1016/j.exphem.2004.01.005

399. de Boer J, Williams A, Skavdis G, et al. Transgenic mice with hematopoietic and lymphoid specific expression of Cre. *Eur J Immunol*. 2003;33(2):314-325. doi:10.1002/immu.200310005

400. Ogilvy S, Elefanty AG, Visvader J, Bath ML, Harris AW, Adams JM. Transcriptional Regulation of *vav*, a Gene Expressed Throughout the Hematopoietic Compartment. *Blood*. 1998;91(2):419-430. doi:10.1182/blood.V91.2.419

401. Kwarteng EO, Heinonen KM. Competitive Transplants to Evaluate Hematopoietic Stem Cell Fitness. *J Vis Exp JoVE*. 2016;(114):54345. doi:10.3791/54345

402. Hétu-Arbour R, Bouali S, Heinonen KM. Experimental Competitive Bone Marrow Transplant Assays. In: Cobaleda C, Sánchez-García I, eds *Leukemia Stem Cells: Methods and Protocols*. Springer US; 2021:195-214. doi:10.1007/978-1-0716-0810-4_12

403. Bowling S, Sritharan D, Osorio FG, et al. An engineered CRISPR/Cas9 mouse line for simultaneous readout of lineage histories and gene expression profiles in single cells. *Cell*. 2020;181(6):1410-1422.e27. doi:10.1016/j.cell.2020.04.048

404. Goodwin LO, Splinter E, Davis TL, et al. Large-scale discovery of mouse transgenic integration sites reveals frequent structural variation and insertional mutagenesis. *Genome Res*. 2019;29(3):494-505. doi:10.1101/gr.233866.117

405. Georgiades P, Ogilvy S, Duval H, et al. vavCre Transgenic mice: A tool for mutagenesis in hematopoietic and endothelial lineages. *genesis*. 2002;34(4):251-256. doi:10.1002/gene.10161

406. Morgens DW, Wainberg M, Boyle EA, et al. Genome-scale measurement of off-target activity using Cas9 toxicity in high-throughput screens. *Nat Commun*. 2017;8:15178. doi:10.1038/ncomms15178

407. Hodgkins A, Farne A, Perera S, et al. WGE: a CRISPR database for genome engineering. *Bioinformatics*. 2015;31(18):3078-3080. doi:10.1093/bioinformatics/btv308

408. Han K, Jeng EE, Hess GT, Morgens DW, Li A, Bassik MC. Synergistic drug combinations for cancer identified in a CRISPR screen for pairwise genetic interactions. *Nat Biotechnol*. 2017;35(5):463-474. doi:10.1038/nbt.3834

409. Ricks DM, Kutner R, Zhang XY, Welsh DA, Reiser J. Optimized Lentiviral Transduction of Mouse Bone Marrow-Derived Mesenchymal Stem Cells. *Stem Cells Dev*. 2008;17(3):441-450. doi:10.1089/scd.2007.0194

410. DeWeirdt PC, Sangree AK, Hanna RE, et al. Genetic screens in isogenic mammalian cell lines without single cell cloning. *Nat Commun*. 2020;11:752. doi:10.1038/s41467-020-14620-6

411. Li W, Xu H, Xiao T, et al. MAGeCK enables robust identification of essential genes from genome-scale CRISPR/Cas9 knockout screens. *Genome Biol*. 2014;15(12):554. doi:10.1186/s13059-014-0554-4

412. Andrews S. FastQC, https://www.bioinformatics.babraham.ac.uk/projects/fastqc/. Published online 2010. https://www.bioinformatics.babraham.ac.uk/projects/fastqc/

413. Krueger F. Trim Galore, https://www.bioinformatics.babraham.ac.uk/projects/trim_galore/. Published online 2012.

414. Dobin A, Davis CA, Schlesinger F, et al. STAR: ultrafast universal RNA-seq aligner. *Bioinformatics*. 2013;29(1):15-21. doi:10.1093/bioinformatics/bts635

415. Liao Y, Smyth GK, Shi W. featureCounts: an efficient general purpose program for assigning sequence reads to genomic features. *Bioinformatics*. 2014;30(7):923-930. doi:10.1093/bioinformatics/btt656

416. Risso D, Ngai J, Speed TP, Dudoit S. Normalization of RNA-seq data using factor analysis of control genes or samples. *Nat Biotechnol*. 2014;32(9):896-902. doi:10.1038/nbt.2931

417. Love MI, Huber W, Anders S. Moderated estimation of fold change and dispersion for RNA-seq data with DESeq2. *Genome Biol*. 2014;15(12):550. doi:10.1186/s13059-014-0550-8

418. Yu G, Wang LG, Han Y, He QY. clusterProfiler: an R Package for Comparing Biological Themes Among Gene Clusters. *OMICS J Integr Biol*. 2012;16(5):284-287. doi:10.1089/omi.2011.0118

419. Korotkevich G, Sukhov V, Budin N, Shpak B, Artyomov MN, Sergushichev A. Fast gene set enrichment analysis. *Bioinformatics*. Preprint posted online 20 June 2016. doi:10.1101/060012

420. Subramanian A, Tamayo P, Mootha VK, et al. Gene set enrichment analysis: A knowledge-based approach for interpreting genome-wide expression profiles. *Proc Natl Acad Sci*. 2005;102(43):15545-15550. doi:10.1073/pnas.0506580102

421. Castanza AS, Recla JM, Eby D, Thorvaldsdóttir H, Bult CJ, Mesirov JP. Extending support for mouse data in the Molecular Signatures Database (MSigDB). *Nat Methods*. 2023;20(11):1619-1620. doi:10.1038/s41592-023-02014-7

422. Kaya-Okur HS, Wu SJ, Codomo CA, et al. CUT&Tag for efficient epigenomic profiling of small samples and single cells. *Nat Commun*. 2019;10(1):1930. doi:10.1038/s41467-019-09982-5

423. Wilkinson AC, Ishida R, Nakauchi H, Yamazaki S. Long-term ex vivo expansion of mouse hematopoietic stem cells. *Nat Protoc*. 2020;15(2):628-648. doi:10.1038/s41596-019-0263-2

424. Wilkinson AC, Ishida R, Kikuchi M, et al. Long-term ex vivo haematopoietic-stem-cell expansion allows nonconditioned transplantation. *Nature*. 2019;571(7763):117-121. doi:10.1038/s41586-019-1244-x

425. Li W, Köster J, Xu H, et al. Quality control, modeling, and visualization of CRISPR screens with MAGeCK-VISPR. *Genome Biol*. 2015;16(1):281. doi:10.1186/s13059-015-0843-6

426. Dempster JM, Rossen J, Kazachkova M, et al. Extracting Biological Insights from the Project Achilles Genome-Scale CRISPR Screens in Cancer Cell Lines. *bioRxiv*. Preprint posted online 31 July 2019:720243. doi:10.1101/720243

427. Crispino JD, Horwitz MS. GATA factor mutations in hematologic disease. *Blood*. 2017;129(15):2103-2110. doi:10.1182/blood-2016-09-687889

428. Grass JA, Boyer ME, Pal S, Wu J, Weiss MJ, Bresnick EH. GATA-1-dependent transcriptional repression of GATA-2 via disruption of positive autoregulation and domain-wide chromatin remodeling. *Proc Natl Acad Sci U S A*. 2003;100(15):8811-8816. doi:10.1073/pnas.1432147100

429. Chambers J, Rabbitts TH. LMO2 at 25 years: a paradigm of chromosomal translocation proteins. *Open Biol*. 2015;5(6):150062. doi:10.1098/rsob.150062

430. Yamada Y, Warren AJ, Dobson C, Forster A, Pannell R, Rabbitts TH. The T cell leukemia LIM protein Lmo2 is necessary for adult mouse hematopoiesis. *Proc Natl Acad Sci U S A*. 1998;95(7):3890-3895.

431. Shevchenko G, Morris KV. All I's on the RADAR: Role of ADAR in gene regulation. *FEBS Lett*. 2018;592(17):2860-2873. doi:10.1002/1873-3468.13093

432. XuFeng R, Boyer MJ, Shen H, et al. ADAR1 is required for hematopoietic progenitor cell survival via RNA editing. *Proc Natl Acad Sci U S A*. 2009;106(42):17763-17768. doi:10.1073/pnas.0903324106

433. Jackson RA, Wu JS, Chen ES. C1D family proteins in coordinating RNA processing, chromosome condensation and DNA damage response. *Cell Div*. 2016;11:2. doi:10.1186/s13008-016-0014-5

434. Schilders G, van Dijk E, Pruijn GJM. C1D and hMtr4p associate with the human exosome subunit PM/Scl-100 and are involved in pre-rRNA processing. *Nucleic Acids Res*. 2007;35(8):2564-2572. doi:10.1093/nar/gkm082

435. Liu LJ, Xie R, Hussain S, et al. Functional coupling of transcription factor HiNF-P and histone H4 gene expression during pre- and post-natal mouse development. *Gene*. 2011;483(1-2):1-10. doi:10.1016/j.gene.2011.05.002

436. Chandrasekharappa SC, Teh BT. Functional studies of the MEN1 gene. *J Intern Med*. 2003;253(6):606-615. doi:10.1046/j.1365-2796.2003.01165.x

437. Marini F, Falchetti A, Monte FD, et al. Multiple endocrine neoplasia type 1. *Orphanet J Rare Dis*. 2006;1(1):38. doi:10.1186/1750-1172-1-38

438. Bugiardini E, Mitchell AL, Rosa ID, et al. MRPS25 mutations impair mitochondrial translation and cause encephalomyopathy. *Hum Mol Genet*. 2019;28(16):2711-2719. doi:10.1093/hmg/ddz093

439. Wang F, Whynot A, Tung M, Denic V. The Mechanism of Tail Anchored Protein Insertion into the ER Membrane. *Mol Cell*. 2011;43(5):738-750. doi:10.1016/j.molcel.2011.07.020

440. Ni M, Black LF, Pan C, et al. Metabolic impact of pathogenic variants in the mitochondrial glutamyl-tRNA synthetase EARS2. *J Inherit Metab Dis*. 2021;44(4):949-960. doi:10.1002/jimd.12387

441. Wilhelm SDP, Kakadia JH, Beharry A, et al. Transfer RNA supplementation rescues HARS deficiency in a humanized yeast model of Charcot-Marie-Tooth disease. *Nucleic Acids Res*. 2024;52(22):14043-14060. doi:10.1093/nar/gkae996

442. Safka Brozkova D, Deconinck T, Beth Griffin L, et al. Loss of function mutations in HARS cause a spectrum of inherited peripheral neuropathies. *Brain*. 2015;138(8):2161-2172. doi:10.1093/brain/awv158

443. Zhang J, Grindley JC, Yin T, et al. PTEN maintains haematopoietic stem cells and acts in lineage choice and leukaemia prevention. *Nature*. 2006;441(7092):518-522. doi:10.1038/nature04747

444. Abbas HA, Pant V, Lozano G. The ups and downs of p53 regulation in hematopoietic stem cells. *Cell Cycle*. 2011;10(19):3257-3262. doi:10.4161/cc.10.19.17721

445. Szklarczyk D, Kirsch R, Koutrouli M, et al. The STRING database in 2023: protein–protein association networks and functional enrichment analyses for any sequenced genome of interest. *Nucleic Acids Res*. 2022;51(D1):D638-D646. doi:10.1093/nar/gkac1000

446. Chuang LSH, Ito K, Ito Y. RUNX family: Regulation and diversification of roles through interacting proteins. *Int J Cancer*. 2013;132(6):1260-1271. doi:10.1002/ijc.27964

447. Komori T. Regulation of skeletal development by the Runx family of transcription factors. *J Cell Biochem*. 2005;95(3):445-453. doi:10.1002/jcb.20420

448. Yoshida CA, Furuichi T, Fujita T, et al. Core-binding factor β interacts with Runx2 and is required for skeletal development. *Nat Genet*. 2002;32(4):633-638. doi:10.1038/ng1015

449. Cunningham L, Finckbeiner S, Hyde RK, et al. Identification of benzodiazepine Ro5-3335 as an inhibitor of CBF leukemia through quantitative high throughput screen against RUNX1–CBFβ interaction. *Proc Natl Acad Sci U S A*. 2012;109(36):14592-14597. doi:10.1073/pnas.1200037109

450. Illendula A, Gilmour J, Grembecka J, et al. Small Molecule Inhibitor of CBFβ-RUNX Binding for RUNX Transcription Factor Driven Cancers. *EBioMedicine*. 2016;8:117-131. doi:10.1016/j.ebiom.2016.04.032

451. Kim MS, Gernapudi R, Choi EY, Lapidus RG, Passaniti A. Characterization of CADD522, a small molecule that inhibits RUNX2-DNA binding and exhibits antitumor activity. *Oncotarget*. 2017;8(41):70916-70940. doi:10.18632/oncotarget.20200

452. Roudaia L, Cheney MD, Manuylova E, et al. CBFβ is critical for AML1-ETO and TEL-AML1 activity. *Blood*. 2009;113(13):3070-3079. doi:10.1182/blood-2008-03-147207

453. Green D, Singh A, Tippett VL, et al. YBX1-interacting small RNAs and *RUNX2* can be blocked in primary bone cancer using CADD522. *J Bone Oncol*. 2023;39:100474. doi:10.1016/j.jbo.2023.100474

454. Haney MS, Shankar A, Olender L, et al. In vivo CRISPR screening identifies SAGA complex members as key regulators of hematopoiesis. *bioRxiv*. Preprint posted online 19 May 2025:2022.07.22.501030. doi:10.1101/2022.07.22.501030

455. Nganga VK, Palmer VL, Naushad H, et al. Accelerated progression of chronic lymphocytic leukemia in Eμ-TCL1 mice expressing catalytically inactive RAG1. *Blood*. 2013;121(19):3855-3866. doi:10.1182/blood-2012-08-446732

456. Zhang B, Kracker S, Yasuda T, et al. Immune Surveillance and Therapy of Lymphomas Driven by Epstein-Barr -Virus Protein LMP1 in a Mouse Model. *Cell*. 2012;148(4):739-751. doi:10.1016/j.cell.2011.12.031

457. O'Connell KE, Mikkola AM, Stepanek AM, et al. Practical Murine Hematopathology: A Comparative Review and Implications for Research. *Comp Med*. 2015;65(2):96-113.

458. Taniuchi I, Osato M, Egawa T, et al. Differential Requirements for Runx Proteins in CD4 Repression and Epigenetic Silencing during T Lymphocyte Development. *Cell*. 2002;111(5):621-633. doi:10.1016/S0092-8674(02)01111-X

459. Ichikawa M, Goyama S, Asai T, et al. AML1/Runx1 Negatively Regulates Quiescent Hematopoietic Stem Cells in Adult Hematopoiesis1. *J Immunol*. 2008;180(7):4402-4408. doi:10.4049/jimmunol.180.7.4402

460. Osato M, Asou N, Abdalla E, et al. Biallelic and Heterozygous Point Mutations in the Runt Domain of theAML1/PEBP2αB Gene Associated With Myeloblastic Leukemias. *Blood*. 1999;93(6):1817-1824. doi:10.1182/blood.V93.6.1817.406k36_1817_1824

461. Growney JD, Shigematsu H, Li Z, et al. Loss of Runx1 perturbs adult hematopoiesis and is associated with a myeloproliferative phenotype. *Blood*. 2005;106(2):494-504. doi:10.1182/blood-2004-08-3280

462. Kuo YH, Zaidi SK, Gornostaeva S, Komori T, Stein GS, Castilla LH. Runx2 induces acute myeloid leukemia in cooperation with Cbfβ-SMMHC in mice. *Blood*. 2009;113(14):3323-3332. doi:10.1182/blood-2008-06-162248

463. Jaruga A, Hordyjewska E, Kandzierski G, Tylzanowski P. Cleidocranial dysplasia and RUNX2-clinical phenotype–genotype correlation. *Clin Genet*. 2016;90(5):393-402. doi:10.1111/cge.12812

464. Northrup DL, Zhao K. Application of ChIP-Seq and related techniques to the study of immune function. *Immunity*. 2011;34(6):830-842. doi:10.1016/j.immuni.2011.06.002

465. Mundade R, Ozer HG, Wei H, Prabhu L, Lu T. Role of ChIP-seq in the discovery of transcription factor binding sites, differential gene regulation mechanism, epigenetic marks and beyond. *Cell Cycle*. 2014;13(18):2847-2852. doi:10.4161/15384101.2014.949201

466. Heintzman ND, Stuart RK, Hon G, et al. Distinct and predictive chromatin signatures of transcriptional promoters and enhancers in the human genome. *Nat Genet*. 2007;39(3):311-318. doi:10.1038/ng1966

467. Beerman I, Bhattacharya D, Zandi S, et al. Functionally distinct hematopoietic stem cells modulate hematopoietic lineage potential during aging by a mechanism of clonal expansion. *Proc Natl Acad Sci U S A*. 2010;107(12):5465-5470. doi:10.1073/pnas.1000834107

468. Wilkinson AC, Göttgens B. Transcriptional Regulation of Haematopoietic Stem Cells. In: Hime G, Abud H, eds *Transcriptional and Translational Regulation of Stem Cells*. Springer Netherlands; 2013:187-212. doi:10.1007/978-94-007-6621-1_11

469. Förster R, Schubel A, Breitfeld D, et al. CCR7 Coordinates the Primary Immune Response by Establishing Functional Microenvironments in Secondary Lymphoid Organs. *Cell*. 1999;99(1):23-33. doi:10.1016/S0092-8674(00)80059-8

470. Zlotoff DA, Sambandam A, Logan TD, Bell JJ, Schwarz BA, Bhandoola A. CCR7 and CCR9 together recruit hematopoietic progenitors to the adult thymus. *Blood*. 2010;115(10):1897-1905. doi:10.1182/blood-2009-08-237784

471. Misslitz A, Pabst O, Hintzen G, et al. Thymic T Cell Development and Progenitor Localization Depend on CCR7. *J Exp Med*. 2004;200(4):481-491. doi:10.1084/jem.20040383

472. Hartigan AJ, Kallal LE, Hogaboam CM. CCR7 impairs hematopoiesis after hematopoietic stem cell transplantation increasing susceptibility to invasive aspergillosis. *Blood*. 2010;116(24):5383-5393. doi:10.1182/blood-2010-01-265454

473. Dieu MC, Vanbervliet B, Vicari A, et al. Selective Recruitment of Immature and Mature Dendritic Cells by Distinct Chemokines Expressed in Different Anatomic Sites. *J Exp Med*. 1998;188(2):373-386. doi:10.1084/jem.188.2.373

474. Sánchez-Sánchez N, Riol-Blanco L, Rodríguez-Fernández JL. The Multiple Personalities of the Chemokine Receptor CCR7 in Dendritic Cells. *J Immunol*. 2006;176(9):5153-5159. doi:10.4049/jimmunol.176.9.5153

475. Enomoto H, Furuichi T, Zanma A, et al. Runx2 deficiency in chondrocytes causes adipogenic changes in vitro. *J Cell Sci*. 2004;117(3):417-425. doi:10.1242/jcs.00866

476. Wu H, Whitfield TW, Gordon JAR, et al. Genomic occupancy of Runx2 with global expression profiling identifies a novel dimension to control of osteoblastogenesis. *Genome Biol*. 2014;15(3):R52. doi:10.1186/gb-2014-15-3-r52

477. Hay J, Gilroy K, Huser C, et al. Collaboration of MYC and RUNX2 in lymphoma simulates T-cell receptor signaling and attenuates p53 pathway activity. *J Cell Biochem*. 2019;120(10):18332-18345. doi:10.1002/jcb.29143

478. Le Gallic L, Virgilio L, Cohen P, Biteau B, Mavrothalassitis G. ERF Nuclear Shuttling, a Continuous Monitor of Erk Activity That Links It to Cell Cycle Progression. *Mol Cell Biol*. 2004;24(3):1206-1218. doi:10.1128/MCB.24.3.1206-1218.2004

479. le Gallic L, Sgouras D, Beal G, Mavrothalassitis G. Transcriptional Repressor ERF Is a Ras/Mitogen-Activated Protein Kinase Target That Regulates Cellular Proliferation. *Mol Cell Biol*. 1999;19(6):4121-4133. doi:10.1128/mcb.19.6.4121

480. Twigg SRF, Vorgia E, McGowan SJ, et al. Reduced dosage of ERF causes complex craniosynostosis in humans and mice, and links ERK1/2 signaling to regulation of osteogenesis. *Nat Genet*. 2013;45(3):308-313. doi:10.1038/ng.2539

481. Xiao ZS, Liu SG, Hinson TK, Quarles LD. Characterization of the upstream mouse Cbfa1/Runx2 promoter. *J Cell Biochem*. 2001;82(4):647-659. doi:10.1002/jcb.1192

482. Perez G, Barber GP, Benet-Pages A, et al. The UCSC Genome Browser database: 2025 update. *Nucleic Acids Res*. 2024;53(D1):D1243-D1249. doi:10.1093/nar/gkae974

483. The Human Genome Browser at UCSC. Accessed December 10, 2020. https://genome.cshlp.org/content/12/6/996.full

484. UCSC Genome Browser. Runx2 gene, mouse (GRCm38/mm10) assembly. Accessed September 10, 2025. https://genome.ucsc.edu/

485. Matthijssens F, Sharma ND, Nysus M, et al. RUNX2 regulates leukemic cell metabolism and chemotaxis in high-risk T cell acute lymphoblastic leukemia. *J Clin Invest*. 131(6):e141566. doi:10.1172/JCI141566

486. Braekeleer ED, Férec C, Braekeleer MD. RUNX1 Translocations in Malignant Hemopathies. *Anticancer Res*. 2009;29(4):1031-1037.

487. Chopin M, Preston SP, Lun ATL, et al. RUNX2 Mediates Plasmacytoid Dendritic Cell Egress from the Bone Marrow and Controls Viral Immunity. *Cell Rep*. 2016;15(4):866-878. doi:10.1016/j.celrep.2016.03.066

488. Wang CQ, Jacob B, Nah GSS, Osato M. Runx family genes, niche, and stem cell quiescence. *Blood Cells Mol Dis*. 2010;44(4):275-286. doi:10.1016/j.bcmd.2010.01.006

489. Sato T, Onai N, Yoshihara H, Arai F, Suda T, Ohteki T. Interferon regulatory factor-2 protects quiescent hematopoietic stem cells from type I interferon–dependent exhaustion. *Nat Med*. 2009;15(6):696-700. doi:10.1038/nm.1973

490. Porritt HE, Rumfelt LL, Tabrizifard S, Schmitt TM, Zúñiga-Pflücker JC, Petrie HT. Heterogeneity among DN1 prothymocytes reveals multiple progenitors with different capacities to generate T cell and non-T cell lineages. *Immunity*. 2004;20(6):735-745. doi:10.1016/j.immuni.2004.05.004

491. Ruiz Pérez M, Vandenabeele P, Tougaard P. The thymus road to a T cell: migration, selection, and atrophy. *Front Immunol*. 2024;15:1443910. doi:10.3389/fimmu.2024.1443910

492. Demerdash Y, Kain B, Essers MAG, King KY. Yin and Yang: The dual effects of interferons on hematopoiesis. *Exp Hematol*. 2021;96:1-12. doi:10.1016/j.exphem.2021.02.002

493. Thompson LJ, Kolumam GA, Thomas S, Murali-Krishna K. Innate Inflammatory Signals Induced by Various Pathogens Differentially Dictate the IFN-I Dependence of CD8 T Cells for Clonal Expansion and Memory Formation1. *J Immunol*. 2006;177(3):1746-1754. doi:10.4049/jimmunol.177.3.1746

494. Aichele P, Unsoeld H, Koschella M, Schweier O, Kalinke U, Vucikuja S. Cutting Edge: CD8 T Cells Specific for Lymphocytic Choriomeningitis Virus Require Type I IFN Receptor for Clonal Expansion1. *J Immunol*. 2006;176(8):4525-4529. doi:10.4049/jimmunol.176.8.4525

495. Hervas-Stubbs S, Perez-Gracia JL, Rouzaut A, Sanmamed MF, Le Bon A, Melero I. Direct Effects of Type I Interferons on Cells of the Immune System. *Clin Cancer Res*. 2011;17(9):2619-2627. doi:10.1158/1078-0432.CCR-10-1114

496. Le Bon A, Durand V, Kamphuis E, et al. Direct Stimulation of T Cells by Type I IFN Enhances the CD8+ T Cell Response during Cross-Priming1. *J Immunol*. 2006;176(8):4682-4689. doi:10.4049/jimmunol.176.8.4682

497. Daniel CJ, Pelz C, Wang X, et al. T-cell Dysfunction upon Expression of MYC with Altered Phosphorylation at Threonine 58 and Serine 62. *Mol Cancer Res*. 2022;20(7):1151-1165. doi:10.1158/1541-7786.MCR-21-0560

498. Delgoffe GM, Kole TP, Zheng Y, et al. mTOR differentially regulates effector and regulatory T cell lineage commitment. *Immunity*. 2009;30(6):832-844. doi:10.1016/j.immuni.2009.04.014

499. Dimova DK, Dyson NJ. The E2F transcriptional network: old acquaintances with new faces. *Oncogene*. 2005;24(17):2810-2826. doi:10.1038/sj.onc.1208612

500. Gao X, Tewari K, Svaren J, Suresh M. Role of cell cycle regulator E2F1 in regulating CD8 T cell responses during acute and chronic viral infection. *Virology*. 2004;324(2):567-576. doi:10.1016/j.virol.2004.04.012

501. Field SJ, Tsai FY, Kuo F, et al. E2F-1 Functions in Mice to Promote Apoptosis and Suppress Proliferation. *Cell*. 1996;85(4):549-561. doi:10.1016/S0092-8674(00)81255-6

502. Nozais M, Loosveld M, Pankaew S, et al. MYC deficiency impairs the development of effector/memory T lymphocytes. *iScience*. 2021;24(7):102761. doi:10.1016/j.isci.2021.102761

503. Chen EY, Tan CM, Kou Y, et al. Enrichr: interactive and collaborative HTML5 gene list enrichment analysis tool. *BMC Bioinformatics*. 2013;14:128. doi:10.1186/1471-2105-14-128

504. Kuleshov MV, Jones MR, Rouillard AD, et al. Enrichr: a comprehensive gene set enrichment analysis web server 2016 update. *Nucleic Acids Res*. 2016;44(Web Server issue):W90-W97. doi:10.1093/nar/gkw377

505. Xie Z, Bailey A, Kuleshov MV, et al. Gene Set Knowledge Discovery with Enrichr. *Curr Protoc*. 2021;1(3):e90. doi:10.1002/cpz1.90

506. Kuka M, De Giovanni M, Iannacone M. The role of type I interferons in CD4+ T cell differentiation. *Immunol Lett*. 2019;215:19-23. doi:10.1016/j.imlet.2019.01.013

507. Mehta AK, Gracias DT, Croft M. TNF Activity and T cells. *Cytokine*. 2018;101:14-18. doi:10.1016/j.cyto.2016.08.003

508. Fortelny N, Farlik M, Fife V, et al. JAK-STAT signaling maintains homeostasis in T cells and macrophages. *Nat Immunol*. 2024;25(5):847-859. doi:10.1038/s41590-024-01804-1

509. Beerman I, Seita J, Inlay MA, Weissman IL, Rossi DJ. Quiescent hematopoietic stem cells accumulate DNA damage during aging that is repaired upon entry into cell cycle. *Cell Stem Cell*. 2014;15(1):37-50. doi:10.1016/j.stem.2014.04.016

510. Genetic Control of the Cell Division Cycle in Yeast | Science. Accessed September 11, 2025. https://www.science.org/doi/10.1126/science.183.4120.46

511. Rapp M, Wintergerst MWM, Kunz WG, et al. CCL22 controls immunity by promoting regulatory T cell communication with dendritic cells in lymph nodes. *J Exp Med*. 2019;216(5):1170-1181. doi:10.1084/jem.20170277

512. Vulcano M, Albanesi C, Stoppacciaro A, et al. Dendritic cells as a major source of macrophage-derived chemokine/CCL22 in vitro and in vivo. *Eur J Immunol*. 2001;31(3):812-822. doi:10.1002/1521-4141(200103)31:3%3C812::AID-IMMU812%3E3.0.CO;2-L

513. Mantovani A, Gray PA, Van Damme J, Sozzani S. Macrophage-derived chemokine (MDC). *J Leukoc Biol*. 2000;68(3):400-404. doi:10.1189/jlb.68.3.400

514. Schall TJ, Bacon KB. Chemokines, leukocyte trafficking, and inflammation. *Curr Opin Immunol*. 1994;6(6):865-873. doi:10.1016/0952-7915(94)90006-X

515. Schall TJ. Biology of the rantes/sis cytokine family. *Cytokine*. 1991;3(3):165-183. doi:10.1016/1043-4666(91)90013-4

516. Kurihara T, Bravo R. Cloning and Functional Expression of mCCR2, a Murine Receptor for the C-C Chemokines JE and FIC (∗). *J Biol Chem*. 1996;271(20):11603-11606. doi:10.1074/jbc.271.20.11603

517. Dutta P, Sager HB, Stengel KR, et al. Myocardial infarction activates CCR2+ hematopoietic stem and progenitor cells. *Cell Stem Cell*. 2015;16(5):477-487. doi:10.1016/j.stem.2015.04.008

518. Cheshier SH, Morrison SJ, Liao X, Weissman IL. In vivo proliferation and cell cycle kinetics of long-term self-renewing hematopoietic stem cells. *Proc Natl Acad Sci*. 1999;96(6):3120-3125. doi:10.1073/pnas.96.6.3120

519. Yager EJ, Ahmed M, Lanzer K, Randall TD, Woodland DL, Blackman MA. Age-associated decline in T cell repertoire diversity leads to holes in the repertoire and impaired immunity to influenza virus. *J Exp Med*. 2008;205(3):711-723. doi:10.1084/jem.20071140

520. Castilla LH, Perrat P, Martinez NJ, et al. Identification of genes that synergize with Cbfb-MYH11 in the pathogenesis of acute myeloid leukemia. *Proc Natl Acad Sci*. 2004;101(14):4924-4929. doi:10.1073/pnas.0400930101

521. Matthijssens F, Sharma ND, Nysus M, et al. RUNX2 regulates leukemic cell metabolism and chemotaxis in high-risk T cell acute lymphoblastic leukemia. *J Clin Invest*. 2021;131(6). doi:10.1172/JCI141566

522. Sun J, Ramos A, Chapman B, et al. Clonal dynamics of native haematopoiesis. *Nature*. 2014;514(7522):322-327. doi:10.1038/nature13824

523. Busch K, Klapproth K, Barile M, et al. Fundamental properties of unperturbed haematopoiesis from stem cells in vivo. *Nature*. 2015;518(7540):542-546. doi:10.1038/nature14242

524. Sehgal I, Eells K, Hudson I. A Comparison of Currently Approved Small Interfering RNA (siRNA) Medications to Alternative Treatments by Costs, Indications, and Medicaid Coverage. *Pharmacy*. 2024;12(2):58. doi:10.3390/pharmacy12020058

525. Zhong G, Chang X, Xie W, Zhou X. Targeted protein degradation: advances in drug discovery and clinical practice. *Signal Transduct Target Ther*. 2024;9(1):308. doi:10.1038/s41392-024-02004-x

526. Snaider S, Zheng Y, Hearing P. Rb-E2F-HDAC Repressor Complexes Control Interferon-Induced Repression of Adenovirus To Promote Persistent Infection. *J Virol*. 2022;96(11):e00442-22. doi:10.1128/jvi.00442-22

527. Alburquerque-Bejar JJ, Navajas-Chocarro P, Saigi M, et al. MYC activation impairs cell-intrinsic IFNγ signaling and confers resistance to anti-PD1/PD-L1 therapy in lung cancer. *Cell Rep Med*. 2023;4(4):101006. doi:10.1016/j.xcrm.2023.101006

528. Ramana CV, Grammatikakis N, Chernov M, et al. Regulation of c–myc expression by IFN–γ through Stat1-dependent and -independent pathways. *EMBO J*. 2000;19(2):263-272. doi:10.1093/emboj/19.2.263

529. Iwase S, Furukawa Y, Kikuchi J, et al. Modulation of E2F Activity Is Linked to Interferon-induced Growth Suppression of Hematopoietic Cells*. *J Biol Chem*. 1997;272(19):12406-12414. doi:10.1074/jbc.272.19.12406

530. Takarada T, Hinoi E, Nakazato R, et al. An analysis of skeletal development in osteoblast-specific and chondrocyte-specific runt-related transcription factor-2 (Runx2) knockout mice. *J Bone Miner Res*. 2013;28(10):2064-2069. doi:10.1002/jbmr.1945

531. Jin Kim H, Min Park J, Lee S, et al. Efficient CRISPR-Cas9-based knockdown of RUNX2 to induce chondrogenic differentiation of stem cells. Published online 18 January 2022. doi:10.1039/D1BM01716K

532. Wilkinson AC, Ballabio E, Geng H, et al. RUNX1 Is a Key Target in t(4;11) Leukemias that Contributes to Gene Activation through an AF4-MLL Complex Interaction. *Cell Rep*. 2013;3(1):116-127. doi:10.1016/j.celrep.2012.12.016

533. Hamey FK, Nestorowa S, Wilson NK, Göttgens B. Advancing haematopoietic stem and progenitor cell biology through single-cell profiling. *FEBS Lett*. 2016;590(22):4052-4067. doi:10.1002/1873-3468.12231

534. Rodriguez-Fraticelli AE, Weinreb CS, Wang SW, et al. Single-cell lineage tracing unveils a role for Tcf15 in haematopoiesis. *Nature*. 2020;583(7817):585-589. doi:10.1038/s41586-020-2503-6

535. Esplin BL, Shimazu T, Welner RS, et al. Chronic Exposure to a TLR Ligand Injures Hematopoietic Stem Cells. *J Immunol*. 2011;186(9):5367-5375. doi:10.4049/jimmunol.1003438

536. Haiyong H. RNA Interference to Knock Down Gene Expression. *Methods Mol Biol Clifton NJ*. 2018;1706:293-302. doi:10.1007/978-1-4939-7471-9_16

Appendices

Appendix I: Reagents used in this thesis, supplier code and supplier.

Reagent	Code	Supplier
Alt-R™ S.p. Cas9 Nuclease V3	1081058	IDT
0.45 µm Syringe Filter, Cellulose Acetate	E4780-1453	Starlab
1 Kb Plus DNA Ladder	10787018	Thermo Fisher
96-Well PCR Plate, Semi-Skirted	I1402-9700	Starlab
Agarose	9012-36-6	Sigma-Aldrich
AMPure XP Beads	A63880	Beckman
Anti-APC microbeads	130-090-855	Miltenyi Biotec
Anti-RUNX2	ab236639	Abcam
BD Pharmigen Transcription Factor Buffer Set	562574	BD Biosciences
Biotinylated Recombinant Human DLL4	10171-H49H-B	Sino Biological
BIT 15 9500 Serum Substitute	9500	Stem Cell Technologies
BST2 FITC	127007	Biolegend
Caffeine	A10431	Alfa Aesar
CD11b FITC	101205	Biolegend
CD11b PE	101208	Biolegend
CD127 – biotin	135006	Biolegend
CD127 APC/Cy7	135040	Biolegend
CD127 FITC	135007	Biolegend
CD127 FITC	135007	Biolegend
CD150 PE/Cy7	115914	Biolegend
CD19 FITC	152403	Biolegend
CD201 APC	17-2012-82	Invitrogen
CD24 FITC	101805	Biolegend
CD25 BV785	102051	Biolegend
CD3 PE/Cy7	300310	Biolegend
CD34 FITC	11-0341-85	Invitrogen
CD4 – biotin	100508	Biolegend
CD4 APC	100516	Biolegend
CD4 APC/Cy7	100526	Biolegend
CD44 BV605	103047	Biolegend
CD45.1 AF700	110723	Biolegend
CD45.1 PE/Cy7	110730	Biolegend
CD45.2 BUV395	564616	BDBiosciences
CD45.2 eFluor450	48-0454-82	Invitrogen
CD45R – biotin	103204	Biolegend
CD45R APC/Cy7	103224	Biolegend
CD48 BV421	103428	Biolegend
CD48 BV785	103449	Biolegend

CD8 APC	100712	Biolegend
CD8 APC/Cy7	100714	Biolegend
CD8a – biotin	100704	Biolegend
CD8a PE/Cy7	25-0081-82	Biolegend
CD90 PE	140307	Biolegend
CELLBIND plates	3337	Corning
c-Kit APC	105811	Biolegend
c-Kit BV421	105828	Biolegend
CUTANA™ Concanavalin A-Conjugated Paramagnetic Beads	21-1401-EPC	Stratech
ddPCR™ Supermix for Probes	186-3010	BioRad
Direct-zol RNA Microprep kit	R2063	Zymo
DNeasy Blood and Tissue Kit	69504	Qiagen
dNTP Mixture	4030	Takara Bio
Doxycycline	J60422.06	Thermo Fisher
Dulbecco's Modified Eagle Medium (DMEM)	15630080	Thermo Fisher
EDTA	17892	Thermo Fisher
Eppendorf DNA Lo-Bind tubes	EP0030108051	Merck
Ethanol	445740010	Thermo Fisher
F12 base media	15172529	Gibco
Fetal bovine serum (FBS)	12303C	Sigma-Aldrich
Fibronectin-coated plates	354409	BD Biosciences
Flt3 BV421	135313	Biolegend
Gelatin from porcine skin	G2500-100G	Sigma-Aldrich
Genome-wide lentiviral sgRNA KO library	136987	Addgene
GlutaMAX™ Supplement	35050061	Gibco
Gr1/Ly6C – biotin	108404	Biolegend
Gr1/Ly6G APC/Cy7	108424	Biolegend
Gr1/Ly6G FITC	108406	Biolegend
Gr1/Ly6G PE	108408	Biolegend
H3K27me3	07-449	Millipore
H3K4me3	39159	Active Motif
IGG-PE control Ab	Feb-02	Cell Signaling
IMDM with GlutaMAX Supplement	31980030	Thermo Fisher
Insulin-transferrin-selenium-X (ITS-X)	51500056	Gibco
Isopropanol	383910025	Thermo Fisher
Mouse CRISPR Knockout Pooled Library (Gouda)	136987	Addgene
Mouse CXCL12 (SDF-1α) Recombinant Protein	PMC1354	Peprotech
N-2-hydroxyethylpiperazine-N'-2-ethanesulfonic acid (HEPES)	15630-080	Gibco
NaOH	A16037.36	Thermo Fisher
NEBNext® Ultra™ II DNA Library Prep Kit	E7645L	New England Biolabs
NK1.1 FITC	156508	Biolegend
Non-Essential Amino Acids Solution (100X) (NEAA)	11140050	Thermo Fisher

Opti-MEM	P5965309	Thermo Fisher
P3 Primary Cell 96-well Nucleofector® Kit	V4SP-3096	Lonza
pA-Tn5 Transposase	C01070001	Diagenode
PEIpro®	76304-534	Avantor
Penicillin/Streptomycin	15140122	Thermo Fisher
Penicillin/Streptomycin/Glutamine (PSG)	10378-016	Gibco
Phusion High-Fidelity PCR Master Mix	F531L	Thermo Fisher
pMCB306	89360	Addgene
pMCB306 lentiviral plasmid	89360	Addgene
pMD2.G	12259	Addgene
Polyvinyl acetate (PVA)	P8136	Sigma
Propidium Iodide (PI)	P1304MP	Thermo Fisher
Proteinase K Solution	25530049	Thermo Fisher
psPAX2	12260	Addgene
Puromycin	A1113803	Thermo Fisher
Recombinant Murine FLT3 Ligand	250-31L-50UG	Peprotech
Recombinant Murine IL-7	217-17-50UG	Peprotech
RUNX2-PE Conjugate Ab	98059	Cell Signaling
Sca-1 FITC	108105	Biolegend
Sca1 PE	108108	Biolegend
Sodium acetate	S2889	Sigma-Aldrich
Sodium butyrate	A11079	Alfa Aesar
Sodium propionate	A8960	Alfa Aesar
Sodium pyruvate (100 mM)	11360070	Thermo Fisher
Stem cell factor (SCF)	AF-250-03	Peprotech
Streptavidin APC/Cy7	405208	Biolegend
Streptavidin Polystyrene Particles	SVP-200-4	Spherotech
SYBR™ Safe DNA Gel Stain	S33102	Thermo Fisher
TAE Buffer (Tris-acetate-EDTA)	B49	Thermo Fisher
TaKaRa Ex Taq® DNA Polymerase	RR001A	Takara Bio
TE Buffer	12090015	Thermo Fisher
Ter119 – biotin	116204	Biolegend
Ter119 APC/Cy7	116223	Biolegend
Thrombopoietin (TPO)	130-108-958	Miltenyi Biotec
Trypsin-EDTA (0.25%), phenol red	25200056	Thermo Fisher
UltraPure™ 1 M Tris-HCl Buffer, pH 7.5	15567027	Thermo Fisher
Viability Dye eFluor	65-0863-14	ThermoFisher
Vivaspin 20	Z614610	Merck
Water, Nuclease-free, Molecular Biology Grade, Ultrapure	15644028	Thermo Fisher

II

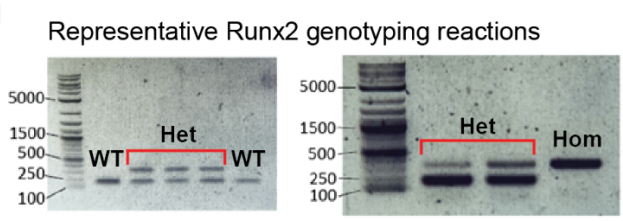

Appendix II: Representative Runx2 genotyping reactions for Runx2^{flox} mouse colony maintenance, described in Chapter 2.4.3. 1 kb^{+} ladder was used in the first lane of the gel. Presence of the flox insert site produces a band of 327 bp, the WT region produces a band of 173 bp.

III

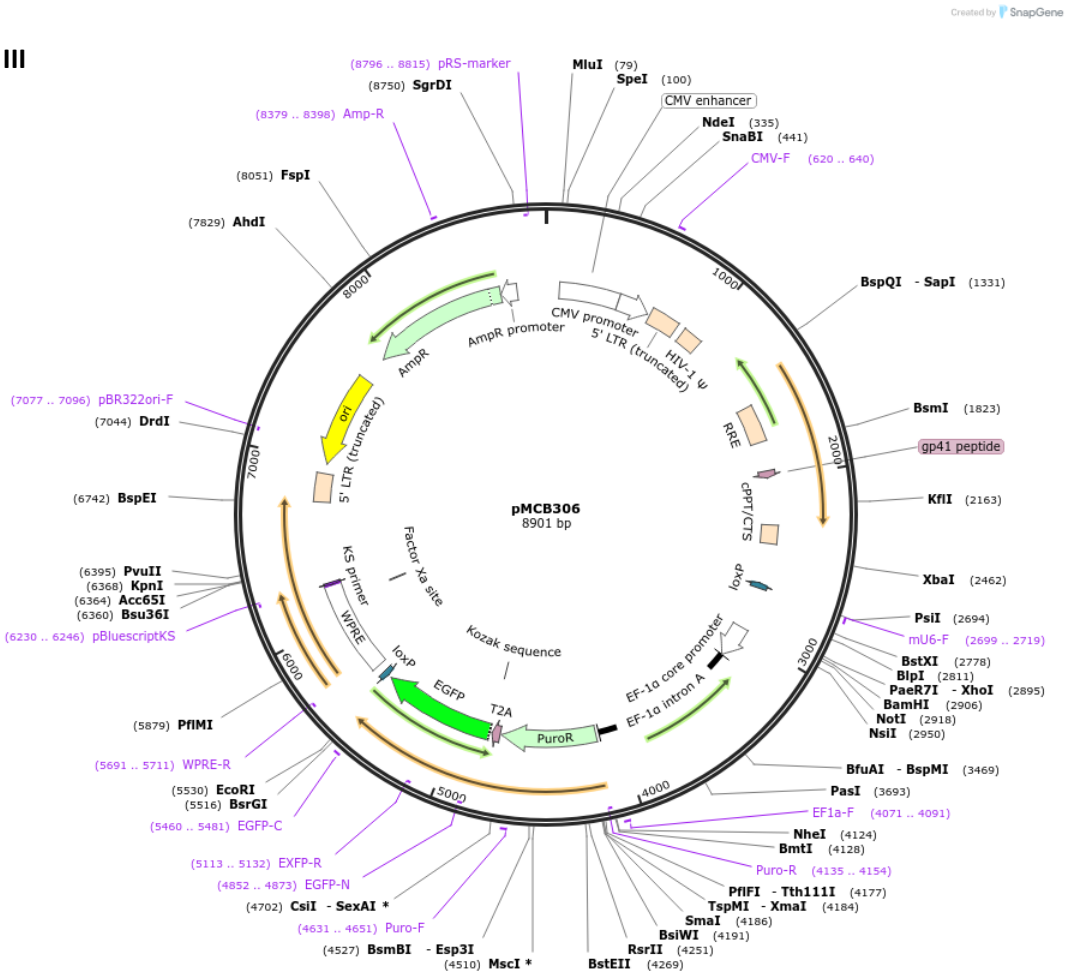

Appendix III: Vector schematic for pMCB306 lentiviral plasmid (Addgene #89360[408]), with a puromycin cassette and GFP selectable markers.

IV

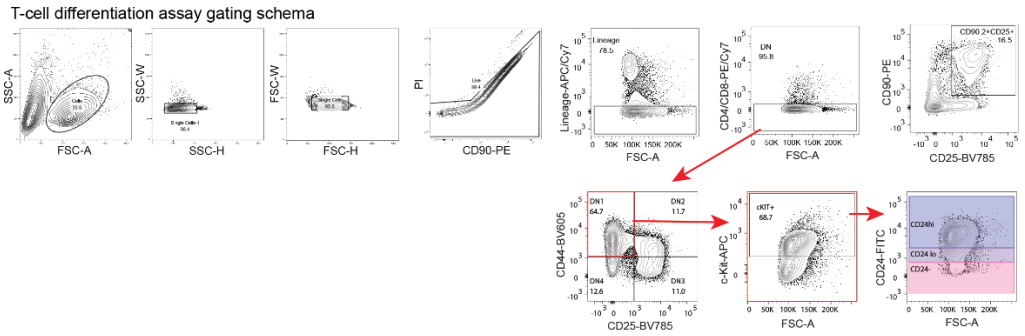

V Bone marrow gating schema

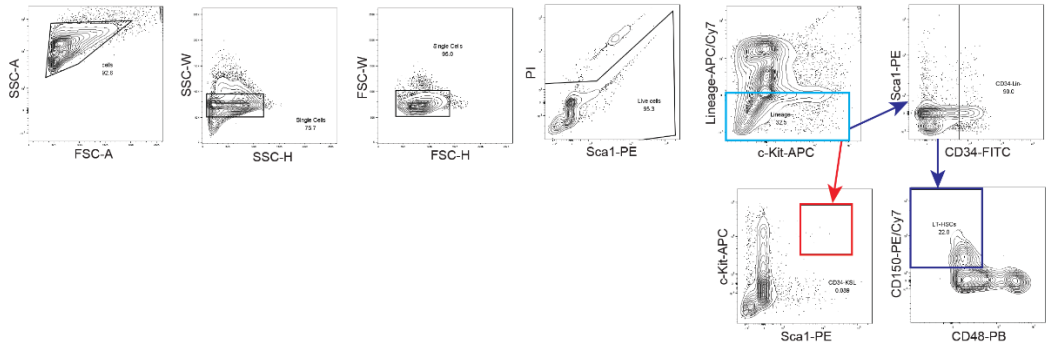

VI Thymus gating schema

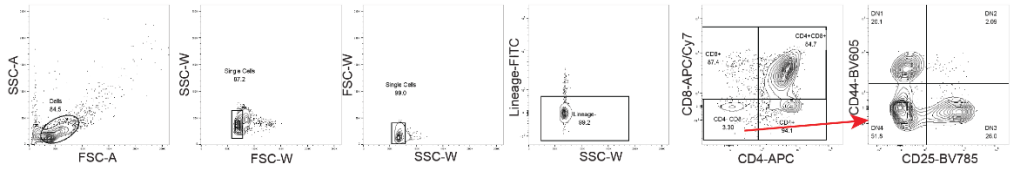

VII Spleen gating schema

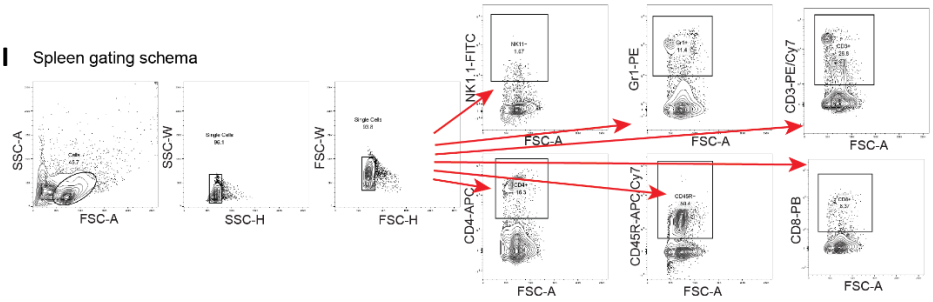

Appendices IV-XIII: Flow cytometry gating schema.

(IV) T-cell differentiation assay gating schema, for methodology described in Chapter 2.

(V) Representative flow cytometry gating schema for bone marrow analysis, described in Chapter 2. Light blue indicates Lin^-, red indicates $c\text{-}Kit^+Sca1^+Lin^-$ (KSL) and dark blue indicates $CD150^+CD48^-CD34^-$KSL (pHSCs).

(VI) Representative flow cytometry gating schema for thymus analysis, described in Chapter 2.

(VII) Representative flow cytometry gating schema for spleen analysis, described in Chapter 2.

VIII Cultured HSC gating schema

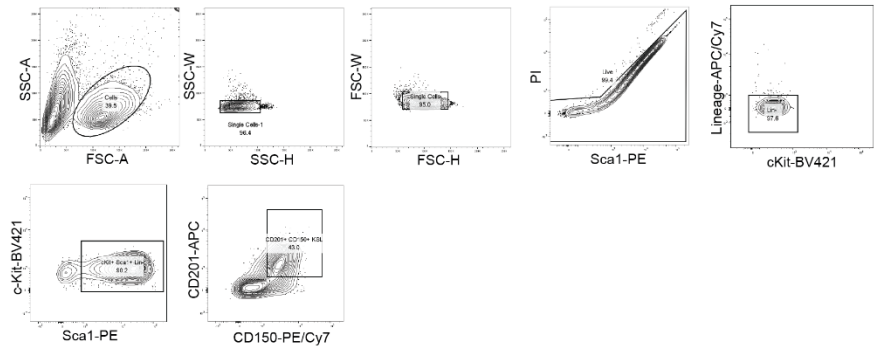

IX RUNX2 intracellular flow cytometry gating schema (*ex vivo* HSCs)

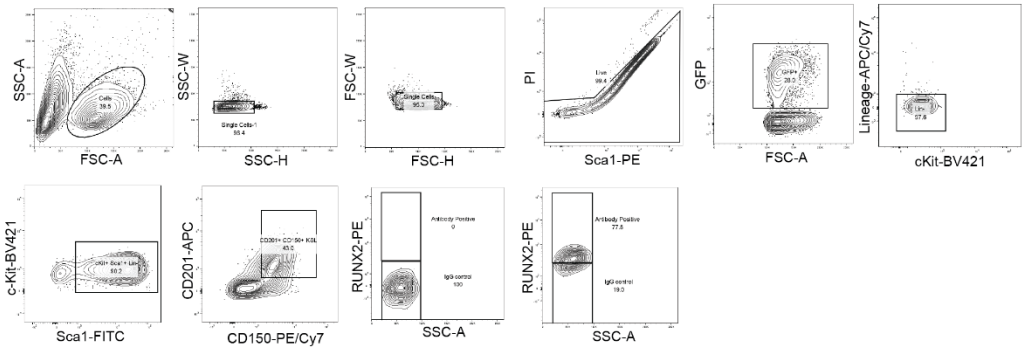

X RUNX2 intracellular flow cytometry gating schema (pDCs in BM)

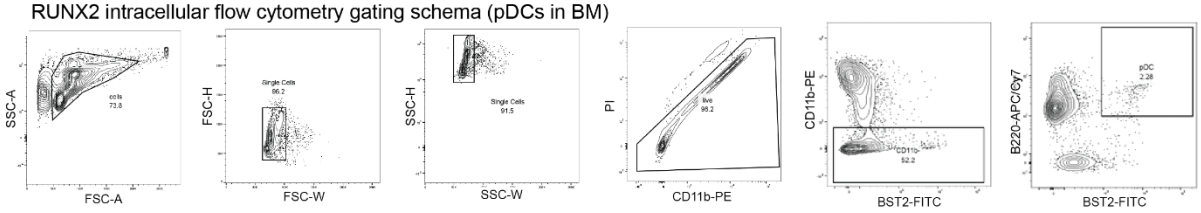

XI HSC competitive transplantation assay peripheral blood gating schema

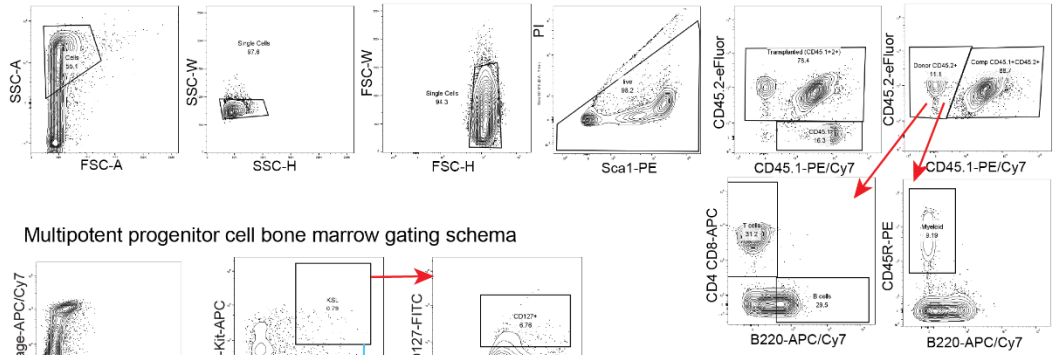

XII Multipotent progenitor cell bone marrow gating schema

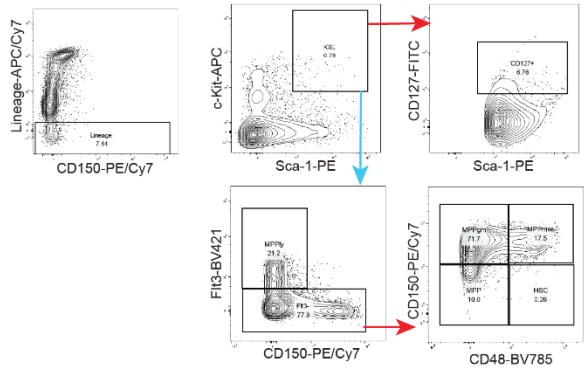

Appendices VIII-XII: Flow cytometry gating schema.

(VIII) Representative flow cytometry gating schema for *ex vivo* cultured HSC analysis, described in Chapter 2.
(IX) Representative intracellular flow cytometry gating schema of RUNX2 on *ex vivo* HSC cultures, described in Chapter 2.
(X) Representative intracellular flow cytometry gating schema of RUNX2 on plasmacytoid dendritic cells (pDCs) in bone marrow, described in Chapter 2.
(XI) Representative flow cytometry gating schema for peripheral blood analysis in competitive transplantation assays, described in Chapter 2.
(XII) Representative flow cytometry gating schema for lymphoid/multipotent progenitor cell panel in bone marrow, described in Chapter 2. Red arrows indicate order of gating and blue indicates end of gating.

Appendix XIII: Genes identified in genome-wide CRISPR screen, in order of beta score (large to small, top to bottom of each column). See Chapter 2.4.6 for analysis pipeline.

Gene target					
Bahcc1	Rabggta	Mrpl34	Copa	Vmn1r155	Gm7429
LOC108168648	Shoc2	Gm10354	Pgm3	Ltv1	Fcf1
Susd6	Dnajb6	Atf4	LOC102634529	Gm6958	Cdc16
Rnf213	Tmed10	Xrcc5	Gm20793	Cog3	Top2a
Fgf3	Gm3667	Snrpc	Krtap16-3	Thoc7	Hinfp
Arih2	Meis2	Emc3	Gins2	Smc2	Rpl18
Dnhd1	Lactbl1	Tefm	Erg	Uqcrc1	Zfp534
Wwp2	LOC102633783	Ercc6l	Hyou1	Exosc7	Napa
Stat2	Wrb	Cflar	Ddx51	Tfam	Sart3
Klrb1f	Prl8a2	Nup205	Wdr7	Polr3b	Lsm3
Ccdc178	LOC101055754	Smc3	Slc3a2	Alg14	Gtf3c4
Cdyl	Gm8094	Ttc4	Gtf3c2	Spc25	Gm3095
Samd1	Rnaseh2b	Sap30bp	Defa33	Gpn1	Zpr1
Ube2e3	Polg	Copb2	Mrpl57	Shq1	Eif2b5
Ccl17	Gm6570	Hist1h2bb	Fam89a	Haus4	Tfrc
Ano9	Safb	Cramp1l	LOC108168588	Crcp	Gm20822
Coq10a	Gps1	Chmp3	Gak	Fadd	Cct3
Runx2	Arpc2	1110008L16Rik	Timm9	Rpf2	Ppp4c
N4bp1	Prpf6	Rusc2	Insig1	Zmat2	Ncbp1
Tph2	LOC102638674	Gm20777	Atp6ap2	Sc5d	Ak6
Lvrn	Tcte1	Sumo2	Gtf3c3	Taf2	Hmgcs1
Htr1a	Cox11	Mms19	Nepro	Gm2046	Orc5
Stat1	1110037F02Rik	Mrps12	Bcs1l	Ube2l3	Rpl17
Olfr644	Vmn1r5	Utp3	Srp14	Gm21292	LOC108168466
Trp53tg5	Pelo	Cnot9	Prim2	Gm5725	Gm2977
Fhl2	Tbcb	Med20	Gins4	Gm3159	Eef2

Grtp1	Fdxr	Scgb1b29	Gm16381	Psmb2	Nars
Olfr360	Clpb	LOC105245406	Wbscr16	Bap1	Gins3
Ccnyl1	Tubd1	Gemin4	Commd3	Sprr2a2	Gm21996
Ccr8	Stt3b	LOC108167321	Clspn	Mvd	Prpf8
D930015E06Rik	Cep295	Kif20a	Rpf1	Polr2b	Gm2237
Fat4	Vmn2r31	Trmu	Sfi1	Ndc80	Mcts1
Pip5k1a	Gm9295	Urb1	Nbas	Gm6818	Smarca5
Thnsl1	Gm33084	Cox18	Psma2	Nkap	Rps3a1
Kif2a	Ipo13	Traf3	Bptf	LOC108169010	Prpf40a
Gskip	Naa15	Gm5415	Gm10698	Usp8	Alg11
Csgalnact2	Tyms	LOC108168587	Defa17	Gm13157	Vmn1r132
Bcan	Gm3259	Gm29758	Vmn2r50	Gm3183	Psmd14
Ackr2	Mettl1	Cfi	Tnpo3	Skiv2l2	Pgam1
4833427G06Rik	Aif1	Yy1	Emg1	Minos1	Ipo11
Zfp397	Vmn1r35	Mrpl40	Slc39a7	Psmd2	LOC108168657
Scimp	Tada3	Zfp708	Noc3l	Ecd	Sf3b2
Pms1	Mon2	Smc4	Mrpl23	2410131K14Rik	Actl6a
Ms4a4c	Elp6	Utp6	Use1	Ankrd49	Imp3
Bbc3	Srfbp1	LOC108168376	Rbm22	Gbf1	Xrcc3
Pten	Gm15319	Selk	Thoc3	Ttc27	Sf3b5
Asap1	Olfr10	Ap5b1	Rpl7l1	LOC108168187	Spin2-ps2
Nsd1	Olfr346	Gadd45gip1	Dph3	Rrn3	Fnta
Tnpo2	Gm4832	Gbp6	Pfdn1	Polr2k	Pold1
Idh3g	Acacb	Gm13212	Ric1	Gm16429	Snrpd2
Plcl1	Sympk	Krtap10-4	Fkbpl	Uhrf1	Ddx10
Dffa	Mbd4	Cox15	Rbbp4	Sae1	Asna1
Olfr893	Aph1a	Pgk1	Mpl	Snrpf	Rpl27
Ankrd33b	Arf1	Romo1	Tubgcp3	Timm50	Mup-ps12
Ly6g5b	Ddx59	Gatb	Eif3c	Rpl6	Dph6
Gm35315	Ppp2r2a	Arih1	Anapc15	Psmc5	Cenpm
P2ry1	Gm20928	LOC108168554	Hlcs	Orc6	Nubp2
Sema3g	LOC102637615	Pold3	Exosc9	Wdr33	Adar
Eda2r	Gm5483	Carm1	Prkrir	Mad2l2	Aurkb
Enpp3	Acly	Ikbkb	Gm3055	Adat2	LOC108168642
Matn4	Zw10	Nol10	Vmn2r121	Pi4kb	Arfrp1
Colgalt2	Serbp1	Hcfc1	Cenpw	Dhx9	Wdr43
Trp53	Zfp931	Hist1h4d	Gm7971	Ruvbl1	Eif2b3

Npvf	Parg	Spcs2	Prpf38a	Nelfcd	Plk1
Baz2a	Nsun2	Cmtr2	Rprd1b	Ube2d3	Acat2
Ctla2a	Prkab1	Gm32211	Usp39	Ggps1	Gm32966
Pou4f1	Leo1	Mipep	Chmp6	Ska2	Wdhd1
Cox6b2	Tnc	Rnaseh1	Gm5157	Kat8	Kars
Nr5a1	Pop5	Snapc5	Gm16404	Taf6	Sap18b
Polr3g	Eif3l	Ppox	Gm8764	Uba3	Ssrp1
Trap1	H2-Q7	Rars2	Amy2a3	Pkm	Ciao1
Evi2b	Mcrs1	Fbxw7	Srp9	Gm13308	Gm21992
Gm29808	Spns1	Cnot10	Rpn2	Upf1	Rpl32
Dapk1	Hus1	Gm3383	Gss	Trip13	Ppp2r1a
Krcc1	LOC108167387	Olfr384	Usp36	Mrpl42	Ncbp2
Avpr1a	Bud31	Emc7	Rpl5	Vmn1r91	Rpl21
Degs2	Rpp40	Actb	Afg3l2	Chtop	Gm26650
Loxl3	LOC100038995	Ska1	Nus1	Pdcd2l	Ticrr
Klhl2	Gm21136	Pet100	Vmn1r163	Eif3a	Sprr2a3
Proc	Ptpn2	Setd5	Pi15	Csnk2b	Hdac3
Grk5	Cnot4	Epg5	Rpl31	Pot1a	Tars2
Spata24	Prr15l	Hnrnpm	Pars2	Guk1	Rpl10
Uhrf1bp1	Gm12407	Gm2022	Nip7	Dync1h1	Dars
Emc9	Olfr954	Pgrmc1	Urod	Copz1	Ssbp1
Crot	Snrnp25	Znhit1	Samm50	Zbtb8os	Cfap20
Gabre	Gm38510	Dph2	Wars	Tsfm	Aars
Sirt1	Gm19470	Taf1d	Atp5b	Supt6	Rpl27a
Tekt3	Il1rap	Sdhc	Sbno1	Gm8256	Golt1b
Plaa	Tbce	Rpp14	LOC105245673	Psma1	Ubl5
Hsdl2	Polg2	Crls1	Nfyc	Mtif2	Rps27l
Cib2	Gm3278	Exoc7	Mrpl43	Tfb2m	Terf2
Mar-02	Lcmt1	Ccdc137	LOC108168679	Hist1h3c	Gm17330
Chia1	Taf10	Hist1h2bj	Nsmce4a	Srcap	Lsm4
Mup7	Cox20	Zfp808	Cap1	Rad9a	Rps10
Haus3	Hist1h1d	Dnajc8	Polr3f	Rpusd4	Vps28
Plxnb2	Cir1	LOC105247075	Gm3005	Acaca	Tex10
Fuca1	Gtpbp4	Taz	Ireb2	Supv3l1	Rps5
Thap4	Ska3	Dcaf7	Gm39972	Scap	Chmp4b
Meis1	Gm42052	Gm5797	Olfr761	Vps4b	Rpl7
Cdc6	U2surp	Ints2	Ap1g1	LOC100041708	Eef1a1
Gm29716	Ccnb1	Tra2b	Hira	Psmd12	Gm20772
Vps18	Hif1a	Gbp9	Kctd13	Efl1	Chd4
Mup21	Pop1	Fam60a	Wbscr22	Npm1	Gm40847
Olfr995	Tuba3b	Suz12	Tipin	Sfswap	Gm40367

Zmat5	Mat2a	Chaf1a	Rrs1	Gm14326	Eftud2
Slc5a6	Macf1	Pmf1	Phb2	Rps21	Dcaf13
Phf12	Bub1	Exosc2	Mdm2	Rps25	Nelfb
Rpl22	Eif5b	Snrpg	Cct7	Pabpc1	Polr2g
Gclm	Fam96b	Smg5	Rbx1	Actr6	LOC100862202
Gm15776	Skint8	Gm41885	Mis12	Vmn1r131	Timm23
Opa1	Nom1	Ces1h	Urb2	Rfc5	Cirh1a
Ube2cbp	Mrpl20	Gjb5	Spin2-ps3	Dut	LOC108167476
Phgdh	Mup10	Sparc	Cops4	Cul2	Stk11
Gml	Coa6	Gm7120	Psmd11	Ubtf	Gm40364
Eif3k	Ranbp1	Slc4a7	Mrps35	Oxa1l	Hspd1
Atp5h	Olfr18	Mtg1	Lsm2	Orc2	Hspa8
Gm32234	Ubd	Rbm14	Alas1	Upf2	Fbxw11
Gm3636	Gemin6	Olfr813	Hist1h2bg	Nup98	Rrm1
Traf2	Mtg2	Fbxo5	Cox14	Ncapd2	Vmn1r101
Efr3a	Dph5	Gm5592	Zwilch	LOC108168534	Las1l
Trappc8	LOC546061	Bud13	Maea	Naa38	Gm7347
Sult2a3	Tomm70a	Cenpe	LOC108167415	Fasn	Taf1a
Atg10	Slc35a2	Morf4l1b	Mtf1	Taf1c	Usp5
Tcstv3	Lrrc39	Twistnb	Rab7	Gata2	Srsf3
Fxn	Slc25a3	Tm2d2	Nop10	Yars2	Nvl
Mmp7	Atg12	Lonp1	Bet1	Ilf2	Nxt1
Nup160	Hoxa3	Alg13	Haus5	Ypel5	LOC10086219 2
Med7	Nup214	Taf1	Atp1a1	Cct5	Mars2
Ints3	Por	Polr2h	Mrpl27	Tubb5	Mrps33
Cdkn2b	Ash1l	Gm5373	Srsf10	Gm40369	LOC108168506
4930521O11Rik	Usp16	Ercc1	Rpain	Zfp972	Rpl9
Zfp959	Tcl1b4	Klra4	Gm4027	Psmd4	Top1
Prmt7	Gm10378	Tubgcp5	Dot1l	Ptpn11	Mcm7
Zfp592	Sptlc1	Srpr	Pus3	Copb1	Snrpd1
Strap	Prdm10	Oraov1	Gm10375	Cox7c	Exosc4
Hivep1	Olfr330	Traip	BB287469	Rad50	Cdca8
Sin3b	Mrps30	Cdc27	Nat10	Rpl36	Ssu72
B3glct	Cfdp1	Scgb2b4-ps	Scgb1b3	Rplp1	Dnmt1
Pex1	Lelp1	Mrps23	Rbsn	Gm4177	Gm20794
Txn1	Umps	Tbcc	Mrps7	Rps24	LOC108168591
B020011L13Rik	Nol8	Ppib	Lars	Mrpl22	Snrnp200
Obp1a	Gm9840	Mphosph6	Cyp51	Ywhaq	Atp6v1a
Epn1	Kcng4	Tceb2	Spdl1	Polr2f	Polr3h

Ubqln3	Vmn1r56	Eif1a	Ppwd1	Snrnp35	Rpa2
Yae1d1	LOC108168176	Mrpl24	Nup107	LOC108168573	Rcc1
Bdp1	Vmn1r111	Ddx19a	Scgb2b11	Pdcd11	LOC108168962
Coasy	Kif18b	Cdc42	Wdr83	LOC108168566	Mdm4
Nufip1	Nrf1	4930433I11Rik	Cdc23	Gm2001	Tbca
Lzts3	Hist1h3e	Rprd2	Polr2l	LOC100041806	Nedd1
Emc2	Cwc25	Vmn1r13	Gm2016	Polr1b	LOC108168572
Dnajc2	Xrcc2	Vmn2r97	Mbip	Gtf2e2	LOC108169061
Grpel1	Smok3b	Ccl21a	Mrpl2	Tamm41	Rpl23
Cenpp	LOC108168658	Snrnp48	Timeless	Mecom	Ddx23
Vmn1r33	LOC102637070	LOC105243090	Meaf6	Gm20827	Gm41476
Cog7	Pym1	Brf2	Orc4	Mrpl47	Polr3a
Gm33726	Pcdhga1	Tmx2	Gm2956	LOC100502592	Ppp1cb
Kri1	Rhox8	Med28	Rps19bp1	Atg9a	LOC108168589
Dnah3	Slu7	Eif4a1	Dohh	Polr3e	Gemin8
Pold2	Cdk13	Mrpl33	Gtf2e1	Cnot3	Hspa5
Dnajc11	Gm2777	Gm8165	Dync1i2	LOC108168652	Mrpl53
Rgp1	Glmp	2700062C07Rik	Arpc4	Rfc2	Gtf2b
Gfi1	Ndufab1	Isy1	Osgep	Cops3	LOC108168600
LOC102637163	Wdr12	Cse1l	Glrx3	Mrps6	Rpl10a
Gm3173	Hgs	Olfr871	Esf1	Vars2	Ddx47
Synpo	Gm5934	Olfr951	Shc1	Mrpl54	Yrdc
Olfr390	Gm4498	Heatr1	Rbmy	Aamp	Rpl39
Utp20	Ubr4	Gm4884	Tubgcp2	Rps19	Trnt1
Gtf3a	LOC101056144	Tlk2	Gm6445	Tufm	Hnrnpl
Gm10424	Med18	Slc7a5	Mrpl12	Cad	2200002J24Rik
Zmym2	Hist1h1c	Commd8	Atp6v1h	Lsm10	Rad51
Irs3	Brap	Hist1h4a	Ccm2	Dhx15	9930104L06Rik
Rfc4	Baz1b	Wash1	Vmn1r149	Trmt6	Supt4b
Tmem208	Spin2e	Gm21608	Cog4	Nploc4	Gm20819
Qrsl1	Mrpl3	Nol9	Ddx52	AA792892	Eif6
Gm21658	Wnk1	Fbxo7	Nuf2	Exoc3	Rcl1
Zscan4f	Tsc1	Atp6v1b2	Pggt1b	Psma7	LOC108168565
Gm7762	Rpl41	Tsen15	Ddx21	Naa50	Nedd8

LOC105245578	Gm38947	Hist1h4b	Cdc5l	Grb2	Mis18a
Vps29	Krtap5-2	Metap2	Hexim1	Dhx36	Gfpt1
Haus2	Ei24	Adat3	Sdhd	Gm10340	Exosc10
Wdr61	Gm7361	Anapc2	Tsc2	Sys1	Tsr2
Uvrag	1700020A23Rik	Anapc1	Pmpcb	Psmg3	Rps27a
Vmn1r20	Nudt10	H2afx	Ippk	Dhx33	LOC108168003
Vmn1r128	Gm38423	LOC108168637	Nop9	Snrpb	Atr
Uqcrb	Hsd17b10	Haus7	Prim1	Eif3g	Gm4216
Usp9x	Supt3	Asf1a	Nifk	Gm17019	Thoc5
Mllt10	Trappc3	BC003331	Smg1	Pfdn2	Rps7
Trappc11	BC061212	Psmg1	Znrd1	Ddx49	Tango6
Cx3cl1	Nfkb2	Pomp	Cpsf4	LOC108169100	Cdc123
Ppm1d	Gm4925	Uqcc2	Stat5b	Cdc73	Birc5
Scrt1	Olfr943	Usp37	Eef1e1	Polr2e	Nrde2
Zfp955b	Prpf19	Lce1e	Mis18bp1	LOC102638047	Trmt112
H2afy	Emc4	Ube2m	Smc6	Ufd1l	Rpl4
Gm11563	Cc2d1a	Dynll1	Exoc5	Deb1	Psma3
Rad1	Rrp1	Mrpl51	Pola1	Vbp1	Cdc20
Bod1l	Lrpprc	Uso1	Mad2l1	Ipo7	Thoc1
Gm8909	Mrpl16	Taf13	Naa35	Iars2	Ddx39b
Sprr2a1	Ddx1	Zmiz1	Alad	Tcea1	Rps26
Srp54a	Olfr774	Gm6164	Cenph	Jak2	Eif2s1
Vmn2r91	Pus7	Eif3j1	Nup93	Cab39	Rps14
Gm9257	Bop1	Ctbp1	Ddx31	Eif3i	Ran
Gm3043	Rnf8	Bms1	Rps9	Rabggtb	Trp53rka
Defa23	Cyc1	Hnrnpu	Krit1	Rpl11	Bysl
Rbm25	Gab2	Nfyb	Nup43	Cbfa2t3	Vars
Cebpz	Mrps31	Vps33a	Sacm1l	Fh1	Prelid1
Blvra	Mylk2	Cenpo	Mettl3	Defa31	Dhx8
Ech1	Nfkbiz	Chchd4	Pola2	Paf1	Dimt1
Gm21319	Vps53	Setdb1	Mrpl9	Usp18	U2af1
Mbd2	Eefsec	Xab2	Polr1a	Polr2a	Pisd
Eif4a2	Amy2a4	Nelfa	Nudt4	Htatsf1	Wdr36
Rbm19	Mrpl15	Psmb3	Mar-05	Gm20898	Rpl34
Orc1	Cycs	Uba1	Sde2	Kdm1a	Gm10666
Olfr1359	Rpn1	Aasdhppt	Chmp2a	Nae1	Gm20854
Zfyve19	Gm10668	Ddx56	Mrpl41	Gm9495	Mars
Vmn1r15	Olfr1249	Cars2	Hacd2	Rsl24d1	Clp1
Exosc5	Mrpl10	Srrd	Gclc	Ldb1	Bub3
Zfp830	Dck	Wdr46	Wdr26	Oip5	Eif2b4
Kifc2	Trmt10c	Mrps10	Wdr4	Cit	Fau

LOC108168602	Acat3	LOC102637947	Tmem203	LOC10086224 5	Pmpca
Tmed2	Dgcr8	Cops2	Rpp21	Rbm8a	Preb
Vps35	Gm30124	Sf3b1	Mtor	Gm21699	Psmb1
Bola2	Mylip	Snrnp70	Mrpl38	Nol6	Rack1
Dph1	Mrps15	Vmn2r98	Hhex	Fitm2	Psma4
Rnf20	Tex21	Lsm8	Wdr75	Farsa	Gm16434
Gm31035	Ino80	Cog5	Txnl4a	Rpl13	Rfk
Cnot1	Mtbp	Rnaseh2c	Polr1d	Gm21977	Cdt1
Gm21586	Zcchc9	Eif3e	Srebf1	Dctn4	Noc4l
Defa24	Olfr1154	Pfn1	Gm11239	Mvk	Vmn1r113
Pno1	Pkmyt1	Rrp7a	Lmo2	Rpl12	Tubg1
Atp6v1f	Cmpk1	Bub1b	Uqcr10	Srsf2	Polr1c
Gcn1l1	LOC108168649	Mrpl49	Mysm1	Eif5	LOC101055672
Scgb1b12	Tab2	Ppp1r8	Gm10058	Snrpe	Kpnb1
Sptlc2	Mtx2	Commd4	Ykt6	Sbds	Pes1
Nsun5	Gm6468	Cops5	Dtymk	Ddx27	Gnl2
Gpr89	Med22	Pias1	Pfdn6	Xpo1	LOC105244208
Tubb4b	Etnk1	Stmn1	Zfp781	Scd2	Dctn6
Rab11a	Prpf3	LOC108168468	LOC102634581	Gm20879	Fdps
Brip1	Rpap3	Plrg1	LOC101055663	Gnb1l	Atp1b3
Mterf3	Zfp935	Dlst	Trim28	Gm4301	Gm10670
Lck	Mrps5	Sdhb	Pgd	Prc1	Sdad1
Gtf2h1	Tti1	Eno1	Cox6b1	Ccdc115	Ears2
Nsl1	Tmem164	Bcl2l1	Spc24	Sp110	LOC101055676
Cog6	2310011J03Rik	Recql4	Rae1	Gmppb	Usp7
E430025E21Rik	Naf1	Tagap1	Gm13249	LOC108167858	Dr1
Defa5	LOC102632102	Tube1	Myl12a	Nxf1	Psmc4
Wee1	Mcmbp	Srm	Gtf2h3	Anapc5	Rpl7a
Atxn2l	Rpap1	Srbd1	Cmip	Kif23	Exosc3
Dido1	Atp5f1	Scfd1	Vmn1r93	Uxt	Cars
Wdr77	Pam16	Pi4ka	Cox16	Phb	Tars
Commd2	Hnrnpk	Ap1m1	Dcps	Lce1j	Mettl16
Txnrd1	Rrp36	Gm7040	Ccdc130	Rint1	Gm7980
Ccar1	Hsd3b5	Hist2h3c2	Med6	Dynlrb1	Rps18
Pdcd2	Mmachc	Ddx3x	Hmgcr	Bccip	Gm7982
Kif3b	Larp7	Tsen34	Nfs1	Gm42078	Hist1h3f
Gse1	Stx4a	2310036O22Rik	Rpl28	Zfp36l2	Utp15
Coa5	Rpa1	Gm21425	Rabl3	Rps8	Gm36327
Suv420h1	Alg1	Olfr983	Supt5	Gm6337	Hist2h3c1

Ccdc22	Mrps17	Med10	Vmn1r112	Mrpl46	Dpagt1
Nbn	Gm21104	Mre11a	Sap18	Cdc45	Ddx54
Knstrn	Dctn1	Nop16	Jtb	Txnl4b	Rangap1
E4f1	Nob1	Dctn2	Mrps16	Tpi1	Dclre1b
Gm13272	Gm21811	Uba2	Anapc11	Defa36	Men1
C130060K24 Rik	Pira2	Ptpmt1	Tubb3	LOC108169043	Map3k7
Usp34	Gm35342	Ythdf2	Mocs3	9530057J20Rik	Gm40378
Mybbp1a	Taf5	Srprb	Prpf4	Tardbp	Wdr1
Cdca5	Gosr2	C87414	Cpsf3l	Mrpl35	Gm40600
Olfr812	Ctu1	LOC105244034	Prmt1	Lars2	Crnkl1
Gm11238	Gm3248	Vps54	Osbp	Ddb1	Mybl2
Ppp1r7	Gm2832	Plag1	Banp	Gfm1	LOC108167809
Lamp2	Xpr1	LOC108168665	Grwd1	Ripk1	Chek1
Rad54l2	Gm8210	Pdcd7	Hsd17b12	Spata5l1	Hist1h2ad
Rmi1	Vmn1r130	Cpsf1	Ddx46	Kit	LOC10816851 6
Zfp574	Nsun4	Mrps2	LOC108168681	Med4	LOC10816856 8
Asic4	Noc2l	Wdr3	Dolk	Rps6	Hist2h2ac
Gm20873	LOC545763	Ppil1	Gm2696	Ncapg2	Rpl30
LOC105245577	Stard7	Atad3a	Dhx37	Ogt	1110004E09 Rik
Zfp384	Hmbs	Mrpl30	Racgap1	Eif4a3	Alg2
Zfp207	Ints4	Chordc1	Vps11	Med31	Vps52
Vmn2r113	Gm13309	Csnk1a1	Tpt1	Rps15a	Sf3b3
LOC108168155	Exosc8	Nsmce1	Gatc	Mrpl39	Psma5
Olfr535	Ndrg3	Vmn1r194	Trappc1	Abt1	Cdk1
Arnt2	Atpaf2	Rev3l	Cept1	Hist1h4f	Hist1h2ao
Gm4565	Cstf1	Vps45	Timm10	Psmd1	Rps29
Gfm2	Morc3	Zc3h13	Hist1h2bh	Actr10	Mdn1
Irf2	Gm4737	Vmp1	Gm6351	Gm20820	Xrn2
Vmn1r220	Cox19	Cenpl	Gm16367	Naa25	Rpl8
Cyp3a16	Pbx1	Rpl37	Aagab	Rbm39	Ctcf
Thap11	Nutf2	LOC105245675	Erh	Tbl3	Dhdds
Rsbn1	Smc1a	Ewsr1	Lsm6	Mrpl18	Gm20815
Myef2	Cpox	Ccdc93	Zc3h10	LOC102639037	Hist1h3g
Sdhaf2	Cinp	Mrpl44	Ankle2	Tuba1a	Fam50a
Gm10591	Haus1	Gm10302	Sars2	Eif4e	Rpl15
Fam32a	Ptpn23	Cdk7	Atp6v0b	Nop2	Hist1h2ac
Nfya	Tubb2a	Psmg4	Gm8229	Smu1	Rps20
Gemin2	Ube4b	Impdh2	Atp6v1e1	Ddx24	Psma6

Sult2a2	Ugt2b35	Atp6v1d	Nudc	Sod1	Chaf1b
Gm11595	Rbm15	LOC105242399	Gm6348	Gltscr2	Atp6v0c
Mucl2	Hsd17b7	Sap130	Pnkp	Ciapin1	Eif2b2
Ipo9	Rsl1d1	Ifna5	Eprs	LOC108167362	LOC108167571
Kifc5b	Sugt1	Pwp2	AY358078	Rps23	Gm8005
Spag5	Gm13242	Haus8	Fbl	Slmo2	Gm40368
Diexf	Gm20910	Lrr1	Dhx16	Psmd8	LOC10816791 8
Rft1	Sco2	Ppp2ca	Ppcdc	Elof1	Rps13
Olfr1129	Dcp2	Mrpl4	Trmt61a	Ahcy	Rars
Gm20604	Ctr9	Ccdc12	Mrps22	Phf5a	Sf3b6
Aldoa	Supt4a	Hist1h1b	Rngtt	Psmc6	Nsdhl
Rdh19	Cct4	Rnf31	Rps2	Dna2	Tk1
Cphx3	Cers2	Prkar1a	Gm2446	Snupn	Tuba1b
Iltifb	Pik3c3	LOC100503923	Eef1g	Ppcs	Mbtps2
Slc38a2	Sf3a3	Pcbp1	Eif1ad	Trappc4	Cct8
Mrps28	Vmn1r203	LOC108168186	Eif3m	Mak16	Espl1
Zfp804a	Olfr1373	Ikbkg	Polr1e	Tsr1	Gm20795
Zfp687	Gm13251	Plk4	Kmt2a	Gm2427	Rnps1
LOC108168467	Gm2457	Lss	Mcm3	Nup85	Aurka
Surf6	Zbtb1	Eif5a	Wdr18	Ncapd3	Gm3685
Fam189a2	Mcm3ap	Atp6ap1	Brpf1	Med14	Snrpd3
Hnrnpc	Huwe1	Rnmt	Ppa1	Tfg	Pdrg1
Fen1	Hist1h1e	Aars2	Lsm5	Hypk	Rps28
Amy2a2	Lce3f	Vmn1r95	Dctn3	LOC105247282	Polr2c
Rnf40	Tmem258	Armc7	Wars2	Mrps21	Uri1
Ctbp2	A530032D15Rik	Dnajc9	Cog2	Psmd3	Rpl18a
Rmi2	Zfp407	Rnasek	Ndor1	Gm5862	Vcp
Stil	Iscu	Srp68	Vmn1r166	Eif3b	Rpl23a
Srp54b	Kif14	Wtap	Gm8068	Arl1	Gm3476
Hscb	Mrpl36	Mrpl17	Srp72	Qars	Nhp2
Map3k11	Tfb1m	Clta	Thoc2	LOC102639021	Mcm2
LOC108168655	Tmub1	Pet117	Mrpl14	Rps11	Sf1
Gm21129	Gm8653	Cmtr1	Mrps9	Exosc6	Rpsa
Vmn1r18	Fip1l1	Ngdn	Nampt	Eif2b1	Rpa3
Gm2666	Ccna2	Med12	Rtcb	Nsf	Gm10408
Hist2h2ab	Isg20l2	Gm8660	Ruvbl2	Nudt21	Rpl35a
Pigl	Fam205c	Mrps18a	Casp8	Haus6	Snrpa1
Chd5	Sars	LOC108168045	Cox5a	Tomm20	Tomm22

Dhx38	Atxn7l3	Frem1	Fzr1	Psmc3	Gm10410
Gm32719	LOC620551	Cox5b	Cpsf2	Vmn1r142	Cpsf3
Olfr297	Ptcd3	Slc7a6os	Uqcrc2	Sdha	Banf1
Capzb	Spin2-ps4	Ints9	Ftsj3	Gm42267	Gars
Uba6	Eif3j2	Ttc14	Cdc26	Gm15433	Vps25
Gm7970	Yme1l1	Tceb1	Gm2003	Ascc3	Ssty1
Mc3r	Mtr	Rbmxl1	Srebf2	Atp6v0d1	LOC108168592
Btg3	Gm3701	Lsm11	Gtf3c1	Dhodh	Snap23
Smarca4	Sult2a5	Sass6	Nup155	Mettl14	Vmn1r118
Coa3	Flad1	Mbtps1	Cactin	Xpo5	Cstf3
Olfr1079	Ap2s1	Eny2	Cenpn	Vmn1r143	Gm14295
Cdh22	Dars2	Msmo1	Phax	Cox6c	Rplp2
Becn1	Gm2799	Telo2	Pmvk	Rpl37rt	Rpl26
Peo1	Lamtor4	Hist1h2be	Triap1	Acd	Kif11
Sf3a1	Arpc3	Gemin5	Mcm4	Arcn1	Hist1h2ba
Fam13b	Polr3k	Ttc1	Sep-07	Sec13	Scd3
LOC105242449	LOC108168683	Gm8212	Ddost	Ints1	Gtf2a2
Ccnd2	Denr	Eif2s3x	Dad1	Cfl1	Polr2j
Cenpi	Dhcr7	A230046K03Rik	Timm22	Nubp1	Gm21248
Wdr48	Vmn1r2	Gm21663	Gpkow	Cox7b	Ddx20
Gm12789	Blm	Nmd3	Ubc	Iars	Psmb4
Lce1f	Scgb2b33	Cwc15	Rnaseh2a	Thg1l	Hars
Sharpin	Srrt	Pcyt2	Krtap5-4	Rps16	Scgb1b2
Gm5935	Gm10436	Tcp1	Elac2	Dnaja3	Ube2i
Ankrd40	Gmps	Gata5	Letm1	Kdsr	Gm37416
Vmn1r16	Cwc22	Speer4c	Atp6v0e	LOC108168067	Abcf1
Znhit3	Pfdn5	Speer4e	Rps27	LOC100041057	Gm42102
Dpf2	1810013L24Rik	LOC108168551	LOC100039029	Gabpb1	Mup13
Emc6	Mcm5	BC052040	Psmd13	Wdr5	Rplp0
Ptar1	Gm5639	Rpl34-ps1	Atp5a1	Rpl37a	Rps17
Top2b	Atp5l	Imp4	Trappc5	Kat6a	Dkc1
LOC108169097	Gm29376	Dnm2	LOC108167806	Rpl35	Pcna
Gm41844	1110059E24Rik	Tbcd	Pum3	Hspa9	Hist1h2ae
Furin	Pstk	Gm8453	Eapp	Gm40814	Tut1
7420426K07Rik	Naa20	Nol12	Abcb7	Top3a	Hist1h4m
Pex2	Gnl3l	Gm35091	Ppp2r3c	Psmg2	LOC102636792
Cc2d2a	N6amt1	Sec22b	Mnat1	Sfpq	Ckap5
Gm3233	LOC108168607	Trmt5	Ercc2	Trp53rkb	Pabpn1

Gm13128	Etf1	Vmn1r170	Gm40595	Mrto4	Rrm2
Vmn1r80	Mcm6	Aqr	Slc35b1	Cdipt	Snf8
EU599041	Sec61b	Olfr1484	Orc3	Rps15	Rps4x
Ssxb9	1810026J23Rik	Mrpl52	Sin3a	C1d	Rpl24
Napg	Sec61g	Zbtb11	Nsa2	Yars	LOC108168556
Myl12b	Nsmce2	Nars2	Zc3h3	Vma21	Gm40365
Dusp12	Dicer1	Nudcd3	Gm40853	Nrbp1	Gm21596
Tm2d3	Dpy30	Mms22l	Tfip11	Gpn2	Sf3b4
Hist1h4k	Wbp11	Kin	Ebp	Gm2854	Gm38418
Ppp1r12a	9030624J02Rik	Tma16	Clns1a	D2Wsu81e	Vmn1r104
2700060E02Rik	Gm906	Zfp335	Pdcd10	Rfc3	Cdc37
Gm42368	Jade2	Rdh9	Ints5	Terf1	Gapdh
Rpp38	Gapdh-ps15	Uba52	Ncaph2	Fars2	Rps3
Sptssa	Cltc	Slc25a26	Tomm40	Prmt5	Gm40862
Olfr128	Fam58b	Rbm28	Adsl	Cbfb	Gm36504
Hoxa9	Elovl1	Gm20806	Gm32584	Gm3147	Gm40363
Wdr24	Polr2d	Gpn3	Rrp12	Gm38699	Dhps
Hrnr	Gins1	Numa1	Psmc1	Gm2784	Vmn1r127
Suds3	Ppa2	Supt16	Fdft1	Yeats4	Rpl3
H3f3c	Olfr1152	Fech	Sf3a2	Msto1	
Rptor	Mrps14	Hspe1	Pgs1	Smc5	
Klk1b4	Sos1	Dnajc17	Vmn1r100	Mrps25	
Gm13271	Seh1l	Gm31009	Ppan	Ddx18	
Tm2d1	Hist1h2bf	LOC108168152	Itpk1	Rpl13a	
Vps39	Aurkaip1	Scgb1b30	Scgb2b6	Gm14393	
Uqcc1	Gm3435	Smarcb1	Rpl19	Nop58	
Pigs	Luc7l3	Fntb	Nle1	Ect2	
Rybp	Krt87	Mtpap	Ddx55	Krr1	
Ap2m1	Irf2bp2	Polrmt	Rpl29	U2af2	
Derl1	Gtf2f1	Arl2	Med11	Rpl14	

Appendix XIV: Significant (padj < 0.05) differentially expressed genes from Runx2-flox pHSC RNA-seq, Runx2-hom vs Runx2-wt. n = 3, sorted by padj small to large, top to bottom of each column. See Chapter 2.8.2 for data analysis pipeline.

gene	log2FC	gene	log2FC	gene	log2FC
Runx2	-2.210678243	Smc4	-0.297924028	Mgat5	0.31403882
Ifi27l2a	1.09242304	Tchp	0.605304025	Cish	-0.432314885
Ifi27	0.711698828	9130020K20Rik	0.989013138	Spats2	-0.634390871
Irf7	0.841013152	AU022793	1.951439771	Hmgn3	-0.493533144
Il18r1	-1.944631545	Tmem167	-0.336980427	Cracd	-0.356561382
Neat1	0.762781422	Gem	-0.606795011	Gm32715	1.826625656
Sell	1.714580175	Skp1	-0.316152315	Cd72	-0.469762779

Gm41107	3.448995922	Mast3	0.290189998	Nfic	0.28096157
Kmt2d	0.525464213	Tbkbp1	0.356938536	Actn1	-0.353286835
Plec	0.527709697	Map1s	0.358298406	Casp12	-0.487069743
Kcnq1ot1	0.861357279	Gm31349	1.72331338	Pex6	0.361176304
Lpl	-2.003776049	H3f3b	-0.349346283	Hif3a	0.509925616
Tox	-1.26050963	Rbm15	0.498921594	Id2	-0.796667217
Itsn1	-0.691429776	Kmt2b	0.36329211	Zfp760	-0.456546814
Oas2	0.671788196	LOC115488769	1.365136993	Hccs	-0.391431673
Nrk	-1.067740388	Trpm2	1.091330997	Cpd	-0.368150104
Ly9	0.742222958	App	-0.567696148	Cul9	0.345788959
Ifi209	2.012595081	Oas1a	0.385042306	Epdr1	-1.172390973
Hdgfl3	-0.616523123	Gm51450	1.179661757	Gm16150	1.516176602
Tnip3	-0.714163358	C920009B18Rik	0.622928379	Il9r	1.563589719
Oasl1	0.710316316	Marveld2	-1.166570231	Pde9a	-0.893874702
H2-T24	0.912204855	Gm10509	-0.573598806	Gm46485	1.439956175
Plac8	0.974238994	Ccdc88b	0.449799625	Hdac7	0.309004695
Siglecg	1.160218378	Pmaip1	-1.148962017	Il6ra	0.530155022
Ralb	0.701673108	Prex2	-0.835580408	Gm4269	2.154628858
Gm39326	1.094773435	Arpp19	-0.36730146	Rin2	-0.862216997
Ifi206	0.989142298	Atp13a2	0.341256385	Ccdc60	-0.803030666
Rgs8	1.916799	Prnp	-0.414414675	Cdcp1	-0.938583769
Sva	7.98860273	Gm20559	0.465744	Entpd5	-0.267638191
Commd10	0.844383229	F830016B08Rik	0.680214694	Slc7a11	-1.362057416
Oas3	0.49390349	Gm34854	1.367756024	Zfp72	-0.747080483
Lat2	0.819971341	Mov10	0.309192116	Rptor	0.307483503
Dgkz	0.405672947	Mpeg1	-1.186487631	Rasgef1b	-0.530414231
Vasn	0.700857625	Klhl21	0.440650802	Tsc22d1	-0.331298152
Tjp1	-0.584112501	Pced1b	0.590812518	Nr4a1	-0.778415193
Nbea	-1.023048595	Rps6ka6	-2.252884658	Sptbn2	1.480411661
Tespa1	0.78510466	Rnf125	-0.431684326	Cttn	-0.649413773
Gm32483	1.242803934	Arhgap29	-0.430066388	Gm39065	0.793715223
BC147527	0.729492999	Nbeal2	0.300763343	Zdhhc15	-0.544395021
Camk2a	0.498417015	Erbb3	0.788280037	Cdk1	-0.294000102
Msrb3	-0.718483492	H2-Ob	0.514109458	Podnl1	-0.668580818
Bsn	0.748488165	Gm4366	-0.552487883	Ddx60	0.454396827
Ccnb1	-0.468188648	Evc2	-1.034701606	Fam83h	1.541208171
Gm32920	7.358608879	Rps16-ps2	-0.448064875	Ubash3a	1.290509327
Oas1b	0.665543057	Lincred1	0.323391075	Golm2	-0.385247258
Gimap3	1.766602514	Bahcc1	0.364471073	Plxnd1	0.28102607
Rnf213	0.468688128	Kpna2	-0.440058926	Tmem33	-0.290729608
Gm1966	0.513638449	Ms4a6c	0.543460516	Tyrobp	0.650441243
Tifab	2.075308758	Reep3	-0.323804318	Ifi203-ps	0.442563663

Podxl	-0.462743507	Alcam	-0.758705575	Plekhg5	0.498197856
S100a11	-0.508665393	Gm31619	0.815379871	Spred3	0.372754234
Dnah8	1.109368495	Gm52296	2.369758639	Rai14	-0.343352803
Mmp14	-1.167134525	Tap1	0.276293707	Zfp825	-0.575118945
Dusp6	-1.098769615	H2-T23	0.343410215	Vill	0.409394258
Serpinf1	-1.416695354	2310015A10Rik	0.537632532	Tmem215	-1.131868172
Snhg20	0.876076804	LOC108167518	0.600691326	Gm39272	1.463569237
Ccl22	-1.619905164	BE692007	0.675647945	Gm40842	2.416003954
Serpinh1	-1.440467133	Dstn	-0.39711602	Rgs1	-0.507081626
Tnfaip8l2	0.792501677	Oasl2	0.416321878	Kdm4b	0.287395398
Gas2l3	-0.587130332	Adgra3	-0.354400511	Atf7	0.305572999
Stxbp6	-0.655477875	Tyk2	0.33519682	Dyrk1b	0.388202153
Trafd1	0.466993632	Gulp1	-1.221945484	F630028O10Rik	0.742923312
BC035044	1.201501447	Gm9385	-0.595424742	Cip2a	-0.319527329
Thy1	-0.754077202	Gm9794	-0.467653024	Sox12	0.335440598
Gm41559	0.844281146	Parp10	0.396600864	Hnf4a	1.118663072
Ifi213	1.688665718	A630001G21Rik	0.400322228	Rabac1	0.304727502
Tmem121	-1.33369115	Rasa4	0.517172575	Slc6a15	-0.70666487
Myh10	-0.495156995	Tmem150b	0.791929253	Gm40231	1.899916334
Pxdn	-2.750236224	Gm15651	1.365057374	Obsl1	-0.898529408
Mx1	0.840171778	Jag2	0.390223028	Depdc1a	-0.474230153
Slc17a8	-2.42092845	Prr12	0.343082714	Vopp1	-0.330596915
Helz2	0.412674701	Ddx3x	-0.314148151	Trpv2	0.338672293
Tlr7	1.129970731	Gm41553	1.310354516	Hook1	-0.277404776
Ccr7	-1.377229166	Yes1	-0.689077158	Zfp219	0.275127491
Stat2	0.499200276	Tceal8	-0.510693134	Kmt5c	0.268588665
Mdga1	0.501689641	Ypel3	0.411932931	Zbtb7b	0.431780869
Hexim2	0.794442346	Jakmip1	0.466690446	B3gnt5	-0.388407797
Rere	0.461768294	Stk17b	-0.369793556	Nfyb	-0.343835188
Ddx4	1.332374078	Smc2	-0.286053416	Prps1	-0.328472982
Il3ra	0.580475013	Flt3	0.31725716	Ccl5	0.654208953
Slc18a1	1.410152429	Hoxa3	0.586169106	Rab18	-0.276301643
Tcaf1	-1.140388478	Gm26679	2.761288395	Gm4258	0.52802863
Arhgap42	-1.262017539	Mis18bp1	-0.360761677	Samd11	1.927492643
Nusap1	-0.412256999	Cd96	-0.554886374	Naip3-ps1	2.027735742
Rasgrp4	0.76400886	Myo15b	0.731540014	Tpx2	-0.254426514
Gm41590	2.75189118	Maged1	-0.326536839	Xaf1	0.357966021
Fhl1	-1.308009278	Serpinb6b	-0.449061062	1600014C10Rik	0.312619394
Ramp1	0.473566741	Gm9522	3.550834145	Gm39273	0.398480025
Slc22a3	0.667458442	Bcas1	2.052147518	Themis2	0.654034134
Gm40309	1.06443555	Rpl38-ps2	-0.638295913	Tmem156	1.669882445

Evc	-1.407977195	Psma3	-0.326255661	Zfp36l2	-0.32995567
Ccr2	-1.856145204	Acvr1b	0.341299523	Myo1g	0.246591909
H2-Eb1	-2.09459308	Gigyf1	0.321139141	Dok3	0.691609436
Gm38485	1.563633353	Igh	0.679758738	Kbtbd2	-0.311241483
C130050O18 Rik	1.566665359	Zfp579	0.465499185	Syne2	0.274073437
Oas1g	0.703692211	Tmprss3	1.41618536	Ccnd1	-0.573317685
Fkbp9	-0.555372746	Hspa4l	-0.363324748	Ddx5	-0.229195177
Arhgap45	0.402241419	Kmt2a	0.248306605	Nsd1	0.264093718
Sdc1	0.774987969	Atp6ap2	-0.307141562	Sh3d19	0.5398978
Ms4a6b	0.655233033	Myo1f	0.330430663	Ifi44	0.412714888
Dhx58	0.439833162	Kif11	-0.299287973	Hmmr	-0.366257443
Itgb2	0.406427995	Adam15	0.347344432	Gm9243	0.946543213
Mpzl1	-0.48098308	Cacna2d4	1.129130462	Nlgn2	0.329540996
Gm16599	1.887995633	Timp3	-0.589405325	Pex3	-0.381774043
Slc44a1	-0.616205483	Gm19708	0.670079242	Neil1	0.534892966
Plch1	-1.689965188	Cd33	0.474640099	Cacnb3	-1.244575505
Gm51544	1.049982156	Zfp983	-0.503228039	B130055M24 Rik	0.427913694
Cd276	-0.627080306	Mfsd12	0.354309156	Tspan2	-0.357066523
Tap2	0.362022219	Mmp12	-1.935869612	Ddx3y	-0.280461709
Itga9	0.797564998	Dapk1	-0.427579949	Gm31657	1.525990565
Ccna2	-0.366934753	Arhgef1	0.309686881	Septin7	-0.24041884
Pld4	0.746195593	Shisa8	0.636137832	Tiparp	-0.428329649
Leng8	0.417816942	Crocc	0.420234239	Bub1	-0.300443862
Gm12828	1.901807044	Parp14	0.331106137	Ccng1	-0.397606419
Taok2	0.351569136	Gm38482	1.610403204	Zbp1	0.550112673
Dnajc6	-0.511222892	BC016579	2.138738242	H3f3a-ps2	-0.758398744
Gm29975	1.832205583	Prc1	-0.326641284	Zfp518b	-0.48007214
Gja1	-0.777357741	LOC108167553	0.651259383	Hs2st1	-0.271415136
Gm51671	1.995324865	Gm51554	2.317312346	Ufm1	-0.338028536
Tcf7	-0.927599511	Syne3	0.317908344	4930502C15 Rik	1.553162065
Hoxb9	-2.274780171	Bpnt2	-0.266931353	Gm41098	0.856953074
Mirt1	0.680455075	Pla2g4a	-0.353734454	Gldc	1.589345758
Pls1	-1.290499013	Hoxb8	-1.709004953	Pls3	-0.63517359
Gm46060	1.779814413	LOC115487747	1.132080445	Ecm1	0.814655278
Tmsb4x	-0.344651418	Fads6	0.781419764	Gm52629	0.938969216
C330026H20 Rik	1.345987106	H2-Aa	-1.522571605	Adgrl1	0.417885609
Gm46371	1.912120019	H2-K2	0.517636277	Macroh2a1	0.245981147
Tent5a	0.913020008	Gm51891	1.629667819	Ehbp1l1	0.284396467
Itgb7	0.616872684	Stat1	0.327746807	Akna	0.317996419
Gm51785	0.891070005	Zfand5	-0.358729013	Lrrc45	0.341099744
Cd24a	-0.39275163	Naa35	-0.394465718	Ptprf	-1.152595762

Hemgn	-0.424915215	Dek	-0.288938077	Fam193b	0.301587484
Gpr174	3.29126309	Cd48	0.332356479	Usp16	-0.338779315
Lrch2	-1.074809594	Gm32262	1.04608667	Ptpn2	-0.316432133
Tnf	-0.747388282	Gabbr1	0.378145086	Hsdl2	-0.359249391
Tax1bp1	-0.298197681	Net1	-0.387122013	Bcl2	-0.352591263
Spry2	-0.813820313	Nptn	-0.357069405	Top2a	-0.226691449
Tnfaip2	-0.499239017	Card9	1.051441199	Mpdz	-0.514566221
Gm13351	1.549581054	Gm43380	1.365858939	Emc2	-0.299668366
Tspoap1	1.08929645	Fn1	-0.98809892	Ccdc9	0.363568499
Bin1	0.493941943	Ptgs2	-1.425511156	Ppargc1b	0.463047702
Kcnd3	-1.240274765	Acvrl1	1.034408405	Gm38865	2.038063811
Gm31166	0.852715268	Ube2c	-0.331429486	Trim25	0.266299741
Igsf10	-1.396652989	Rps6ka3	-0.299730658	Scrib	0.318196723
Vma21	-0.422423375	Hes1	-1.735827433	Capn1	0.3259778
Zfp532	-0.723802487	Prdx6	-0.272019969	Stxbp4	0.520700461
Sdc3	0.685046561	Egr2	-3.378964414	Trim56	0.345925445
Mcf2	-0.999496095	H2-DMa	0.416060375	Gm50589	1.422340063
Nuf2	-0.420675473	Antkmt	0.406524069	Klrg2	1.707067921
Unc5a	0.843292688	Tmed5	-0.281252035	Emilin1	0.272408277
Bst2	0.425555644	Glipr1	-0.341994169	Skil	-0.632951144
Irf5	0.469817306	Txnl1	-0.267720419	Ttll11	1.929995498
Irf6	-0.862875859	Arhgef18	0.267190258	Slc24a3	0.84222958
Gm46213	1.517854986	Vmn2r84	1.558707559	Ptp4a1	-0.342023355
Arhgap9	0.437728735	Cnr2	0.699020968	Gcn1	0.28839074
Adar	0.334790108	Cxcr1	1.74702473	Aqp1	-0.853526516
Col11a2	0.676561715	Apol9b	1.1408978	Mboat7	0.294141987
Pck2	0.312735692	Klhl4	-0.753069595	Bmpr1a	-1.213057554
Nckap1	-0.645677547	Gm51710	2.299156364	Filip1l	-0.44223601
Gm51897	1.384435969	Ckap2	-0.368062096	Prr11	-0.33528724
Hs6st2	-1.450315703	Tbrg3	1.32190872	Rnf13	-0.253101242
Ifi208	0.951584319	Eloc	-0.347810272	Cep55	-0.354351952
Enpp4	-0.41999077	Itgb1	-0.254735504	Gdap10	0.583775331
Uaca	-0.857452073	Gm31253	0.880611264	Rras2	-0.427241862
Cpne8	-1.373242876	Abca4	-0.552925192	Iqsec2	0.411263518
Safb2	0.453085121	Arrb1	0.287243517	Hsh2d	0.433264981
Egfl7	0.435476861	Mapre1	-0.246796457	Gm12843	0.829641668
Dbf4	-0.38360263	Serpinb6a	-0.480737604	Clpx	-0.343185679
Gm52709	1.699129111	Actr3b	-0.695911729	Rps3a2	-0.666590714
Marcks	-0.613963393	Cuedc1	0.392891604	Adgrl2	-0.415559322
Znfx1	0.417455869	Mrvi1	1.188211913	Psma1	-0.272579606
Tmem123	-0.297531662	Gm32908	0.751097555	Camk1d	0.493386133
Stc2	0.740399576	Ssr3	-0.239442925	Fcgr2b	0.716669888
Chd3	0.321519521	Fam3c	-0.314694541	Gm32234	1.082202515
Srcap	0.300069142	Stk3	-0.440814109	Cyb561	-1.143961936

Mbd6	0.34199466	Pbx3	-0.620245251	Dennd2a	-0.843347151
Gm38708	0.747547175	Piezo1	0.30528435	Mcl1	-0.309600194
Slc16a12	0.842815695	Plscr2	-0.464732384	Cdc27	-0.243220306
Cmpk1	-0.317942857	Anln	-0.308595989	Suz12	-0.232619266
Slc35f2	-0.688338925	Tmem50b	-0.453546121	Pml	0.246791795
Padi4	0.341392964	Phf11d	0.835834287	Ppp1r12c	0.262197897
Gm12188	0.779042666	Uprt	-0.348961726	Csgalnact1	0.368987621
Muc13	-0.299009683	Ssb	-0.279379377	Mospd3	0.395205873
Dhx40	-0.644625115	Csrnp1	-0.498932113	Cbfa2t3	0.264482741
Pkn1	0.357624295	Dusp4	-0.670131184	Pnpla8	-0.296884997
Cep250	0.375101696	Chil5	0.883648211	Nap1l1	-0.223042204
Arhgap5	-0.502491375	Gm3534	-5.697647739	Igtp	0.322567159
Arap1	0.285144121	Kcnab2	0.264491294	Insyn2b	1.488734029

Appendix XV: Significant (padj < 0.05) differentially expressed genes from Runx2-flox pHSC RNA-seq, Runx2-het vs Runx2-wt. n = 3, sorted by padj small to large, top to bottom of each column. See Chapter 2.8.2 for data analysis pipeline.

gene	log2FC	gene	log2FC	gene	log2FC
Commd10	0.932062	Ltbp3	0.293592	Hoxb5os	0.600642
Dok3	0.976799	Smim24	0.507007	Hscb	0.434717
Apoe	0.679245	Kif5b	-0.26083	Akirin1	-0.26507
Runx2	-0.51484	Fignl1	-0.37379	Mcm3	-0.23484
Ifi27	0.613973	Plekhg5	0.538963	Ccnd1	-0.53577
H2-Ob	0.493324	Hira	-0.33521	Ergic3	0.264805
2410006H16Rik	0.599339	Trafd1	0.26587	Thada	-0.30515
Gfi1	0.543516	Ncapg2	-0.31943	Son	-0.25919
H2-T23	0.420885	Pno1	-0.48562	Rnasel	0.249856
Ypel3	0.578456	Nlgn2	0.269604	Cdca7	-0.24581
Pink1	0.464891	Tns1	0.321856	Elovl6	-0.23196
Septin11	-0.42219	Eif5	-0.24978	Fut7	0.292316
Dusp6	-0.97661	Psrc1	0.359685	Cops9	0.493639
Skil	-0.77154	Rpl36a	0.354068	N4bp2l2	-0.23518
Hells	-0.54031	Nr4a1	-0.80692	H2-D1	0.205793
Mirt1	0.589475	Vsig10	0.480398	Slfn3	-0.51078
Dnajc6	-0.71442	Ssb	-0.25649	Hnrnpu	-0.19905
Mcm4	-0.38646	Chsy1	-0.32611	Cables1	0.313161
Atp13a3	-0.38952	Mis18bp1	-0.36308	Lcp1	-0.18287
Kpna2	-0.44652	Nolc1	-0.27964	Hsh2d	0.375074
Ptprz1	-1.39512	Hdac11	0.613314	Tfdp1	-0.22111
Dhx9	-0.37202	Set	-0.24595	Lmntd2	0.7002
Tjp1	-0.39569	LOC102634078	0.578695	Myl10	0.422232

Notch3	0.513382	Ipo7	-0.25928	Ppp1r15b	-0.25707
Pik3ip1	0.43035	Clnk	-0.33069	Csf2rb	0.218063
Ifi27l2a	0.738174	Uhrf1	-0.27676	Skp2	-0.3266
Rpl36	0.456801	Hdac7	0.268191	Mmgt1	-0.31667
Hdgfl3	-0.40439	Ralb	0.400391	Foxn2	-0.31197
Irf7	0.524992	Naprt	0.514636	Dkc1	-0.23417
BC147527	0.645873	Haao	0.428306	Commd7	0.279878
Gm36809	0.735465	Bzw1	-0.25355	Cct8	-0.2141
Ankrd37	0.64675	Bbc3	0.446547	Gaa	0.220993
Ak1	0.644446	Tiparp	-0.44991	Rpl39	0.280078
Arhgap45	0.317539	Knl1	-0.34967	Arhgap5	-0.36904
Eif4a1	-0.30808	Rif1	-0.32347	Adpgk	-0.36499
Psmd1	-0.3376	Atad2	-0.28426	Flot1	0.291391
Neat1	0.536956	Rgs11	0.455895	Ulk1	0.243158
Smc2	-0.32789	Nup155	-0.30359	Mrps2	-0.29405
Il18r1	-0.95229	Mboat1	-0.52256	Rps12-ps3	-0.88539
Nop58	-0.31518	Bsn	0.486524	Plin3	0.317249
Syncrip	-0.29014	Col4a2	0.22456	Dgka	0.337003
Fam111a	-0.33926	Tcrb	-0.93237	Rpl32	0.272502
Nup93	-0.41107	Nup205	-0.27067	Actr3	-0.20036
Smarca5	-0.32459	Tfrc	-0.3486	Serpina3f	-0.26201
Gspt1	-0.29288	Slc25a28	0.347571	Tomm70a	-0.23847
Ndc1	-0.42309	Cdc27	-0.26644	Ppp1cb	-0.2085
Usp1	-0.33191	Casp8ap2	-0.33987	Scd1	-0.23052
Hspd1	-0.30108	Pdk2	0.457064	Prkdc	-0.30872
Pck2	0.311647	Tmpo	-0.2263	Eif3a	-0.2046
Snhg20	0.736848	Mir17hg	-0.47821	Gab1	0.355495
Pdzk1ip1	0.496851	Rpl13	0.296136	Rtkn	0.355397
Pola1	-0.3334	Gm46183	1.021169	Pald1	-0.731
Mpeg1	-1.2263	Caprin1	-0.20835	Dcaf13	-0.30073
S1pr3	-0.68026	Abhd8	0.330011	Brca1	-0.31219
Idh3a	-0.3567	Fus	-0.23659	Psip1	-0.23391
Gem	-1.03461	Mill2	0.515879	Smc6	-0.23372
Hs6st2	-1.15634	Rcn3	0.299233	Gmfg	0.241052
Rabac1	0.430898	Ccr7	-0.96894	Sla	0.263098
Ramp1	0.43784	Kntc1	-0.29176	Matk	0.346097
Il15	0.476364	Irf5	0.355601	Rplp1	0.251889
H2-K2	0.547313	Ndufaf4	-0.37412	Rplp2	0.290874
Prps1l3	-0.37277	Amd1	-0.28823	Usp15	-0.24808
Brip1	-0.4363	Col11a2	0.507724	Pcm1	-0.26789
Rasa4	0.41432	Topbp1	-0.24481	Itgb2	0.21732
Psmb9	0.358808	Rps15	0.270167	Wdr77	-0.26632

H2-DMa	0.415518	Gm2a	0.274508	Tmem223	0.393687
Etf1	-0.32198	Kdr	-0.75779	Plppr3	0.285972
Cse1l	-0.32868	Gadd45g	1.086734	Clspn	-0.32487
Utp20	-0.49624	Fn3k	0.732605	Eif3j1	-0.29234
Tecpr1	0.437471	Ppa1	-0.28482	Smpdl3a	0.306167
Pdp1	-0.64591	Zfp467	0.307397	Ncapg	-0.26692
Coro2a	-0.28819	Myc	-0.34888	Prpf40a	-0.19617
Akap8l	0.378541	Zbtb41	-0.33558	Calcoco1	0.288368
Hsp90aa1	-0.29206	Suz12	-0.2624	Jup	0.475058
Nasp	-0.35599	Adamtsl5	0.849975	Galnt3	-0.81522
Fau	0.395876	Eif4g2	-0.21229	Ninj1	0.272571
Idi1	-0.3606	Nucks1	-0.23612	Cybc1	0.247509
Odc1	-0.33568	Tpp2	-0.25048	Pex6	0.28419
Nop53	0.352235	Podxl	-0.26655	Eya1	0.315233
Thap3	0.590588	Xpo1	-0.2588	Tbc1d9b	0.19462
Rbm12	-0.50066	Pcp4l1	0.537865	Als2cl	0.397911
Pla2g4a	-0.33625	Mthfd1	-0.32713	Itgb7	0.396648
Ddx3x	-0.31446	Ezr	-0.29921	Mpl	0.185265
Lat2	0.515181	Pitrm1	-0.25979	Mapk1ip1	0.332688
Dhfr	-0.44955	Gramd1b	0.366129	Ppip5k2	-0.24382
Ncbp1	-0.3804	Aldoc	0.24821	Rps27	0.307963
Procr	0.459873	Lemd2	0.3316	Gng11	0.468593
H2-T22	0.31835	Stxbp4	0.368939	Srsf6	-0.25252
Prps1	-0.36035	Neu1	0.388651	Antkmt	0.317176
Ipo11	-0.41827	Papola	-0.2167	Gpr84	-0.95297
Rrm1	-0.31819	Serpina3i	-1.36404	Eif2b3	-0.48536
Mamdc2	0.595634	Srsf10	-0.24935	Snx20	0.385045
Def8	0.323246	Zwint	-0.25542	Sdad1	-0.24547
Hspa4	-0.28814	Nupl1	-0.27964	Mad2l1	-0.28047
Naa50	-0.28601	Kif20b	-0.27869	Atxn7l1	0.235879
Gm42226	-0.31695	Iqsec2	0.372163	Tipin	-0.25205
Camk2a	0.333366	Eva1b	0.459393	Tbc1d17	0.296706
Gm35189	0.819057	Msrb3	-0.32887	Tnfrsf14	0.246501
Lamb2	0.521419	Ufm1	-0.31896	Rad23b	-0.18515
Top2a	-0.27096	Cad	-0.27557	Acap1	0.23814
Gemin4	-0.45602	Abcf2	-0.32762	Phf1	0.409237
Hat1	-0.34684	Ccna2	-0.23764	Pa2g4	-0.23125
Sdc1	0.61579	Abce1	-0.22722	Baz1a	-0.28799
Plk4	-0.37459	Ccdc86	-0.42979	D2hgdh	0.26254
Dek	-0.27331	Ccne2	-0.55274	2900052L18Rik	0.417229
Il12rb1	0.368357	CYTB	-0.34063	Treml2	0.204414
Oas2	0.379942	Actb	-0.26246	Cox8a	0.327311

H2-T24	0.501049	Mbnl3	-0.30807	Nup107	-0.27765
Hlf	0.394176	Cox14	0.390994	Prtn3	0.342996
Ipo5	-0.26544	Eif2s1	-0.24635	Naa25	-0.23821
Ddx21	-0.30797	Blm	-0.31365	Ubc	0.420886
Tyms	-0.41835	Gm38850	1.134299	Hmgn5	-0.30023
Smc4	-0.25759	Rin3	0.234569	Fen1	-0.30852
Nectin4	0.679562	Tspan7	0.528856	Lmnb1	-0.22352
Pcna	-0.3086	Sf3b3	-0.22264	Rbbp8	-0.274
Ercc6l	-0.43195	Cd37	0.286115	Fos	0.81122
Unc5a	0.755385	Rps21	0.342854	Apba3	0.309201
Zfr2	0.619606	Me2	-0.2905	Fbxl12	0.456441
Ccl22	-1.19601	Rps9	0.280667	Ugcg	-0.32185
Fgf11	0.426932	Tmem167	-0.2536	Zfp971	-0.42466
Cip2a	-0.36067	Pphln1	-0.26756	Fkbp5	-0.28535
Lgals1	0.366221	Trpv2	0.324293	Celf5	0.724975
Fcgrt	0.377755	Glul	0.291676	Odf3b	0.435909
Slf1	-0.44	Ring1	0.436831	Eng	0.189728
Arnt2	-1.30044	Cebpz	-0.27799	Hint3	0.408101
Orc2	-0.38457	Cul9	0.290733	Ncf1	-0.25773
Kpna3	-0.29626	Esco2	-0.39713	Trip13	-0.36279
Vma21	-0.35055	Phf11d	0.595694	Abcb7	-0.24905
Smarcc1	-0.25518	Xpo4	-0.29749	Senp5	-0.27066
Il1r1	-0.28601	Rps23	0.325681	Esam	0.31493
0610010F05Rik	-0.36624	Hdac5	0.278656	Ezh2	-0.20587
Plac8	0.43618	Dusp4	-0.48207	Eml2	0.264102
Ppat	-0.30041	Ptcd3	-0.31719	Hnrnpf	-0.18832
Tap1	0.239199	Pds5a	-0.24551	Ypel4	0.614638
Spire1	-0.47589	Ptpn3	-0.42768	Aldoa	0.201656
Prkar2a	-0.3571	Depdc1a	-0.3866	Pole	-0.2574
Brca2	-0.43066	Trim46	0.466197	Chml	-0.39544
Tbl3	-0.39227	Rpl37a	0.334908	Ift57	-0.26617
Aebp1	-0.99999	Chek1	-0.40361	Syngr1	0.467205
Pde2a	0.613369	Mpst	0.345432	Rpa1	-0.22354
H2-K1	0.218343	Kcnd1	0.707598	Slc50a1	0.277442
Dpm3	0.600805	Gnl3	-0.29308	H2-Ke6	0.295262
Lbp	0.3526	Ints2	-0.32379	Rbm27	-0.2797
Uba52	0.333316	Naa80	0.434183	Naip5	0.359191
Rps19	0.395755	Grik5	0.281312	Tst	0.432007
Dnaja1	-0.27574	Tomm7	0.439666	Atg16l2	0.35284
Syngap1	0.316972	Bpnt2	-0.25396	Arrdc1	0.299332
Ptpn18	0.376367	Rp9	0.280451	Cuedc1	0.317654
Slc7a1	-0.2964	P3h3	0.288601	Ccl4	0.571765
Tox	-0.60693	Hsph1	-0.28754	Nfic	0.232799

Heatr1	-0.37758	Hif1a	-0.28245	Gm36266	0.628353
Man2b2	0.314426	Dhx15	-0.23221	Myo1f	0.249285
Wdr43	-0.30545	Gm8203	-0.78691	Slc22a17	0.410581
Adrb2	0.767207	Por	0.22035	Gpr162	0.448034
Ddit4	0.560957	Lincred1	0.298291	Ywhab	-0.19619
Wdr36	-0.30621	Shcbp1	-0.38983	Ube2n	-0.24371
Nrgn	0.452977	Zscan2	0.454328	Cul4b	-0.2405
Arpp19	-0.30709	Fam110b	0.638958	Cct6a	-0.21842
Mdga1	0.31524	Gabpa	-0.24887	4930579G24 Rik	-0.39694
Azin1	-0.30231	Hspa8	-0.20087	Mrpl54	0.39565
Hmgcs1	-0.2889	Tmem33	-0.26835	Gsr	-0.26191
Sparc	0.562161	Exo1	-0.39014	H2-DMb1	0.422966
Fbxw4	0.519978	Capn5	0.283777	Hus1	-0.30257
Sgsm1	0.440153	Ccl3	0.617443	Ptbp3	-0.20777
Cyp51	-0.2713	Hid1	0.340903	Galnt7	-0.29975
Xpo5	-0.28653	Mib2	0.300804	Zfp638	-0.26182
Pear1	0.29024	Usp31	-0.35963	Gpd2	-0.23951
Nsun2	-0.25344	Ganc	0.348754	Rps16	0.245192
Pbx4	0.567383	Mpdz	-0.44202	Dgkz	0.214103
Coro7	0.236191	Rere	0.262618	Ube2d3	-0.18718
Atp13a2	0.262952	Nop2	-0.2882	G430095P16 Rik	0.761393
Gm41559	0.577511	Nup153	-0.25328	Tmem40	0.265679
Gsdmd	0.285605	Slco3a1	-0.29596	Dnajc2	-0.22759
Mettl7a1	0.414373	Dut	-0.28198	Manea	-0.27714
Slc44a1	-0.46579	Plcb2	0.250755	Zdhhc15	-0.34059
Tnfaip8l2	0.536015	Unc13d	0.234661	Fyco1	0.323806
Ncl	-0.23689	Nol11	-0.30458	Nkapd1	-0.30014
Scd2	-0.23904	Uba7	0.210354	Dtl	-0.23425
Rai14	-0.37794	Mettl27	0.285626	Cyb5b	-0.20941
Rap2c	-0.29059	Csgalnact1	0.332316	Rps18	0.271136
Dis3	-0.34381	Rps10	0.249903	Rpl35a	0.29216
Hexim2	0.527549	Safb2	0.306855	Mcm10	-0.30699
Gas2l3	-0.3587	Nfyb	-0.32322	Narf	0.218778
Mcm6	-0.26262	Pdzd8	-0.26769	Xrcc5	-0.27748
Ddx4	0.902473	Srsf1	-0.21174	Rab6b	0.462389
Gpr25	-1.02576	Tsc22d3	0.35509	Ccdc88b	0.279599
Vill	0.387071	Lig1	-0.26791	Cryzl2	0.398634
Grina	0.354937	Sytl1	0.348109	Hspa9	-0.17462
Ctps	-0.3639	Rufy4	0.61679	Letm2	0.492015
Myof	0.450071	Zdhhc2	-0.44741	Napsa	0.205818
Rpl11	0.316598	Kcnh2	0.515658	Kctd12	-0.21961
Acaca	-0.33216	Larp4	-0.24879	Naa35	-0.25837
Tap2	0.276614	Fam193b	0.348587	Topors	-0.26286

Calm1	-0.26213	Cdk18	0.296842	Naa15	-0.2115
Rpl41	0.365611	Pafah2	0.338691	Bub1	-0.24682
Supt16	-0.29217	Rxrb	0.283617	Dock5	-0.27265
Bend3	-0.44227	Pbrm1	-0.23612	Gabre	0.637483
Lpl	-0.86187	Clcc1	-0.28276	Pprc1	-0.26802
Cybb	-0.88997	Kif11	-0.21703	Sgo1	-0.30674
Slc16a1	-0.32705	Noc3l	-0.33816	P3h4	0.552973
Mat2a	-0.36301	Themis2	0.527292	Igsf10	-0.74712
Npc1	0.304301	Arap1	0.201425	Oas1b	0.327241
Ip6k1	0.268862	Gmps	-0.23604		
Srsf3	-0.29195	Itsn1	-0.22874		

Appendix XVI: Significant (padj < 0.05) differentially expressed genes from Runx2-flox pHPC RNA-seq, Runx2-hom vs Runx2-wt. n = 3, sorted by padj small to large, top to bottom of each column. See Chapter 2.8.2 for data analysis pipeline.

gene	log2FC	gene	log2FC	gene	log2FC
Runx2	-2.42213	Prkch	-0.32587	Ahdc1	-0.32463
F13a1	1.662062	Rab38	-0.32249	Gapt	0.695653
Gda	1.525643	Gypa	1.213001	Snap47	-0.38946
Ly6c2	3.219646	Svil	-0.29165	Sp4	0.324957
C3	1.070515	Nlrp1b	1.316513	Spns3	-0.29534
Igsf6	1.393968	Nebl	0.773182	Dab2	0.89921
Elane	1.573923	Lck	-0.76642	Asah1	0.207334
Gzmb	-1.17178	Pard3b	-0.72707	Naca	0.191194
Sell	1.090943	Ccl3	0.551847	Sytl5	-1.89039
Stom	1.044593	Carns1	-0.61018	Gstt1	-0.75201
Myh10	-1.25669	Rbpms2	-0.54175	Gm48893	1.580332
Ifi209	1.521276	Macroh2a1	0.295619	Arl8b	0.214257
Abcd2	1.539083	Nrgn	-0.55334	Itgb5	0.357311
Lyz2	0.977267	Ubash3a	0.471608	Selenop	0.235222
Hdgfl3	-1.21159	Runx1	0.286547	Thsd1	-0.31177
Commd10	1.269449	Mthfd2	-0.42567	2410002F23Rik	-0.32646
Trappc9	-0.94606	Myo1e	-0.79658	Gm51554	2.02574
Adgrl4	0.905647	Xbp1	-0.26083	Tnks1bp1	-0.44143
Ctsg	0.762851	Ifi211	1.078297	Pfkl	-0.24176
Mycn	-0.77787	Ephb2	0.823346	Carmil2	-0.32477
Mpo	0.641842	Chac1	-0.65027	Ripk1	0.224763
Hmga2	1.015771	Ly86	0.820446	Wnt10b	-0.84471
Abca4	-1.71595	Cavin1	-0.40814	Cd69	-0.24285
Cd33	1.05907	Lama5	-0.42297	Arhgap42	-1.21269
Gas7	1.107469	Acer3	0.423503	Mppe1	0.449374
S100a9	2.266524	Mtus1	0.620577	Tjp2	-0.31149
Emb	0.812729	Mxd1	0.423916	Psd	-0.70723
Thy1	-1.80223	Pla2g4a	-0.30109	F730016J06Rik	2.406062

Il18r1	-2.3848	Pvr	0.530551	Abca1	0.437485
Mgam	2.289369	Gm7694	-0.46408	Zdhhc20	0.239231
Cp	0.951731	LOC115490344	-6.27503	Stard8	0.402242
Tgm2	-1.14139	Gimap1	-0.36642	Pxdn	-3.24633
Atp1a3	1.108795	Il11ra1	-0.55762	Cercam	-0.31843
Adgre1	1.330251	Iars	-0.32186	Arhgef3	0.23944
Prg2	1.392223	Icos	1.136645	D630039A03Rik	-0.45335
Hdc	1.217844	Rbm47	0.958503	Ptk7	-0.35143
Fcgr2b	0.752683	Dram1	0.941506	Srgn	0.193928
Csf1r	0.89798	Rxra	0.873452	Tln1	-0.19025
Gm3534	5.407491	Cebpa	0.31769	Mmp14	-1.47003
Gm42048	-0.88057	Xrcc5	-0.51423	Nrg2	1.177635
Zeb2	0.621179	Cep85l	0.390906	Scube3	-0.82375
Itgam	0.746792	Gla	0.518047	Tpst1	0.457698
Cybb	0.76494	Idh1	0.33822	Morc4	-0.69077
Arx	-2.15729	Zfp36	0.604159	Syde1	-1.6767
P2rx7	1.311133	Lag3	-0.75788	Snx29	0.308398
Dio2	1.39011	Ankrd44	0.307809	F11r	-0.34166
Fgl2	0.795708	Car2	-0.26666	Mfsd14b	0.21531
Sdc2	-1.73299	Ticam2	0.389025	Ptpro	0.742344
Ap3s1	0.772075	Tnfrsf9	-1.36525	Akt2	-0.25889
Tox	-1.53462	Ass1	0.351564	Jund	-0.36915
Tlr7	1.066668	Zfp385a	-0.44172	Ap1s2	0.494837
H2-Aa	-2.6793	P2ry2	0.530755	Pttg1ip	-0.24585
Podxl	-0.9521	Ptbp3	0.245873	Drc7	0.457666
Mpeg1	0.851872	Gpr160	0.633496	Ugp2	0.259413
Rcn3	-0.74778	Laptm4b	-0.52835	Myof	0.565255
Tifab	1.445654	Mgst2	0.897481	Nr3c1	0.226667
Cpa3	0.839707	Nlrp1a	0.624047	Relt	-0.29724
Anxa3	0.849037	Ccr7	-0.88217	Traf2	-0.28223
Pde2a	1.256956	Prkag2	-0.3641	Camk2d	0.346439
Dntt	1.473913	Apaf1	0.280601	Nrg4	0.916726
Mgst1	1.104684	Gm24339	3.616821	Htr7	-3.65351
Stox2	-1.43814	Cd48	0.362807	Ehbp1	-0.54144
Hp	1.227433	Adora2a	-0.59359	App	0.292053
Ccr2	0.776683	Ifi203-ps	0.553318	Btla	1.232377
Syne1	0.686297	Gars	-0.25104	Slamf1	-0.68359
Tie1	-0.64084	Shank3	-0.51107	Def6	-0.2759
Col16a1	-1.1844	Csf2rb2	0.319353	Tpm1	-0.224
H2-Eb1	-2.68416	Thbs1	0.576363	Nadk	0.264846
Ugcg	0.487005	Ppp1r9a	-0.46023	Trp53i11	-0.34551
Zfp532	-3.14514	Samd12	-0.57117	Panx1	-0.30294
Gm32554	2.848474	Gfi1b	-0.42389	Nxpe1-ps	0.775338

Tmem156	0.953394	Myo1f	0.332013	Vamp8	-0.33125
Man1a	0.507056	Sesn1	0.318262	Prnp	-0.50226
Prtn3	0.776737	Hsdl2	0.400134	5930403L14Rik	-1.59175
Hemgn	-0.67314	Inf2	-0.31155	Ifitm7	1.862396
Papss2	0.902293	Slc18a1	1.840846	Camsap2	0.5593
Cxcr2	0.859113	Gnptab	0.296202	Naip6	0.353772
Gm3360	2.217313	Ms4a4c	0.509079	Tmem71	0.271086
Sema7a	-1.03358	Car13	-0.44782	F2rl3	-0.37664
Plac8	0.69485	Bhlhe40	-0.3903	Fads2	-0.25308
Ltb	-0.73875	Tnfrsf14	0.412074	Supt3	0.33574
Alas1	0.788892	Mpped2	-1.00536	Eaf1	0.237834
Slc15a2	1.225704	Fscn1	-1.39871	Klrd1	-0.65003
Stxbp6	-0.69235	Rnf122	-0.68727	Nabp2	-0.32811
Cttn	-0.93915	Abca2	-0.27282	Tedc1	-0.36482
Gm2a	0.55677	Pik3cd	-0.26478	Flna	-0.18565
Ptprz1	-3.75943	Kif21a	-1.55733	Ccdc102a	-0.57817
Akr1c12	-0.64553	Arid3a	0.378083	Eps8l1	0.442771
Mgat5	0.495333	Diaph1	-0.22551	Ptp4a3	-0.2489
Pim2	-0.73522	Vasp	-0.27204	Cep164	0.346451
Clec2i	1.093889	Vps13c	0.2939	Pacs2	-0.2938
Lpl	1.504745	Sgpl1	0.373301	Susd2	-1.06837
Yes1	-2.22489	Serinc3	0.213891	Clec11a	-0.9457
Dscam	-2.17668	Trim5	0.459772	3300002I08Rik	0.357335
Irf8	0.712144	Sdsl	-0.70436	Zfp935	0.349331
Ms4a2	0.801174	Tlr2	0.542116	Nuak2	0.391925
S100a8	1.905182	Camk2a	0.361295	Cdkn1c	-0.70541
Hgf	0.75424	Clec12a	0.387092	Selenot	0.18559
Ccnd1	-1.10046	Ms4a3	0.495892	Pkia	-1.35167
Ifi204	0.801127	Cd44	0.240836	Lrfn4	-0.61774
Mpp1	0.594479	Asns	-0.43003	Cep350	0.19743
Atp13a3	0.449392	Soat1	0.318237	B4galt1	0.198413
Fndc3b	0.639827	Gng12	0.261684	Edem1	0.219523
Arhgef40	-0.88798	Ly9	0.492512	Lamp1	0.240144
Ifi213	0.756341	Bin2	-0.29219	Cd52	0.302838
Akr1c13	-0.55185	P3h3	-0.5076	Stk26	0.202966
Pgr	-1.39253	Ermp1	0.307994	Ephb4	-1.36186
Rgs8	1.808907	Nfatc2	-0.47085	Dctd	-0.25964
Lhcgr	-2.23217	Trpc6	-1.05948	Emilin2	-0.24016
Gpc3	1.0992	Fam107b	0.25145	Adgb	1.940684
Ifngr1	0.478055	Sars	-0.32453	0610010K14Rik	-0.39951
Fkbp9	-0.86379	Samsn1	0.254361	4931406C07Rik	0.254686
Lbp	0.670127	Wars	-0.31443	Celsr1	-0.34853

Tcn2	0.641473	Mogat2	2.061796	Entpd5	-0.23958
Wfdc17	0.840304	Esam	-1.05242	Cep170b	-0.39379
Clec4d	0.655625	Megf8	-0.37469	Phlda2	-1.54739
Cd200r4	0.86625	Vill	0.389987	Cdk19	0.23756
Dock1	-0.74915	Cnn3	0.347472	Cavin3	-0.79981
Cd93	0.510739	Ccl6	0.850981	Strip2	-1.84652
Dnajc6	-0.61359	Slc3a2	-0.37434	Marveld1	-0.29874
Slc17a8	-3.17731	Gyg	0.291895	Ccdc92	-0.97116
Cadm3	-1.33505	Kctd12b	0.744706	Ccdc112	-0.42941
Podnl1	-1.14626	Lad1	-2.01696	Cd2ap	0.251237
Arid5b	0.683794	Gab1	0.484072	Pcmtd2	0.237627
Sema3d	2.617111	Bmx	1.159756	Micu1	0.299594
1810073O08 Rik	1.089096	Crebrf	0.378112	Med25	-0.30854
Nbea	-1.59425	Ctnnal1	-0.62096	Ank	0.247613
Tent5a	0.658431	Scarna9	3.178767	L3mbtl3	0.263473
Mcf2	-1.49781	Ctse	0.429781	Hormad2	-1.94069
Mpl	-0.44637	Plxnb2	-0.33023	Peli2	0.334846
Pld4	0.726688	Med12l	-0.38728	Tlr13	1.066066
Itsn1	-0.61883	Arhgap29	-0.50621	Olfm1	0.888062
Scin	0.409281	Sorbs3	-0.46208	Zfp386	0.274274
Lypd6b	-0.79808	Ifi27l2a	0.476293	Nfe2l1	-0.31709
Cdcp1	-2.55911	Clic4	-0.2756	Gm32908	0.581743
Itih5	-0.47847	Camk1d	0.479791	Armcx2	-0.2879
Slpi	0.962463	Rnase4	2.083474	Sh3bgrl	0.209279
Fads1	-0.47555	Col4a1	-0.27866	Stx3	0.44099
Acot1	1.489342	Prg3	1.588514	Zfp598	-0.25952
Sowahc	2.234559	Nedd4	-0.19911	Osbpl1a	-0.26214
BC035044	0.512658	Aoah	0.432607	Nos1ap	-0.46794
Gimap4	0.74361	Galnt6	-0.29529	Gatad1	-0.21434
Arhgef12	-1.34593	Nupr1	-0.8553	Sele	1.814632
Slc22a4	1.487336	C130050O18 Rik	0.905634	Cebpd	0.524572
Gfi1	0.723846	Coro2a	-0.25562	Tent5c	0.663117
Ngp	1.630215	Slc8b1	0.514538	Trim58	-0.50503
Rab7b	1.126693	Cyria	0.435443	Atp5mpl	0.345238
Cracd	-0.68454	Gm17745	0.604521	Creb5	-0.65657
Irf6	-1.50986	Dok3	0.473255	Slc16a9	0.760755
Sgms2	1.714556	Hk3	0.316152	Gata3	-0.5802
Slc35f2	-0.84316	Amd1	0.318065	Gm52043	1.223266
Itga9	1.140145	Slc4a7	0.286229	Acvrl1	1.056748
AB124611	1.120805	Ccl22	-0.8539	Cmah	0.566241
Gsr	0.459334	Rps27	0.296903	Hnmt	-0.6009
Gpt2	-0.66607	Chst15	0.410845	Cyb5r1	-0.36942
Cd84	0.43823	Srpk1	-0.29887	Fhl1	-1.0104

Egfl7	0.507945	Pik3ap1	0.347426	Klhl24	0.235928
B3gnt5	-0.43807	Slc40a1	0.986497	Map4k5	0.30455
Il1rl1	0.63086	Arhgap18	0.243491	Slc9a3r2	-0.67501
Hs6st2	-1.61319	Arl11	0.387442	Rasgef1b	-0.54079
Ms4a6c	0.54111	Cyth1	0.348526	Plp2	-0.22729
Mx2	0.618655	Tnk2	-0.37775	Gtf2e2	0.258266
Hlf	0.481905	Cx3cr1	0.52019	Snx2	0.228226
Hid1	-1.07263	Fcer1a	-0.77013	Pitpnm1	-0.26092
Lincred1	0.608098	Abcc1	-0.24198	Ptafr	0.347676
Msrb1	0.605411	Dmkn	1.565489	Cd38	1.096943
Spns2	-0.40224	Tars	-0.28431	Nsmf	-0.51609
Rassf4	0.440586	Vash1	-0.36249	Gnb4	0.294746
Tcf7	-1.41633	Atp1b1	-1.36478	Ttc39b	-0.40829
Cebpe	1.240754	Afap1	-2.27429	Gata2	-0.23973
Actn1	-0.57815	Cst7	0.361744	Siglecg	0.806068
Tjp1	-0.42978	Sdc1	0.512904	Acss1	0.440155
Gm31657	0.983493	Pirb	0.710184	Slfn10-ps	0.356687
Nin	0.391581	Ifi206	0.401852	LOC115488500	1.48511
Cdk5rap1	0.896981	Fgd5	-0.8331	Abhd14b	0.474631
Aqp1	0.771232	Mob3a	-0.2795	Arntl	0.428898
Arhgap15	0.413884	Mindy2	0.27897	Ssr2	-0.22309
Cd53	0.453961	Add2	1.165576	Cat	0.197339
Tuba8	-0.59455	9030619P08Rik	-0.65746	Gbx2	-0.62589
Zdhhc15	-0.66986	Nr4a3	-1.30467	Dst	-0.26351
Adamtsl4	1.85507	Mmp19	0.61852	Plekhf2	0.236088
Eda2r	-1.52588	Padi2	0.335498	Fn1	-1.15709
Slc16a12	1.387762	Ctsb	0.264942	Socs2	-0.24319
Havcr2	-0.79636	F10	0.903229	Tspan9	-0.3889
Ctss	0.682816	Pdcd4	0.276574	Herpud1	-0.23983
Mpzl1	-0.82057	Ppm1k	0.470293	Gm51746	2.079425
Cd300lb	0.667329	Slc7a3	-0.94058	Hdac9	-0.34091
Casp12	-0.59162	B4galt6	0.414039	Ephb6	-0.49056
Prkcb	0.716762	Mdfi	-0.41253	Trabd	-0.2696
Itga2b	-0.55779	Pram1	1.465235	Sdr39u1	-0.44275
Vav3	0.472162	Evc2	-1.69704	Scn3a	-2.13896
Olr1	1.964478	BE692007	0.690981	Cdc42bpa	-0.30783
Dpp4	0.597298	Asph	0.328342	Gm52877	0.394657
Tyrobp	0.512875	Ampd2	-0.26505	Heca	0.259979
Fcnb	1.732478	Gimap5	-0.44015	Trp53cor1	-0.4461
Tspoap1	0.919168	Eya2	-0.45695	Cd180	0.252047
Rcor2	-0.70716	Apobr	-0.31127	Dnaaf3	-0.61746
Ralb	0.465029	Cd7	-1.82067	Trmt2a	-0.23454
Kcnd3	-2.56668	Cpt1a	0.24617	E2f7	-0.36485

Kcnk5	-0.44449	Bcat1	-0.44576	Tnpo1	0.167868
Klrb1f	0.724076	Mboat2	-0.34627	Runx3	-0.26398
Klhl4	-1.94056	Gm39896	1.679446	Clic5	0.524536
Lonrf3	0.701698	Nmnat2	0.960118	Cnr2	0.409888
Cpq	0.602048	Fam234a	0.491509	Mier3	0.231593
Sva	7.350128	Scamp1	0.261771	Lipa	0.238839
Dmwd	-0.65112	Spib	-1.17287	Mndal	0.187805
Plekha5	-0.50496	Csgalnact1	0.553746	Ptprm	4.018296
Tbc1d2b	0.40816	Shmt2	-0.25588	Eif6	-0.23002
Serpinh1	-3.04564	Gpr65	0.382797	Cfap74	-1.45514
Dkkl1	-0.89	Gulp1	-0.97812	Cd24a	-0.22181
Fgf3	-0.89299	Ptgr1	0.562071	Apol10b	-3.5692
Lpcat2	0.531719	Wdr26	0.23191	Rab9	0.259785
Wdhd1	-0.41054	H2-T24	0.277535	D430019H16 Rik	-3.13238
Svip	0.543202	Bhlha15	-0.67086	Siah2	-0.37193
Ccl9	0.440703	Ier5	-0.37359	Gm52945	0.535856
Cd72	-0.67444	Plin2	0.331174	Washc4	0.250176
Gm1966	0.349021	Gpr18	1.022228	Fam234b	0.346513
Mecom	-0.51769	Fam110b	-0.96485	Il12a	0.335878
Lrch2	-1.98213	Zmiz2	-0.30634	Eprs	-0.21716
Slc6a15	-0.87128	Nlrc4	0.909999	Ap2m1	-0.19297
Ston2	0.65134	Sbf2	0.650355	Zfp874a	0.322214
Pde4b	0.37113	Ly6i	4.699227	H2-Eb2	-2.05062
Milr1	0.476261	Ermap	1.433451	Gm39326	0.974091
Cd74	-0.81037	Bcl2l1	-0.30168	Mpst	0.336156
Tsc22d1	-0.38512	Stk40	-0.32061	Mcpt8	0.35834
Sesn2	-0.52278	Smpdl3a	0.403486	Mapk12	-0.81572
Evc	-2.23161	Col4a5	-1.38689	Smo	-0.25896
Gm40185	-1.48738	Gng10	0.358778	Rab27b	-0.3844
Adam17	0.327964	Igfbp7	-0.4494	Tspan17	0.728371
Flt3	0.485748	Serpinb10	0.837694	Ctu2	-0.45781
Tdg-ps2	1.433967	Cd14	0.808345	Ccdc85c	-0.52478
Clnk	-0.56523	Rcc2	-0.22777	Ldhb	-0.86166
Slc1a4	-0.68532	Nhsl2	0.295922	Gstm1	0.286931
Shroom4	-0.69261	St6gal1	-0.64301	Ccnd2	-0.18806
Psap	0.35661	Zfp709	0.602836	Sbf1	-0.23389
Sh3d19	0.608123	Neurl3	0.248045	Gm10419	-1.28496
Aars	-0.49012	Slc7a1	-0.26992	Gm51770	2.175715
BC064078	0.58124	Lonp1	-0.25871	AU020206	-0.27382
Myo7a	0.676263	Ttll7	-0.81325	Phc1	-0.30476
Armcx4	0.526638	Angptl6	-1.08537	Gm38733	0.975178
Il5ra	1.487368	Adgre5	0.530165	Trip6	-0.35207
Slc43a2	0.436388	Cars	-0.33262	Iqgap2	0.178573

Arnt2	-2.1751	Pip4k2a	0.245616	Senp7	0.251809
Dnah8	0.95436	Perp	0.35332	Gm29868	1.042246
Dok2	-0.56287	Usp18	-0.32025	Pidd1	-0.37654
Yars	-0.40675	Myb	0.226389	Cc2d2a	-0.97924
Ifitm6	1.066781	Vamp7	0.292667	Hoxb3	-0.42664
Dpysl5	-4.54975	Fam167a	-1.30131	Tert	-0.78815
Fam20c	1.652313	Hsd17b10	-0.30535	Socs3	0.509906
Spats2	-0.58635	1600014C10 Rik	0.289994	Ppp1r12c	-0.24808
Dhdh	0.509698	Sqor	0.482841	Abcb7	0.205925
Uaca	-1.17611	Rhou	1.439182	Samd4	-0.82972
Vsir	0.402618	Rras2	-0.44869	Zfp97	0.505105
Cldn15	1.852195	Zfpm1	-0.36011	Cd47	0.177595
Hspa12b	-0.65558	Pou2f2	0.270618	Pde4dip	-0.293
Fgd4	0.665954	Pecam1	0.235588	Gria3	0.295454
Slc16a10	0.450507	Bcl2	-0.28096	Cdkn1a	-0.23406
Abca13	1.569389	Bicdl1	-0.47682	Rps7-ps3	-0.80099
Cd28	0.619145	Selp	-0.32624	Arhgef25	-0.90801
Ppt1	0.371753	Itm2b	0.229308	Rpl39	0.25809
Sla2	-0.72828	Kcnj2	0.754478	Rps24	0.174167
Prss34	0.77335	5830444B04R ik	-1.70199	Galr3	-0.89447
St8sia4	0.343321	Cast	0.279078	Ccn3	0.305873
Il18rap	-0.35691	Trim35	-0.28535	Relb	-0.36216
Adam11	-1.52547	Tenm4	-2.44486	Gm39198	-0.30627
Nlrp3	1.00748	Mid2	-1.48646	Tmem135	0.237023
Ugt1a7c	0.577587	Ppic	-0.37378	Mettl22	-0.59518
Tmem38b	0.507258	Klf3	0.353514	Cyp39a1	1.034455
Afdn	-0.48115	Lrp8	-0.28307	Lgmn	0.655018
Il6ra	0.550359	Csf2rb	0.225036	Slc2a3	-0.2519
Epdr1	-0.73019	Sat1	0.324214	Dnm1	-2.73018
Zfp462	-0.88066	Cep126	-1.99851	Klf13	0.206188
Rin2	0.91613	Marcks	-0.42333	Nup62	-0.23237
Mc5r	0.40501	Zfp827	-0.94157	Ctsa	0.229947
Gm32920	6.883583	Tdrkh	-0.33438	Col4a2	-0.22316
Stard9	0.784279	Fam3c	-0.34409	Clip1	0.208883
Ndrg2	-0.55333	Dipk1b	-0.39875	D17H6S56E-5	-0.18117
Trib2	1.138412	Gm35853	0.90053	Septin10	0.992628
Gpr25	-1.23651	Als2cl	-0.54189	Ankrd12	0.288569
Ms4a6b	0.483181	Csf3r	0.277556	Slc24a3	0.351125
Siglecf	0.404103	Naip2	0.302753	Maged1	-0.39241
Vars	-0.32856	Mcf2l	-0.58123	Heatr4	3.972572
Lrp1	0.680584	Nars	-0.26154	Ptgds	2.648902
Ramp1	0.448101	Cln5	0.33691	Rnd2	-0.76912

Bmpr1a	-1.3488	Ddr1	-2.26543	Iffo2	0.308621
Krt18	-1.07176	Mettl6	0.300082	Ifi214	3.989414
Pglyrp2	-0.4762	Pygl	0.222707	Mcl1	0.174387
Slc7a5	-0.46138	Zfp658	0.847612	Lrrc41	-0.2708
Ncam2	-2.11249	Phyh	0.498145	Ppp1r13b	-0.2261
Gm29946	-1.23272	Insyn1	-0.81848	Zcchc18	-0.72606
Tbxa2r	-1.03264	Pold1	-0.29888	Arhgap32	0.298623
Otulinl	0.541251	Tnfaip8l2	0.433646	Slc27a1	-0.38373
Stab1	1.109593	Gm36587	1.546512	Ciart	-0.58433
Fzd2	-1.8144	Lats2	0.438654	Ctnnd2	-2.71962
Fsd1l	0.92144	Dtx4	0.358937	Cln8	0.290837
Pdgfrb	-0.41538	Lars	-0.23646	1700030C10 Rik	-0.83812
Slc6a9	-0.69272	Ces2g	0.869217	Atp13a2	-0.20302
Cacnb3	-1.8648	Adam10	0.206967	Atrn	0.242089
Aldh18a1	-0.42867	Mt1	0.408887	Dock5	-0.19067
Cd96	-0.50987	Txnip	-0.32509	Mtus2	1.004201
Zmat3	-0.60441	Tapt1	0.259691	Ipo13	-0.33475
Ggta1	0.350924	Ncoa3	0.244019	Megf11	0.713328
Obsl1	-4.02952	Ikzf4	-0.95864	Clstn1	-0.29223
B3gnt2	0.300245	Cysltr2	-0.55744	Mvp	-0.30773
Adgrg1	-0.32244	Nfam1	0.288546	Hps3	0.282097
H1f10	-0.80751	Lsp1	-0.28479	Ppp3ca	0.196401
Tnip3	-0.37662	Zfp57	-0.63468	Itpr2	-0.26215
Met	0.460142	Rubcnl	0.694276	Gm2560	-3.37237
H1f0	-0.35572	Tns3	0.259738	Ralgps2	0.226716
Cysltr1	0.569453	Fam102b	0.311615	Ugt1a6a	2.100348
Themis2	0.585682	Calcrl	0.26402	Sema4d	-0.2244
Psat1	-0.32649	Pck2	-0.26319	Cyp4f18	1.038851
Ptger2	0.59988	Glrx	0.362877	Mns1	0.32851
Il10rb	0.404739	Peg13	0.301702	Map1s	-0.27212
Myh9	-0.31286	Il6st	0.28093	Cert1	0.207491
Tgfbi	1.061193	Hexb	0.482337	Rnf123	-0.24275
Phldb2	1.119532	Dnmt3a	-0.22321	Kcnip3	-0.58511
Ikbke	0.420298	Cd200r3	0.623616	Gm26512	0.935239
Tnfrsf1b	0.397931	Gm5431	0.793509	Itfg2	-0.35011
Klf12	-0.81216	Klrb1c	1.826478	Olfm4	2.89356
S1pr3	-0.58003	Meis1	-0.25198	Six5	-0.39252
Mars1	-0.31405	Tgfbr1	0.279373	Dip2a	-0.43928
Vamp5	-0.48103	Extl1	-0.91921	Trak2	0.208298
Dusp4	-0.79245	Man2a1	0.276983	Mrgpre	-0.50564
Nucb2	0.681252	Gimap3	2.084896	Ddit3	-0.73561
Plppr3	0.39199	Chdh	1.441723	Gm34181	0.900716
Cd164	0.273477	Trim7	-0.91816	Gm12828	1.183599

H2-Ob	0.433575	Nfkb2	-0.32782	Septin3	-1.22426
Pcp4l1	0.863876	Kctd15	-1.19523	Zhx2	-0.47636
Tcp11l2	0.416438	Nrp1	0.732564	Cmya5	-1.90731
Rai14	-0.52732	Nqo2	0.369663	Hgh1	-0.34048
Npc2	0.355076	Man1c1	0.378443	Ly6e	0.257221
Slc28a2b	1.228028	Hip1r	-0.31834	Itga1	0.584592
Slc22a3	0.294394	Tmem184c	0.450355	Gpr68	-1.02406
Soat2	-0.97179	Dnase1l1	0.43359	Tacc1	-0.18698
Pcyox1	0.340884	Cd200r1	0.322146	Zdhhc8	-0.31495
Slc12a6	0.301389	Cpne2	-0.28791	Usp44	-0.85487
Xlr3a	-3.48539	Gm46162	0.907162	Nudt4	0.224295
Timp3	-0.63692	Kdr	-0.60505	Cdk14	-0.3997
Plekha7	-1.25907	Bbc3	-0.42435	Mtmr6	0.19582
Cd244a	-0.46793	C030002A05 Rik	1.762028	Itgax	-0.69604
Itga4	0.330113	Eif4ebp1	-0.37069	Sorcs1	-0.64923
Clec4a2	1.531213	Sec24c	-0.1944	Mmp25	-2.00115
Sh3pxd2a	-0.46684	Vcpip1	0.244463	Pnp	0.287826
Ceacam1	0.949089	Gm34232	2.6401	Trp53	-0.20098
Slc1a5	-0.35509	Klf9	0.34875	Gm32742	-1.58072
Aldh7a1	-0.41405	Abhd17b	0.263898	Pgm2l1	0.218058
Slc9a7	0.565902	Rab32	0.292288	Map4k1	-0.20993
F2r	-0.30222	Gm42517	-1.81055	Il17re	-0.67882
Far2	0.77416	Metrnl	-0.55986	Sec24d	-0.26312
Abcb4	0.840847	H3f3b	-0.18213	Siglech	-1.09783
Bcam	-1.17439	Cd276	-0.78829	Trib3	-0.88011
Chd7	0.534412	Sp100	0.258387	Tmem201	-0.26019
Exoc3l	-0.6419	Cd83	-0.86274	Mllt3	0.272083
Sirpa	0.328498	Upp1	-0.54211	Pik3cb	0.274351
Atp1b2	0.69929	Mfsd1	0.265937	Ppp2r5a	0.176018
Hsd11b1	1.459666	Clec2d	0.313064	Lpxn	0.366455
Dlg3	-0.39597	Lnpep	0.266419	Cand2	-0.29723
Ifrd1	-0.33497	Mapkapk2	0.287781	Cotl1	0.267625
Dcaf7	-0.26192	Ptgir	0.375	Ssh2	0.194645
Tmx4	0.305373	Adrb2	1.038221	Cactin	-0.24414
Mpdz	-1.20066	LOC115489981	1.995584	Cstb	0.383475
Cxcr4	0.37393	Nod1	0.47583	Skil	0.283645
Rab44	0.408043	Chrnb1	-0.73181		
Rec8	-0.70929	Klri2	-1.89239		
Dsg2	-3.59054	Ncf2	0.250436		

Appendix XVII: Significant (padj < 0.05) differentially expressed genes from Runx2-flox pHPC RNA-seq, Runx2-het vs Runx2-wt. n = 3, sorted by padj small to large, top to bottom of each column. See Chapter 2.8.2 for data analysis pipeline.

gene	log2FC	gene	log2FC	gene	log2FC
Podxl	-1.32637	Gpc3	0.700437	Pdap1	-0.2912
Mthfd2	-1.29049	Amd1	0.312965	Hacd4	0.333875
Wfdc17	1.694064	Arnt2	-1.31185	Cybc1	0.239853
Dntt	2.168582	Gimap9	0.380384	Zfp639	-0.32389
Sell	0.932675	Clec5a	-0.60777	Ankrd13a	0.184784
Emb	0.892491	Evc2	-1.91816	Slc12a2	-0.35465
H2-Ob	1.127832	E2f8	-0.35489	Mettl14	-0.25466
Ifi209	1.261355	Btg2	0.340767	Rps24	0.201137
Ccl9	0.930434	Svil	-0.31002	Tmem50a	0.251687
Adgrl4	0.992714	Car13	-0.48646	Pask	-0.37125
Slc7a5	-1.14371	Ms4a4b	0.432699	Hck	0.382045
Itgam	1.107674	Ptprc	0.266069	Pgap4	-0.55598
Sdc1	1.521953	Mndal	0.28693	Cd83	0.684162
Emp1	1.565058	Xrcc5	-0.49792	Ddx20	-0.26987
Psat1	-0.92165	Prodh	-0.48663	Camsap2	0.573829
Commd10	1.315203	Gulp1	-1.03281	Pglyrp1	0.42025
Gimap4	1.323326	Wdr19	0.526762	Met	0.295409
Irf8	1.090922	Prkcd	0.31255	Odf2	-0.24423
Myh10	-1.04489	Rhob	0.421565	4930555A03Rik	0.539853
Asns	-1.25409	Aagab	0.298252	Rnf141	0.242371
Shmt2	-0.73823	Il2ra	1.065525	Clec11a	-0.92382
Flt3	1.000709	F2rl2	-1.00955	Gm15987	0.852264
Lyz2	0.782107	Lst1	0.454325	Slc2a9	0.374409
Atp1a3	1.336939	Ppp1r16b	0.859729	Etf1	-0.2012
Il10ra	0.702999	Ctsz	0.347566	Per2	-0.54944
Adgre1	1.447993	Parp8	0.308067	Lsg1	-0.25544
Abca4	-1.37591	Rab34	0.857527	Mtrr	-0.33363
Gpt2	-1.11631	Cerk	0.341551	Nf1	-0.29284
Gm2a	0.80189	Hsd17b11	0.349753	Obscn	-1.55543
Ifi204	1.067701	Rassf5	0.286393	Sytl1	0.334668
1810073O08Rik	1.443127	Fxyd5	0.282357	Flna	-0.23378
Itga2b	-0.8869	Lag3	0.561454	Ppan	-0.26597
Ahnak	0.91831	Tlr4	-0.44139	Ankra2	0.362763
Pld4	1.13788	E2f7	-0.49873	Dusp4	-0.49496
Slc3a2	-0.84925	Nt5e	-0.92134	P2ry2	0.389401
Gzmb	-0.98425	Plin3	0.33419	Cdk14	-0.44604
Mgst1	1.343948	Lrrc25	0.681864	Eipr1	-0.36871
Iars	-0.73419	Arhgap29	-0.52517	Taf15	-0.19295
Cd33	1.067421	Msrb3	0.422739	Tdp1	-0.33302
Ly6c2	2.567207	Rel	0.326248	Gm15915	-0.77448

Aldh18a1	-0.87432	Usp1	-0.3003	Atad5	-0.22129
Slc1a4	-1.28413	Calcoco1	0.3336	Ctps2	0.230041
Aars	-0.92916	Fgd4	0.460405	Caskin2	0.431584
Pde2a	1.392885	Irf5	0.426142	Dmwd	-0.34434
Bcat1	-1.17061	Scarb2	0.28545	Paox	0.332899
Cttn	-1.24056	Samsn1	0.265642	Bid	-0.28568
Tlr7	1.11838	Mid1ip1	-0.33774	Esyt1	-0.19067
Gars	-0.7335	Mier3	0.312056	Atp1b3	0.251221
Arx	-2.24783	F2rl3	-0.50432	Ggps1	-0.25426
Ifrd1	-0.74132	Fam107b	0.220629	Iqsec1	0.296298
Clec2i	1.392476	Abr	0.313129	Idh1	0.253993
Man1a	0.618832	Ppfia4	0.9634	Sntb1	-0.41924
Thy1	-1.38811	Cenpf	-0.2837	Pgap6	0.52274
Glul	0.641906	Gstt1	-0.87214	Phf11d	0.425692
Nars	-0.68381	Rps27	0.278254	0610010F05Rik	-0.27492
Gimap6	0.673668	Il16	0.277736	Mob3c	-0.39549
Ccl5	1.062587	Psmg1	-0.36428	Tnfrsf14	0.249118
Chac1	-1.57643	Ncapg2	-0.2681	Tap2	0.22161
Lars	-0.64239	Foxo3	0.27512	E2f4	-0.24377
Hlf	0.793324	Hdac7	0.310002	Vldlr	-0.31079
Csf1r	0.932228	Rars2	-0.3896	Trf	0.232883
Dpp4	0.971115	Mettl7a1	0.337282	Ugt1a7c	0.368549
Lbp	0.787967	Serpini1	0.590269	Smap1	-0.28423
Cd300lb	1.022777	Zfp467	0.468951	Pfn1	-0.257
Wdhd1	-0.72729	Plekhg1	1.47369	Kif11	-0.21317
Myof	1.387341	Cd55	-0.46846	Oxct1	-0.23409
Tars	-0.70988	Dapk1	-0.41218	Unc119	-0.29103
Stom	0.760437	Rpl24	0.247999	Myh9	-0.26631
F13a1	1.100875	Gja1	-0.55588	Abcg2	-0.35773
Cars	-0.81732	C330026H20Rik	2.053366	Fbxw4	0.436054
Slc6a9	-1.46496	Trp53	-0.2688	Gatad1	-0.20674
Psap	0.621845	Shisa8	1.342908	Ifitm1	0.255626
BC064078	1.020757	Ifrd2	-0.36504	Armcx4	0.330909
Ccl3	1.069236	H1f2	0.562658	Amot	0.348423
Ctss	1.000226	Fau	0.24667	Map3k14	0.393945
Yars	-0.74416	Kdm7a	0.422657	Irf2bp2	0.191899
P2rx7	1.263344	Sema7a	-0.41842	Anp32b	-0.25547
Prtn3	0.713475	D230025D16Rik	0.367344	H3f3a	0.21943
Rasa4	0.768185	Atp6ap1	0.286784	Rangap1	-0.21034
Mpeg1	0.909005	Zfp219	0.306005	Oas3	0.209483
Dhrs3	0.942701	Trip13	-0.43056	Reep2	-1.84912
Slc7a3	-2.4133	Hsdl2	0.409459	Pkp4	-0.26535
Tmem71	0.67603	Pecam1	0.263402	Serinc3	0.160466
Slc7a1	-0.67982	Atad2	-0.25987	Vdr	0.409434

Nupr1	-1.97558	Tmem43	0.294233	Pik3cg	0.204088
Ms4a4c	0.882715	Vasp	-0.28606	Eri2	-0.45536
Mars1	-0.59698	Il18r1	-0.68244	Synpo	0.476581
Gm3534	5.047344	Snx20	0.398447	Rpl36	0.211045
Clstn3	-1.10171	Ly6e	0.33955	Pkia	-1.22676
Hemgn	-0.69712	AW112010	0.507193	Eif1	-0.21726
C3	0.735735	Slc6a6	0.270729	Ass1	0.230911
St8sia4	0.558349	Dtymk	-0.29905	Phgdh	-0.22057
Abcd2	1.085119	Pde4dip	-0.39034	Mid2	-1.26698
Gm31657	1.313655	Ckap2l	-0.39912	Pxylp1	0.310868
Tgm2	-0.80842	Washc4	0.297078	Mbd3	-0.24698
Ypel3	0.677396	Gimap3	2.266721	Trnt1	-0.31204
Cybb	0.59208	Mettl16	-0.3501	Nme6	-0.46108
Soat2	-1.76418	Als2cl	0.5693	Dnajc9	-0.23098
Smpdl3a	0.823524	Znrf1	0.299164	Hcfc2	-0.2762
Fam234a	0.983884	Chp1	0.26448	Slc25a32	-0.28246
Prg2	1.175903	Slc18a2	-0.34964	Plag1	0.332097
Fgf3	-1.29506	Nr4a3	0.884681	Rps9	0.182646
Casp12	-0.81808	Smg5	-0.28657	Frs2	0.231177
Dock1	-0.94634	Atp8b2	0.289166	Bnip3	0.195261
Gp5	-1.5147	Sh3bgrl3	0.320556	Uchl3	-0.35326
Satb1	0.739265	Tle2	0.657899	Zfp974	0.528874
Arhgap18	0.509938	Smim14	0.299108	Cep85	-0.29507
Slc43a2	0.664069	Tdrkh	-0.35824	Med22	-0.23294
Cp	0.870386	Ets1	0.573099	Tbpl1	-0.25733
Mtbp	-0.81106	Zfp598	-0.33894	Hnrnpd	-0.25054
Slc35d3	0.992835	Retreg1	0.356484	Sos1	-0.26536
Glrp1	-1.51402	Pde3b	0.33304	Lmbrd2	-0.26197
Egfl7	0.609121	Treml1	-1.32862	Spry4	-1.12767
Ifi213	0.802875	Gfi1	0.48693	Mcf2	-0.57472
Acot1	1.654467	Ak1	0.592415	BE692007	0.528324
Pgr	1.216248	Vill	0.362838	Cd34	0.180474
Slc1a5	-0.67083	Nicn1	0.536755	Inpp5d	0.205014
Sesn1	0.568566	Ccl22	0.80961	Spi1	0.233626
Itgb5	0.822999	Cd300a	0.30448	Trmt2a	-0.22501
Pcp4l1	1.246258	Ano10	0.442017	H1f10	-0.45327
Sdc4	0.844514	Nop14	-0.3002	Gabarap	0.23294
Clic4	-0.49637	Setd6	-0.61889	Gdi2	0.190515
Macroh2a1	0.469807	Ubash3b	-0.34099	Haus7	-0.41843
Rab6b	0.97401	Mapkapk2	0.289539	Arid4a	0.222872
BC035044	0.573508	Blnk	1.522929	Mmachc	-0.34028
Pla2g4a	-0.59683	Cd180	0.337199	Pwp2	-0.27195
Cd93	0.563479	Mx1	0.392264	Ssbp2	0.220666
Hmga2	0.707133	Rasgef1b	-0.67454	Eif2s1	-0.22064

Rab27b	-0.81012	Tpst1	0.522397	Fbxo9	-0.26927
Fcgrt	0.96195	Larp1	-0.22776	Man2b1	0.20665
Gda	0.865221	Trpc1	-1.48875	Neu1	0.363706
Shroom4	-1.02898	Bora	-0.33722	Fundc1	0.251351
Fcer1a	-1.64435	Trpc4ap	0.256178	Epsti1	0.240357
Cd28	0.899469	Epb41l4b	0.272652	Nxpe3	0.249335
Stox2	-1.25305	Evc	-1.60789	Amz2	-0.24921
Ltbp3	0.675438	Hexim2	0.494228	Scml4	0.508548
Mfsd2b	-0.99374	Rxra	0.779249	Stard8	0.379333
Itm2b	0.441801	Dus4l	-0.64774	Pik3r2	-0.2753
Ifi207	0.905501	Pign	-0.29444	Recql4	-0.5118
Ramp1	0.616913	Prxl2c	0.371722	Pip4p1	0.303213
Selenop	0.511052	2610035D17Rik	0.505844	Zfp948	-0.68434
Ly86	1.274625	Ciart	-0.75665	Sema4a	0.462745
Neurl3	0.524744	Pdlim5	-0.37713	Cyp39a1	1.046904
Tcn2	0.643298	Prr5	0.549203	Ripk1	0.202318
Pck2	-0.55745	Tmem176b	0.318909	Niban1	-0.57019
Ugcg	0.468931	Btbd19	-0.7126	Dph6	-0.29551
Slamf1	-1.58392	Rab5b	0.261047	Tspan3	0.220332
Slc26a11	1.22288	Krt7	1.15962	Gm42226	-0.21712
Adgrl2	-0.83733	Pnrc1	0.274055	Pnp	0.286742
Sgpl1	0.641147	Zfp516	0.36343	Riox2	-0.26486
Lat2	0.511067	Pdk2	0.652156	Abtb1	0.284789
Gm1966	0.444453	St3gal2	0.263807	Larp1b	-0.3382
Zfp462	-1.28189	Runx2	-0.2782	N4bp2l1	0.344912
Klhl24	0.455134	Clic5	0.671059	Spns2	-0.18893
Sars	-0.63608	Nup205	-0.25255	Cdc20	-0.24615
Xpot	-0.50415	Adssl1	0.390137	Foxo1	0.37432
H2-T23	0.417908	Nsd2	-0.23706	Serpinh1	-1.13667
Gm3360	1.992686	Cln8	0.394975	Mcm8	-0.34135
Gas7	0.747361	Samd12	-0.52801	Stk39	-0.4383
Pink1	0.530109	Zfyve1	0.356883	Fam234b	0.34193
Ctsb	0.459191	Castor2	0.594611	Myo6	-0.40416
Eprs	-0.51835	Jdp2	-0.37365	Pten	0.176312
Plac8	0.584589	Prmt1	-0.30896	Atr	-0.25538
Sgsm1	1.499547	Grina	0.398982	Foxm1	-0.32391
Pou2f2	0.515482	Slc8b1	0.500592	Fgd3	-0.23821
Pik3ip1	0.539951	Kdr	-0.61358	Rtkn	0.429271
Zeb2	0.466046	Pld2	0.63966	Aph1c	0.537633
Hpse	0.683519	Aqp9	-0.50398	Rhoq	0.282421
Rab7b	1.239371	Ninj1	0.336105	Dynll1	-0.26078
Pik3ap1	0.603462	Tigit	0.413396	Fanca	-0.40861
Gimap8	0.570002	Stc2	-0.55564	Cdk5rap2	-0.25887
Sdc3	0.674929	Kri1	-0.42155	Usp3	0.228836

Cracd	-0.7631	Ifit2	0.284219	Poglut2	-0.25002
H2-DMa	0.615364	Mknk1	-0.40358	Klrb1c	1.614717
Tyrobp	0.691335	Exosc2	-0.35724	Clnk	-0.3023
Tcp11l2	0.603515	Ccnd2	-0.24944	Top2a	-0.18115
Csf2rb2	0.54587	Chaf1a	-0.33669	Dhdh	0.29419
Themis2	0.814388	Slc7a8	-0.42037	Il27ra	-0.30406
Cd200r4	0.833273	Siglecg	1.042058	Fth1	0.229028
Ddit3	-1.08351	Crlf3	0.250455	Rcbtb2	0.267691
Tecpr1	0.656778	Dctd	-0.31441	Rbbp5	-0.22701
Il10rb	0.575736	Set	-0.25791	Trp53cor1	-0.47601
Myo1f	0.475772	Evi5	0.395922	Cenpw	-0.51124
Npc2	0.519052	Trat1	0.656838	Pbk	-0.32037
Padi2	0.63943	Ppfia1	-0.30525	Ube2k	-0.22829
Itgb7	0.510164	Lrrc59	-0.26797	Rbm19	-0.3609
Tspan13	0.41719	Ift81	0.556319	Napsa	0.212798
Klrb1f	0.784585	Prkar2b	-0.24733	Hbp1	0.304454
Hspa9	-0.45267	Slc29a3	0.356085	Adam15	0.246893
Lonrf3	0.839982	Ctsh	1.002351	Strap	-0.21113
Lincred1	0.704082	Lgalsl	-0.56328	Wdr43	-0.18564
Chd5	-1.55958	Srsf7	-0.29339	Trim25	0.181353
Trp53inp1	0.549363	Anp32e	-0.30026	C77080	0.391819
Septin11	-0.44606	D830031N03Rik	-0.60583	Irf1	0.224505
Mycl	1.164537	Rbms1	0.306227	I830077J02Rik	-0.33695
Bmf	0.660649	Lamp1	0.252976	Rpl37a	0.24405
Igh	0.743794	Grap2	0.84846	Psmb9	0.237619
Cpq	0.679436	2810004N23Rik	-0.31735	Sugct	1.037916
Hdgfl3	-0.5903	Cep83	-0.30316	Cenpe	-0.21788
Xlr3b	-2.1019	Rad23b	-0.2099	Npepl1	-0.23305
Gpnmb	1.291584	Cdip1	0.389847	Gm52627	0.970513
Sesn2	-0.69758	Papola	-0.21217	H2-Ab1	0.42859
Alas1	0.620204	Tnfrsf13c	0.825392	Asb1	-0.3174
Trappc9	-0.53965	Edem2	0.270474	Noc3l	-0.24751
Mpp1	0.544306	Pomgnt2	0.495432	Mettl2	-0.28149
Trim30c	0.589149	Celsr1	-0.40003	Dpm3	0.399034
Wars	-0.46897	Plpp5	-0.41656	Ikbke	0.305996
Fgf11	0.690726	Peg13	0.355646	Cnot9	-0.20825
Scpep1	0.519822	Stard9	0.651015	Lrp8	-0.25072
Ube2h	0.489666	Il18	0.74838	Tmem171	0.681791
Sema3d	2.486505	B4galt6	0.429506	Zranb2	-0.19499
Tns1	0.630249	Palm	0.373317	Uvrag	0.219352
Pls1	-1.15393	L3mbtl3	0.308483	Cep162	-0.28894
Timp3	-0.63364	Hpcal1	0.354565	Zgrf1	-0.29864
Pf4	-0.70902	Mill2	0.617012	Fam117a	0.207392
Ifitm6	1.204429	Cdkn1b	0.28905	LOC115487677	-0.64665

Lat	-0.76175	Samd4	-1.07755	Gm10419	-1.25161
Vsir	0.530945	Pfdn6	-0.38556	Syde1	-1.44471
Ctse	0.693068	Rdh12	0.772632	Prg3	1.235683
Phf10	-0.4778	Cish	0.351762	Zfp608	0.231142
Hirip3	-0.60385	Brca2	-0.31824	H2-D1	0.195399
Sgsh	0.911754	Slc18a1	1.690041	Arl11	0.293776
Alox5	-0.85738	Cd44	0.231132	Fbxl20	0.224515
Olfm1	1.582061	Rnf17	2.066408	Gm46478	0.854563
Ifi206	0.505246	Irf7	0.249654	Arhgef18	0.22771
Tnfrsf1b	0.497925	Clec7a	0.980759	Ndc80	-0.28861
Hmgb3	-0.60252	Hmgn2	-0.27772	Fnip1	0.261701
Dtx4	0.621196	Heatr3	-0.29754	Fyco1	0.275151
Elane	0.845095	Trim58	-0.66228	Me1	-0.61288
Crebrf	0.545424	P2rx4	0.344462	Prelid3b	-0.28332
Sat1	0.526633	Gpr25	-0.82362	Fry	-0.35869
Ptprz1	-2.54277	Nop2	-0.27154	Sh3bp5	0.346025
Rai14	-0.65707	Bco2	0.694848	Fam168a	0.229567
Ifi27l2a	0.643505	4933404O12Rik	-0.46773	Alpk1	-0.42917
Epdr1	-0.90505	Tspan17	0.932289	Golim4	-0.21625
Scin	0.376906	Spta1	-0.98526	Ncf4	0.232571
Akr1c12	-0.58906	Klf3	0.353789	Slc12a9	0.415545
Sp100	0.390201	Septin8	-0.33248	Baz2b	0.237588
Dok2	-0.59159	H2-DMb1	0.457757	Adat1	-0.36246
Ppt1	0.446872	Nudcd1	-0.31145	Sorcs1	-0.67257
Tent5a	0.500623	Lipa	0.291766	Adcy6	0.269445
Ccr2	0.685779	Pnn	-0.23821	Otud1	0.608859
Lrp1	0.877482	4931406C07Rik	0.300345	Rnase4	1.643355
Slpi	0.942532	Ncf1	0.266259	Rbmx	-0.26953
Ms4a6c	0.531428	Cbx5	-0.2337	Tstd2	-0.27379
Rgl1	0.685022	Mlh1	-0.33623	Cdk12	-0.22112
Msrb1	0.600039	Pstpip1	0.263682	Baz1b	-0.16665
Nop58	-0.42256	Bmpr2	0.282063	Gm33669	1.590206
Slc9a7	0.74354	Eif3f	0.222709	Pds5a	-0.16223
Eif4ebp1	-0.58141	Cstb	0.438716	Arid3a	0.250181
Trim5	0.617693	Gm26812	-2.11541	Senp5	-0.21402
Milr1	0.518768	Cenpt	-0.48437	Tex30	-0.32436
Gm5431	1.178503	Arhgap45	0.268702	Gtpbp4	-0.2118
Ccn3	0.61761	Arhgef10l	0.386252	Rpn1	-0.19453
Agtrap	0.452559	Sec61a1	-0.23028	Adgrl1	-0.3357
Scn1b	1.078396	Knl1	-0.29129	Rcor2	-0.33204
Rassf4	0.456739	Traf3ip2	0.639402	Cpne3	0.177276
Ptger2	0.767428	Mns1	-0.44185	Heatr1	-0.19036
Cds1	0.736497	Svip	0.387548	Traf1	0.426643
Slc20a1	-0.4951	Ckb	0.938508	Atp6v1e1	0.237916

Ezh1	0.506155	Etv4	-1.06397	Sclt1	-0.34487
Lhcgr	-1.75755	Hmox2	0.308041	Pld3	0.314423
Cldn12	-0.89896	Atp6v1b2	0.268027	Faah	0.357688
Il6ra	0.648484	Cir1	0.307654	Gnat2	-0.82958
Mamdc2	0.857141	Nlrp1a	0.510003	Stk10	0.258707
Pirb	1.015485	Kif20b	-0.27194	Pram1	1.130408
Srpk1	-0.43048	Ddx21	-0.21909	Dstyk	0.264089
Cst3	0.464277	Dglucy	0.321632	Lamp2	0.184192
Gata1	-1.10476	Tmem170b	0.293057	Rhbdd1	-0.32575
Pygl	0.370682	Furin	0.325959	Phldb1	-0.34692
Tbc1d8	0.700255	Map3k3	0.271137	Dennd3	0.220766
Hgf	0.626724	Marcks	0.441434	Cgas	-0.2652
Snx29	0.563939	Zfp131	-0.31783	Mob1b	-0.25847
Angptl6	-1.75112	Il3ra	0.424039	Depdc1b	-0.31838
Igsf6	0.664789	Stx7	0.280902	Srsf2	-0.23383
Acox3	0.568726	Srm	-0.28944	Dmd	-1.27803
Cd52	0.506783	Alg8	-0.36163	Urm1	-0.2721
Cyth1	0.494518	Mad2l1	-0.29339	Rassf2	0.213986
Txndc16	0.64809	Bcl2l1	-0.33221	Rbm44	1.766273
Col16a1	-0.80935	Agpat3	-0.50132	Morc2a	-0.21007
Arl14ep	-0.58389	Cyb561a3	0.275246	Chst12	0.272796
Pcmtd2	0.453825	Pros1	-0.8778	Mtus1	0.454165
Lpl	1.199892	Ptpn11	-0.23726	Vamp7	0.238853
Vwa5a	0.389534	Gm32249	1.034154	Ccr5	1.189061
Rubcnl	1.095439	Prim1	-0.31263	Mapk1ip1	0.446401
Vav3	0.457594	Tbxas1	-0.30686	Pvr	0.400336
Dok3	0.723959	Aldh2	0.225832	Aldh7a1	-0.2484
Sva	7.608586	Adam17	0.231684	Cyth3	0.284618
Cd68	0.531381	Dgkd	0.235074	Cyp20a1	-0.30185
Slc12a6	0.433784	Pgrmc1	-0.29651	Tmpo	-0.16948
Atp9a	1.614787	Prep	-0.30078	Nhp2	-0.27992
Kctd12b	0.990612	Snhg17	-0.47125	Sgf29	-0.32292
Cadm3	-1.108	Gramd1b	0.346661	Zfp33b	0.328905
Zfpm1	-0.54594	Slc15a2	0.681124	Wdr46	-0.24264
Eif2s2	-0.40997	Bmpr1a	-0.98678	Mgme1	-0.29741
Pde4b	0.398983	Sla2	-0.4661	Smad7	0.394817
Smim24	0.67802	Cnot8	0.284535	Prkacb	0.177934
Tnfaip8l2	0.703805	Ifi203	0.273022	Prss16	-0.56551
Ptafr	0.555882	Sox4	0.233285	Spns3	-0.25763
Cyb5r1	-0.65828	Lins1	-0.48404	Racgap1	-0.24104
Drc7	0.745705	Psme3	-0.26335	Eif3j1	-0.2049
Rin2	1.000351	Ltv1	-0.3259	Trmt61a	-0.39213
Gm42048	-1.31291	Xpo5	-0.24059	Angpt1	-0.19126
Cxcr2	0.607985	Kmt5a	-0.23282	Foxo4	0.257403

Arhgef10	1.258552	5031439G07Rik	0.363548	Mettl27	0.338997
Gpr18	1.287455	Nabp2	-0.35346	Taldo1	0.191742
Abca1	0.815649	Plcb1	-1.02104	Birc5	-0.31056
Gm30605	0.745215	Il12b	1.685338	Mgam	0.824095
Gab1	0.687704	Sash1	0.373813	Kntc1	-0.23528
Aff3	0.42332	Srsf10	-0.23479	Clec2f	1.254571
Cyria	0.606269	Znfx1	0.282659	Jpt2	-0.19936
Inpp5k	0.447131	Pola1	-0.24901	Tox	-0.39964
St8sia1	0.817978	Brix1	-0.33463	Hoxa5	0.541861
Asah1	0.343733	Dazap1	-0.32416	Ube2r2	0.213203
Gm17745	0.837389	Tlr1	1.033003	Fam162a	-0.27259
Ggta1	0.417081	C130050O18Rik	0.829657	Zfp637	0.383542
Selplg	0.375432	Dnajc2	-0.25343	Washc2	0.230757
Ephb2	1.101603	Tnfrsf9	-1.07376	Chm	0.233397
Prkca	-0.60606	Tle3	0.30365	Rbm3	-0.2085
Arhgap15	0.402602	Arhgef40	-0.40663	Notch1	0.662868
Mgat1	0.375861	Scamp1	0.261296	Ralgps2	0.226518
Lpar6	0.607377	Map4k5	0.37266	Abcb6	-0.64272
Arhgef3	0.425523	Sp4	0.335298	Mfsd6	0.261777
Clec12a	0.455857	Arhgap5	-0.3244	Ccdc25	-0.34237
Sqor	0.682328	Rpl13	0.191206	Kcnq3	0.438291
Otulinl	0.622868	Gyg	0.264826	Nup93	-0.3039
Ptpro	1.142746	Cbx6	0.247052	Mmrn1	-0.61302
Gbp6	0.71167	Gm20506	1.010707	Cyp4f18	1.015991
Rbpms2	-0.68544	Parp9	0.21795	Khnyn	0.235743
Pcdh7	-0.60457	Pcyox1	0.26553	Il13ra1	0.798611
Nfe2l1	-0.53578	Arhgap11a	-0.22707	Cpa3	0.278227
Cd84	0.362821	Nfe2l2	0.252292	Rexo2	-0.26462
Ctnnal1	-0.90003	Plxnb2	0.299615	Ssr2	-0.19666
Ifnar2	0.3936	Eps8	0.334932	B430306N03Rik	0.597833
Gm32554	2.137771	Itih5	-0.25657	Rpl32	0.178312
Gpr132	0.567664	Capn2	0.316006	Nrxn1	0.362082
Fads1	-0.34685	Ptgs2	-1.05058	Tube1	-0.40997
Eng	0.447443	AA467197	1.585984	Slc16a12	0.804056
Bcl2	-0.38259	Zdhhc2	-0.65839	Epor	-0.8374
Pde5a	-0.75317	Cdc42se2	0.23436	2610318N02Rik	-0.53114
Mxd1	0.495772	Exoc3l	-0.50734	Zcchc3	-0.53054
Tgfbr3	-0.60096	Fmnl2	0.283872	Prkd3	0.200259
Slc4a7	0.390196	U2af2	-0.21442	Exosc7	-0.28622
Tuba8	-0.62004	Lats2	0.431388	Cr1l	-0.20915
Cntln	-0.47574	Tek	-1.23384	Gbx2	-0.61165
Plppr3	0.478871	Cabp1	-1.75957	Hace1	-0.34827
Ifi44	0.360033	Elovl5	0.235863	Dock5	-0.20362
F2r	-0.36037	Sorl1	0.405297	Psmb8	0.190508

Gm39198	-0.50878	Gm41974	1.355452	Sema6d	0.720349
Socs3	0.919413	Dot1l	-0.26619	Cep41	-0.31387
Gimap7	1.109055	Phyhd1	0.6324	Snx9	0.2493
Gpr160	0.811744	Stxbp3	0.317087	Gpr65	0.2738
Xpc	0.404132	Selenon	0.284468	Tep1	0.265668
Arap3	-0.39838	Mindy2	0.237508	Mmadhc	-0.21876
Galnt6	-0.4125	BC016579	1.477917	Gp1ba	-0.50675
Eif3c	-0.36615	Ikbkg	0.246502	Gle1	-0.22637
Tnfrsf26	0.505485	Gar1	-0.36838	Eif1ad	-0.21172
Rbm47	1.208932	Extl1	-0.86905	Nsl1	-0.31491
Sdsl	-0.9326	Pold2	-0.31297	Sacs	-0.23023
Fam3c	-0.47389	Cmtm6	0.233458	Cenpk	-0.37882
Ms4a6b	0.476175	Zfp949	0.365309	Psmc3ip	-0.44686
Gbp5	0.546709	Irak2	0.37932	Ift57	0.225277
Glrx	0.499915	Rora	0.329298	H2-M3	0.267684
Tlr9	0.950189	Ebna1bp2	-0.29575	Tbcb	-0.42597
Kmo	0.814714	Sh3kbp1	0.25404	Eif5a	-0.21634
Zfp385a	-0.48079	Lrrc8c	0.260913	Galnt1	-0.16086
BC147527	0.521947	Ero1a	-0.28964	Ccnd3	-0.21444
Lmo2	0.323527	Susd2	-1.11197	Uggt2	0.502156
Tnk2	-0.55228	Qtrt2	-0.37195	Hhex	0.213819
Ctsf	1.174954	Orc2	-0.27293	Itfg2	-0.37302
Mycn	-0.33535	Slc7a11	-1.43012	Ing5	-0.22147
Shank3	-0.64704	Gpr183	0.722596	Tcof1	-0.23679
Tapt1	0.390926	Kif9	0.850732	Prmt7	-0.24373
Cd69	-0.41062	Nuf2	-0.3217	Psmc3	-0.22585
Gria3	0.530339	Gbp11	1.394453	Hars	-0.25361
Jakmip1	0.492094	Arhgap32	0.36647	Paxip1	-0.25034
Camk2a	0.477524	Tmem38a	0.625291	Cdc23	-0.21263
Anxa6	0.367259	Slc38a2	-0.21211	Sapcd2	-0.54638
Aldh1l2	-1.7067	Abraxas1	-0.41505	Dock10	0.185631
Mpdz	-1.41813	Cers2	-0.22695	Rhoj	-1.84686
Ctsd	0.368557	Nlrp1b	1.065632	Plekha7	-0.70906
Tcf4	0.314025	Kdelr1	0.28575	Abca2	-0.23376
Ttc39b	-0.57264	Gmds	-0.40535	Gm35315	-0.42535
Gstm1	0.453457	Timm23	-0.29932	Tifa	0.252925
Kit	0.371093	Cnot6l	0.199961	Ccne2	-0.37693
Gprc5b	0.928072	Stat5b	0.250921	Tipin	-0.27089
Tifab	0.953708	Atp8a1	-0.28938	Myo5a	0.20781
Clca3a1	-1.74385	Gm43305	1.316103	Ncapd2	-0.19909
Samhd1	0.310885	Limd2	0.219702	Ezh2	-0.19193
Trim35	-0.40843	Hspa12b	-0.39979	Mcm5	-0.21831
Ccr7	0.889478	Rilpl2	0.271706	Atp2b4	0.226295
Esr1	0.561951	Evi2a	0.410461	Dlgap4	0.27543

Ifi27	0.327909	Kif15	-0.27323	LOC115487638	-1.10907
2410002F23Rik	-0.55068	Ccnd1	-0.53376	Atp7a	0.266958
Lonp1	-0.34646	Clec2d	0.35805	Ftsj3	-0.21565
Herpud1	-0.4024	Fam174a	0.365176	Mios	-0.23628
Trim30d	0.376656	Ddx60	0.227161	Ncoa3	0.249923
Cdk19	0.346546	Creg1	0.263205	Ddr1	-1.61215
Tmcc3	1.269478	Snx2	0.233656	Rabac1	0.242741
Usp40	-0.49181	Dlg3	-0.32513	Ankrd44	0.207737
Tmem176a	0.399377	Heca	0.261233	Kctd10	0.23065
Rgs2	0.484329	Ldlrap1	0.290303	Dhx29	-0.29669
Nod1	0.674073	Hoxa3	0.753797	Zwilch	-0.31005
Rasgrp3	1.216691	Cux1	0.223694	Myl12b	0.216055
Nuak2	0.572559	I730030J21Rik	-0.33844	Bmt2	0.210843
Padi4	0.375754	Gbp9	0.544532	Dcbld2	-0.74596
Zbtb4	0.598927	Syne2	0.399208	Galc	0.282866
Pard3b	-0.84345	Nt5dc3	-0.365	Psmc2	-0.21323
Man1c1	0.536962	Ogg1	-0.43485	Ccser1	0.72029
Pqlc3	0.489188	Pnpla7	0.294624	Iqgap2	0.176649
Nop56	-0.33929	Olr1	1.379487	Ftl1	0.195407
Snhg5	-0.66671	Uqcrq	-0.39531	Neo1	-0.94746
Il1bos	-1.61609	Dennd5a	0.209639	Dazap2	0.171646
Bcl2l11	0.522012	S1pr1	0.432755	Rpl17	0.186316
Add3	-0.37944	Nucks1	-0.24034	Ubash3a	0.305015
Lsp1	0.339229	Tenm4	-2.21974	Piga	-0.26754
Tpd52	0.386448	Phldb2	0.821303	Rasa3	0.198942
Lck	-0.84793	Odc1	-0.26952	Ppp1r8	-0.22656
Hs6st2	-1.35271	Birc3	0.233322	Pawr	-1.12307
Arhgef12	-0.98861	Slc2a3	-0.22965	Sipa1l1	-0.22578
Peli2	0.537156	Zfp658	0.78264	Timm50	-0.29176
Dnajc6	-0.45951	Bnip5	0.480985	Dync2li1	0.456841
Fn1	-2.21248	Cpox	-0.34776	Gm32908	0.502895
Adam8	0.879906	Luc7l3	-0.29326	Dnmt1	-0.19472
Hk3	0.422701	Mturn	0.622956	Wdr18	-0.22806
Arpc5l	-0.43998	Iqgap3	-0.3822	Cep19	0.319525
Tnik	-0.56128	Gm46162	0.862648	Arhgap19	-0.22941
Jup	0.866155	Tie1	-0.26082	Runx3	-0.20401
Gm39556	2.579393	Senp1	-0.24983	Rac2	0.173956
Psph	-0.56147	Acvr1b	-0.24809	Bphl	0.287003
Fus	-0.41734	P2ry1	-0.44111	S1pr4	0.271052
Akr1c13	-0.45095	Ifi203-ps	0.534007	Tax1bp1	-0.15392
Fndc3b	0.448965	Zfp532	-0.96749	Coq2	-0.22475
Ddx27	-0.35002	Cnn3	0.273023	Gm40185	-0.67106
Fgl2	0.450722	Bin2	-0.20086	Gimap1	0.195379
Dusp22	1.037592	Sdcbp	0.232211	Jrk	-0.60395

Adipor1	0.335035	Lrrc8d	-0.32425	Tardbp	-0.20325
Btg1	0.373758	Tmem229b	0.28947	Ammecr1	-0.33521
Zup1	0.471664	Lrrc66	-2.09107	Orc5	-0.26241
Fkbp9	-0.55681	Tap1	0.196142	Mcm3	-0.19732
Unc93b1	0.364672	Pitpnb	-0.23846	Fam126a	-0.19647
Pip4k2a	0.334446	Lsm4	-0.29625	Anapc5	-0.16293
Cebpg	-0.46442	Rif1	-0.20319	Brdt	0.763778
Mgat5	0.358835	Flot1	0.23802	Ccp110	-0.31506
Ifngr1	0.340502	AB124611	0.664783	Smc6	-0.17184
Camk1d	0.625603	Rps19	0.192186	Shcbp1	-0.28825
Acsf2	0.372253	Rbl1	-0.23467	Kcnn1	1.067551
Aldh1a1	-1.06915	Dsg2	-2.1466	Cactin	-0.23683
Iigp1	0.386406	Ets2	-0.38034	Tacc1	-0.1854
Ndc1	-0.39557	Paqr3	-0.86417	Adgra3	-0.25763
Ccl6	1.075304	Ago4	0.475784	Nup85	-0.25291
Dpysl5	-3.61232	Prune2	-0.80333	Ddx39a	-0.26555
Sirpa	0.384506	Hps3	0.339374	Dph5	-0.33206
Ccpg1	0.339239	Prpf31	-0.31203	Micu1	0.254294
Coro7	0.38277	Nxpe1-ps	0.777265	Gpr146	0.30749
Baiap2	0.570224	Runx1	0.212211	Ypel4	0.916129
Slc17a8	-1.89516	Ccng2	0.267288	Sptssa	0.248096
Sft2d2	0.324039	Nfam1	0.294618	Rbbp8	-0.23466
Spats2	-0.54983	Kcnk5	-0.26247	Gosr1	0.210272
Gm52877	0.543832	Mapk3	0.27694	Gdi1	0.229523
Icos	1.226962	Tgfb1	-0.20867	Phf11a	1.36259
B3gnt5	-0.39791	Trim14	0.222306	Topbp1	-0.1792
Nup62	-0.40207	Pdss1	-0.5291	Bcap29	-0.21634
Usp35	0.79887	1700019D03Rik	-1.68185	Tom1l1	-0.40139
Nlrp3	0.980343	Fam20c	1.1493	P2ry10	0.517408
Hax1	-0.40516	A630034I12Rik	-0.41529	Xaf1	0.22865
Clec4d	0.492774	Pgm2l1	0.218896	Clec9a	1.336124
Mtfr2	-0.42788	Efcc1	0.534359	Mcm10	-0.26101
Mthfd1l	-0.33915	Niban2	0.281399	Arl4a	-0.22873
Col11a2	0.540048	Nkg7	-0.26163	Bcl11a	0.181537
Anxa2	0.347618	Usp44	-0.96188	Ska2	-0.27513
Gp9	-1.0166	Anxa1	0.278477	Tsr2	-0.2829
Stat4	0.359967	Plxna4os1	0.960995	Gpr137b-ps	0.520739
Tjp1	-0.34966	Gucy1b1	-0.914	Rnps1	-0.20962
Trib3	-1.35881	Insr	0.264242	Lif	-0.76966
Il15	0.501137	Rp2	0.250525	Cenpn	-0.32196
Serpina3f	0.299559	Crybg1	0.688095	Tspan14	0.183929
Nucb2	0.726258	Mcm2	-0.26432	Zc3h12d	0.487077
Eif5	-0.31193	Tpm1	-0.2509	Ppp1r3b	0.219447
Golm2	-0.51575	Nf2	-0.2343	Kat14	-0.20497

Nckap1	-0.91221	Rrp15	-0.3652	Vcpip1	0.185702
Ppic	-0.44831	Igbp1	0.254572	Spire1	-0.30186
Aldoc	0.348421	Recql	-0.31244	Bub1	-0.23761
Slfn5	0.325983	Sowahc	1.429941	Arpc5	0.164948
Rgs8	1.38354	Dennd4a	-0.23061	Nfkb2	-0.23024
Paqr5	0.958052	Nectin1	-0.66042	Pprc1	-0.22356
Ppm1k	0.552628	Psma8	-0.59857	Dph7	-0.3116
Cysltr1	0.553159	Mrpl17	-0.32611	Asah2	0.225342
Cd53	0.392906	Gsdmd	0.266846	Cc2d2a	-0.87575
Stxbp6	-0.42632	Utp25	-0.29557	Ica1	-0.24741
Trpc6	-1.11015	Gm26947	1.318089	Tnf	-0.45805
Sox6	-1.1428	Hmgn5	-0.29194	Cdt1	-0.2324
H2-T22	0.340348	Actr3b	-1.3704	Tmem51	0.446176
Ip6k1	0.311149	Rpusd2	-0.38828	Anapc15	-0.34774
Robo4	1.008816	Ctla2a	0.266346	Cyfip1	0.180197
Hgh1	-0.5866	Myom1	-1.41407	Tspyl4	-0.5335
Cep164	0.49592	Lpar1	1.652048	Supt3	0.278071
Gbp2	0.482873	Vps26c	0.356183	Def6	-0.18627
Tinagl1	1.603138	Cmah	0.620436	Ormdl3	-0.25898
Cdc42bpa	-0.48249	Slc36a1	0.327593	Egln3	0.176538
Adamtsl4	1.52054	Pold1	-0.30306	Zadh2	-0.21133
Il12a	0.565659	Spred1	-0.20842	Itsn1	0.213354
Ghitm	-0.36088	Abcd1	0.293641	Morc4	-0.53549
Palld	0.986275	Hells	-0.25526	Prkx	0.244085
Ap3s1	0.398584	Gsr	0.245675	Eva1b	0.499356
Ifi211	1.137094	1600014C10Rik	0.262655	Ino80e	-0.25381
Samd14	-0.73691	Prx	-0.62504	Rbbp9	0.338875
D17H6S56E-5	-0.34174	Eif2a	0.208087	Hipk1	0.178398
Il1r1	0.314522	Ston2	0.440848	Sgo1	-0.26693
Mettl1	-0.58577	Dio2	0.554073	Chpt1	-0.29623
Rcsd1	0.328907	Zrsr1	0.429048	Nsun5	-0.43235
Mpo	0.374809	F830016B08Rik	0.457992	Gm30189	-0.42121
Dtx3l	0.276749	Ssh2	0.258901	Cables1	0.262161
Ctsa	0.36541	Ccr1	0.672578	Efr3b	-0.69938
Cth	-1.83219	Azin1	-0.23636	Fhdc1	0.989498
Fam102b	0.384273	Myef2	-0.26565	Atad3a	-0.21083
Uqcrh	0.432743	Prex1	0.263088	Foxj2	0.299929
Ldlrad4	0.563214	Smc2	-0.2097	Arntl	0.387274
Ccl4	0.677326	Cd79b	0.472485	Cdca7	-0.1904
Lgmn	0.968593	Aurka	-0.33383	Dlst	-0.17396
Gsn	0.4391	Rad51	-0.33905	Snx8	0.3182
Tnfaip2	-0.37966	Rcc1l	-0.35018	Gpr157	0.452709
Pcyt1a	0.330712	Spag5	-0.31391	Rftn1	0.21832
P3h2	-2.21525	Mtss2	-1.31966	Ly9	0.344128

Ckap4	0.352695	Lrrc8b	-0.27866	Pcyt1b	-0.23725
Sting1	0.358674	Kansl1l	0.270442	Septin5	-1.12523
Entpd1	0.578517	Sdr39u1	-0.4786	Pigg	-0.32292
H2-T24	0.321016	Siah2	-0.39095	Lyplal1	-1.33893
Angptl2	0.69231	Iffo2	0.35858	Vis1	0.991114
Hsd17b1	-0.99607	Cyp11a1	0.419934	4930503L19Rik	-0.3592
Bckdha	0.385476	Tada2b	-0.42262	Slc17a5	0.381649
Haao	0.461576	Fbxo16	-1.48301	Haus3	-0.21374
Gm4951	0.415256	Mgst2	0.698978	Arl4c	0.368739
Tspan2	0.459419	Ypel2	0.444802	Il17ra	0.19133
Cast	0.369798	Irf2	0.220608	Ripor3	-1.14788
Gcnt2	0.31047	Gprin3	0.755637	Ahctf1	-0.16645
Evl	0.524598	Prpf18	0.257969	Hs6st1	0.25262
Mki67	-0.33743	Slamf7	0.918378	Gfod1	0.226844
Tra2b	-0.35414	Sidt2	0.257117	Ankrd49	-0.23127
Slc35b1	-0.54294	Zcchc24	0.531295	Macrod2	-0.71407
Kpnb1	-0.26064	Ebi3	0.268036	Gnl3	-0.20187
Nomo1	-0.30923	9530068E07Rik	0.219022	Mlec	-0.15218
Elk3	0.316924	Nrgn	-0.3421	Cd164	0.162024
2900026A02Rik	0.458684	Ddah2	0.334912	Srprb	-0.20702
Chst15	0.471942	Fyn	-0.28287	Snx33	0.366285
Il6st	0.434335	Stk16	-0.27621	Snap47	-0.29648
Srsf1	-0.34239	Nectin4	0.484938	Gabpb2	-0.20644
Stat2	0.317375	Gla	0.396938	Mat2a	-0.19217
Ctps	-0.37285	1810058I24Rik	0.303818	Ubr7	-0.19845
Alox5ap	0.310824	Rtl5	0.426122	G3bp1	-0.16225
Fads3	0.776603	Ranbp1	-0.30533	Ubxn2a	-0.2242
Cd200r1	0.424865	Map3k8	0.363411	Cavin1	-0.25859
Rap1b	-0.33311	S1pr3	-0.36826	4930579G24Rik	-0.3324
Zdhhc15	-0.52985	Pbxip1	0.254801	Dpf2	-0.17281
Cxcr4	0.385087	Ankrd27	-0.21709	Bmx	0.81502
Kbtbd11	0.379756	Wdr76	-0.27881	Haus5	-0.3149
Cebpa	0.345413	Adgrg7	-0.36961	Cers6	-0.19611
Gpr171	0.365592	Tdg-ps2	0.99095	Tgfbi	0.653971
Rgs7bp	-0.67883	Lrch2	-1.15217	Prss34	0.421925
Grn	0.29015	Gngt2	0.530386	N4bp3	0.482084
Ank	0.367606	Nox1	-0.48997	Tmem38b	0.283879
Arid5b	0.525604	B2m	0.243345	Ptger3	-0.29796
Slc16a9	1.056637	Fcho2	0.310998	Rsu1	-0.19018
Pbx1	-0.35881	Zc3h18	-0.2497	Zik1	-0.38591
Gapt	0.879207	Ppp3ca	0.226096	Cltb	-0.35582
Il7r	0.924888	Gaa	0.25614	Mrpl57	-0.33018
Ampd2	-0.31988	Mcl1	0.213478	Rsad1	-0.3059
Lifr	0.824652	Cdcp1	-0.97915	Snhg1	-0.2864

Rin3	0.362566	Abcc1	-0.23064	Itm2c	0.216637
Wdr26	0.258933	Spred2	-0.28366	Pop1	-0.3094
Gltp	0.323744	Ifi208	0.365436	Tceal8	-0.30313
Sdad1	-0.29755	Nbea	-0.57599	Mical3	-0.38131
Ehd3	-1.636	Fis1	0.265703	Senp7	0.218339
Tbl2	-0.38529	Htra3	1.29677	Denr	-0.22925
Mppe1	0.616127	Pfkm	0.239744	Homez	0.28969
Zfp831	0.499226	Endod1	-0.33809	Tnfrsf1a	0.190635
Dusp5	0.429758	Tbcc	-0.4345	Slc15a4	0.261136
Myo1e	-0.85549	Ccna2	-0.28388	Gt(ROSA)26Sor	-0.40404
B3gnt2	0.279279	Cyp2j9	0.589532	Gm2629	0.386707
Pfdn5	0.361636	Bop1	-0.28893	Rtel1	-0.30397
Rara	0.515869	Lrp5	0.287841	Tmem135	0.210622
Ablim1	0.318819	Glmp	0.293514	Fut4	0.315483
Nat10	-0.34674	Tubgcp4	-0.42368	Osbpl1a	-0.19629
Klhl23	-0.49814	Cdca8	-0.33394	Metap1	-0.20814
Ncf2	0.299347	Slc38a9	0.453081	Kbtbd8	-0.493
Calcrl	0.35762	Pik3c2a	0.317778	Il12rb1	0.255421
Mn1	0.681683	Tns3	0.267236	H2bc4	0.39262
Map1lc3b	0.317036	Chd1l	-0.28953	Mrpl38	-0.25741
4833407H14Rik	0.637785	Slamf9	-1.06352	4833420G17Rik	0.213282
Papss2	0.539519	Laptm4a	0.215197	Usp31	-0.22309
Col18a1	-0.71629	Zfp874b	0.351675	Prmt3	-0.1869
Ppfibp2	0.653574	Fmo5	0.505227	Slc35b4	0.209362
Atf5	-1.67745	Zdhhc21	-0.242	Snx24	0.469079
Dap	0.31636	Hipk3	0.214734	Hp	0.325629
Uaca	-0.95023	Fscn1	0.760342	Selp	0.234171
Plin2	0.370514	Peg10	-0.68805	Selenbp1	0.237283
Dnase1l1	0.549552	Hexb	0.457268	Pfkfb4	0.339393
Khdrbs3	-0.99651	Klrd1	0.548696	Serinc5	0.276323
Rcc2	-0.26051	Ncapg	-0.28118	Noc2l	-0.18142
Maml3	0.439791	Btbd3	0.336641	Ncstn	0.185992
H2-Oa	0.658854	Actl6a	-0.2544	Slc8a1	-0.39708
Eda2r	-1.01016	Osgin1	1.014671	Cdca2	-0.21231
Spata6	0.488699	Elac2	-0.28161	Melk	-0.30399
D030028A08Rik	-0.55536	Clcn5	0.308249	Gng10	0.222256
Fzd4	-1.00481	Wdr35	0.696071	Bhlha15	-0.42508
Pygm	0.899847	Dnajc21	-0.29506	Fam124b	-1.78704
Tmem156	0.580453	Adrb2	0.952676	Esam	-0.63524
Tbc1d31	-0.41755	Lyn	0.22521	B3galt4	0.438861
Polq	-0.45061	Pfkp	-0.24205	Tmco1	-0.19813
Als2	-0.31183	Incenp	-0.24991	Elapor2	-0.36758
Lyst	0.417409	Kdm5b	0.233126	Hnrnpm	-0.17309
Gata2	-0.31153	Abhd4	0.253513	Hnrnpu	-0.16193

Rrp12	-0.38918	Rrp8	-0.30984	Hexa	0.194676
Efcab11	-0.78023	Wdr74	-0.32276	Xlr	-0.90989
Vamp5	-0.42759	Eps8l1	0.438938	Jun	0.750164
Cd244a	-0.43123	Farsb	-0.2593	Lap3	-0.21567
Lpcat2	0.436507	Snrnp40	-0.24735	Dennd6a	0.198224
Lpxn	0.537376	Inpp4b	-0.32872	Sertad3	0.369883
Ctsg	0.296656	Mospd2	0.299583	Pacsin2	-0.20209
Csf2rb	0.308673	H3f3b	-0.18583	Ran	-0.20314
Slc6a15	-0.67986	Asap2	-0.35146	Alg3	-0.38361
Ids	0.403575	Ranbp9	0.232593	Diaph3	-0.21389
Mxi1	0.337405	Lsm12	-0.27931	Gm51657	0.839076
Spc24	-0.44248	Tubgcp2	-0.25455	Laptm4b	0.297684
Map3k1	0.353492	Nudcd2	-0.25865	Atp10d	0.323075
Utp20	-0.3222	Ppp1r15b	-0.20737	Ctu2	-0.34159
Gm13073	-1.95894	Fndc3a	0.200414	Ndufv1	-0.21263
Gm12185	0.451815	B3gnt8	0.517672	Tulp4	0.956916
Phf11b	0.598234	Atp10a	0.240515	Zfp60	0.273783
Camk2d	0.445531	Tagap	0.355146	Tacc3	-0.24065
Mia2	-0.29238	Timeless	-0.23695	H2-DMb2	0.630313
Cpt1a	0.283413	Fuca2	0.258191	Srsf3	-0.19542
Dgka	0.480194	Mef2c	0.192215	Gm16553	0.97613
Ybx3	-0.27412	Polr1b	-0.24232	Gm39896	1.224934
Dnah8	0.819554	Cebpd	0.476709	Uchl5	-0.23905
Pabpc4	-0.30035	Heatr9	1.12686	Atg14	0.298404
Snn	0.453959	Cep295	-0.30318	5430416N02Rik	-0.46088
Ccar1	-0.30341	Pira2	1.661522	Ptpn12	-0.17143
Card6	0.788349	Laptm5	0.20781	Orc6	-0.27564
Mybbp1a	-0.25748	Tmem65	0.374325	Gabbr1	0.299746
Arhgap9	0.317186	Cirbp	-0.28375	Oasl2	0.160018
Cd37	0.305007	Nup155	-0.21855	Mybl2	-0.25278
Grb10	-1.09043	Ezr	-0.27072	Tmem107	-0.40915
Sgk3	0.330986	Surf6	-0.26273	Patl2	1.174887
P2rx3	-1.66847	Plekhb2	0.265566	Renbp	0.239361
Tgfbr2	0.35183	Slc35f2	-0.41227	Ttc12	0.585681
H2-K1	0.247215	Hspa8	0.23285	Slc7a7	0.569392
Rnasel	0.301887	Kif13b	0.314357	Hus1	-0.22185
Ddit4	-0.4082	Lamb2	0.724157	Nup50	-0.17431
Wdfy2	0.400609	Espl1	-0.29305	Dnmt3b	-0.24407
Ctsl	0.413699	Fyb	0.205292	4930512H18Rik	0.495257
Cat	0.280373	Trim34a	0.23929	Jak1	0.14342
Rufy4	0.662239	Gns	0.252648	Kif1b	-0.28973
Dedd2	0.37188	Il4ra	0.226699	Iqsec2	0.299268
Mfge8	0.342154	Aldh1b1	0.473727	Mphosph10	-0.22259
Phyh	0.588358	Esco2	-0.41051	Gm30779	1.048333

Cx3cr1	0.556595	Basp1	0.273723	Espn	0.778586
Havcr2	-0.53151	Hnrnpab	-0.22862	Ptgir	0.267309
Myl10	0.882604	Fam214b	0.552985	Clu	-1.44001
Glis3	1.050919	Atp11a	-0.3773	Ddx1	-0.1822
Cox6a2	-1.61053	Suox	0.485217	Ino80d	0.205299
Tyms	-0.43461	A330074K22Rik	1.338404	Lsm11	-0.28923
Podnl1	-0.64172	Mlkl	-0.24814	Zscan2	0.276312
Bmp2k	-0.36312	Zfp783	-0.40835	Syne1	0.300083
Smap2	0.290929	Ptar1	-0.27389	Utp15	-0.20495
Bcl6	0.711751	Gm36809	0.623424	Hdc	0.344657
Mmp19	0.661433	Trim30a	0.198331	Cpne2	-0.19749
Sbf2	0.766964	Pmaip1	0.27934	Syncrip	-0.15387
Zfp874a	0.441063	Soat1	0.261355	Dbp	0.541177
Vash1	-0.37028	Plekha5	-0.26926	Zfp180	-0.41534
Dyrk1b	0.435615	Adgre5	0.474323	Cks1b	-0.2576
Fhl1	-1.24378	Dkc1	-0.25308	Tac4	-1.1744